博士学位論文

化学交換と電解濃縮による同位体分離の研究

Study of isotope separation via chemical exchange and electrolytic enrichment

令和 4年2月8日

大阪産業大学大学院

人間環境学研究科人間環境学専攻

RITTIRONG ANAWAT

Doctoral Dissertation

Study of isotope separation via chemical exchange and electrolytic enrichment

February 2022

Graduate School of Human Environment

Osaka Sangyo University

RITTIRONG ANAWAT

Doctoral Dissertation

Authored by

RITTIRONG ANAWAT

Supervised by

HAZAMA RYUTA

February 2022

Graduate School of Human Environment

Osaka Sangyo University

Abstract

^{48}Ca is a double beta decay nuclide (ββ) with a natural abundance of 0.19%. It is used in CANDLES (CAlcium fluoride for studies of Neutrino and Dark matters by Low Energy Spectrometer) project to study neutrinoless double beta decay (0νββ). CANDLES aimed to investigate the lepton number non-conservation towards the understanding of a matter and anti-matter asymmetry, Majorana nature of neutrino, and the absolute mass of the neutrino. However, in order to search for such an ultra-rare event, a large amount of ^{48}Ca is required. The industrial-scale isotope enrichment methods are inapplicable for calcium isotope. Therefore, this research aims to investigate the cost-effective way to enrich calcium via chemical exchange using DC18C6 crown-ether. The first milestone is the production of grams scale for super heavy elements production. Afterward, a kilogram scale is profitable for the medical use of ^{46}Ca and ^{47}Ca as an in vivo radiotracer, then towards a ton scale for the CANDLES project. Simultaneously, the increasing demand for lithium isotope for the energy supply on tritium production from ^{6}Li in the nuclear fusion reactor, a pH controller of ^{7}Li, is outstripping the current supply of lithium isotope production. This research, on the use of crown-ether and liquid-liquid extraction, could benefit the isotope separation and enrichment and potentially replace the mercury amalgam method that causes the environmental problems.

The isotope composition analysis was measured by (reaction-cell) ICP-MS (RC-ICP-MS) (Agilent 7700 and 7900) and compared to TIMS (TRITON, and MAT261). Careful collection of the isotope composition measured by ICP-MS was described to overcome the mass bias. The comparison measurement of calcium isotope composition measured by ICP-MS and TIMS was found to be in good agreement (CC = 0.72, and 0.72 for TRITON and MAT261, respectively), indicating that the measurement by ICP-MS had a reliable outcome. On the other hand, spike ^{7}Li samples were used to assure the measurement of lithium isotope composition and assure the obtained separation factor.

Liquid-liquid extraction (LLE) using DC18C6 crown-ether was carried out, and several fundamental factors were studied, including the presence and absence of crown-ether in the organic phase, the extraction time, various feed concentrations, temperature dependencies (– 15 to 45 °C), solid-liquid extraction, and the contribution of 12M HCl were carried out. The distribution coefficient (D) of lower Ca and Li concentrations showed a significant increase under the presence of 12M HCl. The separation factor (α_{org}) was consistent with aqueous solvent at 0.991±0.004 for HCl acid and 0.990±0.004 for aqueous solvent (30% w/w). Multistage iterations of calcium were carried out. The results indicated the enrichment of ^{48}Ca under the presence of HCl acid. The maximum separation factor (α_{aq}) of $^{48}Ca/^{40}Ca$ was increased up to 1.007±0.004 on HCl solvent. In contrast, the aqueous solvent was found to be 1.004±0.004 at the 6^{th} iteration. The iteration stages required to achieve ten times enrichment were 2112 and 3793 for HCl and an aqueous solvent, respectively.

The other concentrating element is tritium electrolytic enrichment, which, like calcium and lithium, is an isotope exchange reaction dominated by the nuclear mass effect of the lighter isotope. The tritium enrichment was carried out by the electrolytic using solid polymer electrolyte (SPE) film. This research carried out the improvement on the temperature cooling system. We applied the water and air circulation system and assured that those samples were acceptable. The water circulation system enhanced the enrichment factor up to 13.9±0.2, and the combination of the air circulation system improved the enrichment factor up to 16.0±0.2.

This study was conducted toward the international joint research project between Thailand and Japan. The motivation of this collaboration was the nationwide survey of tritium in Thailand before the operation of firstly nuclear power plants. Tap water samples were collected from Thailand. Shinshu University and Kyoto University also collaborated for trace element determination. The study can improve Thailand's international nuclear safety and safeguard potential.

Keywords: Isotope, Isotope Separation, Enrichment, Crown-ether, Liquid-Liquid Extraction, Calcium, Lithium, Tritium, Electrolytic Enrichment

ACKNOWLEDGMENTS

The author would like to express gratitude to the dedicated and encouraged Professor Ryuta Hazama, and Takaaki Yoshimoto for their consolation, enrollment, support, and motivation until this doctoral thesis was fulfilled. Also, the gratitude to the dissertation committees, Prof. Tatsuya Suzuki, Nagaoka University of Technology, Prof. Tatsuhide Hamasaki, and Prof. Shingo Otsuki, Osaka Sangyo University.

The author would like to express gratitude to the many people who gave generously of their time and knowledge to fulfill this doctoral thesis, including Prof. Tatsuhide Hamasaki, and Nanthapong Chantaraprachoom, Faculty of Design Technology, Osaka Sangyo University, for the support of laboratory equipment, and the support on the ion chromatography measurement, Prof. Ryo Horikoshi, Faculty of Design Technology, Department of Environmental Science and Technology, Osaka Sangyo University for the support on the use of chemical reagent, and micropipette, Emer. Prof. Tadafumi Kishimoto from Research Center for Nuclear Physics (RCNP), Osaka University for the use of ICP-MS measurement, members of CANDLES, Osaka University for the valuable opportunity to present the thesis contents and update at the collaboration meeting, Prof. Masao Nomura for TIMS measurement, and Prof. Ayaki Sunaga from Kyoto University for the simulation of the ion-crown complex.

The author would like to express warm gratitude to Pannipa Noithong, a senior doctoral student who continuously provides support, encouragement, and suggestion to the author on many necessary steps toward this achievement.

Moreover, this work was supported by JSPS KAKENHI Grant Number 16H04636 Grant-in-Aid for Scientific Research(B) from MEXT (Ministry of Education, Culture, Sports, Science, and Technology), Japan, and JSPS Biliteral Joint Research Projects with Thailand NRCT Grant Number JPJSBP120209203. The author was supported by the Japanese Government (MEXT) Scholarship.

CONTENT

List of abbreviations

Abbreviations	Explanation
0νββ	Neutrinoless double beta decay
2νββ	Two neutrino double beta decay
18C6	18-crown-6 Crown-ether
AAS	Atomic Absorption Spectrometry
Aq	Aqueous phase
BE, Org	Back-extracted, Organic phase
CANDLES	CAlcium fluoride for studies of Neutrino and Dark matters by Low Energy Spectrometer
CC	Correlation coefficient
CE	Crown-ether
D	Distribution coefficient is the ratio of the total analyte (solute) in the extract (organic) to its total analyte in the aqueous phase (aqueous)
DC18C6	Dicyclohexano-18-crown-6
DSA	Dimensionally Stable Anodes
ESCR	External Standard Channel Ratio
ICP-MS	Inductively Coupled Plasma Mass Spectrometry
IR	Isotope ratio, counting ratio
JRIA	Japan Radioisotope Association
K	The extracted ratio indicated by the ion content between raffinate to feed

Abbreviations	Explanation
LB7	Liquid scintillation counter AccuFLEX LSC-LB7, Hitachi, Ltd. (Japan)
LLE	Liquid-Liquid Extraction
LSC	Liquid scintillation counting
MWA	Metropolitan Waterworks Authority of Thailand
OSU	Osaka Sangyo University
PWA	Provincial Waterworks Authority
R	Tritium recovery factor
RC-ICP-MS	Reaction-cell ICP-MS
RO	Reverse osmosis
SPE	Solid Polymer Electrolyte film for tritium enrichment
SRM 915b	Standard Reference Material of calcium from NIST
SUS316	Stainless steel electrode
TIMS	Thermal Ionization Mass Spectrometry
TINT	Thailand Institute of Nuclear Technologies
TIT	Tokyo Institute of Technologies
α	Separation factor is a parameter determined as an isotope ratio (R) between the aqueous phase (or organic phase) compared to feed.
ε (‰)	Enrichment coefficient (α-1)
η	Mole ratio (η) is defined as a ratio of ion-crown complex to a total crown-ether in the organic phase
δ	The relative difference in isotope abundance (δ) between calcium sources and the NIST standard

CHAPTER ONE: Introduction

1.1. Introduction

This study investigated the isotope separation technique to determine the feasibility of isotope separation and mass production of the enriched isotope using the chemical exchange technique. Liquid-liquid extraction (LLE), also known as solvent extraction, was used to separate calcium and lithium isotopes. The primary purpose is to enrich calcium-48 (^{48}Ca) isotope to study neutrinoless double beta decay by CANDLES (CAlium fluoride for studies of Neutrino and Dark matters by Low Energy Spectrometer) project. Meanwhile, the electrolytic enrichment of tritium using SPE film was also investigated, which will be useful for the JSPS joint research project between Japan and Thailand.

Chapter 1 deals with the interesting isotopes, applications, separation techniques, and isotope composition analysis using mass spectrometry and scintillation counting. Section 1.2 is the research objectives of this doctoral dissertation. Section 1.3 deals with the principle of isotope, isotope effect, and example of isotope separation for nuclear fuel cycle. Sections 1.4 to 1.6 begin with concentrating isotopes, such as calcium and lithium, their applications, possible isotope separation techniques, and the liquid-liquid extraction (LLE) method that was investigated in this study. At the same time, the isotope composition was analyzed by inductively coupled plasma mass spectrometry (ICP-MS) with a comparison of thermal ionization mass spectrometry (TIMS). Section 1.7 compromises to another concentrating isotope, tritium (^{3}H), including tritium in environmental, electrolytic enrichment of tritium., and the liquid scintillation counting techniques for measuring ultralow level tritium.

1.2. Research objective

This research aims to investigate the isotope separation of calcium, and lithium by chemical exchange using crown-ether. The main purpose is to find a cost-effective method for the isotope separation and isotope enrichment feasibility of ^{48}Ca for the study of neutrinoless double beta decay by CANDLES (CAlium fluoride for studies of Neutrino and Dark matters by Low Energy Spectrometer) project. Studying chemical exchanged reactions in single-stage isotope separation on a small scale could lead to very large-scale isotope enrichment and mass production. The separation of lithium isotopes was also studied for future demand on energy supply and frontier nuclear fusion research.

Moreover, tritium (^{3}H), one of the hydrogen isotopes, was also investigated and improved on the separation technique of electrolytic enrichment. The improvement could enhance the capability of tritium enrichment and measurement. The JSPS joint research project on natural tritium concentration in a water sample collected from various regions of Thailand has been carried out along with the collaboration of the Department of Environmental Science and Technology, Osaka Sangyo University, Kasetsart University, Thailand Institute of Nuclear Technology (TINT), Thailand, Kyoto University, Kyoto, Japan, and Shinshu University, Nagano, Japan. The purpose is to evaluate the national tritium level in environmental water before the first nuclear facility operation in Thailand. The collaboration's goals are to record the most recent tritium levels in environmental water from various regions of Thailand prior to the imminent operation of nuclear facilities and improve Thailand's international nuclear safety and safeguards.

1.3. Isotope and isotope separation

1.3.1. Isotope

The atom is no longer the tiniest particle. Over a century, scientists have discovered subatomic particles and the standard model of particle physics. In 1897, J. J. Thomson made the first discovery of subatomic particles. Thomson measured the deflection of cathode rays and discovered that it was proportional to the potential difference between the electrode plates, indicating that cathode rays were negatively charged particles. Thomson called this particle an "electron." [1]. Thomson emphasized the study of the electron mass after the precise determination of the electron charge by A. H.Wilson in 1909. Thomson discovered that the electron has a mass of 1/1800 that of the hydrogen atom, which at the time was the smallest nuclei. These discoveries demonstrated that the atomic is not homogeneous and indivisible. Afterwards, many studies on atomic particles were carried out after this discovery at the beginning of the twentieth century, especially the radioactive material and radiation studies. E. Rutherford emphasized the Curies' and H. Becquerel's discovery of radioactivity. He also studied the law of radioactivity disappearance and classified radioactive materials based on their half-life [2]. The half-life is the time it takes for half of a radioactive species to decay.

In 1921, F. Soddy was awarded the Nobel prize in chemistry for the discovering of the chemistry of radioelements and the existence and nature of isotopes by observing the three radioactive series of natural elements [3]. Because gamma rays are high-frequency electromagnetic radiation, his research with E. Rutherford demonstrated that the emitted gamma rays do not affect the daughter atomic weight. Furthermore, he investigated the difference in nuclear properties of the isotope and developed an understanding of displacement law. **Fig 1.1** shows the displacement law by F. Soddy.

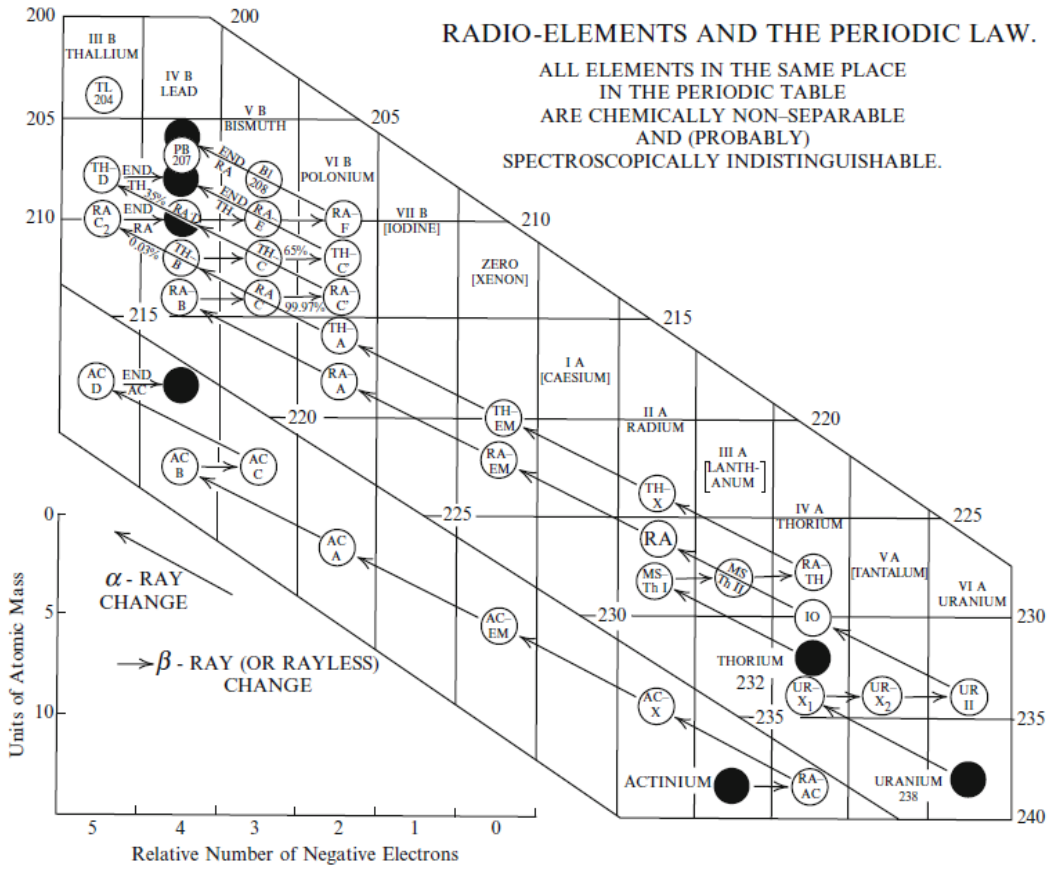

Fig 1.1 The displacement law of the radioactive decay by F. Soddy brought to the understanding of isotope [3].

In conclusion, although the number of electrons surrounding the nucleus is the same, he discovered that chemical elements are not homogeneous in the inner nucleus. His discovery established the existence of isotopes.

Meanwhile, the discovery of neutral particle in the nucleus in 1932 by the former student of E. Rutherford, J. Chadwick, explored the idea of heterogeneous nuclide [4]. Chadwick bombarded lighter atoms with alpha particles from a polonium source and observed the ejected radiation, which was neutral, penetrable, and slightly heavier than the proton mass. The neural particle was known as a neutron. Finally, the understanding of the nucleus and the evidence of the existence of the isotope was fulfilled.

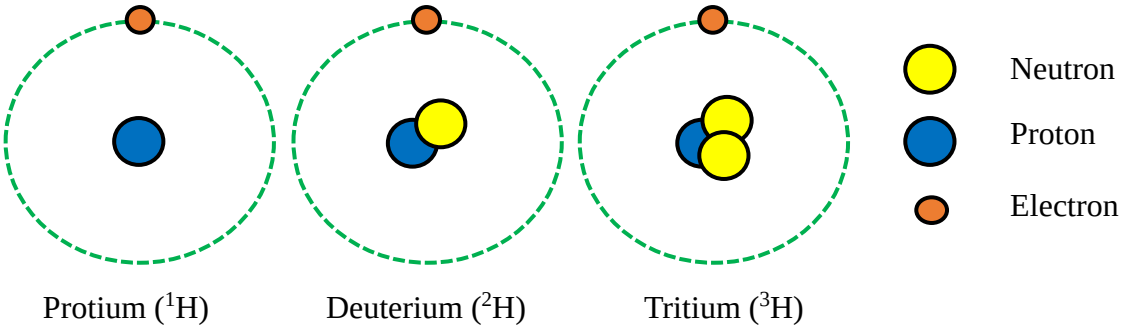

Fig 1.2 Hydrogen isotopes of protium (^{1}H), deuterium (^{2}H), and tritium (^{3}H).

The discovery of the subatomic particle, including proton, electron, and neutron, allows a better understanding of the isotope. To understand the isotope idea is to understand that the nucleus is made up of proton, which has a positive charge equal to the charge of the nucleus, indicating the atomic number of elements, and neutron, which is neutral in charge number. The number of an electron surrounding the nucleus is equal to the atomic number as well. The mass number is the total of mass proton and neutron in the nucleus. Eventually, the isotope is a type of atom that differs in neutron number but has the same proton number (atomic number). **Fig 1.2** shows the example of hydrogen isotopes species consisting of protium (^{1}H), deuterium (^{2}H), and tritium (^{3}H). The natural abundance of hydrogen is only for protium and deuterium, which has 99.9844% and 0.0156%, respectively [5]. On the other hand, tritium is a natural radionuclide produced from the Earth's atmosphere via the interaction of ^{14}N (n, 3H) ^{12}C **(Table 1.1)**. These isotopes have the same chemical properties. Deuterium or tritium can replace one of the hydrogen atoms in a water molecule (H_2O), called tritiated water. Tritium is a radioactive isotope that emits a beta particle. Tritium is used as a tracer in a research field, a medical diagnosis, nuclear activity observation, and a frontier physics research purpose. The separation of these isotopes is not difficult due to the significant mass differences between the hydrogen, deuterium and tritium atoms. Nonetheless, the separation of the heavier isotope is difficult. Many constraints exist in

the production of enriched isotopes for the desired application. The chemical property, natural isotope abundance, and cost-effective method are challenges.

Table 1.1 Isotope abundance of hydrogen and their origin [5]

Isotope	Natural abundance (%)	Nuclide	Origin
Protium (^{1}H)	99.9844%	Stable	Natural
Deuterium (^{2}H)	0.0156%	Stable	Natural
Tritium (^{3}H)	-	Radioactive	Cosmogenic radionuclide

For a more convenient understanding, the isotope composition is expressed in the percent and/or isotope ratio between two concentrating isotopes. This explanation is helpful to study the isotope separation and enrichment, the isotope dating of material, and the origin of the element [6]. For example, this study aims to study the calcium isotope enrichment, the natural isotope abundance of ^{48}Ca is 0.187%, and ^{40}Ca is 96.941%. The isotope ratio of ^{40}Ca to ^{48}Ca equals 0.00193. More details on calcium isotope are presented in section 1.4.

Fig 1.3 shows the table of nuclides and a type of decay of the isotopes. The isotope composition of all elements has been determined in this diagram. The stable isotope from Z = 1 to approximately 20 is located at the defined valley of stability. The isotope diagram trends to shift from the line of Z (number of protons) = N (number of neutrons) after approximately Z = 20 to the region of a neutron surplus. This is because the electric charge of the positively charged protons in the nucleus increases as Z increases. The required number of neutrons must be present to stabilize the nucleus and keep it from splitting apart. Moreover, **fig 1.3** also presents the type of radioactive

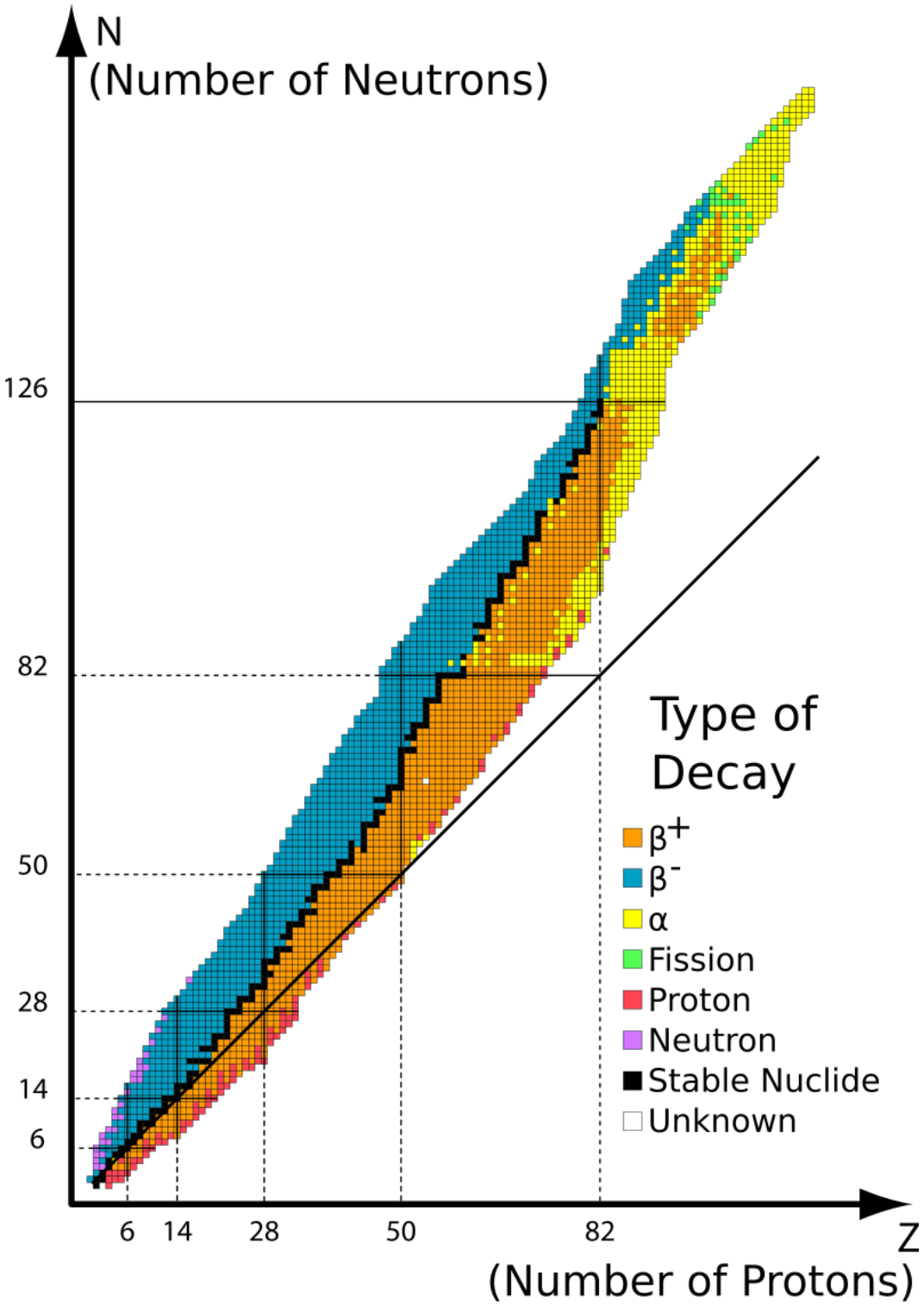

Fig 1.3 The table of nuclides and a type of decay. [7]

decay. The lighter radioisotope mainly emits the electron (β^-) or positron (β^+) particle, while the heavier isotope instead emits the alpha particle (α = nucleus of helium ($^4_2$He)). This is because the heavier isotope is more unstable than the lighter isotope. It would

rather emit the large particle of alpha, making the nucleus stable, than the lighter beta emission. The most remarkable is the fission, indicating the division of the heavier nuclide into two lighter daughter nuclides. The nuclear fission reaction is famous since it is used as a fundamental nuclear power reactor for the energy supply.

1.3.2. Isotope effect

As mentioned, the isotope is the type of atom which has a difference in neutron number. The isotopes mostly have the same chemical properties due to the electron surrounding the nucleus, which indicates the chemical reaction and property of the element. Nonetheless, the element from the different sources sometimes has a difference in isotope composition, called isotope fractionation. Isotope fractionation is a potentially helpful method for determining the origin of the element, material dating, and many historical field studies [5]. However, because of the difference in isotope mass, the vibrational frequency when the chemical reaction is bonded also changed, resulting in the different constant rate of reaction [5, 8, 9]. The kinetic isotope effect (KIE) was studied to better understand the isotope effect caused by different chemical reaction rates.

The kinetic isotope effect (KIE) is a phenomenon that occurs when isotopic substituted molecules react at different rates, as known as the isotope effect on rates. The difference in isotope mass causes different vibrational frequencies, resulting in different chemical reaction rates. The KIE was determined by the ratio of the rate constant between contributed lighter and heavier isotopes, and KIE was determined by the following equation (1.1):

$$KIE = \frac{K_{lighter}}{K_{heavier}} \tag{1.1}$$

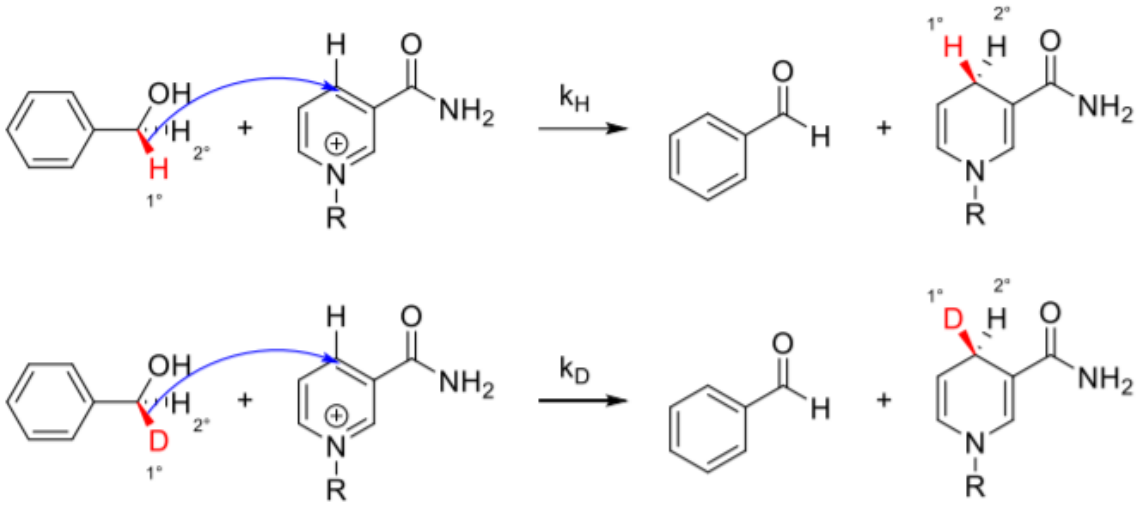

Fig 1.4 Isotopically substitution of deuterium [9]

where K is a rate constant of the contributed isotope, the subscripts of lighter and heaver indicate the lighter and heavier isotope contribution, respectively. The KIE value is always greater than unity. For example, the most famous experiment to understand the kinetic isotope effect is the replacement of protium (^{1}H) by deuterium (^{2}H) [9]. The KIE of protium and deuterium is defined as the following equation (1.2).

$$KIE = \frac{K_H}{K_D} \tag{1.2}$$

where K_H and K_D define as a rate constant of protium and deuterium, respectively. The rate constant of the chemical reaction on protium is higher than deuterium. **Fig 1.4** shows the example in the chemical reaction of isotope substitution of deuterium instead of protium. For a better understanding, potential energy surface (PES) was evaluated.

It is well known that the potential energy surface (PES) is the parameter that is used to indicate the chemical reaction. PES shows the coordination reaction and the change in position of the atoms in the chemical reaction. A chemical reaction will occur if the free energy overcomes the transition stage. As mentioned, the different vibrational

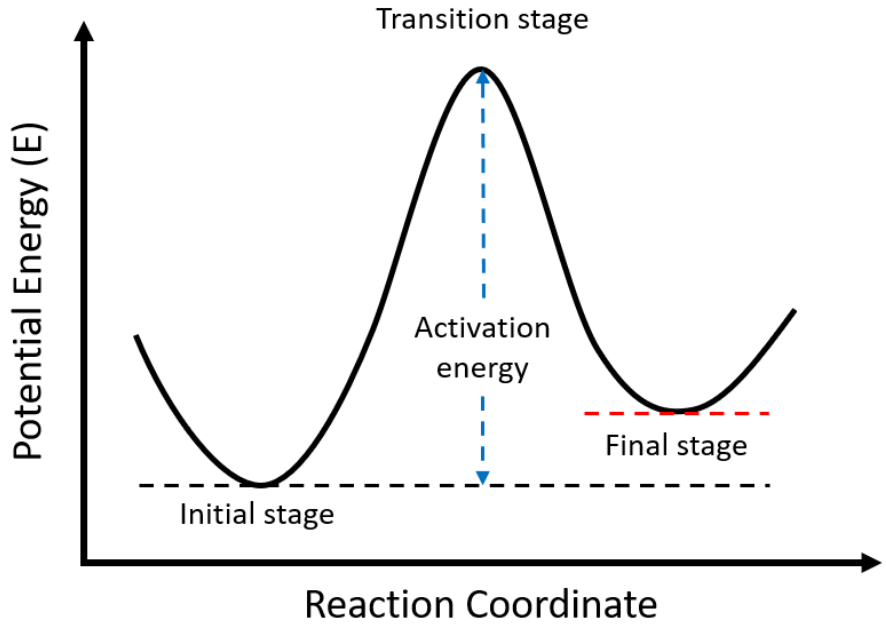

Fig 1.5 The classical transition stage of chemical reaction.

frequency is caused by the replacement of different isotope species, resulting in different chemical reaction rates. The lighter isotope provides a slightly greater chemical reaction compared to the heavier. The chemical isotope effect states that when a chemical substance initially consists of different isotopes of the same element, the chemical reaction favors the lighter isotope over the heavier isotope. As a result, the chemical reaction rate constant to the lighter isotope is higher than the heavier isotope, indicating that less energy is required in the chemical process [9]. **Fig 1.5** indicates the classical transition state theory of chemical reaction. However, the classical model did not concern the different nuclear properties on the different isotopes present in the chemical reaction (assume no isotope effect). The transition stage concerned with the nuclear property and isotope effect was semiclassical [8, 9]. **Fig 1.6** presents the semiclassical transition stage with the various isotopes of hydrogen. The different required activation energy of protium (H), deuterium (D), and tritium (T) result in the difference of zero-point energy (ZPE) at the ground and transition stage. This

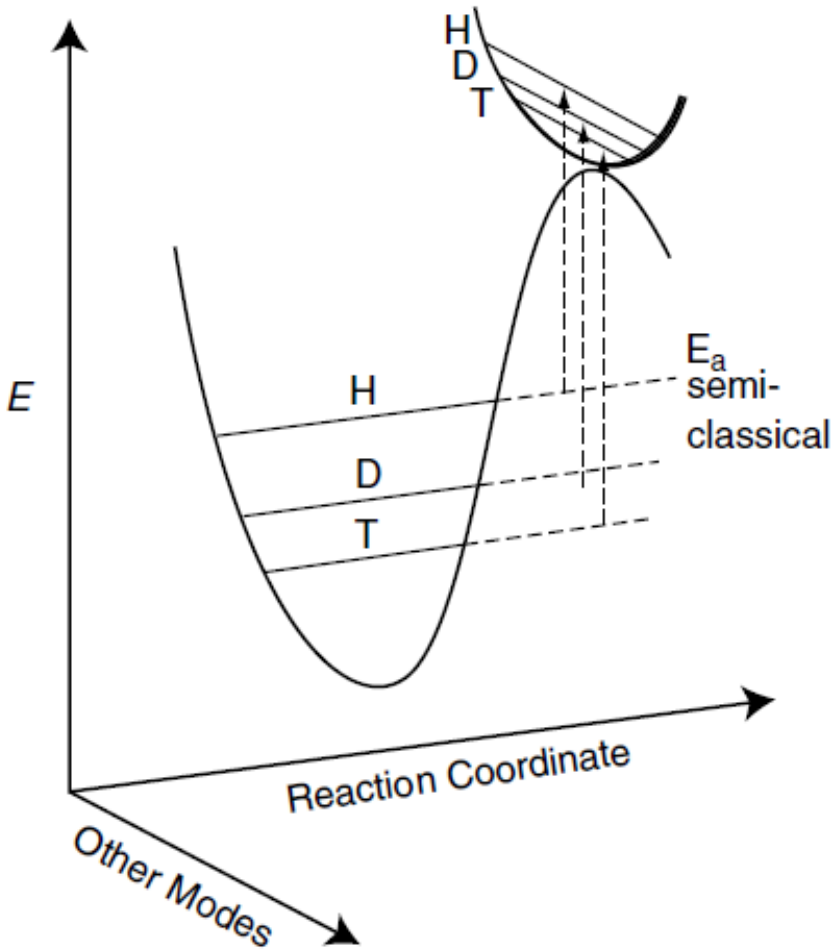

Fig 1.6 The semiclassical transition stage and the primary kinetic isotope effect (1º KIE.) [8]

phenomenon explains the isotope effect in a chemical reaction that protium would be transferred faster than deuterium and tritium.

The semiclassical model divides the kinetic isotope effect into primary and secondary kinetic isotope effects. The primary kinetic isotope effect (1° KIE) refers to the isotope effect in reactions in which the concentrating isotope is broken or formed in the rate-determining step. The 1° KIE can provide a significant isotopic substitution since the chemical bond was broken apart. Meanwhile, the secondary kinetic isotope effect (2º KIE) represents that the concentration isotope is not broken or formed in the

rate-determining step. However, the concentrating atom becomes the main chemical reaction substance. [9, 10]. 2º KIE results in the ZPE presenting in the transition stage, making the isotope substitution smaller than the 1º KIE.

In the case of isotope exchange separation, the difference in zero-point energy and the other factors were contributed. The calculation of equilibrium constant (K) was expressed by Bigeleisen-Mayer [11] as the following (1.3) to (1.6).

$$AX + BX' \rightarrow AX' + BX \tag{1.3}$$

$$K = \frac{[AX'][BX]}{[AX][BX']} \tag{1.4}$$

where X and X' represent the heavier and lighter isotope of the X element, respectively. A and B indicate the chemical species that contributed to the isotope exchange reaction. K could be calculated by the reduced partition function ratios (rpfr) of the above chemical molecule participating in the reaction.

$$K = \frac{(s/s')f_{BX}}{(s/s'')f_{AX}} \tag{1.5}$$

$$(s/s')f = \prod_{i=1}^{f} \frac{u_i \exp\left(-\frac{u_i}{2}\right)/[1-\exp(-u_i)]}{u_i' \exp\left(-\frac{u_i'}{2}\right)/[1-exp(-u_i')]} \tag{1.6}$$

where *(s/s')f* represent the reduced partition function ratios (rpfr) of the chemical species contributing to the exchange reaction, *f* is the degree of freedom of molecular vibration, $u_i = (hv_i/kT)$ and $u_i' = (hv_i'/kT)$, v_i, and v_i' indicate the vibrational frequency of the molecule contains heavier, and lighter isotope, respectively, h is the Planck constant, k is the Boltzmann constant, and T is the absolute temperature (Kelvin). According to the rpfr, expressed by the Bigeleisen-Mayer equation, the vibrational frequency of the chemical exchange and the temperature contribute to the separative effect. The higher temperature and the lower frequency results in the lower u, the *(s/s')f* approaches unity, and the separative effect is disappeared. In contrast, the lower temperature and high frequency, the *(s/s') f* approach 0.5 and the separative effect is out

standing in the difference zero-point energy, and the separative effect is become significant.

Additionally, Bigeleisen-Mayer equation [11] described only the nuclear mass effect contribution to the isotope exchange reaction. In 1989, Y. Fujii et al. [12] reported an anomalous isotope effect of ^{235}U in the isotope exchange via a chromatographic method. It was found that the fractionation between ^{234}U and ^{235}U is much smaller than the one between ^{235}U and ^{236}U. The isotope shift of ^{235}U breakdown the nuclear mass effect line indicated that it might be from the nuclear spin effect of odd number isotope. Further discussion on the existence of odd/even number isotope and the nuclear spin effect was carried out [13 – 15]. These findings indicated the breakdown of the nuclear mass effect line in the isotope exchange reaction. Additionally, K. Nishizawa et al. [16] reported the isotope fractionation in liquid-liquid extraction of strontium using crown-ether in 1995. The results pointed out a similar relation to the nuclear charge distribution. The 'change in mean-square nuclear charge radii $\delta(r^2)$' on the difference isotopes results in the difference of charge distribution (proton) in the nucleus. A change in the energy caused the nuclear field shift effect, known as the nuclear size and shape effect [17 – 24].

In conclusion, the major contributions of isotope shift consist of three components, including nuclear mass effect, nuclear field effect, and nuclear spin effect. In 1996, J. Bigeleisen [25] published the new nuclear field shift effect correction on his theory. The following equation 1.7 is the Bigeleisen new theory.

$$ln\,\alpha = ln\,\alpha_0 + ln\,K_{anh} + ln\,K_{BOELE} + ln\,K_{hf} + ln\,K_{fs} \qquad (1.7)$$

where $\ln\alpha_0$ corresponded to Bigeleisen-Mayer approximation on the reduced partition function ratio (rpfr). K_{anh} represents the correction term of the anharmonic vibration. K_{BOELE} is the Born-Oppenheimer approximation correction on the isotope mass effect.

K_{hf} is the contribution of the hyperfine splitting effect (spin effect). Moreover, K_{fs} is the nuclear field shift effect (nuclear size and shape effect). According to the Bigeleisen's new theory, the isotope shift effect could be reduced to the following equation 1.8 [26 – 27].

$$\varepsilon = \frac{hc}{kT} v_{fs} b + \frac{1}{24}\left(\frac{h}{2\pi kT}\right)^2 \frac{\Delta M}{MM'} a \quad (1.8)$$

where v_{fs} is a field shift (wavenumber), a, and b are the scaling factor of nuclear mass effect and nuclear field effect, respectively. The other is a constant value of Planck constant: h, the velocity of light: c, Boltzmann constant: k, Temperature (Kelvin): T. M and M' indicated the mass of heavier and lighter isotope, respectively. This equation indicates that the temperature effect was contrary to the separation properties. When the temperature approaches infinite, the separative effect disappears.

Understanding KIE and Bigeleisen-Mayer theory opens the isotope separation via chemical exchange. As a result, the appropriate chemical reaction could be used to separate the concentrating element's isotope. At the same time, it raises the prospect of significant isotope enrichment and mass production.

1.3.3. Isotope separation

At present, the application of enriched isotope material was used wildly from the medical diagnosis and treatment, frontier physics research, nuclear power fuel, and industrial-scale purposes. The isotope separation techniques were studied and improved through the centuries. For example, the isotope enrichment of uranium toward the nuclear power plant fuel is one of the most famous isotope enrichments and mass production. The fissile isotope used in the nuclear fission power station is mostly uranium-235 (^{235}U), with a natural abundance at 0.72%. Most uranium isotopes that occur in the natural is ^{238}U (99.27%) (**Table 1.2**). 4 – 5% of ^{235}U is required in most of

the current nuclear power reactors [28]. The produced energy from the nuclear fission of uranium can reach up to 500 GJ/kg of uranium, which is far beyond the energy produced by coal. The nuclear fission principle and fission chain reaction are shown in **Fig 1.7**. The processes for the uranium fuel cycle are shown in **Fig 1.8**.

Table 1.2 Majority naturally occurring uranium isotopes [29].

Isotope	Natural abundance (%)	Nuclide	Decay
^{234}U	0.005	Radioactive	SF, α
^{235}U	0.720	Radioactive	SF, α
^{238}U	99.274	Radioactive	SF, α, $\beta^-\beta^-$

SF = Spontaneous fission

First of all, the uranium resources are well known that natural uranium is found in the earth's crust and is dependent on the geological factor. The majority of uranium deposits are discovered through geological searches. It necessitates the integration of regional geology, structural geology, geophysics, geological mapping, and geochemistry. Then, the first stage of uranium extraction is mining. Recently, the most effective method of uranium extraction is called in-situ-leach (ISL) or in-situ-recovery (ISR) [30]. The extracted uranium ore from the mine is processed through several milling and extracting techniques to obtain the uranium ore concentrates (UOCs), known as the yellowcake (U_3O_8, and UO_2). Afterwards, the conversion stage turns the yellowcake into the UF_6 via several various techniques [31]. The UF_6 is the easiest sublimes of a uranium compound, resulting in the most applicable uranium substance for the gaseous isotope separation techniques [28 - 30].

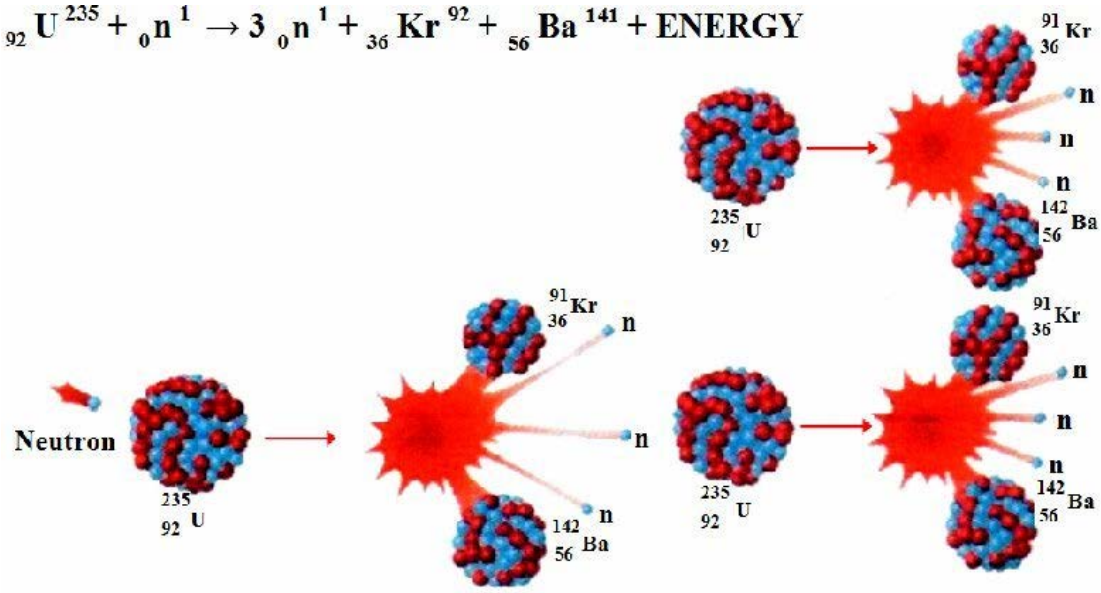

Fig 1.7 Fission chain reaction of uranium-235 (^{235}U) [28]

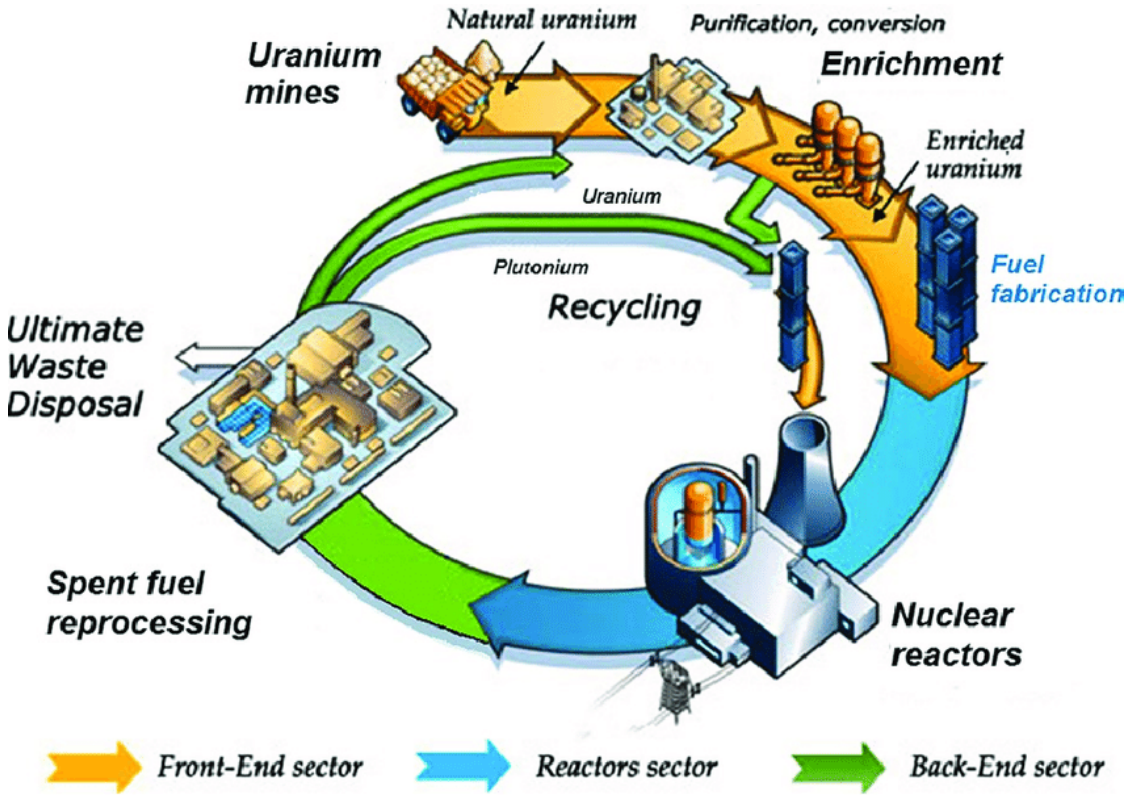

Fig 1.8 Uranium nuclear fuel cycle [30].

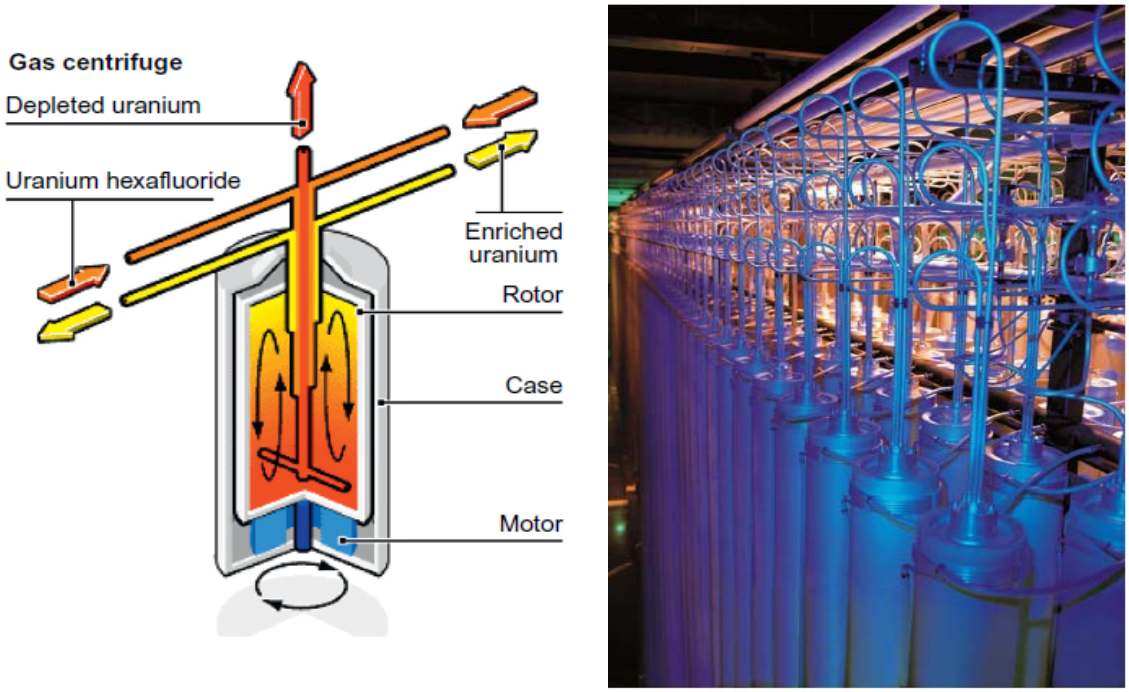

Fig 1.9 The cylindrical device for the gas centrifuge of uranium enrichment [32].

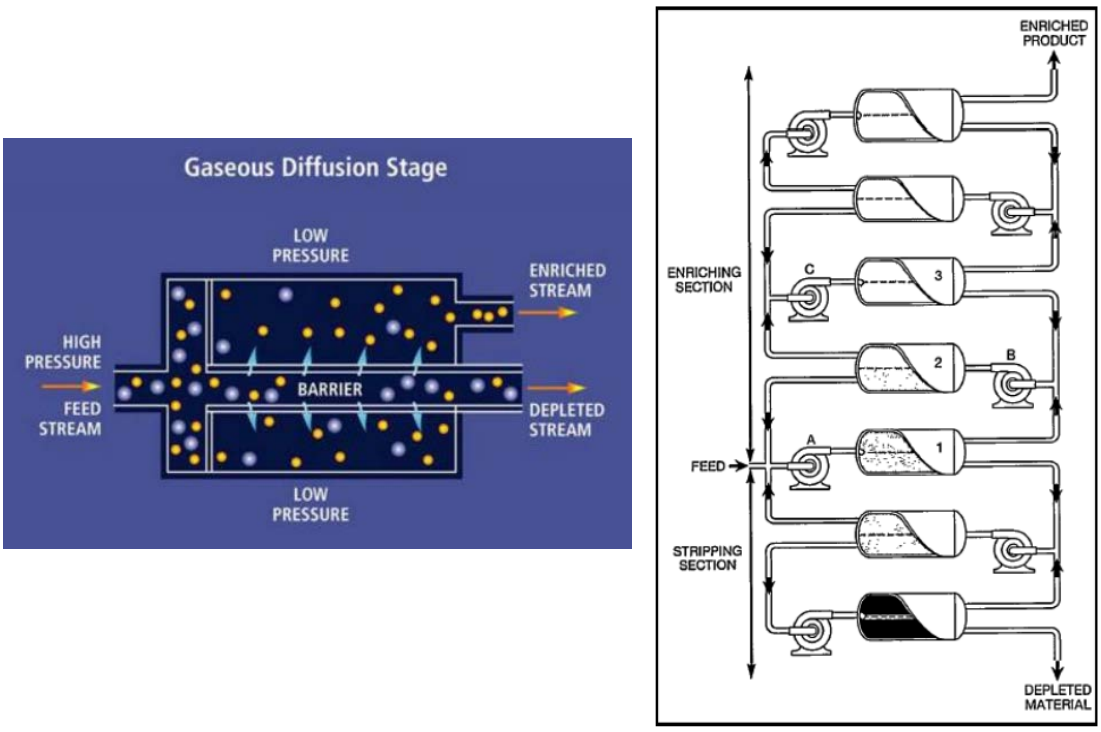

Fig 1.10 The gas diffusion techniques and schematic diagram of the cascade enrichment [33].

The isotope separation method for the enrichment of ^{235}U to achieve the desired ^{235}U concentration consists of a gas centrifuge and gas diffusion. These processes required a

gaseous compound of uranium. The feed uranium passes through several thousand vertical spinning tubes in the gas centrifuge to separate the heavier isotope of ^{238}U (depleted) from the lighter isotope of ^{235}U (enriched). **Fig 1.9** shows the cylindrical device for the gas centrifuge of uranium enrichment. Meanwhile, **fig 1.10** indicates the gas diffusion technique via membrane barrier and schematic diagram for the cascade enrichment. The industrial-scale production of these two methods is applicable under the gaseous chemical compound. Nevertheless, the element with no gaseous compound, such as calcium, is inapplicable under these two industrial-scale production methods.

The cascade theory addresses the separation process and the multiplication problem in the production of enriched isotopes by determining the optimal separation condition, including the number of stages and the enrichment factor for each stage. Because the isotope effect is generally small, the isotope separation method necessitates

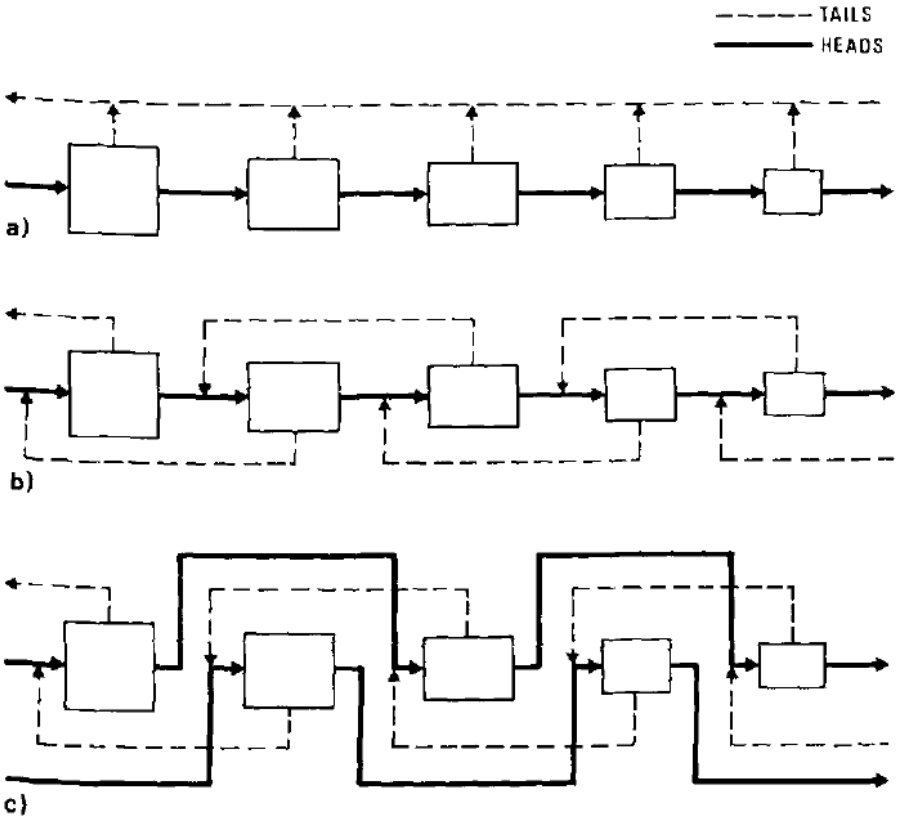

Fig 1.11 The example of cascades, including simple cascade (a), countercurrent cascade (b), and countercurrent symmetric cascade (c) [34].

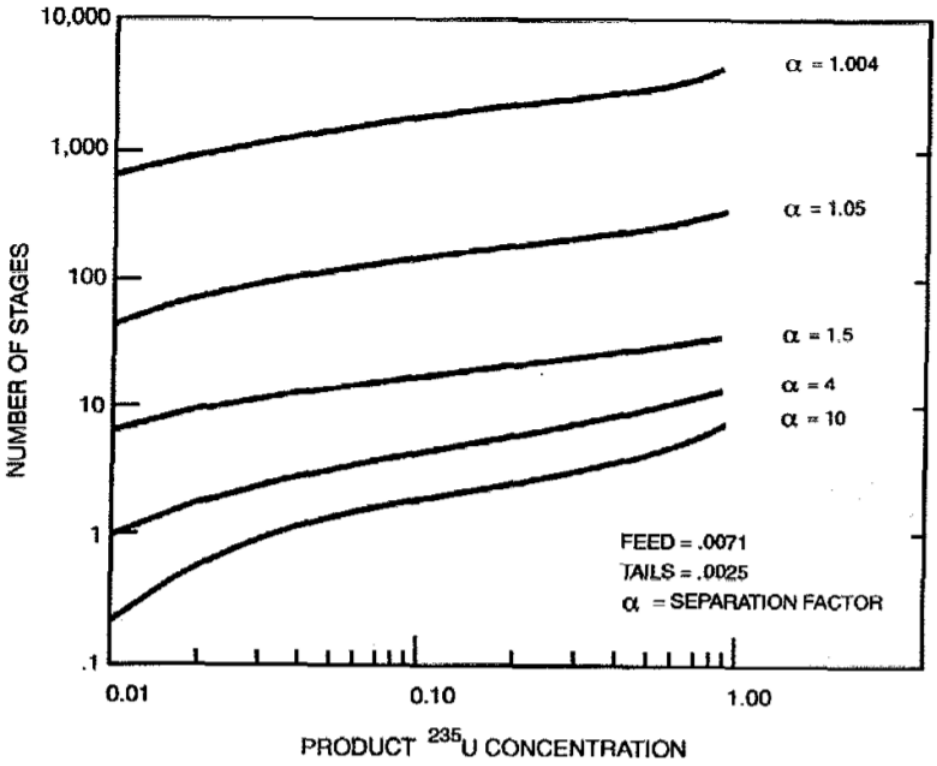

Fig 1.12 The number of stages required to provide a desired product concentration increases as the separation factor decreases [35].

several isotope separations repetitions to obtain the desired enriched isotope concentration. This cascade theory allows the estimate of the mass production of enriched isotope on the desired concentration of the target isotope. **Fig 1.11** depicts the example of cascades, including simple cascade (a), countercurrent cascade (b), and countercurrent symmetric cascade (c). **Fig 1.12** illustrates the number of stages required to provide a desired product concentration increases as the separation factor decreases.

A parameter identifying the enrichment status is called "enrichment factor (α)". The stage enrichment factor is defined as an isotope ratio (R) between the production head and the feed, as shown in equation 1.9:

$$\alpha = \frac{R_{head}}{R_{feed}} \tag{1.9}$$

where R is an isotope ratio of the concentrating isotope. In the case of uranium enrichment is usually indicated by $^{235}U/^{238}U$. Another proper parameter is enrichment coefficient (ε), indicating the current enrichment status, after several separation stages compared to feed (equation 1.10).

$$\varepsilon = \alpha - 1 = \frac{R_{head} - R_{feed}}{R_{feed}} \quad (1.10)$$

Afterwards, the enriched ^{235}U at the desired concentration is ready for nuclear fuel fabrication. This process transforms a fissile material (enriched uranium) into a designed product specific to the nuclear power plant's requirements. Eventually, the spent fuel will be transferred to the final stage of the nuclear fuel cycle, the reprocessing plant for the recycling, or the waste deposit and management section.

As mentioned in the isotope enrichment section, the industrial-scale isotope enrichment techniques are inapplicable for the element with no gaseous compound, such as calcium. Besides the industrial scale isotope separation techniques of a gas centrifuge and gas diffusion, the other electromagnetic, chemical, and laser separation methods were proposed. The isotope separation techniques are explained in the following section.

1.4. Calcium and lithium isotope

1.4.1. Calcium isotopes

Natural abundance of calcium (Ca) isotope composition occurring in six different isotopes, including ^{40}Ca (96.941%), ^{42}Ca (0.647%), ^{43}Ca (0.135%), ^{44}Ca (2.086%), ^{46}Ca (0.004%), and ^{48}Ca (0.187%). The application isotope of calcium is used for many purposes. For example, calcium was used to study the bone diagnosis, uptaking a radioisotope of calcium-45 (^{45}Ca: $T_{1/2}$ = 162.7 days), calcium-47 (^{47}Ca: $T_{1/2}$ = 4.5 days), and calcium-49 (^{49}Ca: $T_{1/2}$ = 8.72 mins), which have a low energy beta decay [36]. The

radioactive calcium is absorbed by a specific organ, such as bone, allowing the radiological technologist to diagnose the symptom. The production of an appropriate radioactive calcium-47 (^{47}Ca) was the interaction of ^{47}Ca and neutron via ^{46}Ca(n,ɣ)^{47}Ca. However, the natural abundance of ^{46}Ca was extremely low, resulting in the rare production of ^{47}Ca. The appropriate enrichment is required to achieve a large amount of stable isotope before the production of radioactive calcium. On the other hand, the stable calcium was applied to study calcium absorption and the mechanism of plants imbibing nutrients by investigating the calcium-44 (^{44}Ca) isotope fractionation [37]. Moreover, calcium-48 (^{48}Ca) nuclide is the highest neutron excess amount the stable nuclide. It was used as a key element in synthesizing a super heavy element. ^{48}Ca bombards the target heavy stable element creating the new artificial super heavy element (Z>110) [38].

Furthermore, the following is the goal of this study. The 2015 Nobel prize in physics was awarded to the discovery of neutrino oscillation by T. Kajita, a Japanese physicist from the Institute for Cosmic Ray Research (ICRR), University of Tokyo, Japan. T. Kajita shared the Nobel prize with A. B. McDonald, a Canadian physicist from the Sudbury Neutrino Observatory (SNO) [39]. Their finding indicated that the neutrino and other subatomic particles have mass, resulting in extreme competition to search for the absolute neutrino mass. One of the potential methods to achieve the absolute neutrino mass and the mystery of matter anti-matter asymmetry is the search of Majorana particles. E. Majorana, an Italian theoretical physicist, proposed that the neutrino and the antineutrino are identical, and that the lepton number is not conserved. The neutrinoless double beta decay (0νββ) can be investigated this property because the 0νββ can only occur when a neutrino is a Majorana particle [40, 41]. The finding is beyond the lepton conservation law, leading to the violation of the standard model (**Fig1.13**). There are many challenges to achieving the absolute neutrino mass through neutrinoless double beta decay, but it has not

been yet observed. The primary criteria to observe the 0νββ is the discrimination of the signal and background. Improving the detector's energy resolution could also enhance energy discrimination. As a result, a lower level of background signal is required, including the 4π active shield and underground laboratory passive shield to prevent cosmic ray interference, among other things. Furthermore, it is well known that the primordial radioisotope from nature is inevitable and significantly affect the measurement. Therefore, the signal should be far beyond the background signal, resulting in the requirement of a high $Q_{\beta\beta}$ value and a large amount of double beta decay nuclide. Moreover, not all double beta decay nuclides are the best candidate in the search for 0νββ. **Table 1.3** shows the current projects, $Q_{\beta\beta}$ (keV), the isotope, natural abundance, and lower limit of the half-life ($T_{1/2}^{0\nu}$) on the search of 0νββ.

Table 1.3 Current projects and the nuclides used on the search of 0νββ [41].

Isotope	$T_{1/2}^{0\nu}$ ($\times 10^{25}$ years)	$Q_{\beta\beta}$ (keV)	Natural abundance (%)	Experiment	Reference
^{48}Ca	$>5.6 \times 10^{-3}$	4,263	0.187	CANDLES III	[42]
^{76}Ge	>8.0	2,039	7.8	GERDA	[43]
	>1.9			MAJORANA DEMONSTRATOR	[44]
^{82}Se	$>3.6 \times 10^{-2}$	2,998	8.7	NEMO-3	[45]
^{96}Zr	$>9.2 \times 10^{-4}$	3,348	2.8	NEMO-3	[46]
^{100}Mo	$>1.1 \times 10^{-1}$	3,035	9.8	NEMO-3	[47]
^{116}Cd	$>2.2 \times 10^{-2}$	2,813	7.5	AURORA	[48]
^{128}Te	$>1.1 \times 10^{-2}$	867	31.75	C. Arnaboldi et al.	[49]
^{130}Te	>1.5	2,527	34.08	CUORE	[50]
^{136}Xe	>10.7	2,459	8.9	KamLAND-Zen	[51]
	>1.8			EXO-200	[52]
^{150}Nd	$>2.0 \times 10^{-3}$	3,371	5.6	NEMO-3	[53]

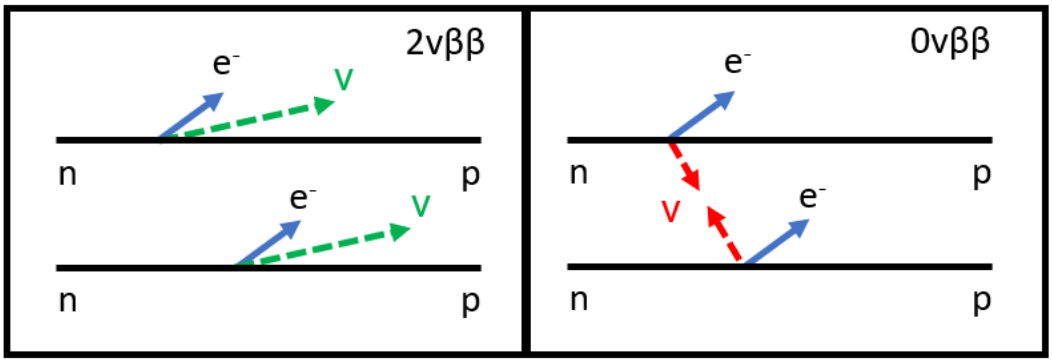

Fig 1.13 Double beta decay (2νββ) and neutrinoless double beta decay (0νββ).

^{48}Ca is one of the double beta emission nuclides. It has been used to study the neutrinoless double beta decay (0νββ) by CANDLES (CAlium fluoride for studies of Neutrino and Dark matters by Low Energy Spectrometer) project in Kamioka Observatory, Japan [42]. The advantage of ^{48}Ca is the highest $Q_{\beta\beta}$ value ($Q_{\beta\beta}$=4,267.98±0.32 keV [54]) among the other ββ isotopes. This $Q_{\beta\beta}$ value is beyond the primordial radioactivity from ^{208}Tl (gamma emission at 2,615 keV) and ^{214}Bi

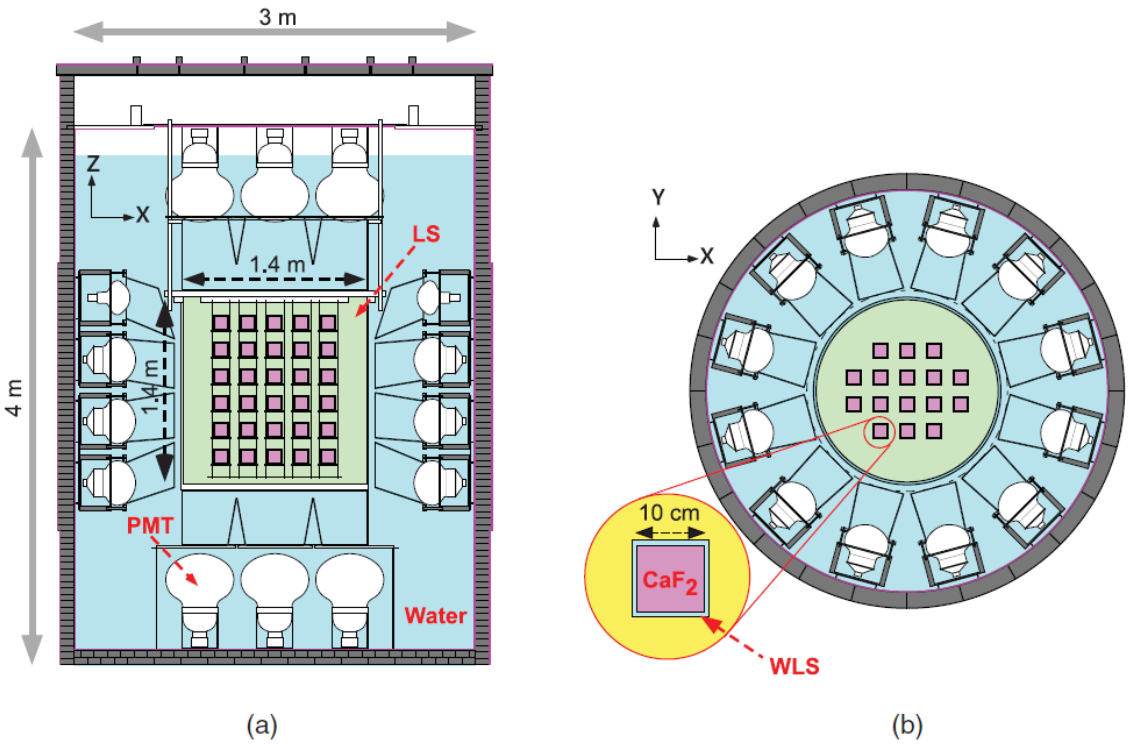

Fig 1.14 The schematic diagram of CANDLE III detector [42]
(a = side view, and b = top view)

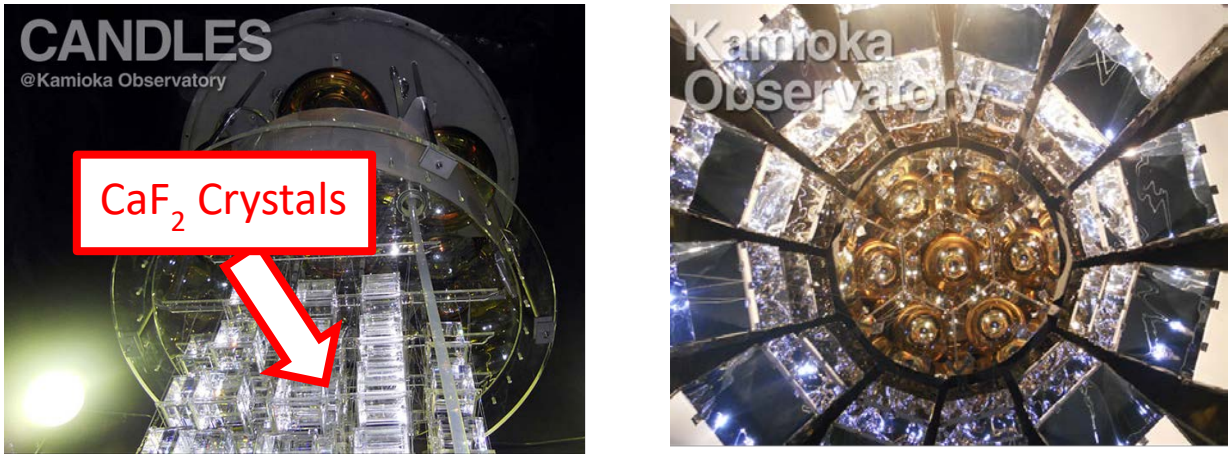

Fig 1.15 The CANDLE III detector, side view and top view [55]

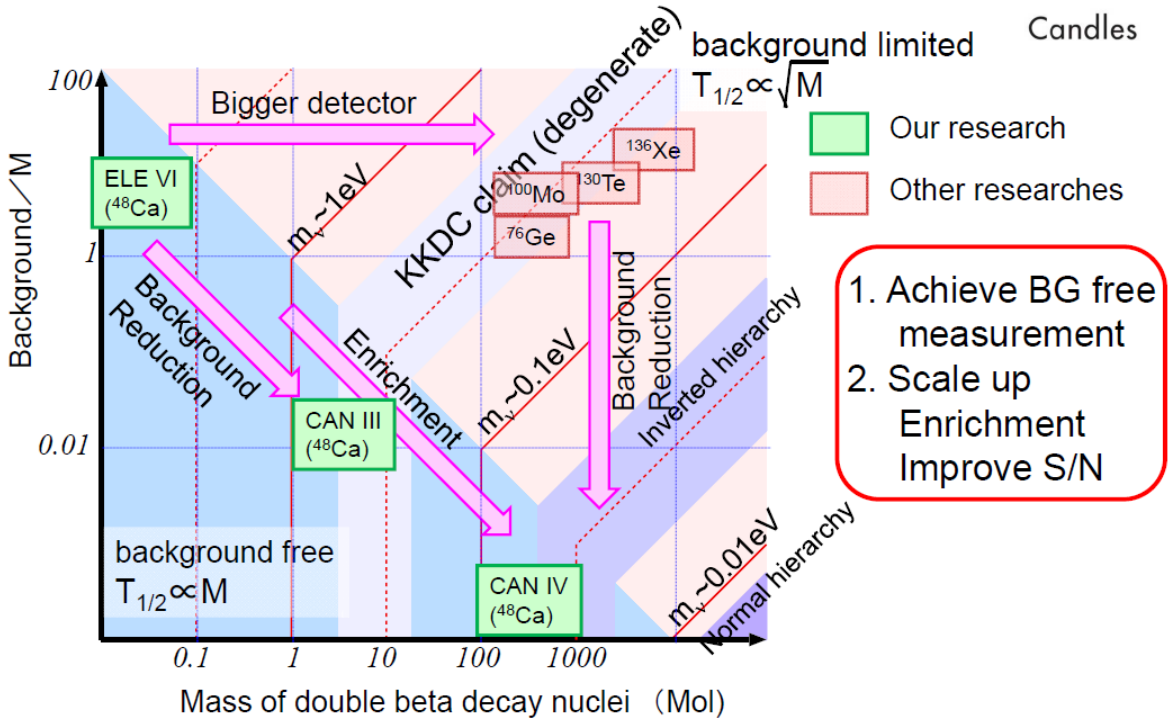

Fig 1.16 The CANDLE project strategies [55]

(daughter nuclide of ^{222}Rn, emits beta with the energy up to 3,270 keV), resulting in the most effective among the candidate nuclides. Moreover, calcium is one of the most abundant elements globally, resulting in a large amount of potentially available calcium. Therefore, calcium can enhance the detection efficiency by making a ton scale of the source emerge detector itself (source = detector). **Fig 1.14** indicate the schematic

diagram of the CANDLE III detector, including CaF_2 crystals, liquid scintillator (LS), wavelength shifter (WLS), large photomultiplier tubes (PMT) [42]. **Fig 1.15** shows the actual CANDLE III detector at Kamioka Observatory. CANDLE III, the current progress, employs 96 pieces of CaF_2 crystal (3.2 kg/piece), yielding 157 kg of total calcium and approximately 0.30 kg of ^{48}Ca. The future improvement of the CANDLES project is CANDLE IV (CAN IV), aiming to achieve the large scale of double beta nuclide (^{48}Ca). **Fig 1.16** shows the strategies of the CANDLES project. The previous improvement to achieve the search of $0\nu\beta\beta$ by ELEGANT VI (ELE VI) was carried out, aiming for the background free measurement. After that, the CANDLE-III to IV (CAN III to IV) detector, aiming to increase the double beta nuclide (^{48}Ca) by the isotope enrichment. A large amount of enriched ^{48}Ca nuclide is required to increase the detection efficiency. Unfortunately, the industrial scale of the isotope enrichment of calcium is difficult because the calcium has no gaseous compound. Therefore, only the electromagnetic separator is available, resulting in the small production yield (ten grams a year) and costly material (250,000 USD/gram) of the enriched ^{48}Ca. Thus, this research aims to find a cost-effective method to enrich ^{48}Ca isotope.

1.4.2. Calcium isotope separation

As mentioned, the industrial scale of the isotope separation and enrichment required a gaseous compound. Calcium has no gaseous compound at room temperature, resulting in that it is inapplicable for large scale isotope enrichment. The isotope separation of calcium is possible through the electromagnetic separator (Calutron, SU20), chemical exchange method, electrooptical separation, electrophoresis, and laser isotope separation method.

Electromagnetic separator method

A calutron is an electromagnetic separator developed by E. Lawrence during the Manhattan project at the Y-12 facility near Oak Ridge, Tennessee, USA. The primary purpose is to produce large quantities of enriched ^{235}U [56]. However, after establishing the industrial-scale production of ^{235}U by gas diffusion and gas centrifuge, the electromagnetic separation method was declared obsolete, and the facilities were shut down. The electromagnetic separation uses a large amount of electromagnetic field to separate the ion which different isotope or difference in mass. **Fig 1.17** indicates a diagram of the beta calutron electromagnetic separator and its mechanism. **Fig 1.18** shows the 12 g of 96% $^{48}CaF_2$ crystal produced by Calutron to study double beta decay. However, the electromagnetic method is too expensive and impractical for large-scale isotope separation since the low production rate (approximately ten grams a year).

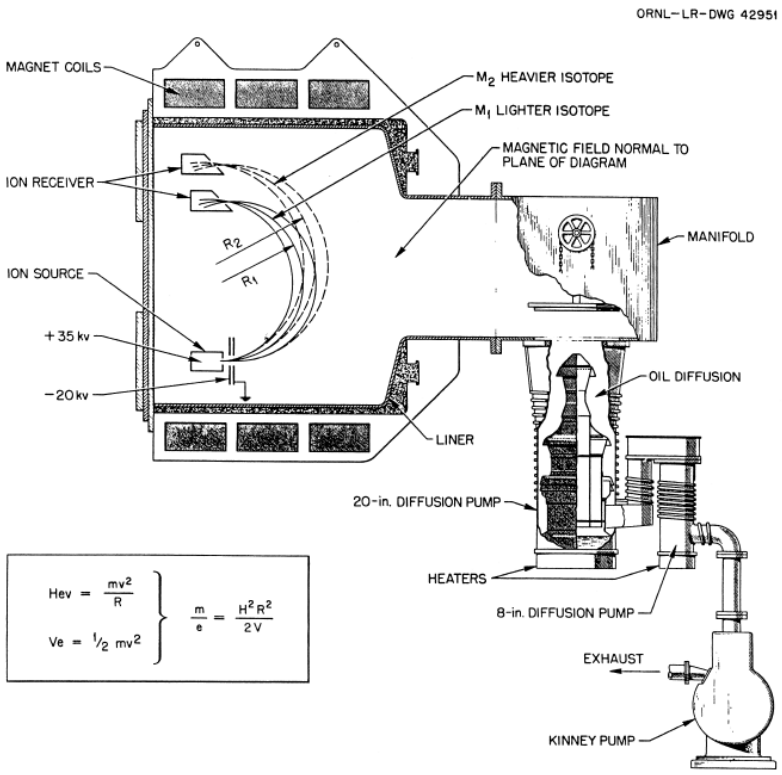

Fig 1.17 The diagram of beta calutron electromagnetic separator [57]

Fig 1.18 $^{48}CaF_2$ crystal produced by Calutron for the study of double beta decay [56]

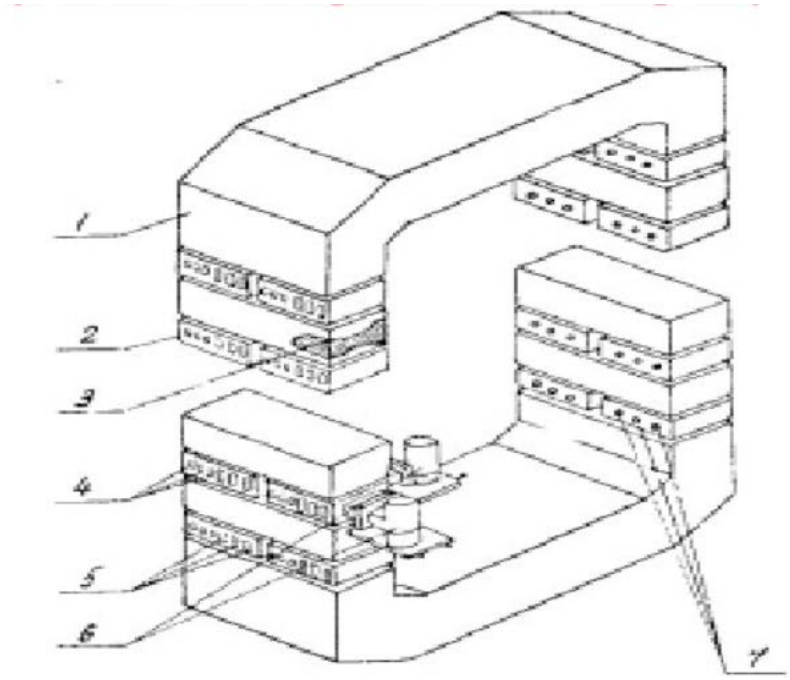

Fig 1.19 The schematic diagram of SU20 electromagnetic separator [58] 1) Housing, 2) Separation tank (Chamber), 3) Electromagnetic coils, 4) Ion source seats, 5) ion receiver seats, 6) diffusion pumps, and 7) observation openings.

Nowadays, the production of calcium isotope is the Russian developed electromagnetic separation of calcium isotope by Lesnoy in Sverdlovsk Oblast, called SU20 [54]. The SU20 was used to separate the calcium isotope toward the production

of $^{40}Ca^{100}MoO_4$ crystal to study neutrinoless double beta decay via ^{100}Mo isotope. To study by $^{40}Ca^{100}MoO_4$ crystal, it requires a high purity of ^{40}Ca. **Fig 1.19 and 1.20** depicts the schematic diagram of the SU20 electromagnetic separator. However, the productivity of ^{48}Ca by electromagnetic separator is small, and only a few grams are available per year [58].

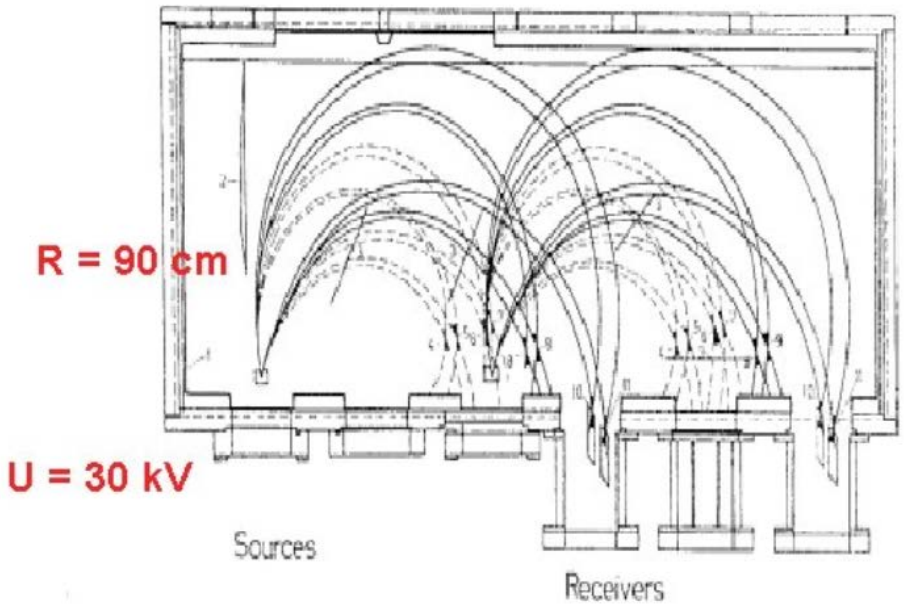

Fig 1.20 The schematic diagram of SU20 electromagnetic separator [58]

Chemical exchange method

The chemical exchange method by redox system method was provided by D. Zucker and J. S. Drury [59]. The purpose was to establish large-scale production of ^{46}Ca, which was used in the production of ^{47}Ca, for the medical diagnosis application. The redox system method is the chemical exchange reaction between the calcium solution [calcium formate ($Ca(HCOO)_2$)] and mercury (Hg). The redox system method poses the significant isotope effect by the following chemical exchange reaction (equation 1.11):

$$^{46}Ca_{(Hg)} + {}^{40}Ca^{2+}_{(solution)} = {}^{40}Ca_{(Hg)} + {}^{46}Ca^{2+}_{(solution)} \qquad (1.11)$$

where the subscripts indicate the calcium phase, including mercury and electrolyte solution. The chemical exchange reaction results in the isotope effect of calcium between two phases. The results revealed that the single-stage separation factor for $^{46}Ca/^{40}Ca$ is 1.008 and for $^{48}Ca/^{40}Ca$ is 1.010. On the other hand, mercury is a severe environmental problem and harmful to humans and other living things. The large-scale production using mercury base will be problematic and challenging to scale up the mass production. The improvement on this method was carried out by S. Saito et al. [60]. Saito used graphite-based instead of mercury and firstly performed the electrolysis in a constant current mode with the electric current at 0.1 mA. This report shows that the lighter isotope was fractionated into the graphite, resulting in the heavier isotope enrichment in the electrolyte solution. The single-stage separation factor of $^{48}Ca/^{40}Ca$ ranged from 1.0010 to 1.0072 at 50 ºC. **Fig 1.21** shows the working station of Saito's

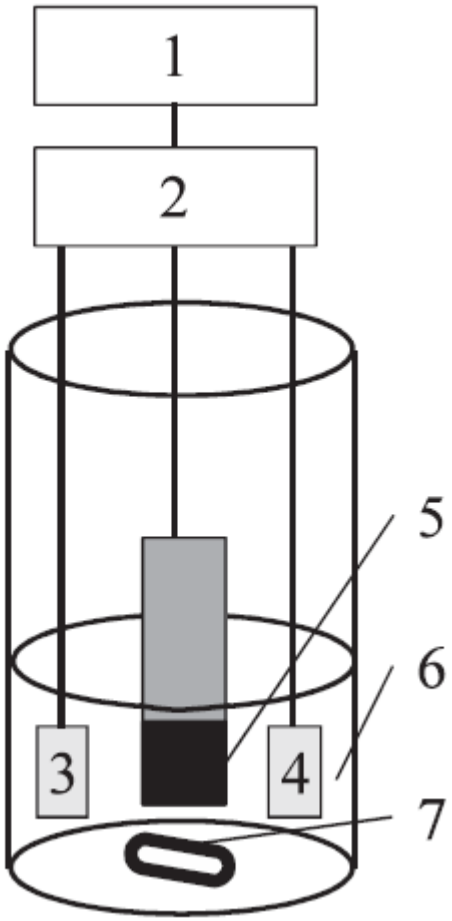

Fig 1.21 The working station of redox system with graphite electrode [60]
1) data acquisition unit, 2) power supply, 3) reference electrode, 4) counter electrode (anode), 5) working electrode (cathode), 6) electrolyte solution, and 7) stirrer tip.

redox system. However, compared to the mercury-based method, enrichment and mass production feasibility is lower due to the small separation factor. Moreover, the contributed calcium content in these chemical exchange methods is limited to only 65 mmol (Hg based) and 0.037 mmol (graphite based), indicating that this method is inapplicable for large-scale mass production.

Another isotope separation by the chemical exchange reaction is the chromatographic method. The chromatographic is one of the most famous and broadly applied for chemical separation, purification, and chemical analysis. Mainly, it is a potentially effective method for ion-exchange separation. The isotope effect is observed based on the chemical exchange between aqueous and solid (resin) phases. The lighter isotope was fractionated into the resin phase, and the enriched aqueous would be eluted to the collector. This method is promising for the large-scale production of isotope separation since it is simple and easy to accumulate the enriched phase. **Fig 1.22** depicts the mechanism of the crown-ether resin method reported by S. Umehara [61]. The chemical exchange reaction between the aqueous phase containing calcium and crown-ether resin shows in equation 1.12:

$$^{48}Ca^{2+}_{(resin)} + {}^{40}Ca^{2+}_{(solution)} = {}^{40}Ca^{2+}_{(resin)} + {}^{48}Ca^{2+}_{(solution)} \qquad (1.12)$$

where the subscripts indicate the calcium phase, including crown-ether resin and aqueous solution, resulting in the fractionation of heavier isotope enrichment at the eluting solution.

Many studies on calcium isotope enrichment using the crown-ether resin chromatographic method were investigated. For example, S. Umeraha et al. [61] reported the calcium isotope fractionation using benzo-18-crown-6-ether embedded in fine porous silica beads. The crown-ether resin chromatographic was conducted over a 1 m, 20 m, and 200 m migration length. In the case of 200 m migration length, 12 sets

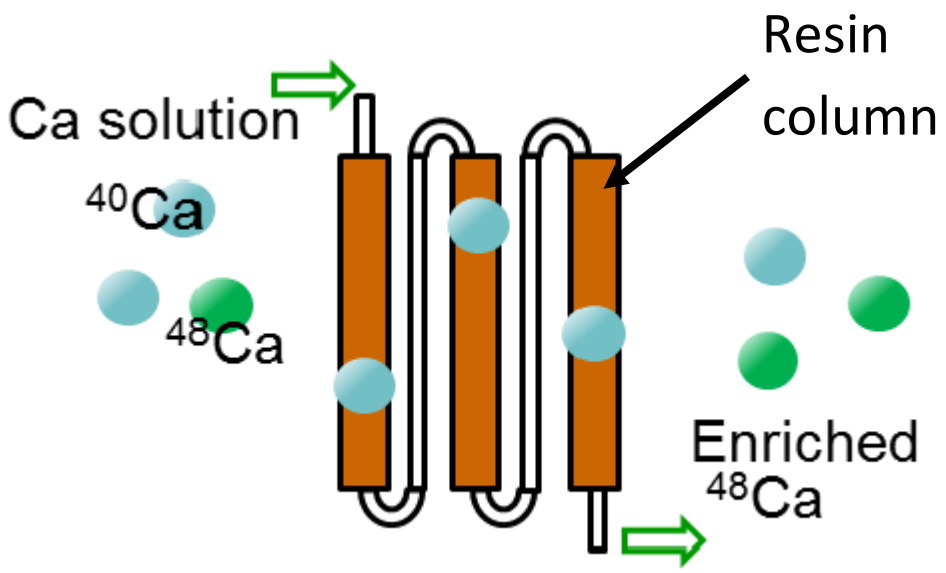

Fig 1.22 The mechanism diagram of resin chromatographic method on the calcium isotope separation [61]

of 1 m column were repeatedly used until the front boundary reached 200 m. The feed solution is 0.1M $CaCl_2$ in 9M HCl acid. The results showed that increasing migration length increases the maximum enrichment factor. The maximum isotope ratio ($^{48}Ca/^{40}Ca$) of the 200 m system was found to be 0.002595 against 0.00194 for the natural abundance (0.002039, and 0.002230 for 1 m and 20 m length). Additionally, the resin chromatographic experiment was carried out using benzo-18-crown-6-ether for 1 m migration length by K. Hayasaka et al. [62]. It was found that the calcium absorption in the crown-ether resin increases proportionally to the HCl concentration. The appropriate HCl concentration is required higher than 6M and strongly absorbed in crown-ether resin at 9M HCl **(Fig 1.23).** The maximum isotope ratio ($^{48}Ca/^{40}Ca$) was found to be 0.002025. The isotope fractionation was almost the same as S. Umehara's study [61]. Moreover, S. Nemoto et al. [63] revealed the liquid chromatography of calcium isotope fractionation using benzo-18-crown-6 ether benzo-15-crown-5 ether resins. Furthermore, S Nemoto calculated the optimized structure of the ion-crown complex and the isotope effect and the MO calculation via Bigeleisen-Mayer equation

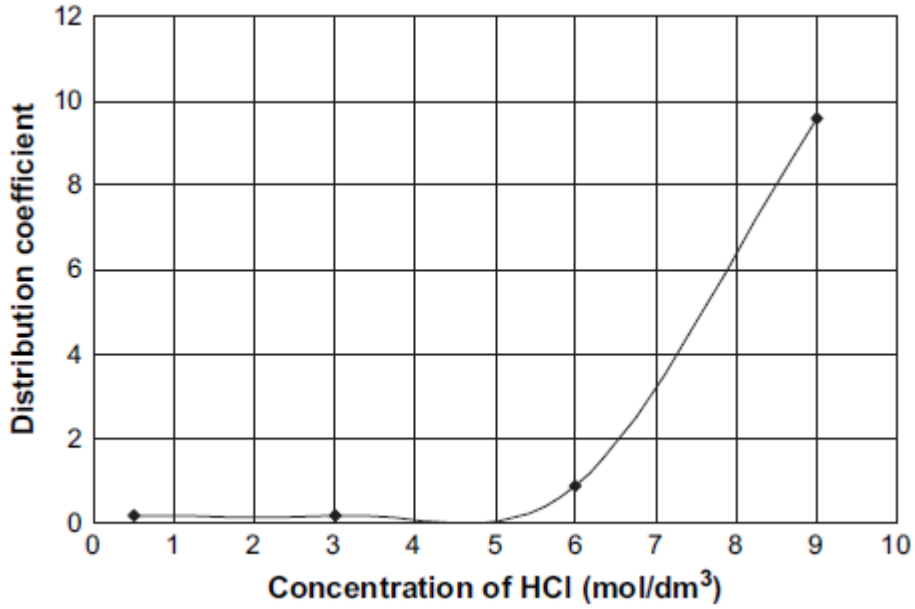

Fig 1.23 Distribution coefficient of calcium between benzo-18-crown-6 resin and HCl aqueous solution. [62]

on the rpfr. The results corresponded to K. Hayasaka's study and emphasized the requirement of HCl acid for the absorption of crown-ether. Furthermore, the optimized structures of the calcium ion-benzo-18-crown-6 (B18C6) complex and calcium ion-benzo-15-crown-5 (B15C5) complex were shown in **fig 1.24**. In the case of the B18C6 ion complex, the calcium ion located in the center of the B18C6 molecule and the distance between calcium ion and six oxygen atoms were nearly the same. Meanwhile, these atoms were also nearly coplanar. The reason was that the calcium ionic radius fits the cavity size of B18C6. The anions contribution ($2Cl^-$), in the case of the absence of HCl acid, was found to be bonded to the calcium ion from one side and another side of the plane. As for the absorption under the contribution of HCl acid, the HCl atom interacts with the anion cap of the ion-crown complex molecule. Even though, there was no experimentally reported on the number of HCl molecules, this work expected that the ion-crown-HCl formation would increase with increasing HCl concentration.

Moreover, the optimized structure under the same conditions was revealed with B15C5 crown-ether resin. Nonetheless, since the cavity size of B15C5 is smaller than

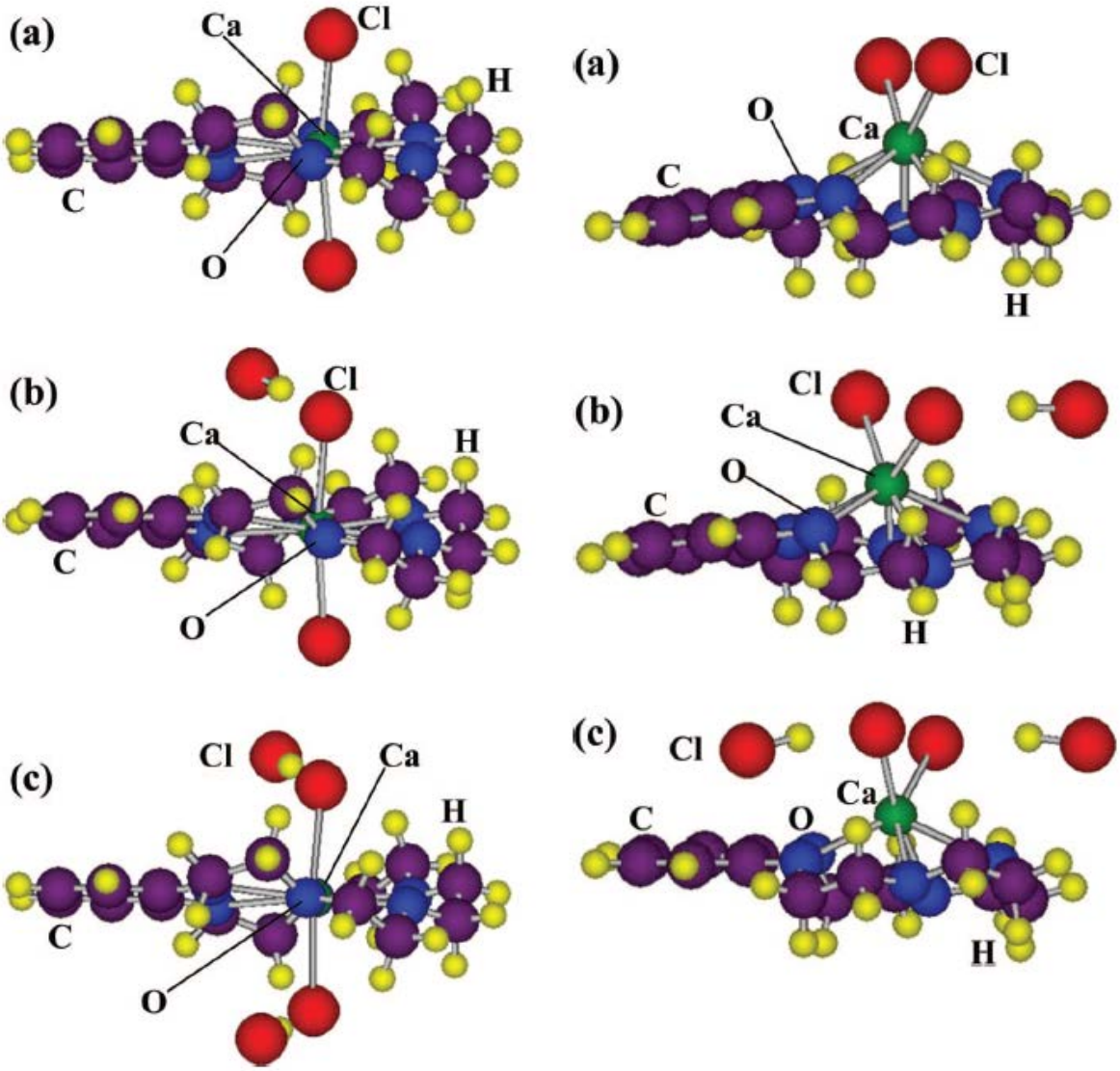

Fig 1.24 The optimized structures of calcium ion-benzo-18-crown-6 (B18C6) [Left] complex and calcium ion-benzo-15-crown-5 (B15C5) complex [Right].
(a) = without HCl contribution, (b, c) = HCl contributed to the formation with low and high concentration, respectively [63].

B18C6, the calcium ion is located slightly out of the plane. The contributed anion (Cl^-) bonded to the calcium ion in only one side of the plane. The HCl atoms interact with the Cl^- ion the same way as B18C6's formation. The experimental result on the isotope fractionation was concluded that B18C6 is larger than B15C5, which was in good agreement with calculated isotope fractionation via rpfr. Nonetheless, higher HCl concentration in feed solution resulted in a smaller value of isotope fractionation in both

B18C6 and B15C5. These results indicated that the HCl acid was mandatory to increase calcium absorption through the crown-ether resin separation. Another improvement was reported by T. Sato and T. Oi [64], who replaced the HBr solution instead of the HCl solution. They expected that HBr, a softer base than HCl solution, would be the better medium for the crown-ether resin extraction. The result indicated the same behavior as HCl solution that the increases of HBr concentration decrease the isotope fractionation. Meanwhile, the magnitude of the calcium isotope fractionation was nearly equal to the HCl solution of S. Nemoto works. In conclusion, the presence of acidity solution could enhance the formation of ion-crown complex, but the isotope fractionation was more negligible under the high concentration of acidity solvent.

The chemical exchange chromatographic via resin crown-ether is possible for the isotope separation and calcium enrichment. This method has the advantage that simple and easy to accumulate the enriched solution via the front boundary. However, it is not yet applicable and impractical for mass production because the time required for the highest fractionation, 200 m migration length, was approximately ten days. The calcium concentration contributed to the separation process is very small (0.1M). Moreover, a high HCl or HBr acid concentration is necessary to increase calcium absorption to the resin. Finally, the B18C6 resin is costly and requires a large amount of crown-ether resin in the chromatographic method.

Electrophoresis is one of the well-known methods for chemical separation and analysis of the charged particle under the uniform electric field and relative water or fluid. It can be applied to separate the particle with the same charged but different size or chemical compounds such as DNA, RNA, and protein. To apply this method to isotope separation, the migration length must be increased to allow for sufficient isotope separation because the isotope effect is usually small. Countercurrent electrophoresis

(CCE) was potentially fulfilled the requirement of long migration length. Countercurrent electrophoresis was based on the flow of the electrolyte. The faster ion (lighter isotope) will travel through the fluid stream, while the slower ion (heavier isotope) will be carried back. However, it is still not enough for practical large-scale enrichment production due to the tiny isotope fractionation. At the same time, the small diameter of capillary electrophoresis (< 0.1 mm) provided a significant separation factor of $^{48}Ca/^{40}Ca$ under the strong electric field, and a short time required is achieved. Nevertheless, the problem of the capillary electrophoresis is only the tiny among can be processed, indicating that it is inapplicable for large-scale production [65]. Simultaneously, the larger diameter was carried out using cation exchange resin (Li^+) as a migration medium. [66]. **Fig 1.25** shows the schematic diagram of the large diameter countercurrent resin exchange method. The maximum separation coefficient of $^{48}Ca/^{40}Ca$ was found to be 8.7×10^{-4}, and the $CaCl_2$ concentration was 2M, indicating that this method has an advantage of high conversion but low separation coefficient. Nonetheless, a longer migration length and longer processing time are required. Therefore, this method is inapplicable for large-scale production. In conclusion, a

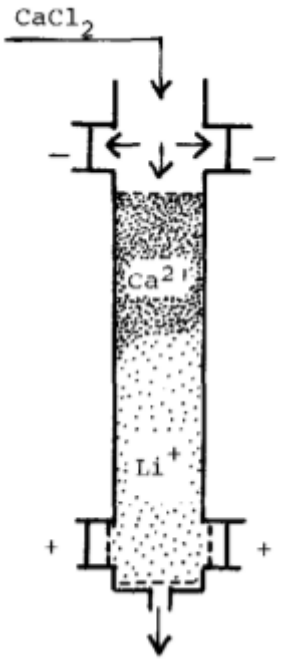

Fig 1.25 The schematic diagram of the large diameter resin exchange counter current method for the separation of calcium isotopes [66]

smaller diameter under the strong magnetic field provides good separation and shortens the required time, but only a tiny amount is possible. On the other hand, the larger gives the opposite result, indicating that it is applicable for enrichment production. However, the longer migration length and longer time required is problematic to large-scale production.

Recently, T. Kishimoto et al. [67] developed a new isotope separation and enrichment method called multi-channel countercurrent electrophoresis (MCCCE). The major objective is the large-scale production of ^{48}Ca towards the study of neutrinoless double beta decay. The improvement could overcome the obstacles of small production yield, shorten the time required, and provide a good separation factor. Moreover, not only calcium, but this method allows the possibility to apply on other isotopes. MCCCE was improved based on the requirement of a large cross section area and strong electric field, maintaining the separation factor and the high contribution of ion content. Making a boron nitride (insulating material) multi-channel migration path allows the electric field to be applied. **Fig 1.26** depicts the mechanism of the calcium isotope separation

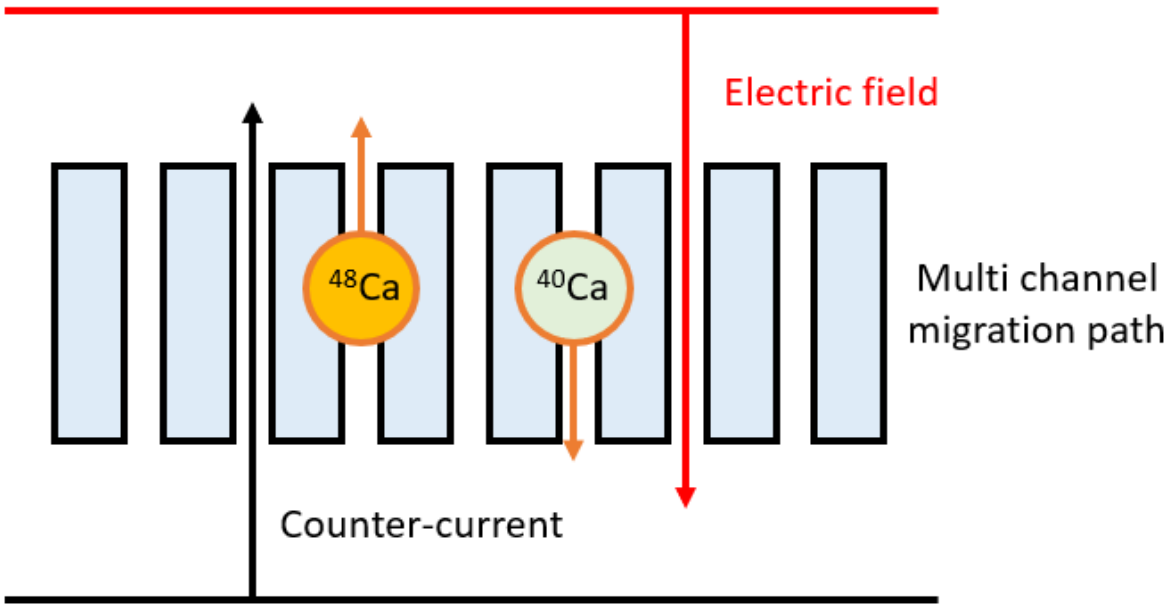

Fig 1.26 The mechanism of the isotope separation by MCCCE [67]

via MCCCE. When operating, the electric field forces the calcium ion to move in the opposite direction of the flow. Because of the difference in the mass of calcium isotope, the heavier isotope moves slightly slower than the lighter isotope. As a result, isotope separation is possible. T. Kishimoto et al. reported the maximum enrichment factor of $^{48}Ca/^{43}Ca$ to be 3.08. The estimation of the enrichment factor of $^{48}Ca/^{40}Ca$ was supposed to be 6.05 under the supplied voltage of 170 V. The $CaCl_2$ concentration in the separation was 0.01M. It was noted that the extracted calcium is only a tiny amount of the original feed. Further improvement of the applicable extraction condition and scale up the production yield is still required. Finally, the additional advantage of this method is that it could be possible to apply for any other isotope or compound with a charge and specific mobility under the water or fluid.

Another isotope separation method is electrooptical isotope separation. This method is based on the threshold dependence of the dipole moment of the nonrigid molecule under infrared laser radiation. The selective laser excites the molecules containing the concentrating isotopes to the upper vibrational state with a small dipole moment. The nonrigid atomic beam emitted from the high temperature crucible under the vacuum chamber interacts with the infrared laser, resulting in the excitation of the selective isotope. The excited isotope was separated from the remaining isotope (the ground vibrational state with a significant dipole moment) under the non-uniform electric field. This property allows for the evaluation of the isotope separation and enrichment. However, this method required a few criteria to achieve the separation property, including light atom (Li, Na, and Ca), similar in melt-vapor systems, the dipole moment must be strongly related to the vibrational quantum number, the concentrating isotope shall have an excited vibrational state, and the time shift of the excited isotope shall have a sufficient period for selection of nonrigid molecule. S. S.

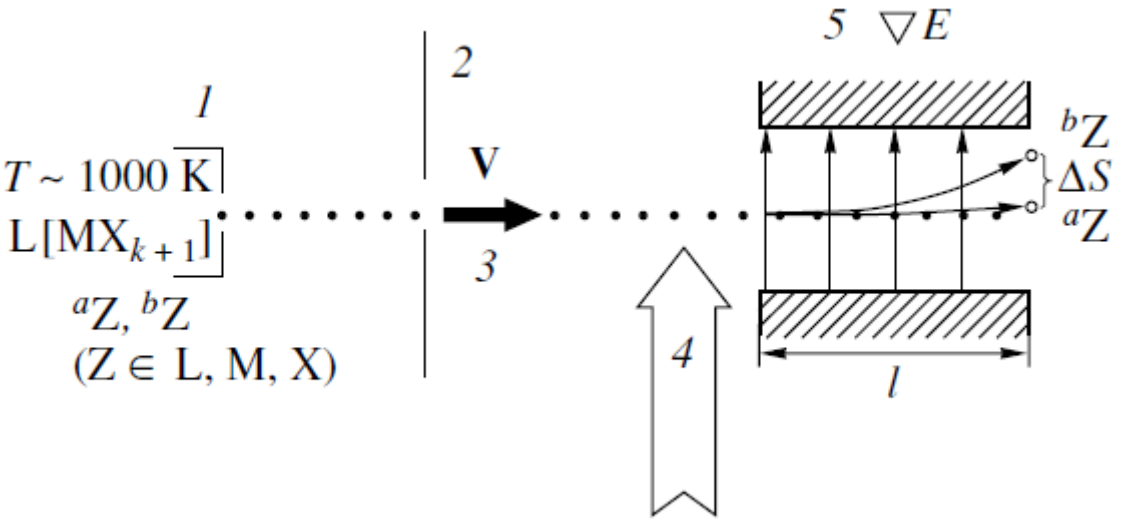

Fig 1.27 Setup and principle of electrooptical isotope separation. [68]
1) crucible contains the inorganic species salt, 2) vacuum chamber, 3) nonrigid beam, 4) infrared laser, and 5) region of nonuniform electric field.

Nabiev et al. [68] reported the electrooptical separation method in the enrichment of calcium isotope towards the purpose of the study of double beta decay. **Fig 1.27** shows the setup of S. S. Nabiev et al. works. S. S. Nabiev reported using CaF_2 (fluorite) as an inorganic species of calcium source. CaF_2 almost has a specific property of highly chemical resistivity even at high temperature and are a good candidate under the mentioned requirement. The separation result showed that the $^{48}CaF_2$ isotope could be effectively separated and collected at the rate of 5 – 10 mg/h. At this rate, the production was significantly greater than the electromagnetic separator. Nonetheless, this method has many requirements and was difficult to perform. For example, the inorganic specie is CaF_2 has a very high melting point at 1691 K, resulting in the specific instrument and crucible, which has high temperature tolerance, being required. Moreover, the production rate of this method is still far from the requirement to achieve isotope enrichment and mass production.

Finally, the laser isotope separation (LIS) poses significant enrichment feasibility of the ^{48}Ca isotope. The laser isotope separation is a selective method

targeting the ^{48}Ca isotope. The narrowband laser with a specific frequency corresponding to the calcium was utilized. The isotope effect occurs by a difference in energy isotope shifts (**Fig 1.28**). The advantage of this method is that it allows the element having no gaseous compound at room temperature can be separated, resulting in the enrichment feasibility and the mass production of calcium as well.

Recently, K. Matsuoka et al. [69] reported the isotope separation of ^{48}Ca using laser isotope separation toward the study of neutrinoless double beta decay. The laser isotope separation was divided into two deference mechanisms, including the deflection and ionization methods. (**Fig 1.29**) Their research presented both methods and the time of flight (TOF) detection field. Metallic calcium, as a calcium source, was heated in the crucible at approximately up to 600 °C. The atomic beam of calcium passed through the specific collimator then the calcium vapor was deflected by irradiating the diode laser with the wavelength of ^{40}Ca (422.6723 nm). Atomic beams were bent using the

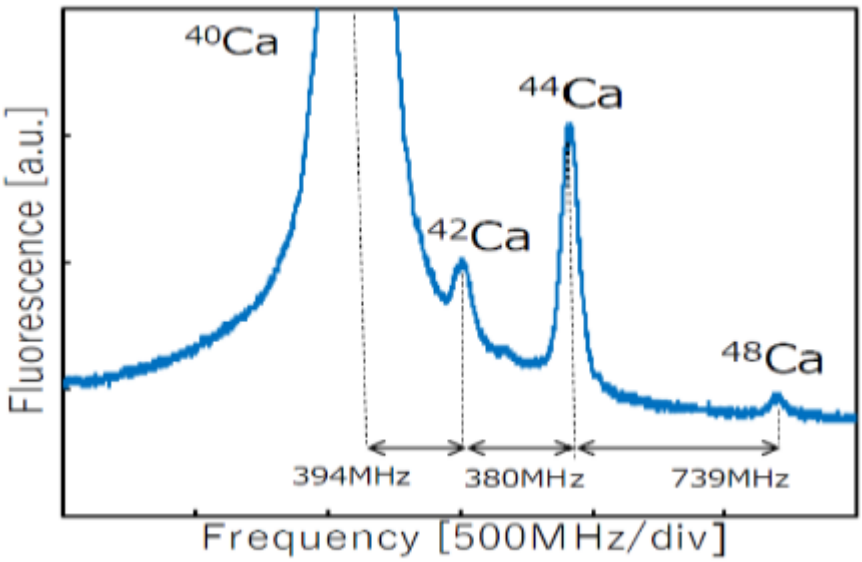

Fig 1.28 Absorption spectrum of calcium, and isotope shifts. The peak indicates the natural abundance of each calcium isotope [69]

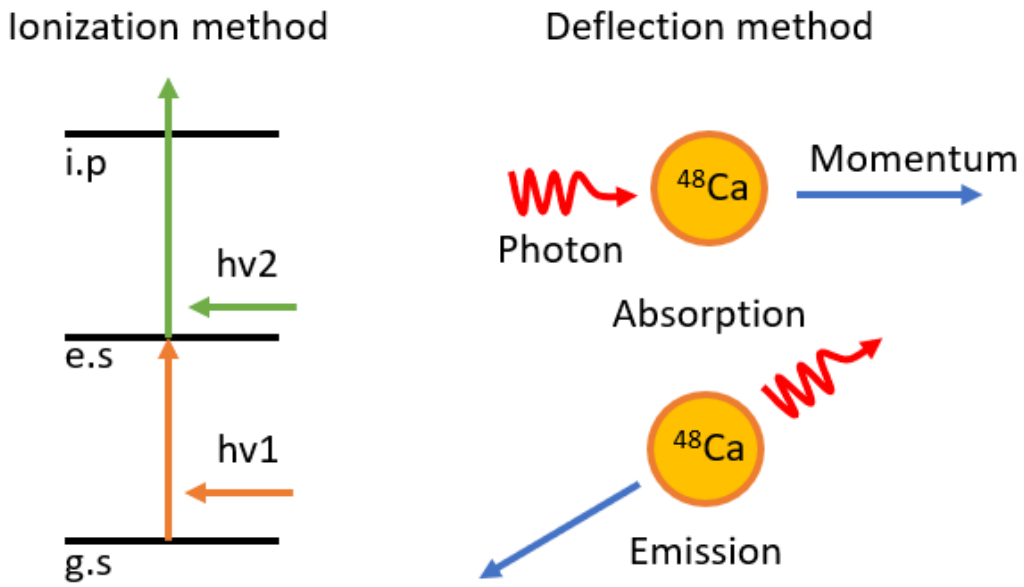

Fig 1.29 Laser isotope separation (LIS) mechanism, ionization method, and deflection method

deflection method by causing momentum transfer by repeatedly exciting and de-exciting atoms with photons from a diode laser several hundred times. Afterwards, the ionization laser is required in the x-axis direction to measure the deflected ion by TOF detection unit (**Fig 1.30**). As for the ionization method, the vapor was excited by a selective laser, including selective laser and dry laser. The ionization occurs by absorbing the two photons from the lasers and then being measured by TOF (**Fig 1.31**). As a result of the deflection method, the spatial difference between the two spectra peaks was 4.1 mm, corresponding to a deflection angle of 12.5 mrad. The calculated recovery rate of ^{48}Ca content in the atomic beam compared to the atomic beam was revealed in **Fig 1.32**. By optimizing the position of the recovery plate, the deflection method achieved a recovery rate of 19.6 % and a concentration level of 5.5 %. On the other hand, the TOF spectra of the ionization method showed that the enrichment could be increased up to 90% using the optimal wavelength laser and density of the atomic vapor. The concentration of ^{48}Ca was found to be higher for the ionization method than

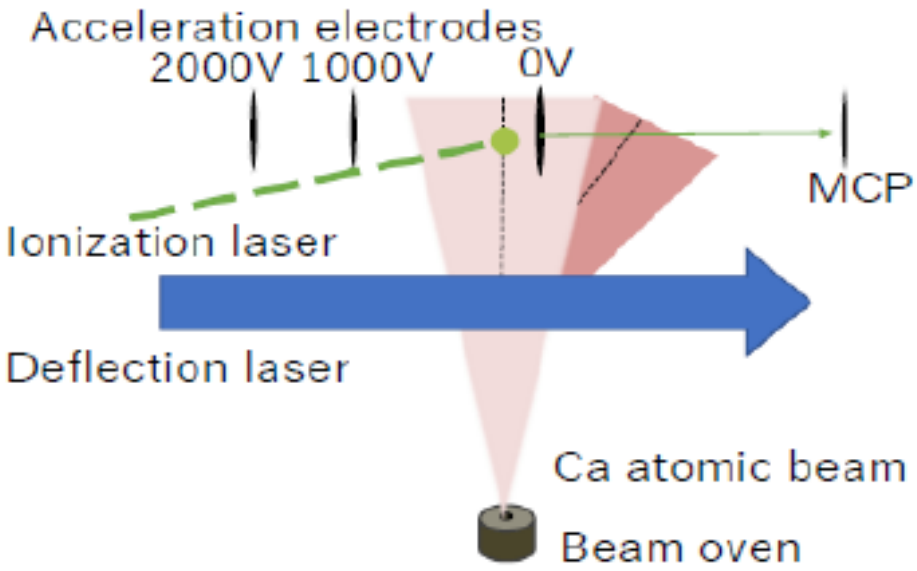

Fig 1.30 Laser isotope separation (LIS), deflection method [69]

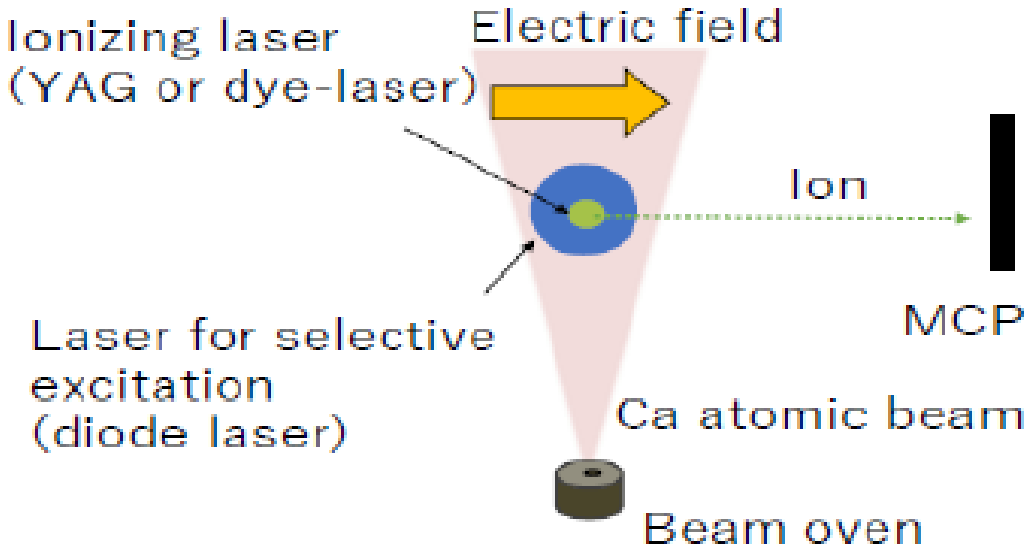

Fig 1.31 Laser isotope separation (LIS), ionization method [69]

the deflection method. However, the recovery rate is lower than the deflection method because the dye laser used for concentration was a pulse laser.

This laser isotope separation method has an advantage that it is simple and inexpensive method for isotope separation. Further improvement is underway and aims

to achieve large-scale production at the first milestone of 1 mol/year. However, the improvement of mass production was required, such as developing a ^{48}Ca collection system, increasing atomic beam density and power, large size crucible and chamber, etc.

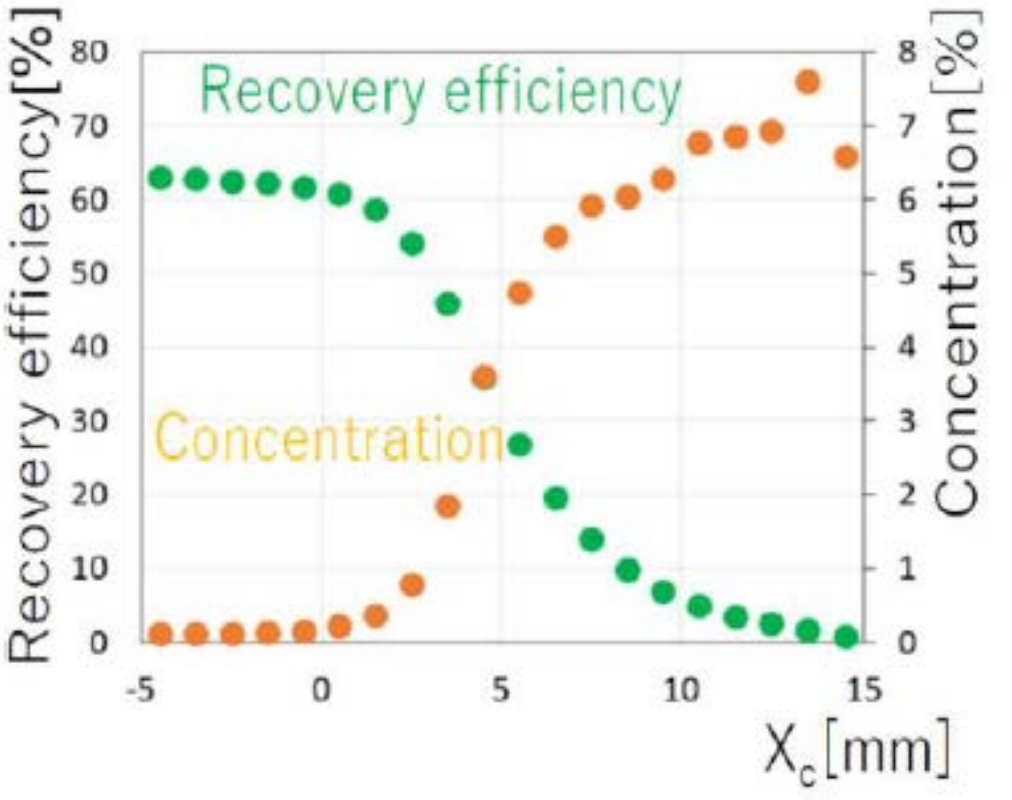

Fig 1.32 Plot of recovery rate (green) and concentration rate (red) assuming that all atoms on the right can be recovered from a point X = Xc [69]

1.4.3. Lithium isotopes

Besides the calcium isotope, lithium (Li) stable isotopes (^{6}Li and ^{7}Li, with the natural abundance ratio of 7.53% and 92.47%, respectively) will soon be demanded. Both lithium isotopes have their specific applications. Lithium-6 (^{6}Li) is mainly used as a neutron absorber in a nuclear fusion reactor due to the large neutron absorption cross section (~940 barn for thermal neutron). Its reaction produces alpha particle and tritium (T) atom via ^{6}Li(n,α)T reaction [70]. According to this nuclear reaction, ^{6}Li (>30%) is usually used as a raw material of tritium production as a fuel in a nuclear fusion reaction [71]. **Fig 1.33** depicts the principle of nuclear fusion reaction via tritium breeding reactor and the fuel cycle of tritium. The heavier isotope of ^{7}Li (>99.9) uses as a pH controller in the coolant of the pressurized water nuclear reactors and as a coolant in the molten salt nuclear reactor [70]. Since the ^{7}LiOH has a suitable pH controller property. It is usually added to the pressurized water nuclear reactors coolant to prevent corrosion. Furthermore, another application of lithium is the coolant of molten salt reactor (^{7}LiF), which is a trend to be developed in the present. The reason is that the molten salt reactor allows the use of Thorium-232 (^{232}Th) as a fissile material which has several benefits, such as the natural resources is larger than uranium [73].

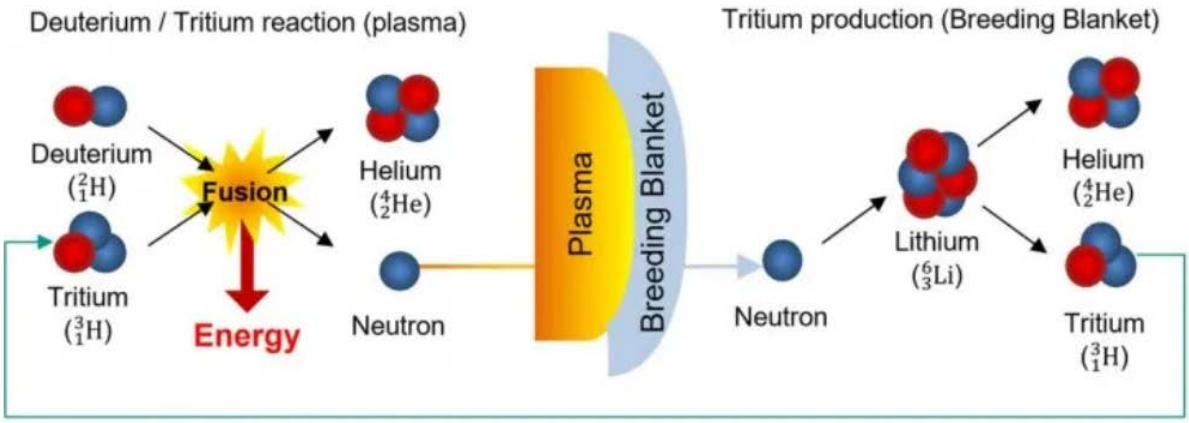

Fig 1.33 Principle of tritium breeding fusion reactor [71]

Moreover, the fission products have a much shorter half-life, resulting in the more accessible waste management. Other advantages of molten salt reactor included safety and efficiency. The molten salt reactor has the advantage of not requiring water as a coolant. As a result, the less risk of steam explosion is promising. The expended property of the salt could manipulate the nuclear fission reaction. Therefore, the salt expended could indicate the current status of the nuclear reactor. The safety valve would trick the freeze plug and immediately separate the fuel of the reactor core to completely shut down the reactor in the case of unwanted high temperatures. The molten salt reactor operates at a high temperature. Therefore, the generated electricity from the steam cycle could have more efficiently. **Fig 1.34** shows the schematic diagram of the molten salt reactor.

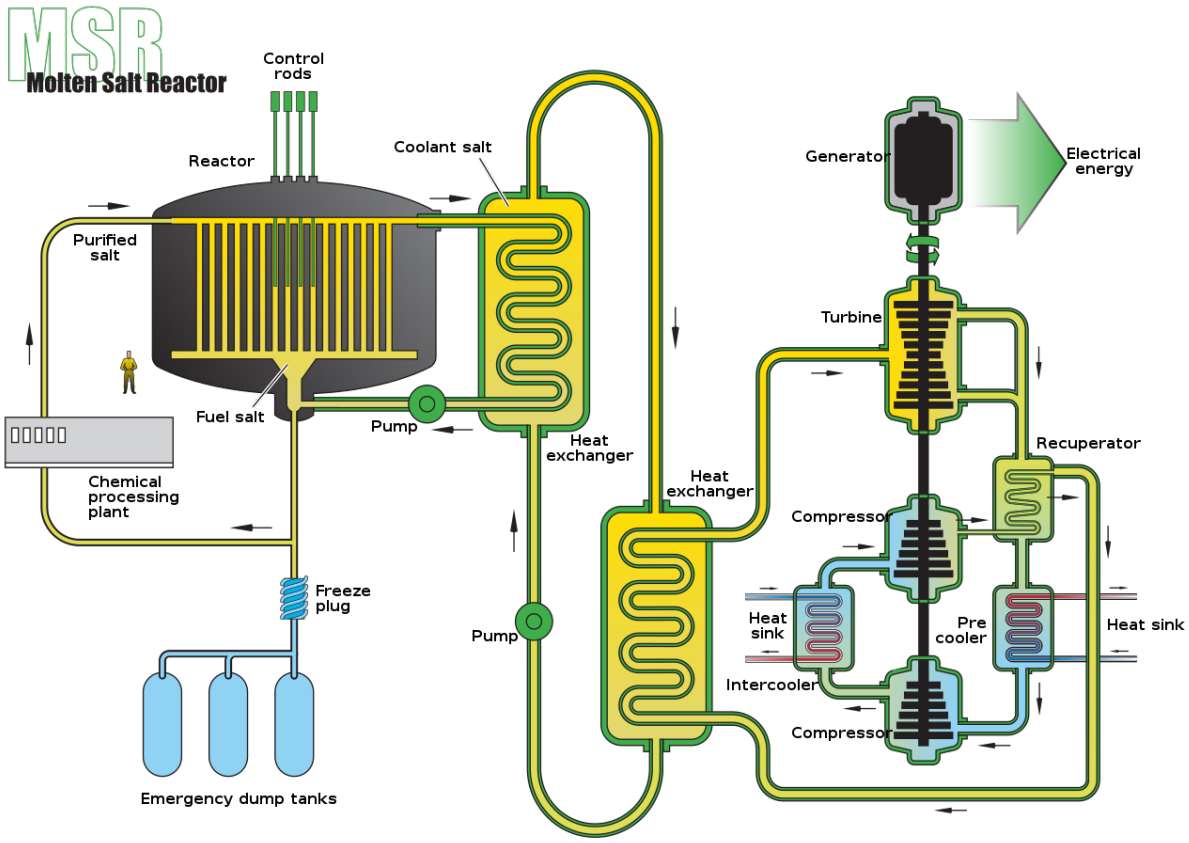

Fig 1.34 The schematic diagram of molten salt reactor [74]

As mentioned, the lithium isotope potentially plays an importance role on the carbon-free energy supply, including the fusion reactor and the molten salt reactor. Nevertheless, since the ^{6}Li could capture a thermal neutron from nuclear fission reaction, resulting to the production of tritium inside the coolant. A high concentration of ^{7}Li is required by removing the ^{6}Li. Here is the competition of the isotope separation of lithium. The industrial scale production of lithium isotope enrichment is the mercury amalgam method. However, mercury poses severe environmental issues and is harmful to human health and living creature. The other potentially methods are improved and proposed through the century.

1.4.4. Lithium isotope separation

The industrial scale production of lithium isotope separation technique so far is mercury amalgam method. Oak Ridge Y-12 National Security Complex (Y-12 NSC) used about 11,000 tons of mercury for lithium isotope separation from 1950 to 1963. Several reports on this amalgam method have revealed [75]. Even with the high value of isotope separation coefficient and a mass production obtained from this method, but approximately 350 tons of mercury were lost to the environment from the production site. Because mercury poses severe environmental issues and is harmful to human health and living creature [76], the U.S. government decided to ban lithium production after the investigation of mercury discharged from the facility in 1963. [76]. Therefore, there was many research on the replacement of the isotope separation technique instead of the mercury amalgam method. The potentially isotope separation technique included ion exchange crown-ether resin chromatography, laser isotope separation, electrochemical method, the ionic liquid extraction system, and dispersive liquid-liquid microextraction.

For ion exchange crown-ether resin chromatography, the principle and mechanism are the same as calcium isotope separation which was mentioned in the previous section (section 1.4.2). Y. Ban, M. Nomura, and Y. Fujii [77] reported the isotope separation of lithium using ion exchanged crown-ether (Monobenzo-15-crown-5: B15C5) resin packed column. The results indicated that the maximum isotope ratio of $^{7}Li/^{6}Li$ was found to be 13.36±0.05, while the feed ratio was 12.34±0.05 (2σ). Finally, the enrichment coefficient (ε = α-1) was determined to be 0.0127 when operating at 35°C. At the same time, the previous work of Kim et al. [78] report the same separation techniques, but the chromatographic was carried out by elution chromatography, while Y. Ban, M. Nomura, and Y. Fujii works were carried out by displacement chromatography. Elution chromatography is appropriate for the separation of low concentrations of ions. The results revealed the single stage separation factor of ($^{6}Li/^{7}Li$) to be 1.053. In conclusion, the isotope separation is significant when carried out by a low concentration of lithium (LiCl). Nevertheless, the practical

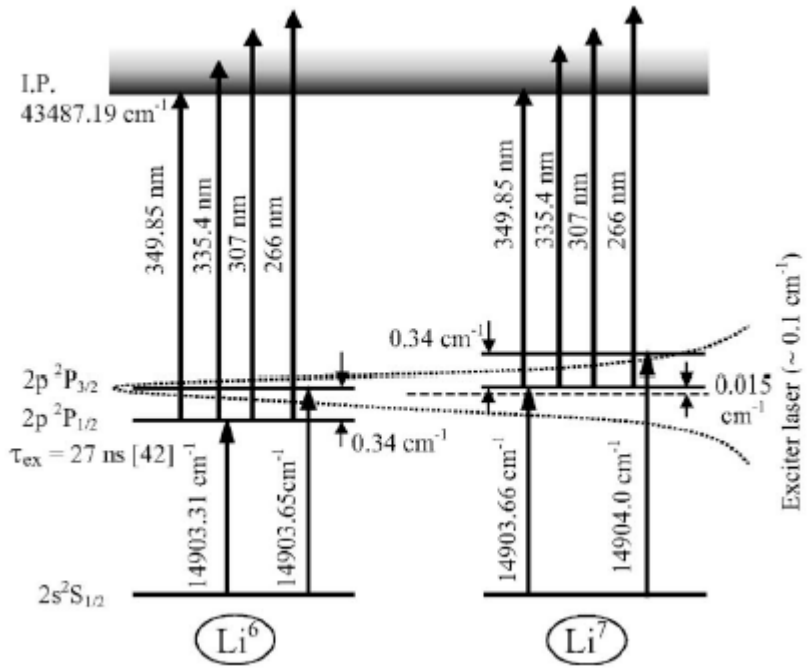

Fig 1.35 Two-step photoionization scheme of lithium isotopes. [79]

achievement to establish a large-scale and mass production, displacement chromatography was performed. 0.55M LiCl dissolved in methanol, and 12M HCl was utilized. The difference between the two methods indicated that the separation factor depends on the concentration of the isotopes in both phases. To optimize the separation coefficient and the amount of lithium ion absorbed by crown-ether resin could potentially scale up the mass production.

As for the laser separation techniques, T. Arisawa et al. [79] reported the lithium isotope separation using a two-step selective photoionization method. The atomic beam of lithium was excited by a dry laser and was ionized by a YAG laser. This method has the same mechanism as ionization laser isotope separation of calcium isotope. The results revealed the high separation factor and can be separated ^{6}Li up to 90% concentration when turning the dry laser wavelength to the energy level of $^{2}P_{1/2}$ of ^{6}Li. Moreover, the results revealed a relationship between the concentration of $^{6}Li^{+}$ and the intensity of the exciter beam. It demonstrates that as the exciter power density increases, the concentration of ^{6}Li decreases dramatically. Another report on the same two-step ionization method was revealed by M. Saleem et al. [80] along with the TOF analyzer. M. Saleem et al. demonstrated that this technique could potentially be used for lithium isotope separation. The obtained results corresponded to T. Arisawa's report on the same magnitude of a dry laser. They also revealed that the much higher energy density of the exciter laser also limits the resolution of the fine structure levels of the lithium isotopes, resulting in a loss of enrichment of 6Li due to the power-broadening effect. In conclusion, a two-step ionization laser could potentially increase the ^{6}Li concentration to 90%. However, the disadvantage of this technique is that it requires a complicated instrument and needs to be improved to collect separated isotopes (**Fig1.35**).

The electrochemical method on the separation of lithium isotope is based on electron charge transfer, known as Marcus's theory [81]. It is a fundamental chemical process when an electron moves from one species to another, either through an intermediate complex or in a single step. J. R. Black et al. [82] announced the electrochemical isotope effect on the lithium isotope. Metallic lithium was placed from 1 M $LiClO_4$ in propylene carbonate (PC) on planar nickel electrodes. The chemical reaction occurs by the following equation 1.13.

$$LiClO_{4(PC)} + e^- = Li_{(s)} \quad (1.13)$$

J. R. Black et al. explored that the light isotope (^{6}Li) is preferentially partitioned into the lithium metal. The enrichment coefficient of ^{7}Li/^{6}Li ranged from -21.6 to -30.5‰. The deposition rate (mol/m^2 s) of the metal lithium needs to be concerned to evaluate the isotope separation and large-scale mass production. It was found that the maximum deposition rate is $55.5\times10^{-5,}$ and it is inversely proportional to the separation coefficient.

Currently, the electromigration method was demonstrated by M. Wang et al. [83]. This method was based on the different abilities of ^{6}Li and ^{7}Li to combine with crown ether (B15C5), which resulted in a different ability of dissociation under an

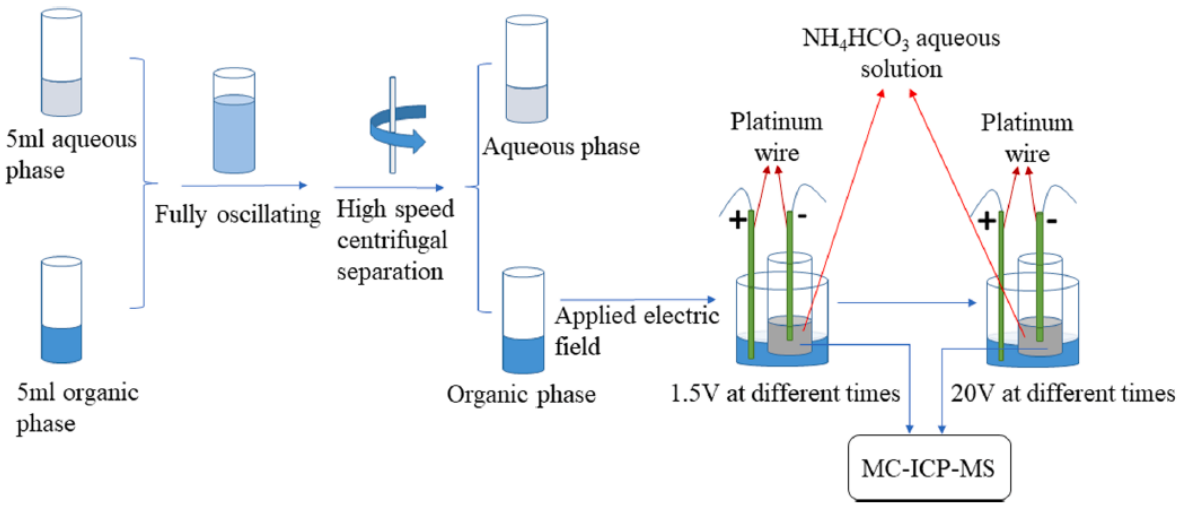

Fig 1.36 The schematic diagram of electromigration combine with crown-ether method [83].

electric field. After extracting lithium ions into the organic phase, an electric field was applied between the organic and aqueous phases to cause the lithium ions in the organic phase to migrate to the aqueous solution. The isotope effect was observed in the process of lithium ions migration. As a result of low voltage, ^{7}Li was firstly moved from the organic phase to the aqueous phase. After that, at high voltage (20V), the lighter isotope of ^{6}Li was migrated. **Fig 1.36** depicts the schematic diagram of electromigration combined with the crown-ether method on the electromigration combined with the crown-ether organic solution. The low voltage supply of 1.5 V found that the enriched ^{7}Li in the aqueous phase compared with the initial lithium isotope value ($\delta^{7}Li = -7.6‰$) of the organic phase. It could be concluded that the organic phase contains the enriched of a lighter isotope of lithium more than the heavier one. The reason why the first electromigration under lower voltage has a heavier enriched is that the organic phase contains both lithium ion-crown complex (selectively ^{6}Li) and lithium ion-uncrown (random). The migration rate of ion-uncrown is much faster than crown-complex, resulting in the migration of heavier isotope under the week electric field more than the lighter one which has a crown-complex formation. Afterwards, the migration of the lighter isotope under the strong electric field resulted in the deformation of ion-crown-complex. The aqueous solution after electromigration of 20 V results from lighter enrichment. The maximum isotope fractionation was found to be – 21.5‰. This new method may reduce crown ether dissolution loss and has the advantages of simple equipment and easy migration control. However, the disadvantage is that the whole process took about 72 hours of consumption time. Moreover, the extracted lithium concentration in the aqueous phase is extremely small (ppm). Further improvements are required, such as larger voltage, a larger amount of lithium loaded to an organic solution, other organic solutions.

The crown ether-ionic liquid on the lithium isotope separation was recently investigated by H. Sun et al. [84]. This method used the ionic liquid as the co-extractant and Dibenzo 15 crown 5 (DB15C5) as the extractant. The maximum separation factor (α) was found to be 1.031±0.001. The advantage of this method is simple and environmentally friendly. Ionic liquids have numerous advantages as extraction solvents, including low vapor pressure, being essentially non-volatile, having low toxicity, having stable physical and chemical properties, and having an adjustable structure. H. Sun et al. also announced the multi-stage counter current extraction (5 stages) for the enrichment of ^{6}Li isotope. After the 5th stage, the abundance of ^{6}Li in the organic phase could reach 7.80%.

W. Zhu et al. [85] reported the same separation techniques using the organic liquid film method. It was improved as a new method of lithium isotope separation. It transports gas into the organic extraction phase, where it condenses into small organic liquid bubbles. These buoyant bubbles then pass through the lithium salt solution phase. Meanwhile, the organic liquid film undergoes the expected isotope exchange. The maximum separation factor (α) was found to be 1.037±0.002 using LiI as a feed. **Fig**

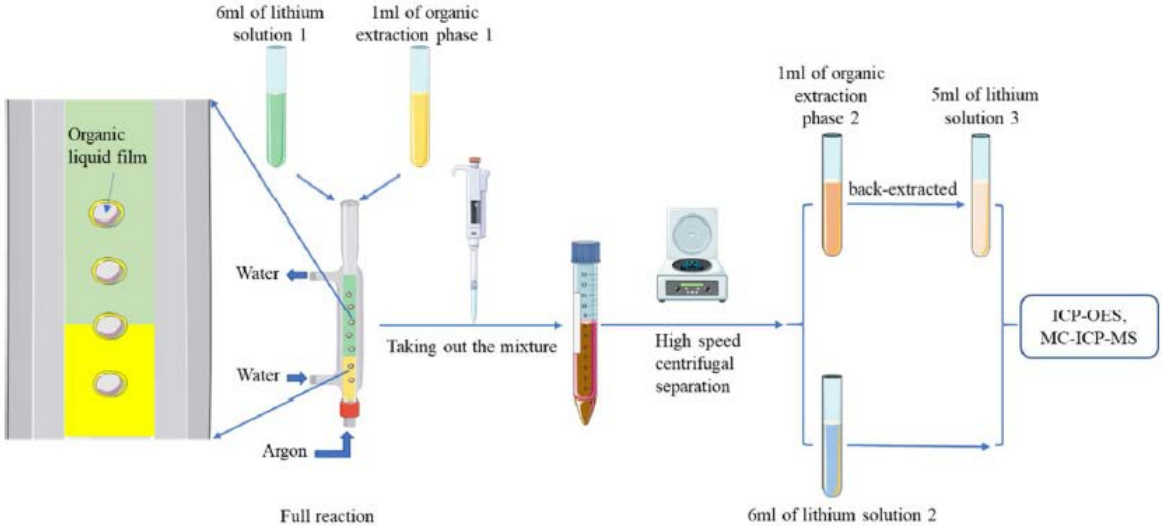

Fig 1.37 The flow diagram for lithium isotopes extraction and separation by using an organic liquid film extraction system. [85]

1.37 shows the mechanism of isotope exchange on the ionic liquid film method. The results also investigated the effect of extraction temperature, indicating that the extraction capacity of the extractant for lithium ions and separation factor decreases as the temperature rises. In conclusion, the organic liquid film extraction system provided a good separation factor of ^{6}Li isotope up to 1.037±0.002. This method has a significant benefit to the mass production of isotope separation. Further studies on the cascade and multi-stage iteration under the applicable conditions are required.

Another isotope separation technique that is easy and simple is membrane separation. T. Hoshino and T. Terai [85] reported the newly developed lithium isotope separation, called ionic-liquid impregnated organic membranes (Ionic-Liquid-i-OMs). This separation technique was based on lithium's ionic mobility between cathode and

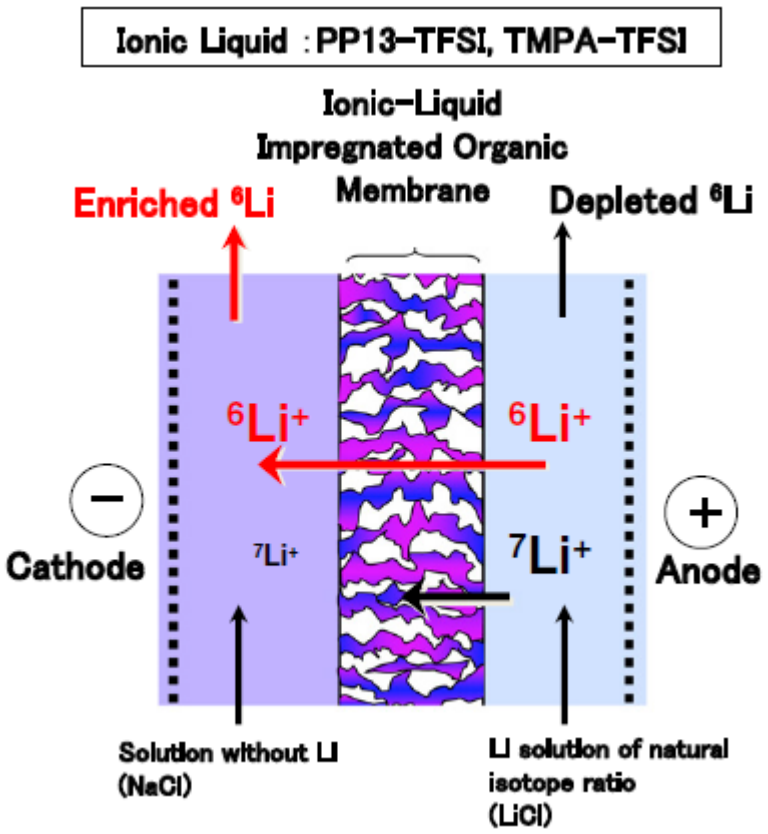

Fig 1.38 The principal mechanism of 6Li enrichment using an ionic liquid impregnated organic membrane [86]

anode through the ionic-liquid membranes. The lighter isotope has ionic mobility greater than the heavier isotope, resulting in the enrichment of the lighter isotope on the cathode cell. The advantages are the high separation factor, inexpensive, and easy to scale up for mass production. **Fig 1.38** shows the principle of ^{6}Li enrichment using an ionic liquid impregnated organic membrane. The separation factor of ^{6}Li was found up to 1.40 under a low electric current of 100 μA and gradually decreased as an electric current increased up to 10 mA. The higher current at 30 and 100 mA has no isotope effect, indicating that this was excessive electrodialytic current. The results indicated the large separation factor under electrodialytic separation using ionic liquid impregnated organic membrane method. However, only a small lithium ion could contribute to this separation. The moving rate of lithium contents was quite small, resulting in this method being inapplicable for large-scale and mass production. Moreover, to stabilize the ionic liquid membrane, assure durability, and prevent the outflow of ionic liquid, the protection cover is required, resulting in the thickness dependency described in another work of T. Hoshino and T. Terai [87].

One of the effective isotope separation techniques for lithium is called the dispersive liquid-liquid microextraction (DLLME) system. This method was invented by M. Rezaee et al. [88] to determine organic compounds in water. However, this method posed the feasibility of isotope separation, too. DLLME is a novel sample-preparation technique offering high enrichment factors from low volumes of water samples. It is modified from the solvent extraction method, and its phase ratio is greatly reduced compared with the other methods, resulting in a large separation factor. In this DLLME, the separation factor depends not only on the extractant but also on the type and volume of dispersive solvents. This property was totally different from the other liquid phase microextraction (LPME) and required a miscible in the organic and

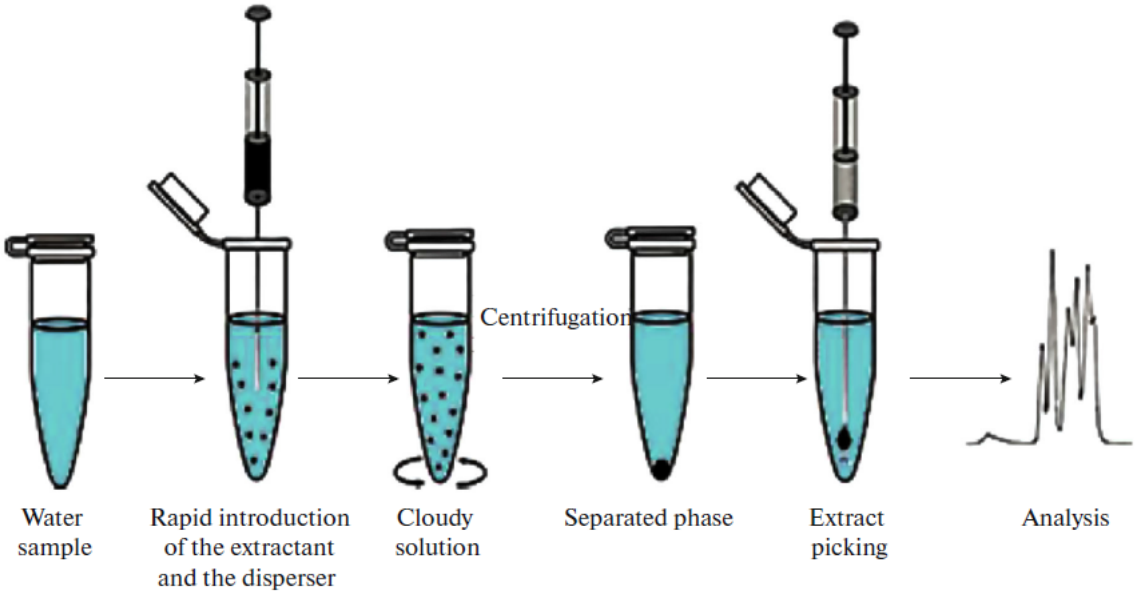

Fig 1.39 The scheme of implementation of dispersive liquid–liquid microextraction [89]

aqueous phase. **Fig 1.39** shows the scheme of implementation of dispersive liquid–liquid microextraction.

M. Davoudi and M. H. Mallah [90, 91] investigate the DLLME on lithium isotope separation by $H_2O/C_2Cl_4/C_3H_6O$ and benzo-15-crown-5 (B15C5). The results found that the ^6Li was transferred from the source phase (feed) to the receiving phase through the formation of the ion-crown complex. The maximum separation factor was 1.082±0.0021, indicating the highest separation factor among the use of B15C5. This method has several advantages profiting to the isotope enrichment, including fast, simple, inexpensive, less amount used of organic solution, reproducible technique with the use of low sample volumes. However, several factors need to be careful. For example, a higher volume of sample leads to a gradual decrease in extraction efficiency and the solubility of the analyte with high polarity.

1.5. Liquid-Liquid extraction using crown-ether

Chemical extraction using liquid-liquid extraction (LLE), known as solvent extraction, mainly uses in the selective extraction of unwanted ions in the reprocessing facility, detoxifications, recovery of precious metals, and chemical separation of metal complex [92]. The relative solubilities in two different immiscible organic and aqueous phases allow the ion exchange and separation of a concentrating ion. As said, due to the mass differences in each isotope, the vibrational frequency and chemical reaction rate also differ, resulting in the isotope effect on the ion exchange.

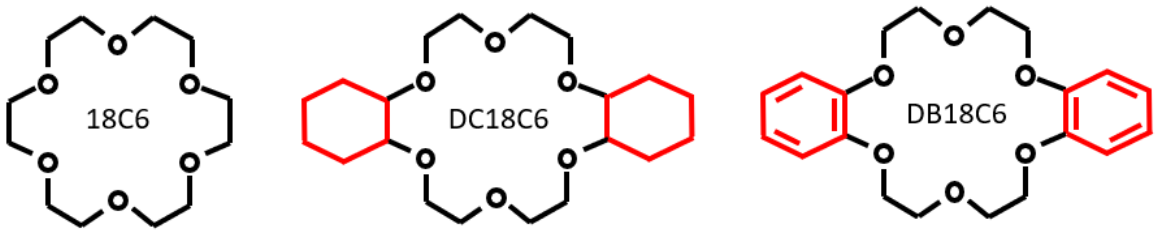

Fig 1.40 The molecular structure of 18C6, DC18C6, and DB18C6

This research used crown-ether (CE) as a chemical carrier of calcium or lithium ion by ion-crown complex formation. Crown-ether is known as a host-guest macrocyclic polyether. Crown-ether has a unique physical structure forming in the shape of a crown molecule. For example, the firstly synthesized crown-ether molecule by C. J. Pedersen in 1971 [93] is called 2,3,11,12-dibenzo-1,4,7,10,13,16-hexaoxacycloocta-2,11-diene (dibenzo-18-crown-6: DB18C6). It is the crown-ether molecule with 18 molecules of C, and 6 molecules of O forming in the shape of the crown. Additionally, the side chain of crown-ether has two benzo molecules located at 2, 3, and 11, 12 of a carbon atoms. Moreover, C. J. Pedersen indicated the formation of the crown-ether compound with the alkali and alkali earth cation by measuring the shift of the ultraviolet spectrum. Eventually, he won the Nobel prize in chemistry in 1987 to discover crown-ether, which benefits the field of chemical extraction [94]. After the

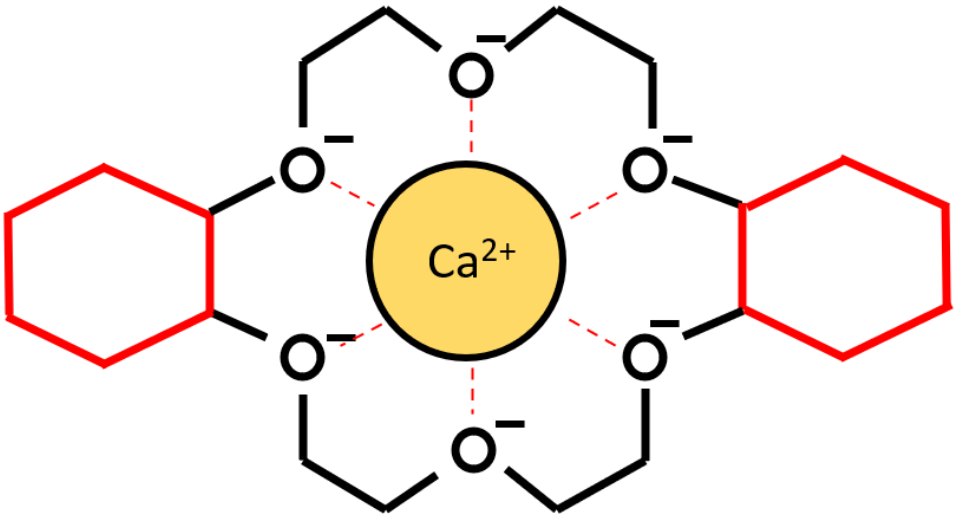

Fig 1.41 The formation of calcium ion complex with DC18C6 crown-ether.

synthesis of DB18C6 was successful, several experiments were carried out to explore the other forms of a crown-ether molecule. Several types of crown-ether molecules were discovered, resulting in the more efficient chemical extraction and purification due to forming more stable complexes with alkali metals. **Fig 1.40** depicts the molecular structure of 18C6, DC18C6, and DB18C6 [95]. The difference between side-chain indicates the physical properties of the crown-ether molecule, such as the solubility in organic and water, stability of the ion-crown complex, and the melting point. The cavity size (hole) of crown-ether is determined by the total number of carbon and oxygen atoms, as the total number of crown atoms increases, the cavity size increases. **Table 1.4** shows the cavity size of crown-ether in the Angstrom unit obtained from X-ray diffraction data. The electrostatic attraction between the cation's positive charge and the negative dipolar charge on the six oxygen atoms symmetrically arranged around it in the polyether ring causes the formation of the ion-crown-ether complex. Therefore, the relative diameter of the cavity size and the cation diameter is important. **Table 1.5** shows the cation diameter in the Angstrom unit. Moreover, the cavity of the macrocycle, the size of the cation, the number of donor atoms in the macrocycle, the planarity of the macrocycle, the alkalinity of donor atoms, and the bond strength

Table 1.4 The cavity size of crown-ether in Angstrom unit [94]

Crown-ether molecule	Cavity size (Å)
12-crown-4	1.2 – 1.5
15-crown-5	1.7 – 2.2
18-crown-6	2.6 – 3.2
21-crown-7	3.4 – 4.3

Table 1.5 The cation diameter in Angstrom unit [98]

Cation	Diameter (Å)
Li	1.36
Na	1.94
K	2.66
Ca	1.98
Cu (I)	1.92
Zn	1.48
Rb	2.94
Sr	2.26
Ag	2.52
Cd	1.94
Cs	3.34
Ba	2.68
La	2.30
Au (I)	2.88
Hg (II)	2.20
Tl (I)	2.80
Pb (II)	2.40
Ra	2.80
NH_4	2.86

between the cation and solvent are thought to be factors that can affect complex formation. As a result, this research focuses on the selective extraction of calcium ions using dicyclohexano-18-crown-6 (DC18C6) crown-ether, which has an appropriate cavity size to calcium ion. **Fig 1.41** depicts the formation of calcium ion complex with

DC18C6 crown-ether. According to **table 1.4 and table 1.5**, both calcium and lithium have a relative diameter to 18-crown-6 molecule. It is noted that lithium has better formability to 12-crown-4 and 15-crown-5 more than 18-crown-6 [96]. Moreover, Truter and Pedersen [97] reported the ion-crown complex that the crown-ether molecule could possibly be distorted when the cation has a smaller size.

Chemical isotope exchange with macrocyclic polyether by liquid-liquid extraction is well known to be an effective method for isotope enrichment of various cationic elements, especially on light elements such as lithium or calcium and tellurium [99, 101, 102]. A large separation factor was obtained using cryptands (a combining structure between polyether and bicyclic diamines: **Fig 1.42**) or crown-ether [97]. Nevertheless, cryptands have a high-water solubility, the application of large scale and mass production was limited. As mentioned, crown-ether has various properties depending on the molecule's side chain. For example, DC18C6 could be dissolved in an organic solvent such as chloroform [99], resulting in the best candidate for liquid-liquid extraction, which required two immiscible phases.

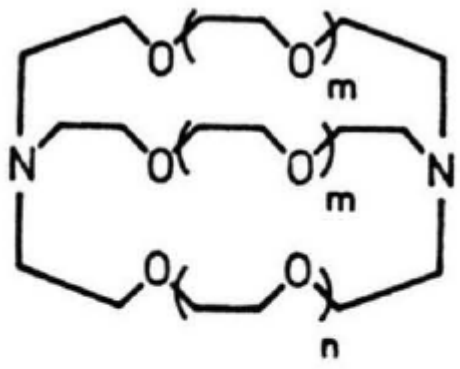

Fig 1.42 [2,2,1] and [2,2,2] cryptands [97].

The isotope effect of calcium using crown-ether (DC18C6) and liquid-liquid extraction was firstly reported by B. E. Jepson and R. DeWitt [99]. The chemical exchange occurs by the following equation 1.14:

$$^{40}Ca^{2+}_{(aq)} + {}^{48}CaL^{2+}_{(org)} \rightarrow {}^{48}Ca^{2+}_{(aq)} + {}^{40}CaL^{2+}_{(org)} \qquad (1.14)$$

where *L* represents the macrocyclic crown-ether dissolved in organic solvents. The subscriptions, org and aq, indicate the organic and aqueous phases. The chemical exchange between calcium ions indicates that crown-ether selectively absorbed the lighter isotope via the ion-crown complex. The discovery revealed the possibility of the isotope separation by liquid-liquid extraction technique. The separation factor of $^{44}Ca/^{40}Ca$ was 1.0010±0.0002 using chloroform and $CaCl_2$ (> 3M) as an organic and aqueous phase. This method has the advantage that a high concentration of calcium could be used, becoming an excellent candidate for the large-scale isotope separation and enrichment **Fig 1.43** depicts the schematic diagram of the liquid-liquid extraction and the isotope effect of lighter calcium isotope. The organic phase crown-ether was mixed with an aqueous calcium solution. The crown-ether selectively absorbed the lighter isotope more than the heavier. The loaded crown-ether was back-extracted by water. Compared to the other chemical extraction such as the crown-ether resin chromatographic method, LLE contributes to calcium concentration through the extraction process approximately 10 times higher than the chromatographic method.

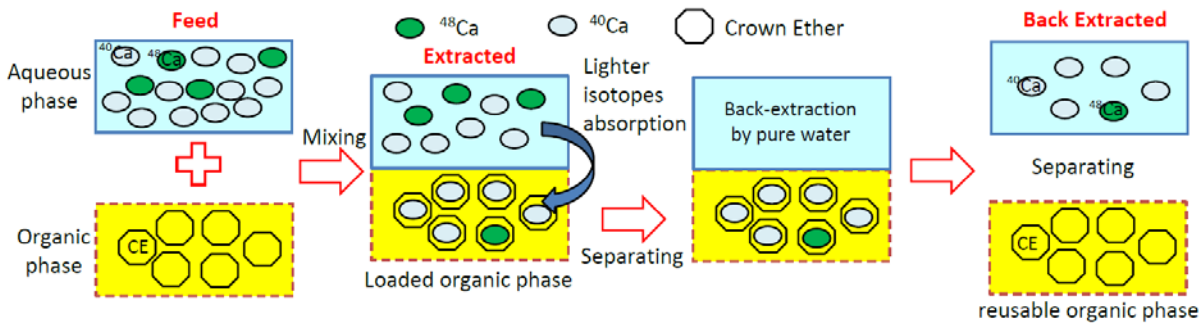

Fig 1.43 The schematic diagram of the liquid-liquid extraction

This advantage of LLE profits the mass production of the isotope enrichment. Although the LLE using crown-ether has simply, uncomplicated, large separation factor and good contribution of cation content. However, the multi-stage iteration or cascade enrichment is required to achieve large-scale and mass production. The designed experiment which could enhance the separation factor and contributed content is challenging.

R. Hazama et al. [100] expressed the calculation of the chemical isotope effect of calcium on liquid-liquid extraction using DC18C6 crown-ether. The evaluated result showed the contribution ratio of the field shift effect and the hyperfine splitting shift effect to the mass effect of the calcium isotopes exchange for the first time. The contribution ratio described that the mass-effect of calcium was dominated the field shift effect, especially ^{48}Ca and ^{40}Ca, which has a doubly magic number of 20 and 28. His demonstration indicated that the isotope effect of ^{48}Ca and ^{40}Ca on DC18C6 crown-ether came from the nuclear mass effect more than the field shift effect or hyperfine splitting shift, providing the promising separation method via crown-ether. However, the odd number of ^{43}Ca has a hyperfine splitting effect that contributes to the separative property. Further experimentally investigation will be explained in this dissertation.

Besides calcium, lithium isotope separation is also possible under the liquid-liquid extraction towards the enrichment and mass production. Several researchers reported the lithium isotope using liquid-liquid extraction. For example, K. Nishizawa et al. [101] investigated the lithium isotope separation using benzo-15-crown-5 (B15C5) via liquid-liquid extraction using chloroform and lithium iodine (LiI) system. The results indicated the formation of an ion-crown complex. Several factors were also revealed, including the effect of crown-ether concentration on the distribution coefficient, minimum time required to reach the chemical and isotope equilibrium,

effect of lithium species, and extraction temperature. The separation factor ($^{6}Li/^{7}Li$) was ranged from 1.002±0.002 to 1.035±0.002. Another important work of K. Nishizawa et al. is on the effect of salt concentration [104]. As mentioned, the advantage of LLE is the high contribution of cation to the crown-ether, which results in large-scale and mass production. Therefore, the appropriate concentration of aqueous solvent becomes the prior manner. K Nishizawa et al. reported the relationship between separation and distribution factors and LiCl concentration to be dependent. As the raised of LiCl concentration, the separation factor and distribution coefficient increased. The maximum separation factor ($^{6}Li/^{7}Li$) was 1.045 under the 10 – 12M LiCl concentration. They concluded that the population of the crown ethers occupied by the lithium ion is large in the concentrated solution, which is favorable for isotope separation and mass production.

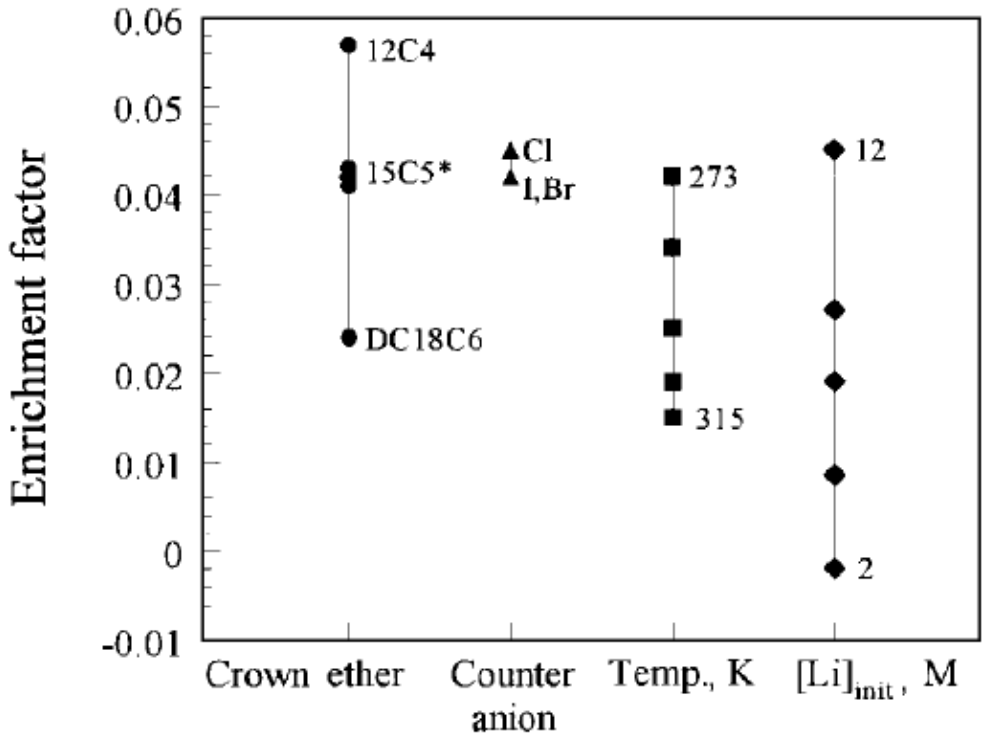

Fig 1.44 The summarization of lithium isotope separation by crown-ether liquid-liquid extraction on various extraction factor [105]

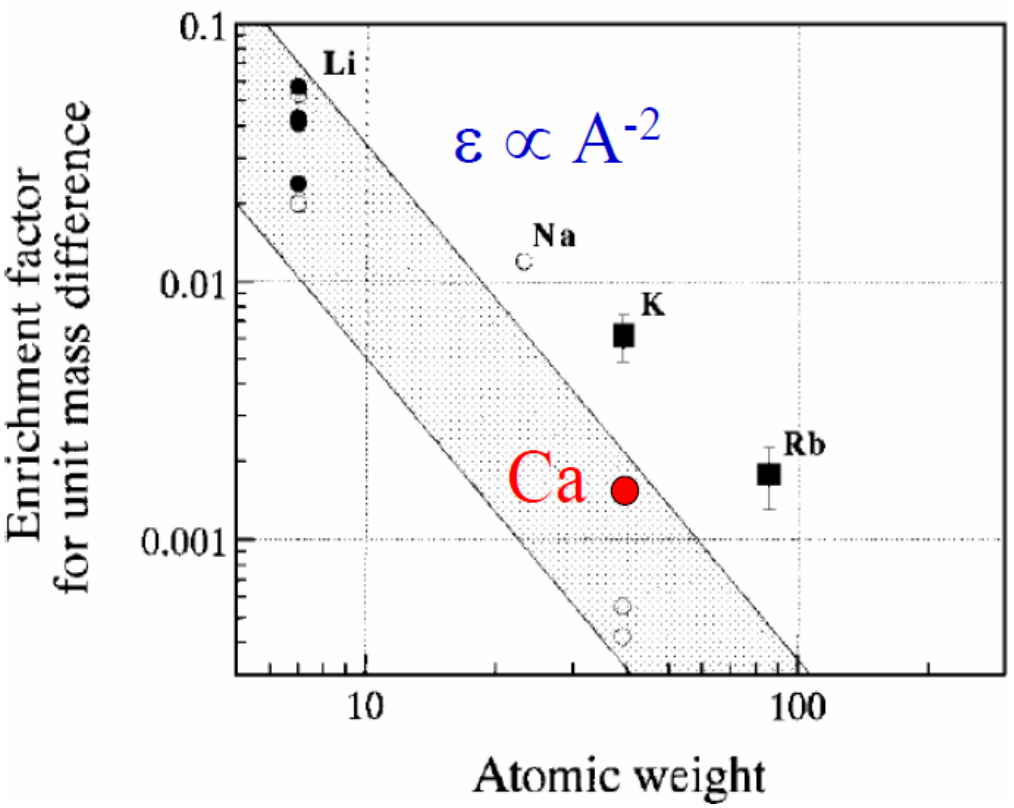

Fig 1.45 The estimation of calcium isotope effect according to Alkali metals results. The gray area shows a linear line with a slope of –2, which has a range of ε_u = 0.01~0.07 at A = 6.9 (Li). [105]

In conclusion, K. Nishizawa and T. Fujii [105] summarized the lithium isotope separation via LLE with various factors, including the type of crown-ether, lithium species, extraction temperature, and feed concentration (**Fig 1.44**). This result could be applied for further study on the other isotope separation. Moreover, K. Nishizawa and T. Fujii also reported the enrichment factor for alkali metals on the unit of mass. As for alkali earth, calcium could potentially be enriched by the same method and unit of mass. The estimation of the calcium isotope effect is shown in **Fig 1.45.**

The most advantage of liquid-liquid extraction using an organic solvent containing crown-ether is that it can be applied to microchip separation. The microchip, known as a microreactor, provides fast and high conversion of the extraction process, resulting in mass production feasibility [106, 107]. The advantage of microchip isotope

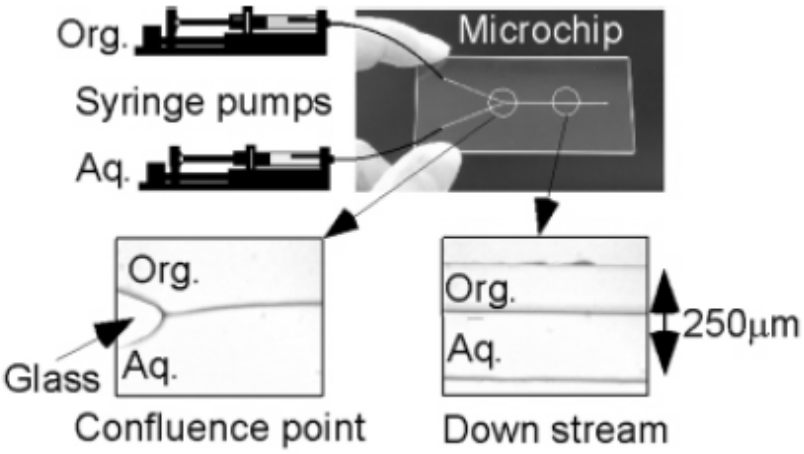

Fig 1.46 The glass microchip and liquid-liquid extraction of organic and aqueous phase [107]

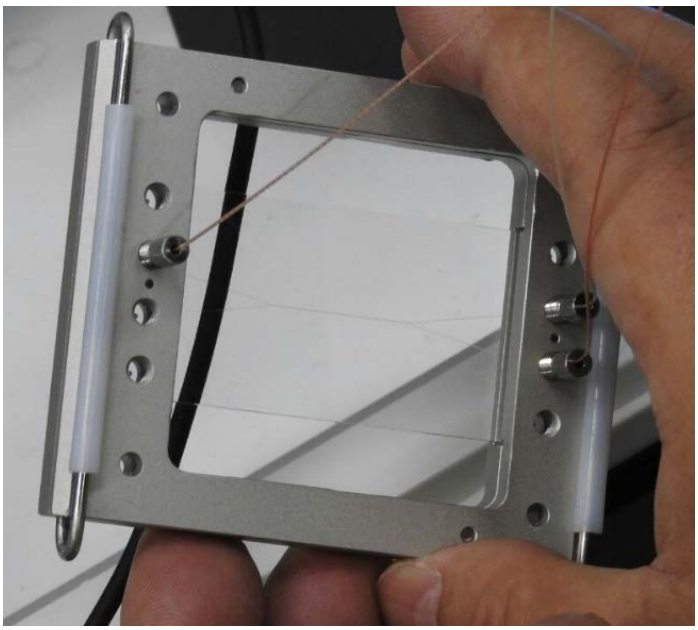

Fig 1.47 The glass microchips with Y junction

separation is that the microchip or microwell fabricated on a glass microchip provides a short molecular diffusion distance, large specific interfacial area, and small heat capacity. These advantages result in a highly effective chemical reaction inside the microchip. The organic and aqueous phases were introduced to the microchannel by syringe pumps, a stable liquid-liquid interface formed a chemical exchange reaction. The outcome of a chemical reaction can be obtained without stirring. Moreover, due to the stable flow of two immiscible solvents, separation is possible at the outlet of the

Fig 1.48 The glass microchips with Y junction during the operation

microchip channel. **Fig 1.46** depicts the glass microchip on the liquid-liquid extraction of the organic and aqueous phases. **Figs 1.47 and 1.48** show our first trial on microreactor extraction.

The mass production prospect using liquid-liquid extraction equipment, the Pulse column and mixer settler are mainly used for industrial production. Pulse column is the type of liquid-liquid extraction equipment which is used in nuclear fuel reprocessing plants. The key to reprocessing is to separate the spent fuel from the radioactive material. The column allows contact between two phases. The immiscibility and density allow the separation of both phases. Pulsed columns work on a similar principle, but the agitation is provided by the solutions' reciprocating pulsation rather than the movement of the internals column. **Fig 1.49** illustrates a pulsed column designed by Bateman [92]. For mixer settlers, it usually is used for commercial-scale production. **Fig 1.50** shows the schematic diagram of the box-type mixer settler. This equipment allows the mixing of the organic and aqueous phase in the mixing

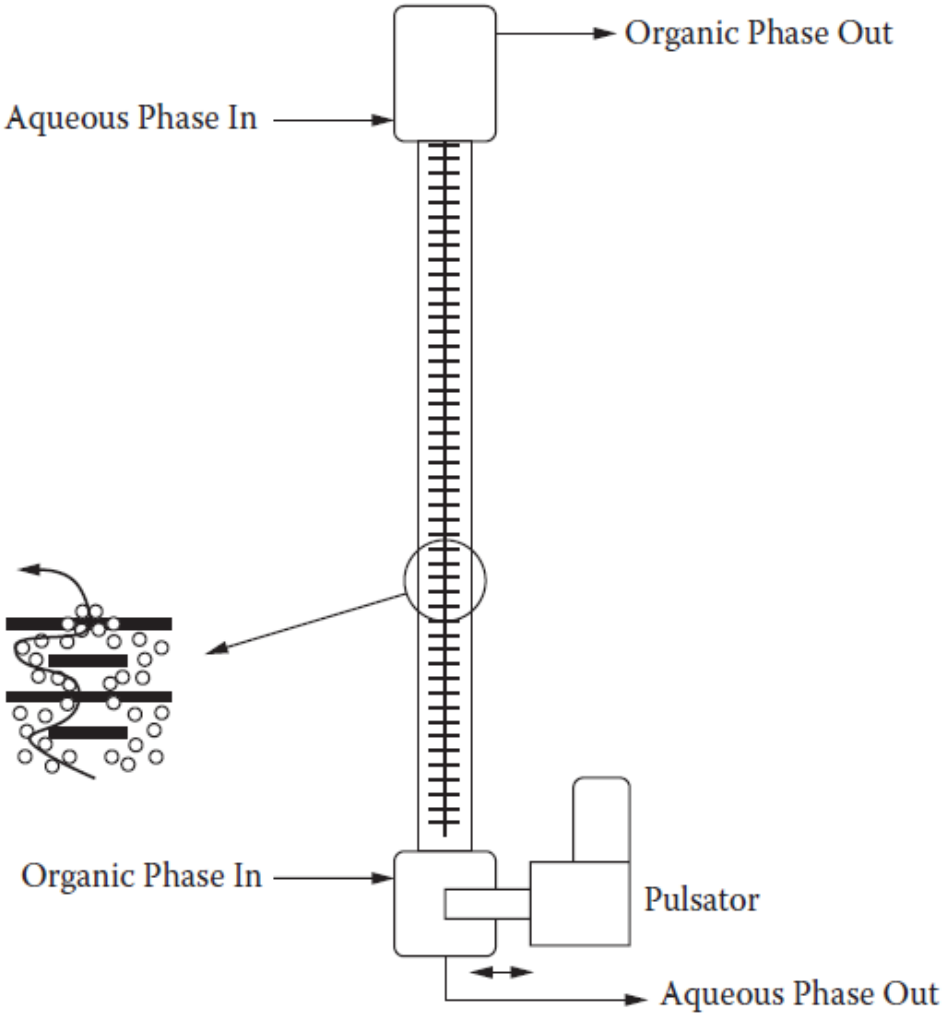

Fig 1.49 Pulsed column designed by Bateman [92]

compartment, and then the mass transfer takes place. Afterwards, the mixing solution overflowed on the settling compartment. The difference in density can separate each phase into the outlets or adjustable overflow weir.

This research studied the several fundamental factors of liquid-liquid extraction and provided the prospect of enrichment and mass production. **Table 1.6** compares the isotope separation and enrichment feasibility advantages and disadvantages.

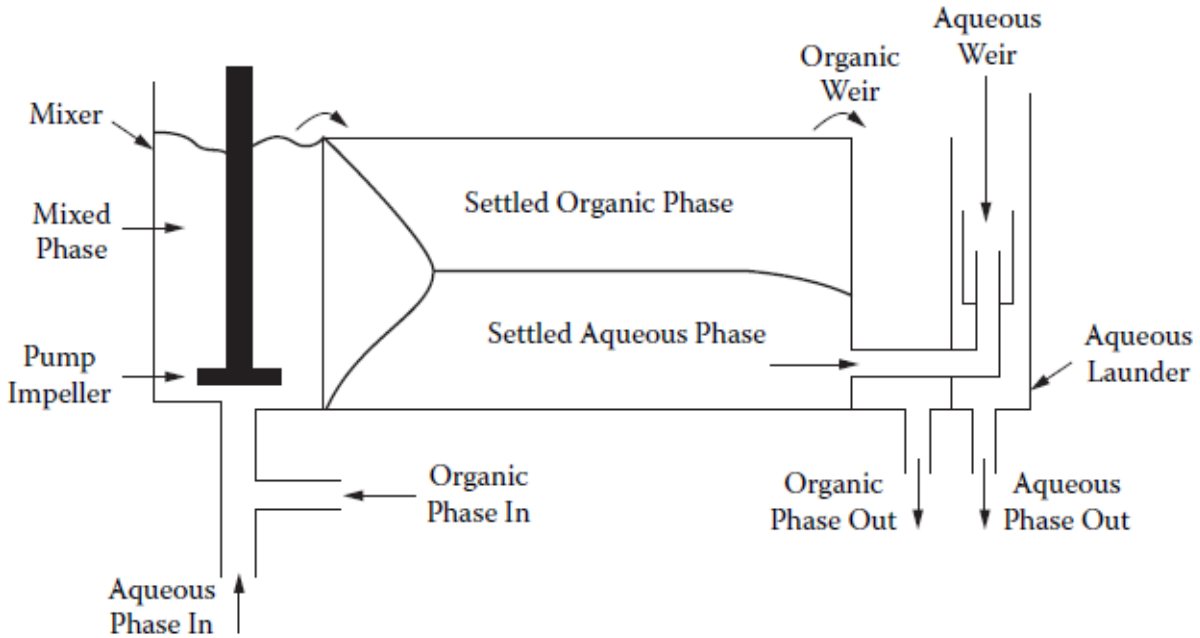

Fig 1.50 The schematic diagram of box type mixer settler [92]

Table 1.6 The advantages and disadvantages of possible isotope separation techniques

Isotope separation techniques	Advantages	Disadvantages	Ref.
Chemical exchange			
- **Crown-ether LLE (This research)**	- Moderate separation factor (α) - High concentration of feed solution is allowed (>3 M) - Easy operation and uncomplicated - Fast and high conversion - Can be applied to microreactors for a mass production	- Extractants loss - Solubility problem - The designed experiment for cascade enrichment is challenging	- 92, 99, 101, 104, 105
- **Cryptands LLE**	- Moderate to high separation factor (α) - High concentration of feed solution is allowed (>3 M) - Fast and high conversion	- Extractants loss - Solubility problem - The designed experiment for cascade enrichment is challenging - High water solubility, multi-stage iteration is limited	- 103
- **Redox method**	- Moderate separation factor (α) - Easy operation and uncomplicated	- Mercury based poses serious environmental issues - Inapplicable for large-scale production	- 59, 60
- **Ion exchange chromatography**	- Moderate separation factor (α) - Simply and easy to accumulate the enriched solution	- Time consumption - Low conversion - Acidity solvent is necessary	- 61, 62, 63, 64

Isotope separation techniques	Advantages	Disadvantages	Ref.
- **Electrochemical method**	- Moderate to high separation factor (α) - Moderate concentration of feed solution (1M)	- Low conversion - In applicable for large-scale production - Time consumption	- 81, 82
- **Electromigration (Combined with crown-ether)**	- Moderate to high separation factor (α) - Reduce the extractants loss - Easy operation and uncomplicated	- Time consumption - Low conversion	- 83
- **Crown ether-ionic liquid**	- Moderate to high separation factor (α) - Easy operation and uncomplicated - Environmentally friendly	- Low conversion	- 84
- **Organic liquid film extraction**	- Moderate to high separation factor (α) - Easy operation and uncomplicated	- Low conversion	- 85
Membrane separation	- High separation factor (α) - Inexpensive - Possible to scale up for the mass production	- The maintenance of membrane is required - Low conversion - Small reproductivity	- 86, 87
Dispersive liquid-liquid microextraction (DLLME) system	- High separation factor (α)	- High sensitivity chemical process - Difficult to control	- 88, 89
Electromagnetic separator	- Highly selective separation factor (α) - Applicable for a high concentration production	- Expensive - Small production yield - Required a large facility	- 55, 57, 58

Isotope separation techniques	Advantages	Disadvantages	Ref.
Electrophoresis	- Moderate separation factor (α) - Widely applicable for any charged compound which has mobility in fluid or water	- Time consumption - Trade-off relation between extracted amount and separation factor (MCCCE could overcome this obstacle) - Only the low concentration is allowed	- 65, 66, 67
Electrooptical isotope separation	- Highly selective separation factor (α) - Greater production yield compared to the electromagnetic separator	- Only light atoms (Li, Na, and Ca) - The source needs to be a nonrigid molecule, resulting in a high melting point. -	- 68
Laser isotope separation (LIS)			
- **Ionization method**	- Highly selective separation factor (α) - Atomic beam sources are relaxed compared to electrooptical isotope separation - Simple and inexpensive	- Specific instruments are required - Small production yield	- 69
- **Deflection method**	- Highly selective separation factor (α) - Atomic beam sources are relaxed compared to electrooptical isotope separation - Simple and inexpensive	- Specific instruments are required - Small production yield	- 69

1.6. Isotope analysis by mass spectrometry

Nowadays, it is well known that mass spectrometry is wildly used as an analyzer in many research and application fields such as chemistry, biochemistry, pharmacy, medicine, and many related fields of science. Mass spectrometry has an outstanding performance among the other analytical method including, detection limit, sensitivity, and highly rapid chemical analysis method. One of the best advantages is that mass spectrometry can process the isotope composition analysis. In contrast, the other chemical analysis methods such as atomic absorption/emission spectrometer and liquid chromatography cannot be performed.

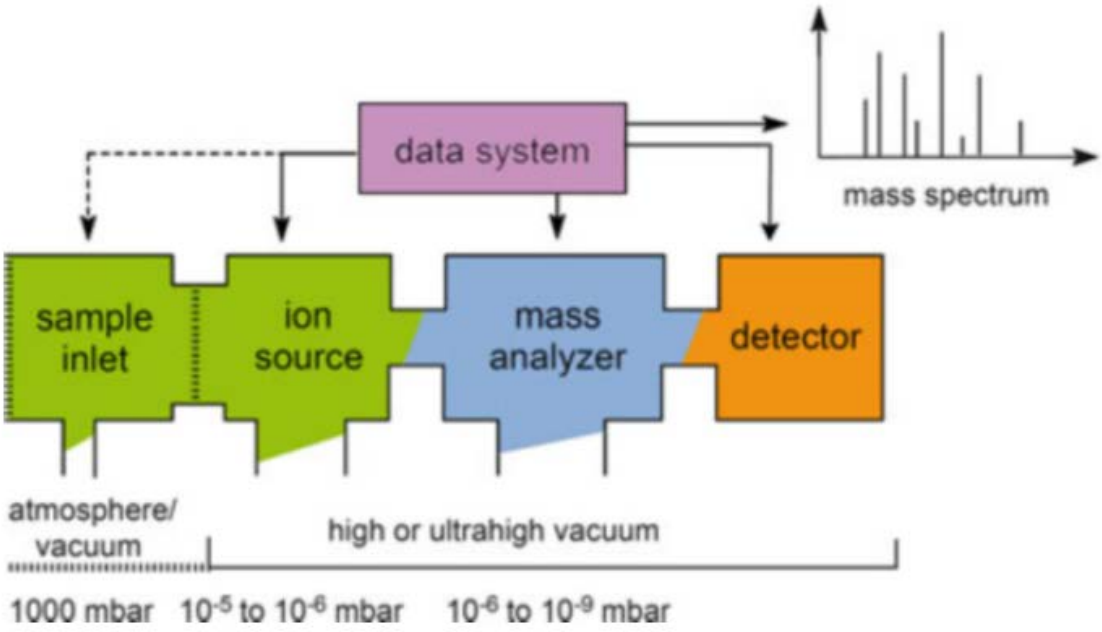

Fig 1.51 The mass diagram of mass spectrometer compartments [108]

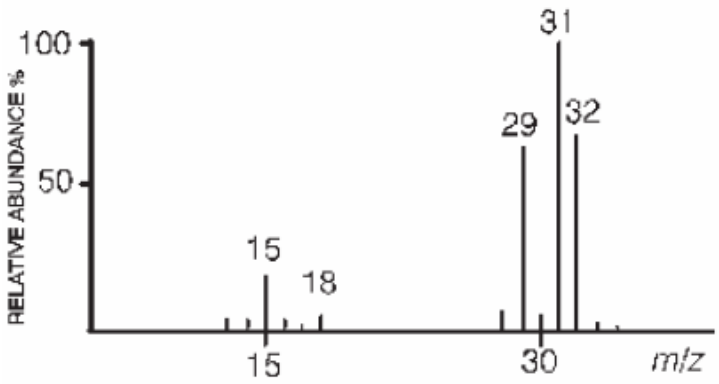

Fig 1.52 The example of mass spectrum [109]

The basic understanding of mass spectrometry analysis is the compartments. A mass spectrometer consists of four essential sections, including sample injection, ion source, mass analyzer, and detector (**Fig 1.51**). Except for the sample inlet, all the mass spectrometer compartments operate under a high vacuum level (>10^{-5} mbar). By any suitable method such as flame, plasma, photon, the thermally generated ions are affected by static or dynamic electric or magnetic fields. The detector collects the

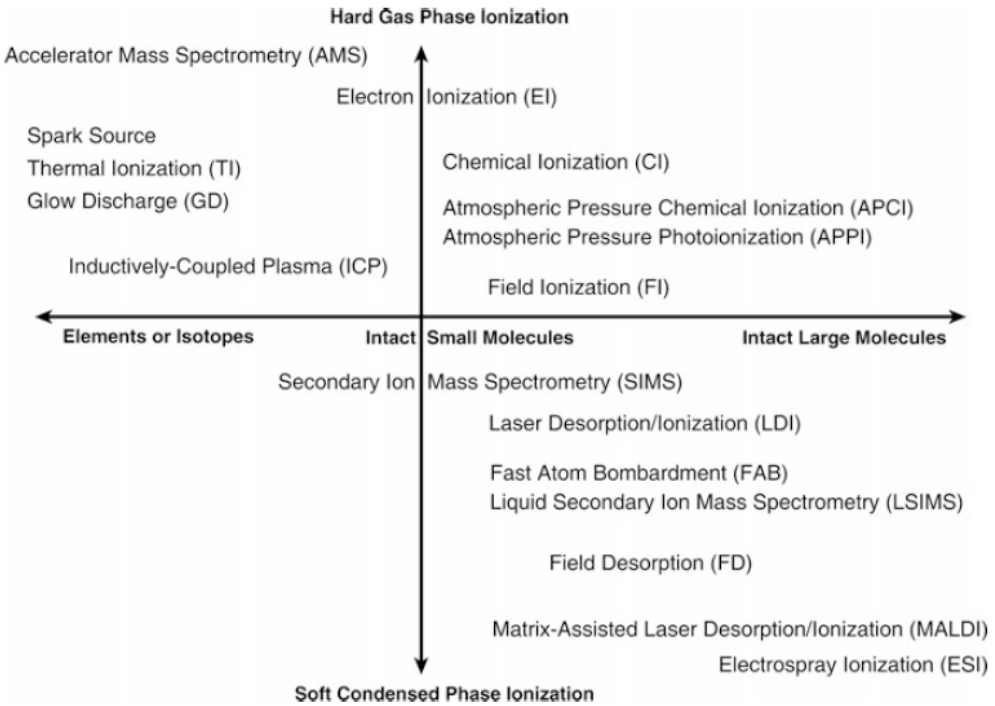

Fig 1.53 The mass spectrometric techniques for various application estimated by relative hardness or softness [108].

separated ion and displays it by mass to charge ratio (m/z) [108, 109]. The mass spectrum represents the signal intensity and m/z. The intensity of this peak is proportional to the abundance of that ion (**Fig 1.52**). **Fig 1.53** depicts the mass spectrometric techniques for various applications estimated by relative hardness or softness. In this research, the primary purpose is to investigate the isotope composition of calcium and lithium. The isotope analysis method used in this research is mainly on ICP-MS and precise measurement for comparison by TIMS.

Inductively Coupled Plasma Mass Spectrometry (ICP-MS) is one of the most famous mass spectrometry for analyzing elements and isotopes. The widespread acceptance of ICP-MS can be attributed to its relatively robust yet versatile sampling mode. The atomization and ionization occur in the radiofrequency of argon plasma at atmospheric pressure [108]. The plasma torch is made up of three quartz tubes coaxially aligned and inserted along the central axis of a water-cooled RF coil. The ignition is done by an electric spark then the coil feeds the plasma by coupling electric energy into the gas. Because the magnetic field induces ion mobility, it heats (6,000 – 10,000 K) the gas while maintaining plasma stability (**Fig 1.54**). The sample is fed to the plasma by the carrier of argon gas. This carrier gas passes through a nebulizer, causing a liquid

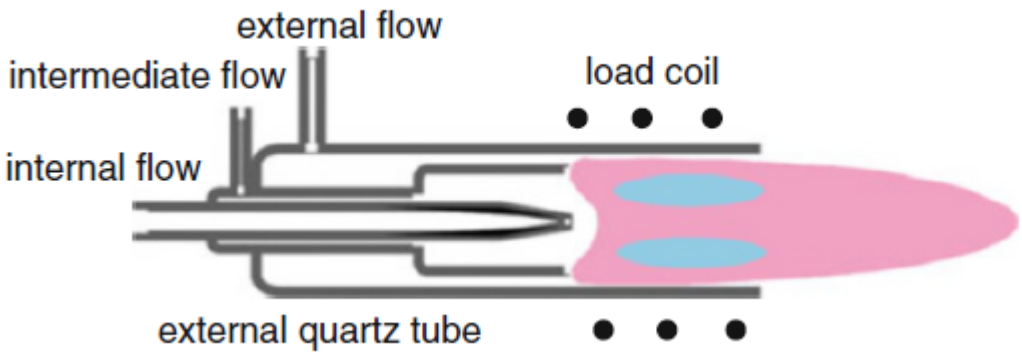

Fig 1.54 The schematic diagram of ICP touch [108]

sample to dissipate and transfer as micrometer-sized droplets. Then the sample droplet was vaporized, atomized, and ionized inside the ICP. Due to the most outstanding characteristic, the ICP-MS allows the measurement of ultralow-level concentration (ppt) and the multielement measurement simultaneously.

Because the most isotope abundance of calcium is ^{40}Ca, which has the same mass number as argon isotope (^{40}Ar: n.a. = 99.604%), it results in atomic interference [110]. Additional reaction or collision-cell ICP-MS can overcome this obstacle. The reaction or collision cell ICP-MS has been widely accepted as an efficient technique for removing polyatomic interference. The reaction or collision cell consists of RF multipole ion guides enclosed in a cell pressurized with a gas [111]. It.is introduced before the mass analyzer, aiming to eliminate atomic interference using reaction or collision gas (**Fig 1.55**). The reaction mode used a reaction gas to remove known interference from the analyte. This was ascribed to the charge transfer reactions of the atomic ions with the argon gas target. **Fig 1.56** shows the ionization potential of reaction gas, indicating the atomic interference. The black circles are the element which are

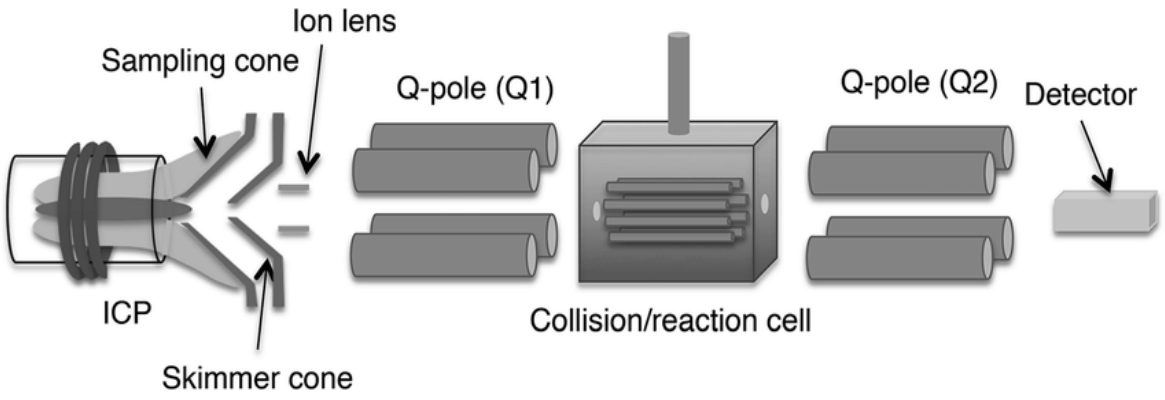

Fig 1.55 Schematic diagram of ICP-MS-MS with collision/reaction cell. [111]

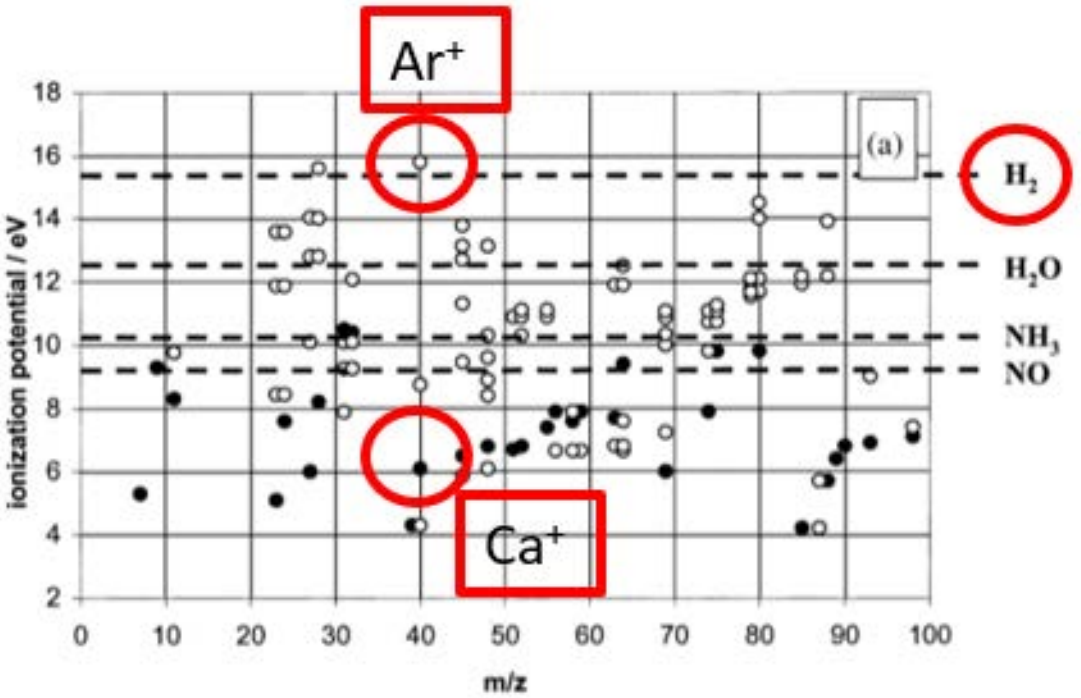

Fig 1.56 The ionization potential of reaction gas [112]

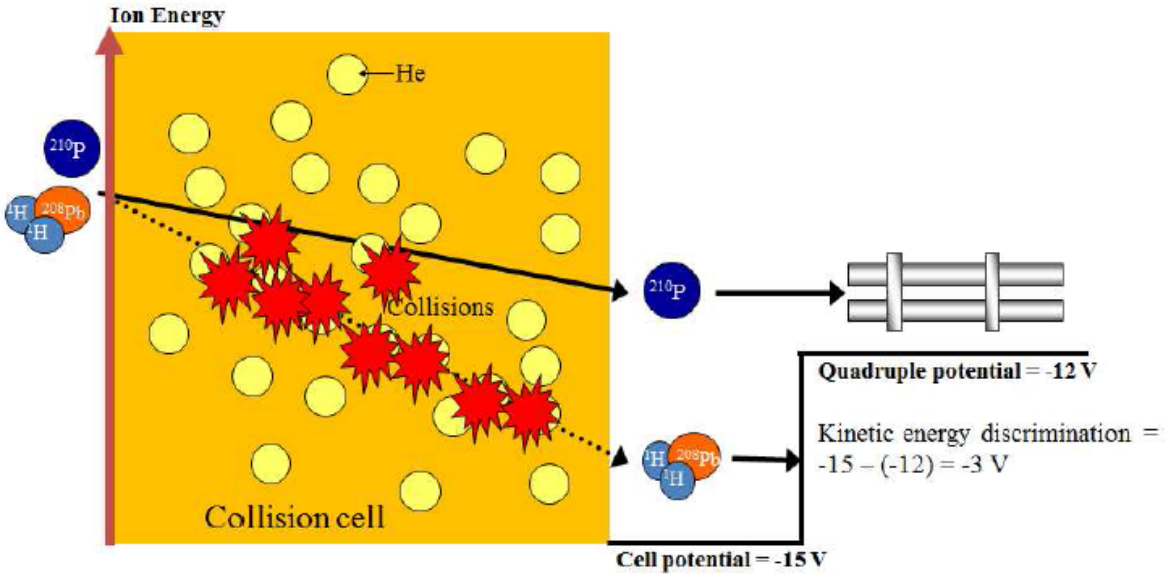

Fig 1.57 kinetic energy discrimination mechanism for collision cell ICP-MS. [113]

interfered by the white cycle. The horizontal line indicates the IPs of the potential reaction gas. The ion species above the line are exothermic and possible for charge transfer for the reaction gas. According to f**ig 1.56**, calcium and argon gas have interfered at the m/z of 40. Argon is exothermic for charge transfer with H_2 gas and

others, while calcium is endothermic to other gases. On the other hand, collision mode uses non-reactive, and the kinetic energy discriminations (KED) was used to separate based on the size selectively. The KED is usually used when the polyatomic interference is larger than the analyte, resulting in more collision than the analyte. **Fig 1.57** illustrates the kinetic energy discrimination mechanism.

Thermal Ionization Mass Spectrometry (TIMS) is famous and widely used for many inorganic isotope analyses and trace element analyses, especially on the isotope composition of calcium. As mentioned, the atomic interference of calcium measurement is caused by the argon isotope for ICP-MS measurement. Nonetheless, TIMS is based on the thermal ionization (TI), known as surface ionization, by the electric current on the metal filament (rhenium or tungsten filament). The sample is heated under the vacuum to a high temperature (400 to 2300 ℃). The production of atomic ions occurs by the electron transfer from the sample to the filament for the positive charge and opposite transfer for negative analytes [109]. The atomic beam of analyze is no longer interfered by the carrier argon gas as ICP-MS. The advantage of TIMS is the high precision measurement (‰), which results in a reference measurement for comparing calibration samples. However, TIMS is limited to the organic sample measurement and is not suitable for multi-element determination, while ICP-MS is robust and multielement analysis is employed [108].

1.7. Tritium

This research also studies the enrichment and measurement of tritium isotope. Tritium is a radioactive nuclide with a half-life of 12.32 years, emitting a beta particle at the maximum energy of 18.6 keV (**Fig 1.58**). Tritium occurs naturally when secondary cosmic rays (fast neutron) interact with a nitrogen atom in the atmosphere via ^{14}N (n, ^{3}H) ^{12}C. An average production rate of tritium is estimated to be 0.5 - 1.9 atoms/cm s [114]. Tritium can transport from the atmosphere to the earth surface through the hydrological cycle by replacing one of the hydrogen atoms in the water molecule. Not only the natural tritium but also the artificial tritium caused by atmospheric thermonuclear tests during 1953 – 1963. Tritium level in precipitation collected in Vienna (Austria) was raised up to 3177 TU [115] (1 TU corresponds to 1 tritium atom in 10^{18} hydrogen atoms and is equal to 0.118 Bq/L [116]). Furthermore, nuclear activity such as nuclear power plant operation, nuclear accidents, and the nuclear reprocessing plant could potentially be tritium sources. For example, the nuclear reactor accident at Fukushima Dai-ichi nuclear power station, Japan, on March

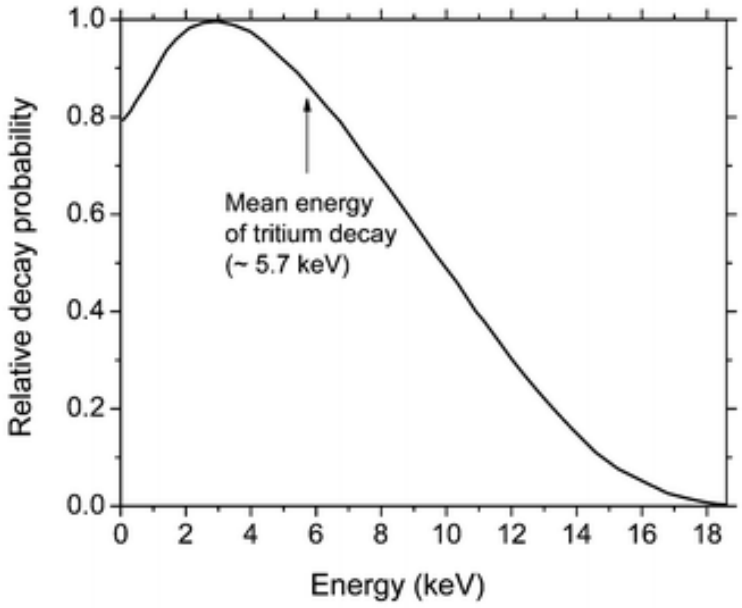

Fig 1.58 Tritium energy spectrum of beta emission [114].

11th, 2011, resulted in the sharply increasing tritium level in the rainwater sample collected at Tsukuba, approximately 30 times higher than the typical sample level [117]. The environmental survey of tritium activity concentration in natural and/or in the consumed water sources is necessary to assure the exposure of radioactive tritium to human health. Recently, however, tritium level in environmental water decreased over time and returned to normal level (Less than 0.3 Bq/L [115]) since the atmospheric thermonuclear tests were banned in 1963. The ultralow level tritium is difficult to measure without additional enrichment even using the world lowest background liquid scintillation counter, providing the limit of detection at less than 0.5 Bq/L.

This research also aims to demonstrate the baseline level of tritium concentration in environmental water, including tap water, rainwater, surface water, and groundwater collected from various regions in Thailand. This research operates under the joint international research project between the Department of Applied Radiation and Isotope, Kasetsart University, Thailand Institute of Nuclear Technology (TINT), Thailand and Department of Environmental Science and Technology, Osaka Sangyo University. The motivation of this collaboration is the nationwide survey of tritium in Thailand before the operation of firstly nuclear power plants, fuel reprocessing or heavy water production facilities. This collaboration investigated the regional distribution: latitude and longitude distribution tendencies and seasonal variations. Since Thailand is now constructing TRIGA-type Research Reactor (10000kW) at northern Ongkharak, Nakhon-nayok. Moreover, the understanding of tritium behavior and baseline level could be used to observe and improve international nuclear safety and safeguard efficiently.

1.7.1. Electrolytic enrichment of tritium

As mentioned, the measurement of tritium requires enrichment since the tritium level is now nearly the detection limit of the liquid scintillation counting (LSC) system. The most famous tritium isotope enrichment technique is the electrolytic method. Electrolytic enrichment is the easiest and acceptable method to enrich tritium in water samples. This method is based on the electrolytic reaction using the different reaction rates of a water molecule to an electric current. The water molecule containing only hydrogen atoms is easier to be electrolyzed than the molecule containing deuterium or

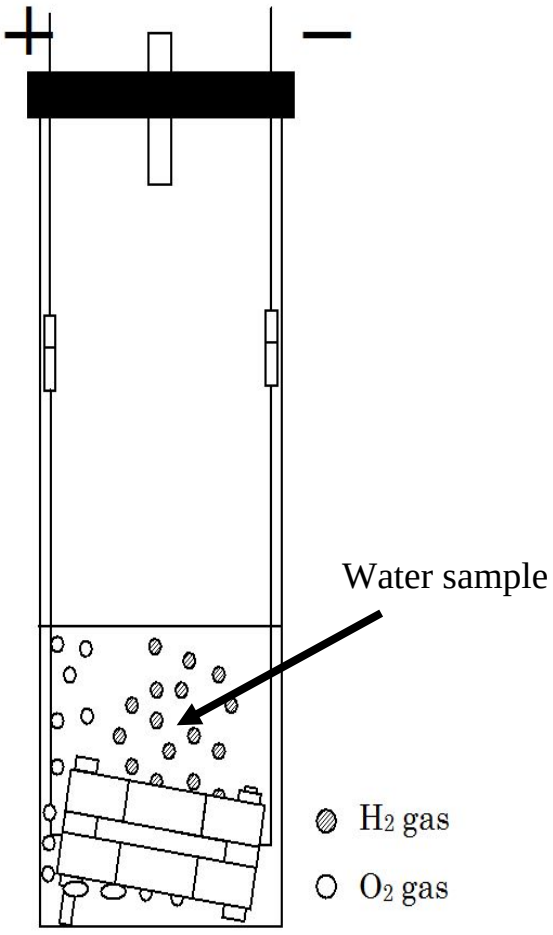

Fig 1.59 Schematic diagram of alkali electrolyte apparatus.

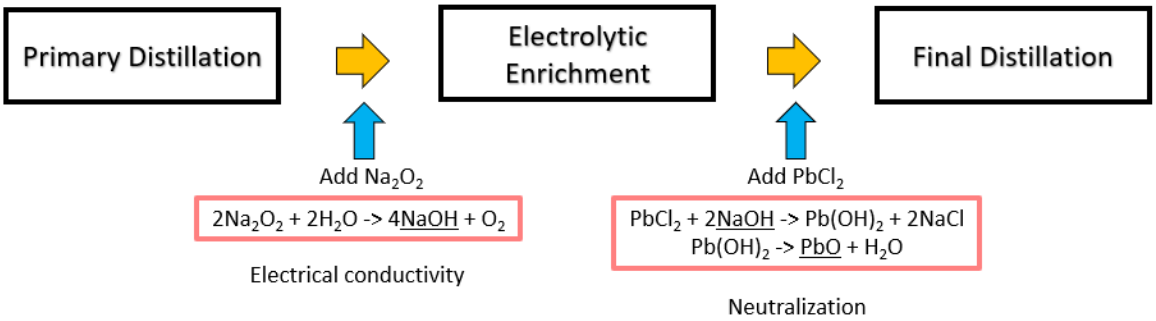

Fig 1.60 Alkali electrolyte chemical treatments and processes.

tritium atom [118]. Because electrolytic enrichment removes the water molecule containing hydrogen atoms, the tritium concentration increased after the electrolytic process was completed. The electrolytic enrichment of tritium can be classified into two methods, including alkali electrolyte and solid polymer electrolyte. As for the alkali electrolyte, it appears in the electrolytic cell. Additional reagent (Na_2O_2) is needed to add to the water sample for electrical conductivity. The advantage of the alkali electrolyte is that the electrolytic cell could be connected in series, providing several enrichments simultaneously. However, the produced gases of oxygen and hydrogen are accumulated in the same location. Therefore, to avoid the explosion caused by the

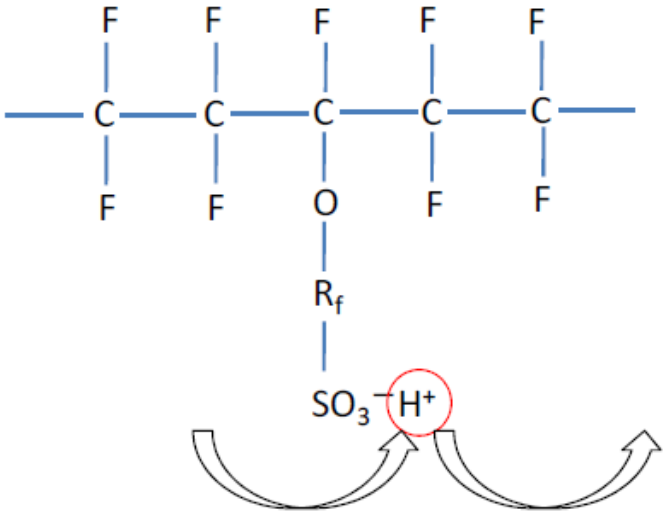

Fig 1.61 SPE film's structure and hydrogen wades through the SPE film by side chain SO_3^- group [118].

mixed gases, the electric current supply to the cell is limited. Moreover, after the enrichment is finished, the samples must be neutralized by another chemical reaction, and additional distillation is required to remove the precipitant from the water sample. **Fig 1.59 and 1.60** depicts the schematic diagram of alkali electrolyte and alkali electrolyte required chemical treatments and processes. On the other hand, the solid polymer electrolyte (SPE) film was applied to the tritium enrichment by Saito Masaaki in 1996 [119]. The SPE membrane made from the carbon-fluorine backbone chain with perfluoro sidechain contains SO_3^- group (**Fig 1.61 to 1.63**). The hydrogen ion passes through the SPE film to the cathode, receiving the electron and becoming hydrogen gas. In contrast, the oxygens ion forms the gaseous at the anode, resulting in the separation of produced gases. The advantages of SPE film over alkaline electrode are that it does not require an additional reagent for electrolysis, it acquires faster sample preparation, producing oxygen and hydrogen gas are separated, reducing the risk of explosion, high electric current is allowed for enrichment, and the enrichment factor is not limited, depending on sample volume. [118]. However, the disadvantage of SPE film is that the

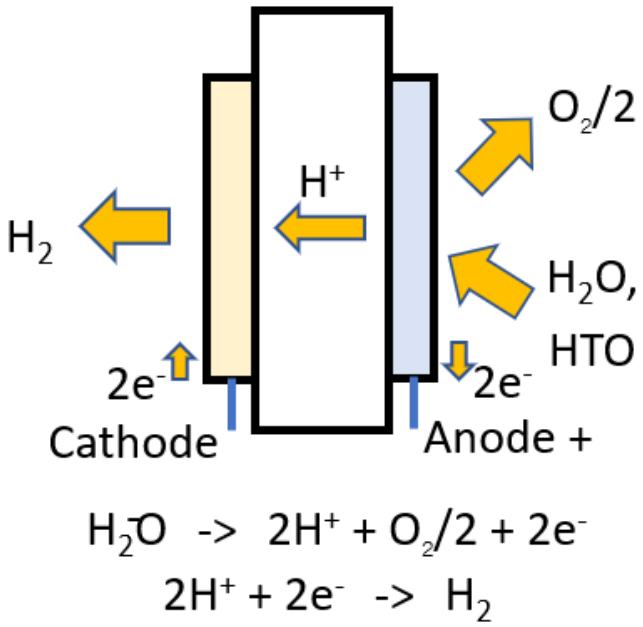

Fig 1.62 Electrolytic enrichment by SPE film.

sample can be introduced and enriched one by one. The tritium recovery factor (R) and enrichment factor (α) was determined by the following equation 1.15 and 1.16:

$$R = \frac{T_f V_f}{T_i V_i} \tag{1.15}$$

$$\alpha = \frac{T_f}{T_i} \tag{1.16}$$

where T is the tritium activity concentration (Bq/L), and V indicates the water sample volume. The subscripts f and i demonstrate the water sample after and before enrichment, respectively.

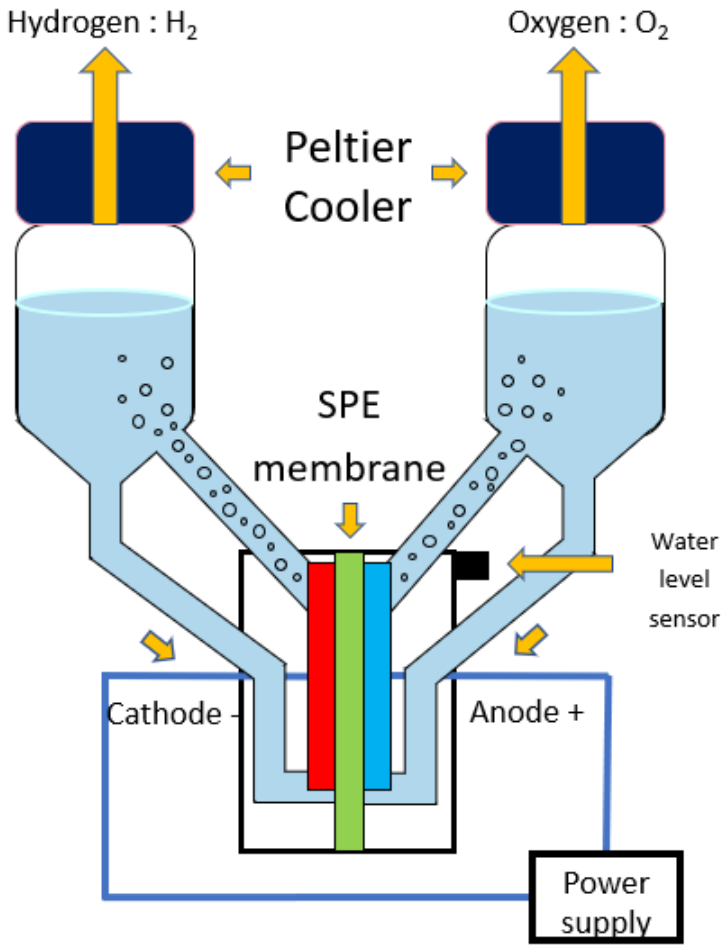

Fig 1.63 Schematic diagram of electrolytic enrichment by SPE film.

1.7.2. Tritium measurement by liquid scintillation counting (LSC)

There are various methods for radioactive analysis depending on the type of radiation emitted from the radioactive source. The appropriate method for radiation detection and measurement is necessary. For example, gas ionization is based on the interaction between radiation and gas. A proportional counter is a gas-filled detector with a property of the signal corresponding to the radiation energy. Geiger-Mueller counter, the most firstly developed radiation detector. Semiconductor detector allows the measurement of electromagnetic radiation such as gamma or X-ray and the multi-channel analyzer. In this research of tritium measurement, the most efficient and useful measurement of tritium (beta emission) is scintillation counting. However, tritium in the environmental sample occurs in liquid form. Therefore, liquid scintillation counting (LSC) is introduced.

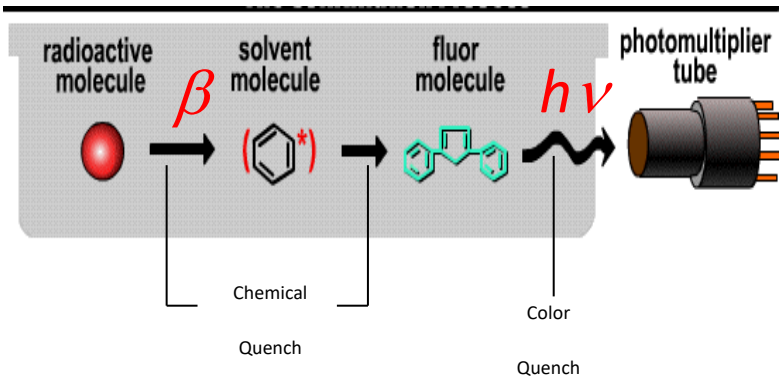

Fig 1.64 Kinetic energy transfer from emitted radiation to light emission.

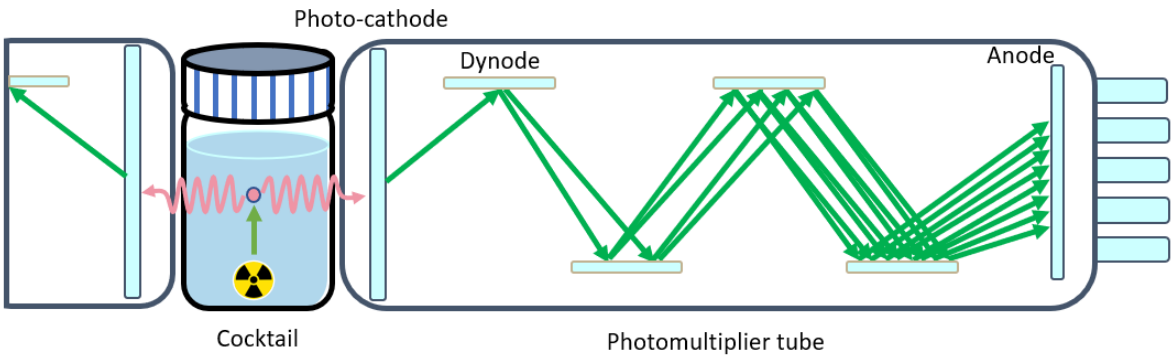

Fig 1.65 liquid scintillation counting mechanism.

Liquid-scintillation counting (LSC) is the type of scintillation counting widely applied to the radioactive material that can be dissolved as part of the scintillator solution. The scintillation detector is based on the scintillation light produced in a particular material. The light emission occurs by the kinetic energy transfer from the radiation and is proportional to the radiation energy. The scintillator should have an excellent kinetic energy transfer property, linear conversion to light energy, transparency for delivering the produced light to the detector, and good detection efficiency [119]. In the case of liquid scintillation, the water sample was homogeneously mixed with the organic scintillation solution, called the scintillation cocktail. The liquid scintillation provides a good detection efficiency since the sample and scintillator are mixed. The aromatic ring of the solvent molecule receives the energy from the beta particle. It transfers the energy to the primary scintillator, and the fluor molecule emits the photon in a visible light wave range. The emitted light is converted to electrons by the photocathode of the photomultiplier tubes (PM tubes) (**Fig1.64 and**

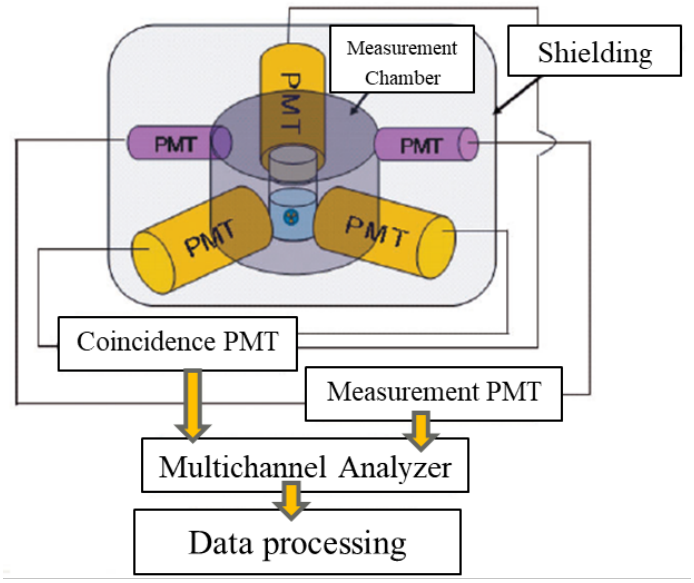

Fig 1.66 LSC LB7 schematic diagram.

1.65). The technique is used to count low-level beta activity such as that from carbon-14 (^{14}C) or tritium.

In this research, we introduce the low background Liquid Scintillation Counting (Hitachi Aloka AccuFLEX LSC-LB7), one of the best performance low-background LSC in the world. It provides the maximum counting efficiency of unquenching tritium samples up to 60%. The LSC LB-7 consists of two photomultiplier tubes, triple coincidence photomultiplier tubes, active and passive shields. Triple coincidence photomultiplier tube provides better signal discrimination than only double photomultiplier tube, resulting in the lower detection limit at 1000 minutes measurement of 0.4 Bq/L. **Fig 1.66 and Fig 1.67** illustrate the schematic diagram of LSC LB7 and compare the detection limit of the double and triple photomultiplier tube system.

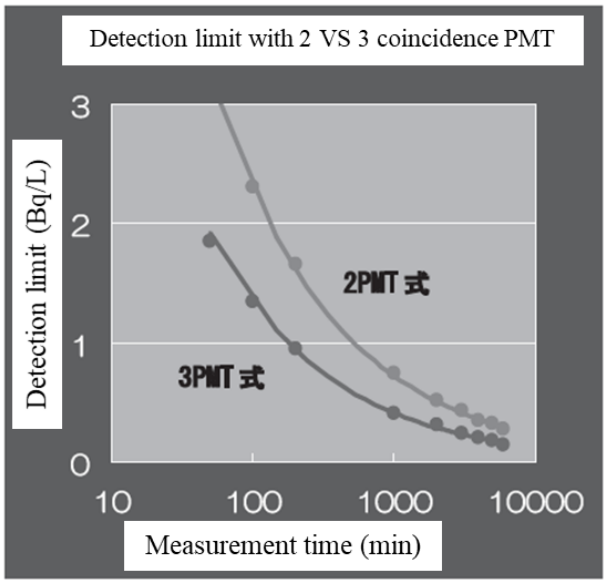

Fig 1.67 Comparison of tritium detection limit between double and triple photomultiplier tube system.

CHAPTER TWO: Material and method

2.1. Introduction

This chapter deals with the material and method, which was carried out to study isotope enrichment and mass production. As mentioned in the introduction chapter, the chemical exchange reaction was used to study the isotope separation of calcium and lithium. Meanwhile, the electrolytic method was applied to the enrichment of tritium. Section 2.2 presents the material and the method of chemical exchange isotope separation of calcium and lithium using liquid-liquid extraction. This section consists of the conditions of chemical exchange, the frame of the study, the ion content analysis using atomic absorption spectrometry (AAS), and isotope analysis using ICP-MS. Section 2.2 mainly describes the electrolytic enrichment of tritium and ultralow-level measurement using LSC.

Materials and instruments

1) DC18C6 crown-ether (98% purity), Sigma Aldrich (Germany).
2) 18C6 crown-ether (98% purity), Sigma Aldrich (Germany).
3) Chloroform ($CHCl_3$, > 99% purity), FUJIFILM Wako Pure Chemical Industries, Ltd. (Japan).
4) Calcium chloride dihydrate ($CaCl_2 \cdot 2H_2O$ > 99% purity), FUJIFILM Wako Pure Chemical Industries, Ltd. (Japan).
5) Hydrochloric acid (HCl, 35% – 37%), FUJIFILM Wako Pure Chemical Industries, Ltd. (Japan).
6) Nitric acid (HNO_3, 68%), Tama Chemicals Co., Ltd (Japan)
7) Standard reference material SRM 915b ($CaCO_3$), NIST (US)
8) Ca standard solution Ca 1000, FUJIFILM Wako Pure Chemical Industries, Ltd. (Japan).
9) Li standard solution Li 1000, Nacalai Tesque Inc. (Japan)

10) Chloride standard solution, Sigma Aldrich (Germany)
11) Spike lithium samples with various ^{7}Li concentrations, including 94.14%, 96.35%, and 98.20%, were obtained from the Tokyo Institute of Technology (Japan).
12) 1 mol / L sodium carbonate solution, KANTO CHEMICAL CO., INC (Japan)
13) 1 mol / L sodium bicarbonate solution, KANTO CHEMICAL CO., INC (Japan)
14) Milli-Q water purification system, Merck Millipore (US)
15) Magnetic stirrer
16) 50 mL, and 100 mL wide-mouthed PP container, AS ONE CORPORATION (Japan)
17) 14 mL PP container, Maruem (Japan)
18) 250 mL amber reagent glass bottle, AS ONE CORPORATION (Japan)
19) Separation filter (No.2S) size 150Φmm, Advantech Toyo Co., Ltd. (Japan)
20) ICP-MS tuning solution, Agilent technologies (US)
21) Atomic absorption spectroscopy (AAS: AA-6800), Shimadzu CORPORATION (Japan)
22) Ion chromatography (Dionex IC system-1100), Thermo Scientific (US)
23) Inductively coupled plasma mass spectrometer (ICP-MS: Agilent 7900), Agilent Technologies (US)
24) Thermal ionization mass spectrometer (TIMS: TRITON X, and MAT261) Thermo Scientific (US), and Finnigan MAT (US)

2.2. Liquid-liquid extraction (LLE)

In this research, liquid-liquid extraction was carried out to determine the isotope fractionation and study the enrichment feasibility using crown-ether (DC18C6). **Fig 2.1** shows the single-stage extraction and back-extraction process. Feed solutions (aqueous phase: AP) is $CaCl_2$ for calcium extraction and LiCl for lithium extraction. The organic phase (OP) contains DC18C6 crown-ether (CE) was used as an extractant. Both aqueous and organic phases were mixed in the 200 mL Erlenmeyer flask using a magnetic stirrer with the volume ratio of 1/10 (20mL/200mL) (**Fig 2.2**). The mixing solutions were kept in a 500 mL separation funnel for a complete phase separation for 10 minutes. The loaded organic solution was back extracted by stripping with pure water with the same volume ratio for 10 minutes using magnetic stirrer. The mixing solution was kept in the 500 mL separation funnel for 10 minutes for a complete phase separation for 10 minutes (**Fig 2.3**). The aqueous solutions, including feed, extracted (raffinate), and back-extracted phase, were diluted to the appropriate concentration and

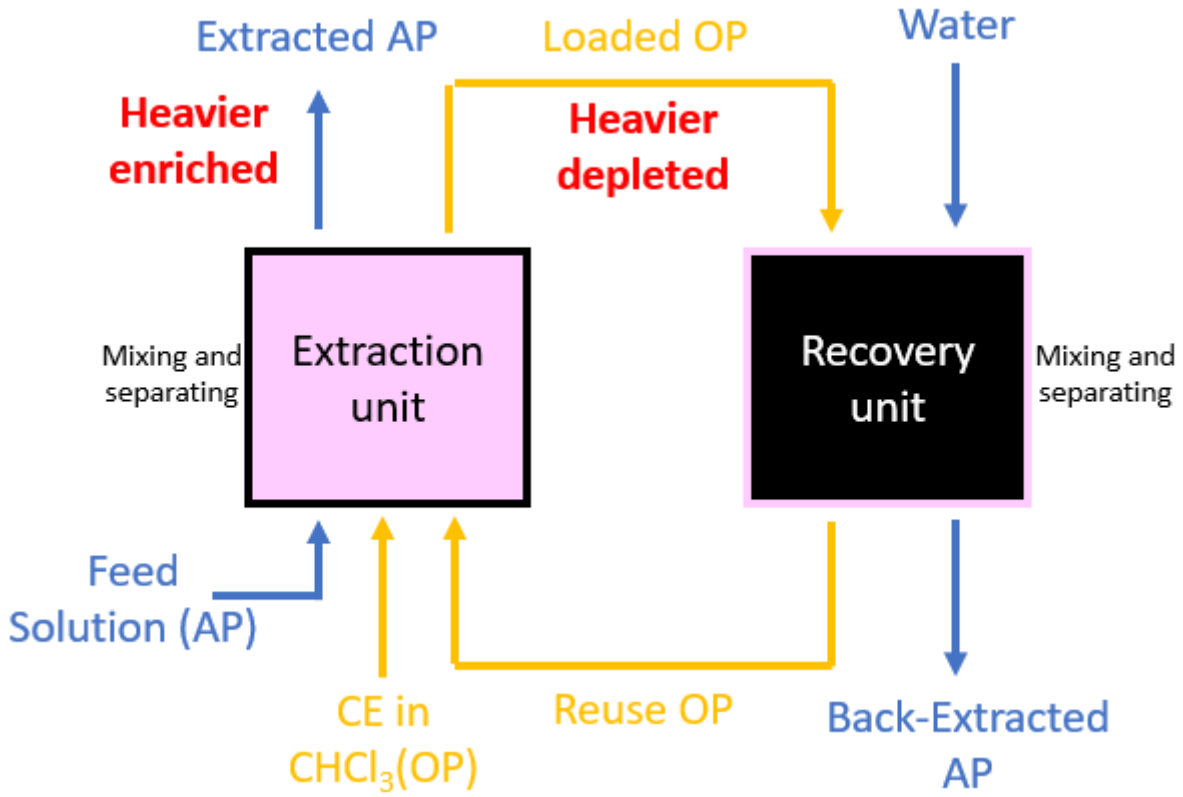

Fig 2.1 Single-stage liquid-liquid extraction

Fig 2.2 The mixing of organic and aqueous phase by magnetic stirrer

measured the cation content using atomic absorption spectroscopy (AAS: AA-6800), Shimadzu (Japan). The anion contribution was measured by ion chromatography (Dionex IC system-1100), Thermo Scientific (USA). The isotope composition was determined by reaction-cell Inductively coupled plasma mass spectrometer (ICP-MS: Agilent 7900), Agilent Technologies (USA), Thermal ionization mass spectrometer (TIMS: TRITON X, and MAT261), Thermo Scientific (USA), and Finnigan MAT (USA).

Several fundamental factors were examined to investigate the isotope effect and estimate the isotope enrichment feasibility. The following conditions investigated the frame of the study.

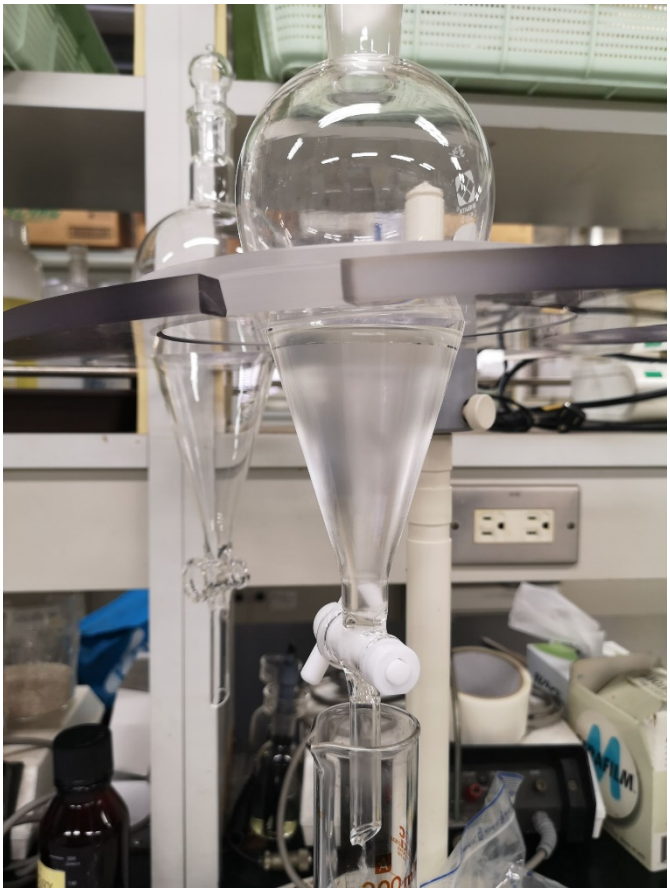

Fig 2.3 Phase separation in separation funnel

1) The presence and the absence of crown-ether

Purpose: To confirm the chemical reaction between calcium/lithium to DC18C6 crown-ether in the organic solution.

For the presence of the crown-ether system, the organic phase was 200 mL of 0.07M DC18C6 dissolved in chloroform. On the other hand, the absence of a crown-ether system was only chloroform. The aqueous solution was 20 mL 3.3 M $CaCl_2$ (aq) (30% w/w), and 8.4 M LiCl (aq) (30% w/w). The extraction time was 1 minute and 10 minutes for back-extraction. Each standing time is 10 minutes in the separation funnel. The extraction was performed at room temperature. Moreover, the back extraction was performed at least twice to assure that all the ion was back-extracted from the crown-ether completely.

2) Extraction time

Purpose: To investigate the minimal time required to make the chemical reaction equilibria.

To investigate the chemical reaction between crown-ether and calcium/lithium ion at equilibrium, the various extraction time was examined. Also, the extraction time must be short of estimating the isotope enrichment and mass production via LLE. Therefore, the minimum time required could potentially improve the enrichment process. This research tested the various extraction times from 1 sec, 1, 10, 30, and 60 minutes. The back-extraction time was fixed at 10 minutes.

3) Aqueous phase concentration

Purpose: To find the optimal concentration for the best extraction efficiency and investigate the isotope effect on various aqueous phase concentration

The appropriate condition of aqueous phase concentration is one of the primary factors in LLE. Because that the extraction efficiency is dependent on the aqueous solution concentration. The calcium and lithium concentrations were investigated by 10%, 15%, 20%, 25%, 30%, and 40% w/w aqueous solution. Other factors such as crown-ether concentration, extraction time, and extraction temperature are fixed at the same condition.

4) Acidity solvent extraction system

Purpose: To confirm the behavior of crown-ether absorption to calcium/lithium ion under the acidity solution.

According to the crown-ether resin chromatographic method, this method required a high concentration of HCl or HBr solvent to observe calcium absorption to crown-ether. This research on LLE using crown-ether was performed under the same

idea. The use of HCl acid was investigated to observe the acidity solvent under various aqueous phase concentrations. 12M HCl acid was used as a solvent of 10, 20, and 30% w/w system of calcium extraction ($CaCl_2$ (HCl)). At the same time, 0.3, 3, and 30% were performed for lithium extraction (LiCl (HCl)). The additional measurement of the anion contribution was carried out by ion chromatography to compare aqueous solvent and HCl solvent. The ratio of anion/cation was investigated.

5) Volume ratio extraction system

Purpose: To find the appropriate volume ratio suitable for isotope separation and production

The various volume ratios of extraction conditions were investigated to find the optimal conditions for the chemical exchange and isotope fractionation. This section also estimates the calculated results depending on the extracted ion. We expected the isotope fractionation in the extracted aqueous phase in this experiment. Furthermore, the smaller aqueous phase volume was applied for the separation techniques using

Fig 2.4 Phase separation using filter

separation filter (No.2S) because the separation funnel is inappreciable for the small volume extraction. Therefore, the filter separation (**Fig 2.4**) on various aqueous phase concentrations was carried out and compared to the separation funnel.

6) Extraction temperature

Purpose: To study the extraction temperature dependency

The single-stage extraction was investigated under various extraction temperatures. The organic (0.07M DC18C6 crown-ether) and aqueous (30% w/w) system was incubated at a constant temperature using an incubator for 1 hour. The extraction temperature was studied from -15ºC, 0ºC, 15ºC, room temperature (22±0.5ºC), 30ºC, and maximum at 45ºC. The purpose is to investigate the extraction temperature dependencies. The results could be compared to other research of the extraction dependencies to find an appropriate condition for the excellent extraction efficiency.

7) Solid-liquid extraction (SLE)

Purpose: To investigate the solid-phase extraction using organic phase containing crown-ether and improve to the other type of crown-ether with a water-soluble property such as 18C6.

The solid phase of $CaCl_2 \cdot 2H_2O$ and LiCl was applied for the extraction of calcium and lithium, respectively. The purpose is to identify the chemical reaction between crown-ether and solid-phase cation sources. This study could be applied to the water-soluble type of crown-ether, such as 18C6, for better cost-effective extraction, isotope separation and enrichment production.

8) Multistage iteration

Purpose: To study the isotope enrichment for multi-stage iteration to achieve and estimate the enrichment feasibility.

This study aims to observe the enrichment of heavier isotope (^{48}Ca) on the extracted aqueous phase (production stage) and estimate the isotope separation production. To increase the isotope fractionation in the extracted aqueous phase, the multi-stage iteration was investigated along with the measurement of calcium content in each stage, resulting in the estimation of enrichment via LLE.

9) Prospect for the enrichment of calcium and lithium isotope

This section deals with estimating mass production according to the acquired results from the above experiment. We aim to calculate the required number of iterations to achieve the ten times isotope abundance of ^{48}Ca by the first milestone of 1 gram of enriched production.

The parameters identify the extraction condition consist of three parameters, including the distribution coefficient (D), Mole ratio (η), and separation factor (α).

1) Distribution coefficient (D), as known as distribution ratio, is the ratio of the total analyte (solute) in the extract (organic) to its total analyte in the aqueous phase (aqueous). D is defined by the concentration of analyte in organic phase (M_{org}) divided by its concentration in aqueous phase (M_{aq}) (equation 2.1). D is often quoted as a measure of how well-extracted a species is.

$$Distribution\ coefficient\ (D) = \frac{M_{org}}{M_{aq}} \quad (2.1)$$

2) Mole ratio (η) is defined as a ratio of ion-crown complex to a total crown-ether in the organic phase. η is used to determine the extraction efficiency under different

conditions, such as separation between batch and filter separation (equation 2.2). The ion-crown complex is determined as an extracted organic phase in this extraction.

$$Mole\ ratio\ (\eta) = \frac{mole\ Ion{-}crown\ complex}{mole\ total\ crown{-}ether} \tag{2.2}$$

3) Separation factor (α) is a parameter determined as an isotope ratio (R) between the aqueous phase (or organic phase) compared to feed. This parameter is a useful method to determine the isotope fractionation for each phase, shown in equation 2.3.

$$\alpha = \frac{R_{sample}}{R_{feed}} \tag{2.3}$$

where R is an isotope ratio of the concentrating isotope. This research focuses on calcium (^{48}Ca to ^{40}Ca, ^{42}Ca, ^{43}Ca, and ^{44}Ca) and lithium isotope (^{7}Li to ^{6}Li). As mentioned, the crown-ether trend to absorb the lighter isotope, therefore the isotope fractionation in the organic phase (back-extracted) is usually less than unity. On the other hand, the extracted aqueous phase (raffinate) is supposed to have a separation factor greater than unity (enrichment). Furthermore, the enrichment coefficient (ε) is identified as the current enrichment status (or isotope fractionation) after several separation stages compared to feed. It is usually expressed in permil (‰) [120] value (equation 2.4).

$$\varepsilon\ (‰) = (\alpha - 1) \times 1000 = \left[\left(\frac{R_{sample}}{R_{feed}}\right) - 1\right] \times 1000 \tag{2.4}$$

2.3. Ion content analysis

This section describes the cation content analysis by atomic absorption spectroscopy (AAS: AA-6800), Shimadzu CORPORATION (Japan), and anion analysis by Ion chromatography (Dionex IC system-1100), Thermo Scientific (US) at Osaka Sangyo University, Daito, Osaka. AAS uses the principle that atoms can absorb light at a specific, and unique wavelength, resulting to the quantitatively analysis of ion concentration in the unknown sample (**Fig 2.5**). AAS provides a robust and laborless method with good accuracy measurement. AA-6800 could perform a real-time background correction using the deuterium (D) lamp method for calcium measurement at the wavelength of 190 – 430 nm (λ_{Ca} = 422.7 nm). This advantage results in the easy and uncomplicated measurement of calcium. However, the lithium required a careful correction of the background signal because the wavelength of

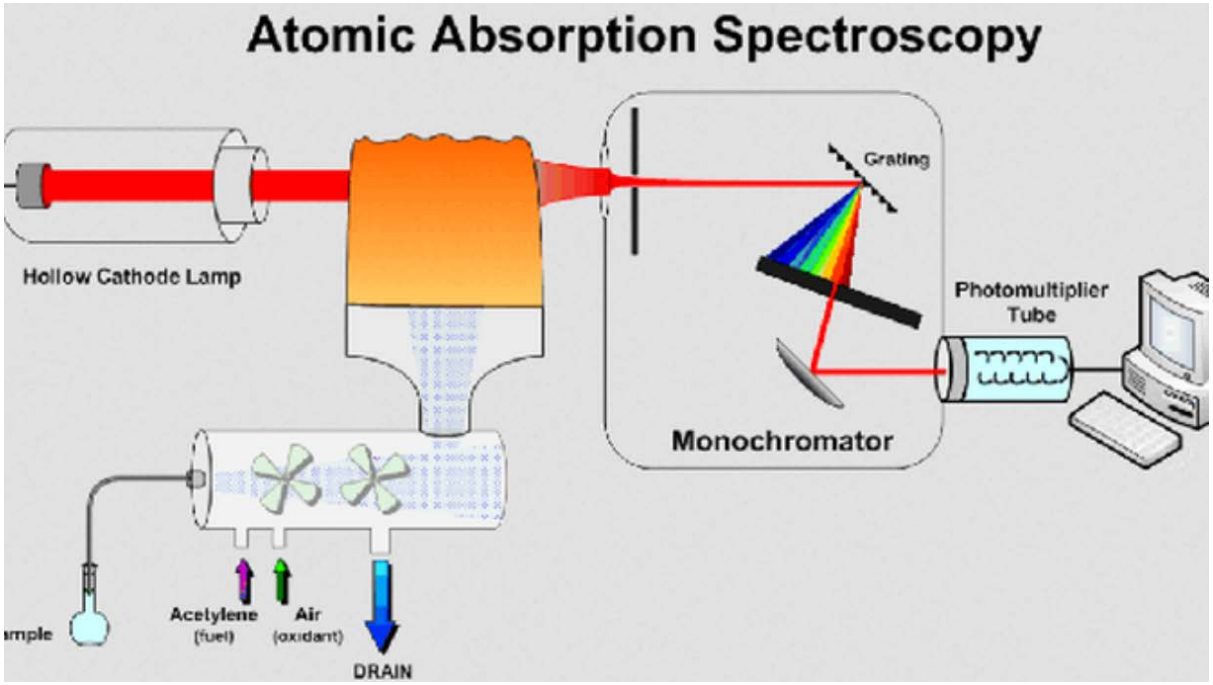

Fig 2.5 Atomic absorption spectroscopy [121]

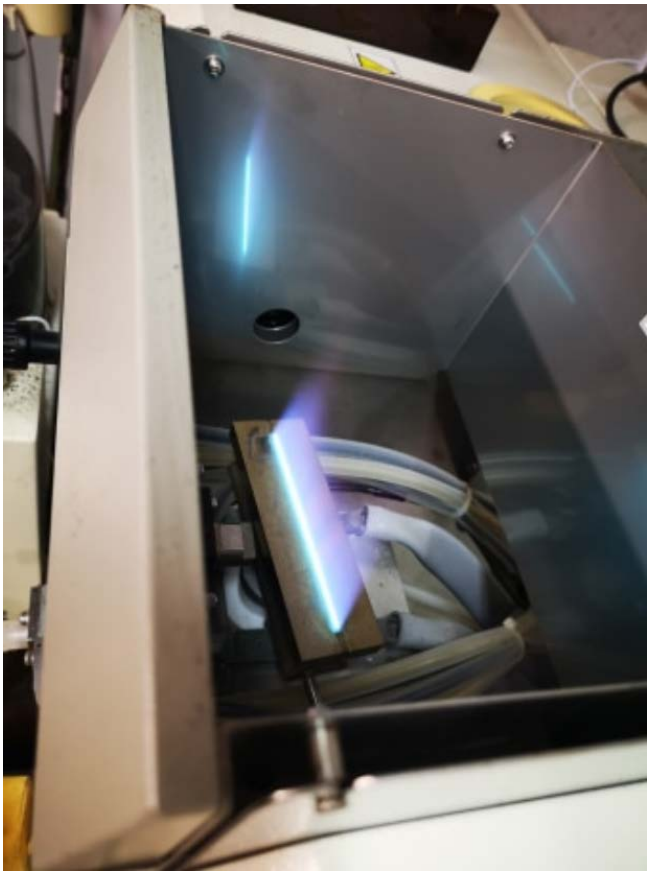

Fig 2.6 Oxide acetylene flame of AAS AA-6800

lithium absorption is out of the range of deuterium lamp (λ_{Li} = 670.8 nm) [122]. The measurement mode was set at flame AAS using oxide-acetylene flame at high temperature (**Fig 2.6**).

The standard calibration samples were prepared at various concentrations, ranging from 0.5, 1, 2.5, 5, and 10 ppm for calcium measurement using standard calcium solution Ca 1000, FUJIFILM Wako Pure Chemical Industries, Ltd. (Japan). In the case of lithium, the calibration curve was determined by 0.1, 0.5, 1, 2.5, and 5 ppm concentration using standard lithium solution (Li 1000, Nacalai Tesque Inc. (Japan)). The reason is that the sensitivity of AAS measurement on lithium is higher than the calcium, and to avoid the memory effect, only low concentration is allowed. Furthermore, all samples must be diluted within the range of calibration sample concentration for improved measurement accuracy and reliability. Every measurement was determined by the relative sample concentration (ppm) and atomic

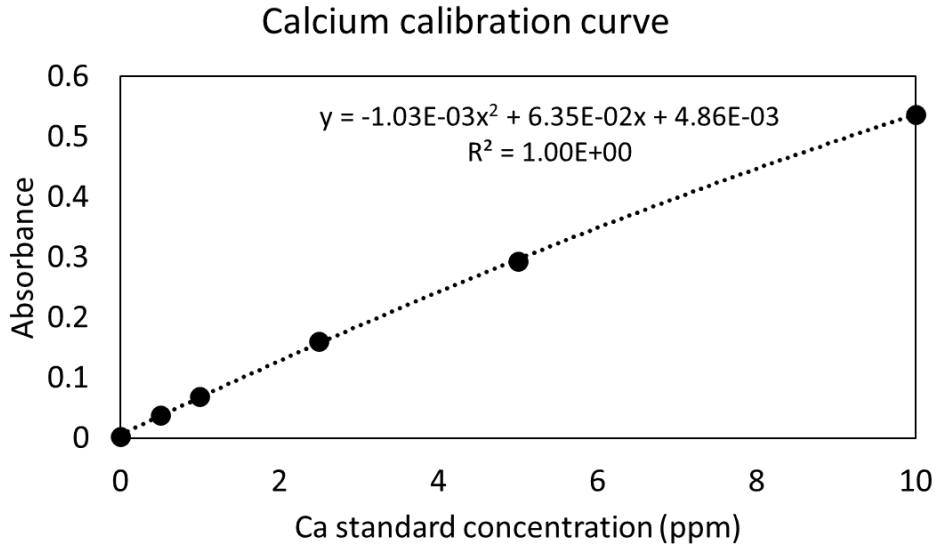

Fig 2.7 Example for the calcium calibration curve

(0 (water), 0.5, 1, 2.5, 5, and 10 ppm)

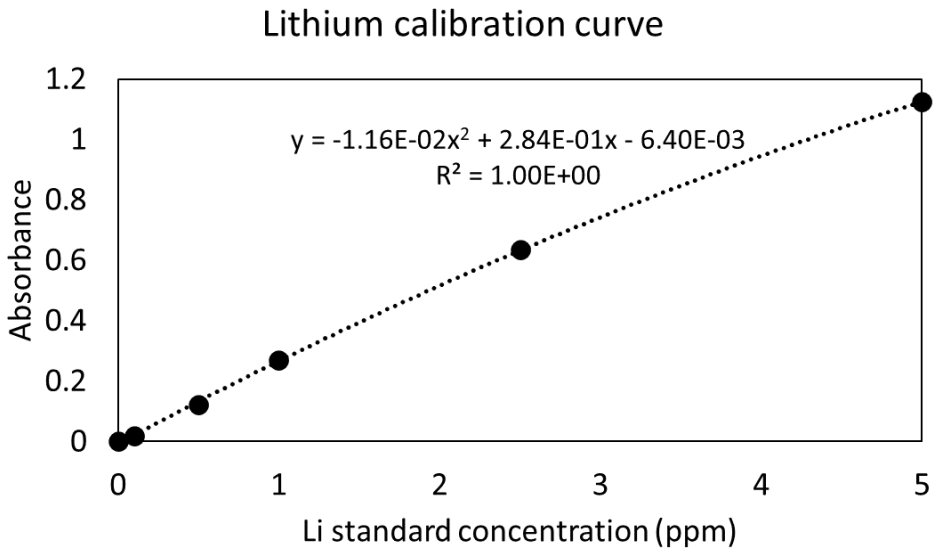

Fig 2.8 Example for the lithium calibration curve

(0 (water), 0.1, 0.5, 1, 2.5, and 5 ppm)

absorbance (abs). The second-order polynomial fitting was used to determine the equation. **Fig 2.7** and **Fig 2.8** show examples of the calcium and lithium calibration curves, respectively. At the time of measurement, the diluted samples were fed to the AAS and waited until the signal became stable. Then the signal was recorded for 5 seconds and repeated three times for each sample (**Fig 2.9**).

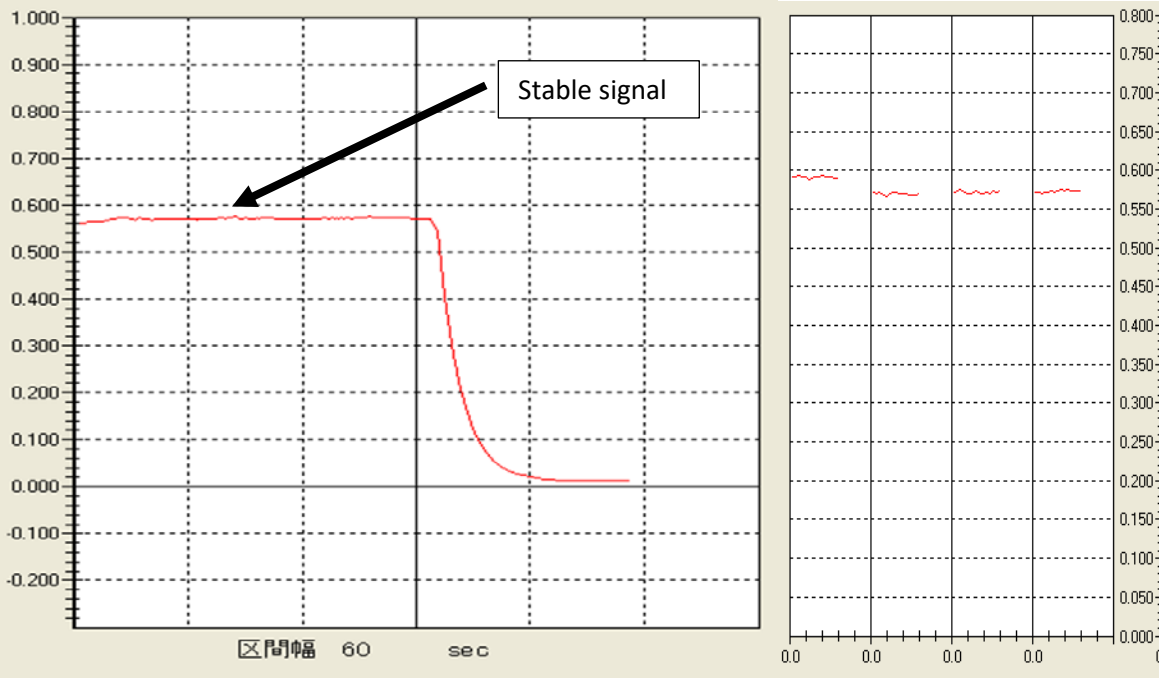

Fig 2.9 Measurement signal and signal logging

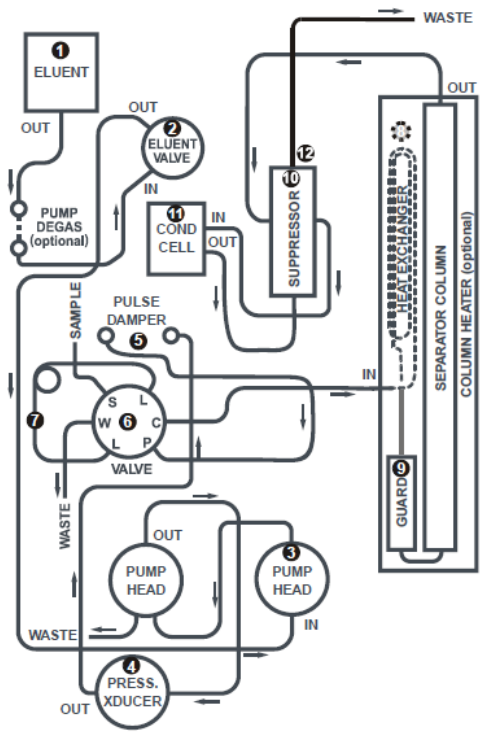

Fig 2.10 Schematic diagram of Dionex Aquion system [123]

On the other hand, the anion content, in this study is only Cl^- ion, was evaluated by ion chromatography (Dionex IC system-1100), Thermo Scientific (US). IC is a chemical separation method based on the interaction between resin (column) and the ion in the eluent. Ions move

at different speeds through the columns of the ion chromatographer depending on their affinity for the specific resin, and they separate from each other based on differences in ion charge and size. The smaller size and less in charge ion have faster mobility in the eluent. As a result, the faster ion will be eluted first. The electrical conductivity is measured after the sample pass through the column. **Fig 2.10** shows the schematic diagram of the Dionex Aquion system. The chromatogram was plotted by the conductivity and time, indicating the peak for each element depended on the eluted time. Using a calibration sample, the area under the peak (μS×min) of each known content can represent the ion content. **Fig 2.11** depicts the chromatogram of chloride standard calibration samples (0 (water), 0.1, 0.5, 1, 2.5, and 5 ppm). Moreover, to assure the total cation of Ca and Li, the measurement of the cation was conducted for a comparison to AAS. **Fig 2.12** shows the chloride, calcium, and lithium calibration curve measured by ion chromatography.

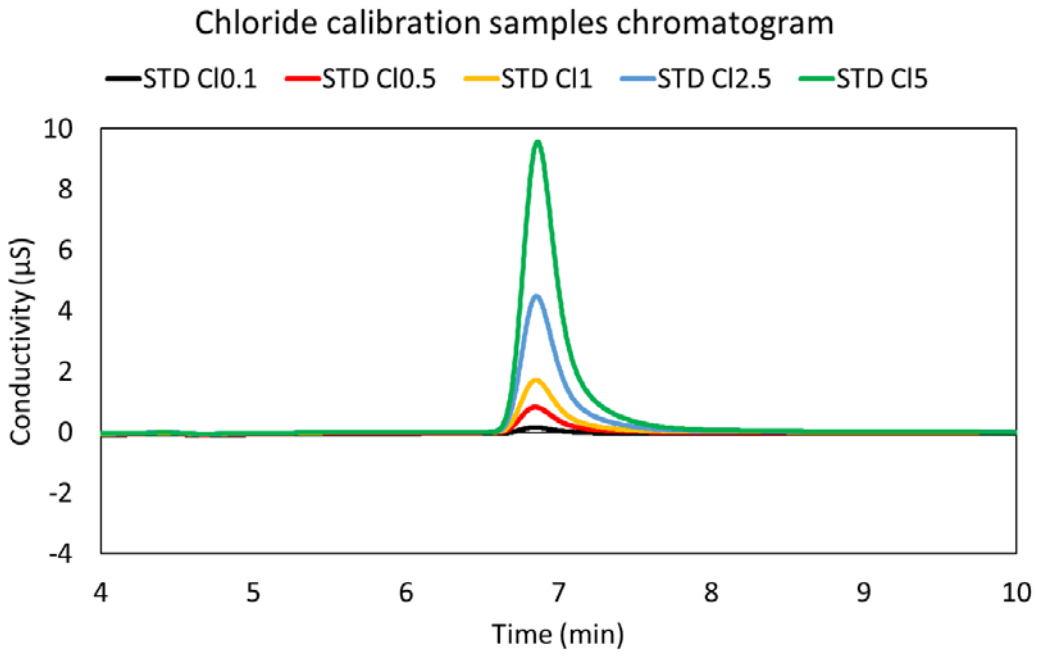

Fig 2.11 Chloride standard solution's chromatogram

(0 (water), 0.1, 0.5, 1, 2.5, and 5 ppm)

Table 2.1 The setup and order of anion, and cation measurement using Dionex AS-AP Autosampler and Dionex ICS-1100

Conditions	Anion set up	Cation set up
Column	IonPac^{TM} AS23	IonPac^{TM} CS16
Target ion	Cl^-	Ca^{2+}, Li^+
Pressure. Lower Limit	200 psi	100 psi
Pressure. Upper Limit	2500 psi	2500 psi
Inject mode	Push Partial	Push Partial
Partial cut volume	50 µL	50 µL
Cycle time	30 min	30 mins
Draw Speed	9.4 µL/sec	9.4 µL/sec
Draw Delay	2 sec	2 sec
Disp. Speed	19.2 µL/sec	19.2 µL/sec
Wash Disp. Speed	19.2 µL/sec	19.2 µL/sec
Buffer Wash Factor	2.000	2.000
Sample Height	5 mm	5 mm
Wash Volume	1000 µL	1000 µL
Inject Wash	After Inject	After Inject
Data collection rate	5 Hz	5 Hz
Cell Temperature	35 °C	40 °C
Column Temperature	35 °C	40 °C
Suppressor type	ASRS_4mm	CSRS_4mm
Suppressor current	25 mA	90 mA
Flow	1 mL/min	1 mL/min
Time	30 mins	30 mins
Eluent	4.5mM Solium Carbonate solution and 0.5mM Sodium Hydrogen carbonate solution	30mM Methanesulfonic Acid solution
Sample volume	1.5 mL	1.5 mL

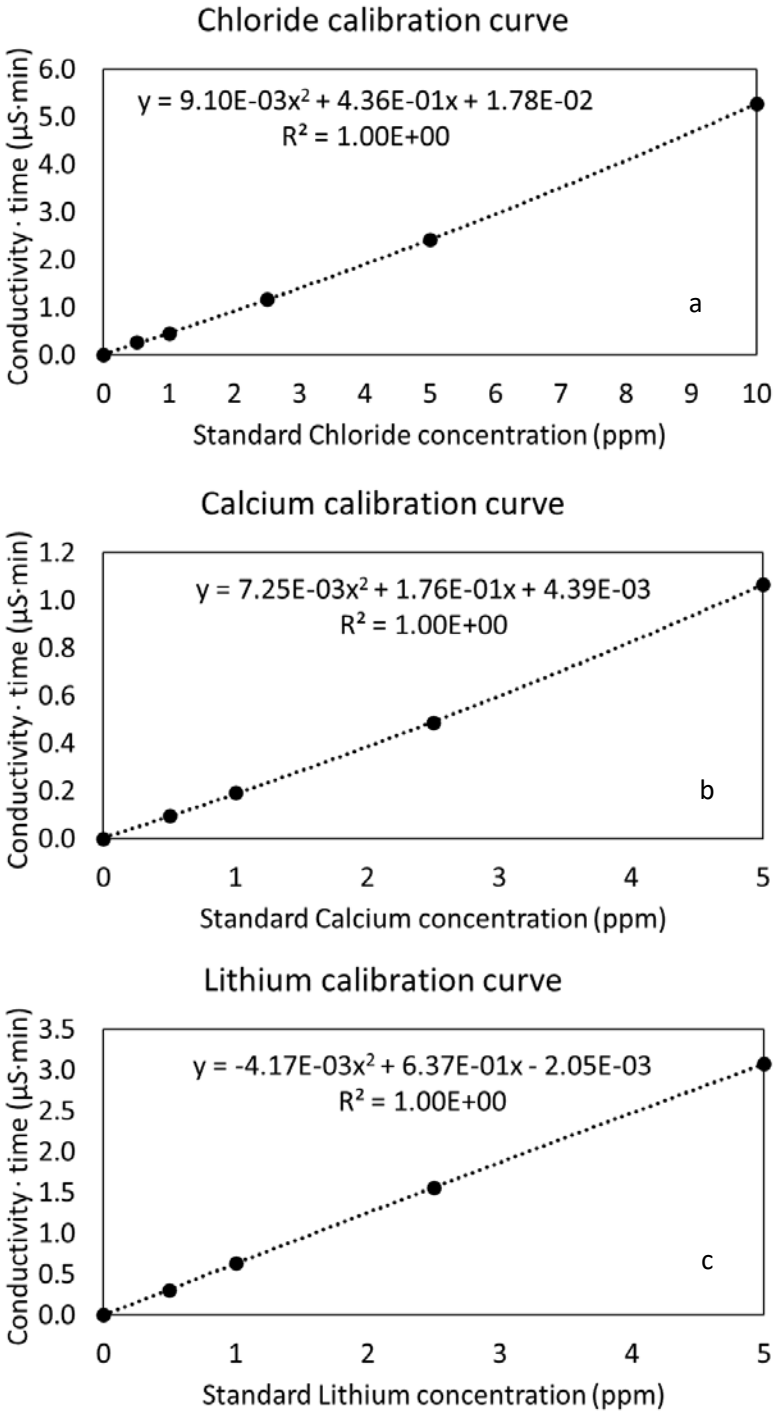

Fig 2.12 (a) chloride calibration curve (b) calcium calibration curve, and (c) lithium calibration curve measured by ion chromatography

2.4. Isotope composition analysis

This research employed the reaction-cell ICP-MS (RC-ICP-MS) (Agilent 7900) as the main analyzer for isotope composition and fractionation analysis. The following paragraphs describe the measurement conditions, criteria, and sample preparation for each measurement of calcium and lithium, respectively.

2.4.1. Calcium and lithium isotope analysis by ICP-MS (Agilent 7900)

ICP-MS carried out the isotope analysis with an additional H_2 gas as a reaction gas. The reaction gas could significantly reduce the isobaric interference of argon gas, allow the measurement of ^{40}Ca isotope. On the other hand, lithium was analyzed by no-gas mode since lithium has no atomic interference problem. However, since the ICP-MS is designed for the ultralow-level quantitative analysis of elements, the determination of isotope composition is possible under some specific conditions. To ensure the acquired data's reliability, several countermeasures and improvements were considered.

First of all, it is well known that mass bias is the most critical obstacle for the isotope analysis by ICP-MS. Mass bias is defined as the deviation of an isotope ratio, measured by ICP-MS, from the actual value for the ratio present in the sample. H. Andren et al. [124] summarized the source of mass bias on isotope analysis by ICP-MS. The report indicated several reasons for the mass bias, i.e., the supersonic expansion of the ion beam behind the sampler in case of boron analysis and the leached of metal ions from the use of extraction lenses. However, the four main reasons reveal the typical behavior of mass bias. First, the mass bias per amu decreases with increasing atomic number, resulting in higher mass bias when measuring the low mass element (>10%). Second, the mass bias depends on the ICP-MS instrument such as nebulizer, spray chamber, and cone. The third reason is the self-induced matrix effect, which is

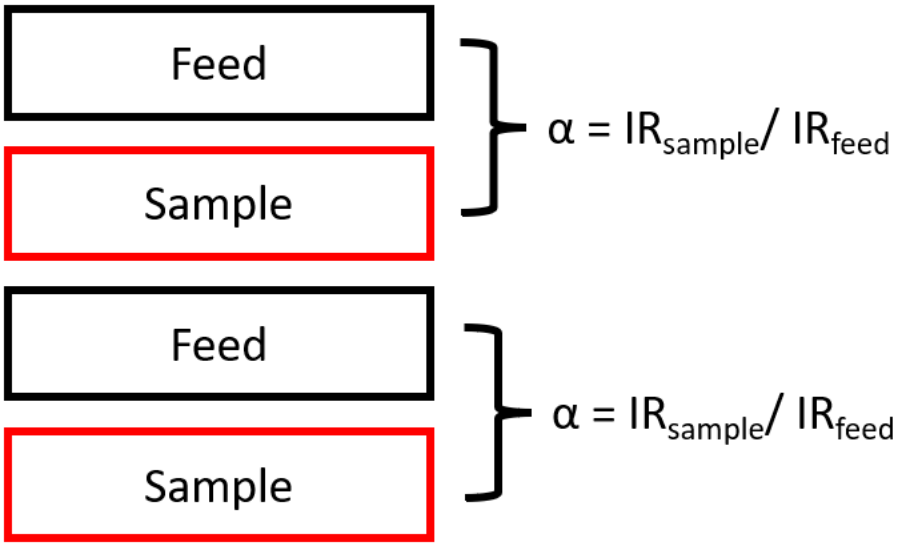

Fig 2.13 Feed sample bracketing sequence techniques and the calculation of separation factor (α)

caused by the sample type, including sample concentration, nitric acid concentration, and impurities. Finally, prolonged measurement is the last reason for mass bias [125, 126].

In conclusion, we employed the measurement of calcium isotope analysis by preparing the sample based on the following criteria. First, the calibration samples were prepared at three different concentrations, ranging from 0.1, 1, and 1.5 ppm, ensuring the mass bias concentration dependent. Then, all of the samples were prepared at one ppm to avoid the drift from the self-induced matrix effect. The nitric acid was added at 1.5 % w/w. Additionally, 5% w/w nitric acid was used to eliminate memory effect or unwanted interference in the ICP-MS measurement cleanup procedure after the measurement of each sample.

To solve the prolonged measurement problem, feed bracketing sequence techniques were applied to the measurement sequence qualifying the sample isotope ratio to the current feed sample (Fig 2.13). This technique allows the precise calculation of separation factor (α) without the mass bias caused by the prolonged measurement.

Table 2.2 The contaminant sample conditions for the observation of mass bias caused by organic solution

SN	Water (mL)	Contaminant (mL)	Dilution order*	mL of 100 ppm Ca standard solution	[Ca] ppm	$^{48/43}$IR ± σ
SN0	10	0	-	0.1	1.00	1.780±0.003
SN1	0	10	-	0.1	1.00	2.612±0.058
SN2	9	1	10^{-1}	0.1	1.00	1.809±0.004
SN3	9.9	0.1	10^{-2}	0.1	1.00	1.785±0.004
SN4	9.99	0.01	10^{-3}	0.1	1.00	1.783±0.005
SN5	9.999	0.001	10^{-4}	0.1	1.00	1.782±0.004
SN6	9.9999	0.0001	10^{-5}	0.1	1.00	1.780±0.004

*Dilution order = contaminant / solution (v/v)

Finally, the mass bias could be occupied by the sample impurity, such as the contamination of the volatile organic solvent, resulting in insufficient nebulization and plasma extinguishment [127]. To solve the problem, increase the dilution ratio with water. Nonetheless, we designed the experiment to examine the magnitude of the mass bias caused by the low dilution ratio sample. The contaminant solution (back-extracted) was obtained from the empty extraction (without calcium contribution) to ensure the same matrix as other samples. 0.1 mL 100 ppm of standard calcium solution was added, making the final concentration of all samples at one ppm. **Table 2.2** indicates the experiment condition of sample number (SN) 1 to 6. Various contaminant and dilution order was obtained and measured by ICP-MS on the no-gas mode. The results indicated that the isotope ratio of ^{48}Ca/^{43}Ca was significantly influenced by the high contaminant solution (SN1 and SN2) (**Fig 2.14**). As a result, because our sample concentration requirement is one ppm and the contamination result indicated a dilution ratio greater

than 100 folds, the unknown sample concentration must be at least 100 ppm to ensure measurement reliability.

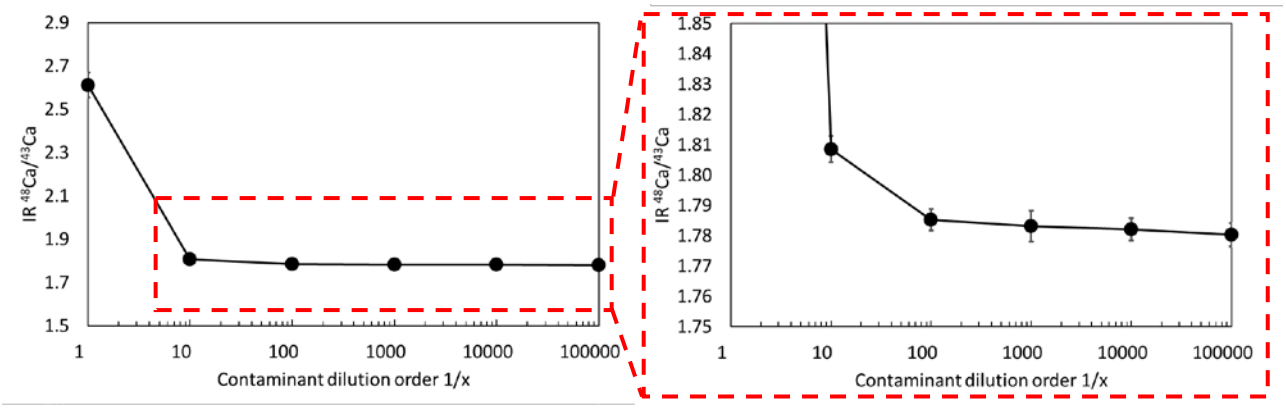

Fig 2.14 The contaminant's effect and the required dilution order

Fig 2.15 Acquire parameter panel for the setup of calcium analysis by no gas and H_2 gas mode.

The measurement software was carried out by the Mass Hunter workstation software. The preparation for analysis begins with the purging of hydrogen gas (for calcium) to the reaction cell by a flow rate of 6 mL/min for 15 minutes and 30 minutes in the case that the gas cell has not been used for a long time. Before the plasma was

ignited, the following checklists checked the hardware settings for six checkpoints at the startup pane. Then the setup was added to the queue, and the plasma was ignited.

- Hardware setting: Torch Axis
- Hardware setting: EM
- Hardware setting: Plasma correction
- Standard Lens tune
- Hardware setting: Resolution /mass axis
- Hardware setting: Performance report

Fig 2.16 Peri Pump/ISIS tap setup

After all the startup items were adjusted, the batch file was created. The setup was checked on the concentrating element and its isotope. At the acquire parameter pant, the replicates and sweeps/replicates were set at 10 and 1000, respectively (**Fig 2.15**).

At the Peri Pump/ISIS tap, the setting on Pre-Run indicates the time and nebulizer pump speed (0.3 rps) for the sample uptake (40 secs) and the waiting time (40 secs) until the signal is stable. At the Post-Run, the probe rinse for sample and standard was set at 10 secs at 0.3 rps nebulizer speed. The rinse port at 5% nitric acid and pure water port was set for 60 secs at 0.1 rps nebulizer speed (**Fig 2.16**). **Fig 2.17** depicts the tuning tap of H_2 gas with the flow rate of 6 mL/min and the energy discrimination of 3V.

After that, we selected the autotune by the ICP-MS tuning solution, Agilent technologies (US). Autotune provides a basic optimization parameter of ICP-MS. The autotune optimized the analysis using the isobaric numbers 59, 59, and 205 for H_2 gas mode adjustment. In the case of the analytes tap, it allows the adjustment of concentrating isotope and the measurement display of quantitative report. The full quant tap sets the calibration curve parameters for quantitative analysis. This research made the calibration samples for 4 points, including 0 (water), 0.5, 1, and 1.5 ppm for calcium measurement, and 5, 10, and 15 ppb for lithium analysis (**Fig 2.18**).

The following paragraph describes the calculation of each isotope analysis of calcium and lithium and the criteria to assure the obtained result. The obtained data were analyzed by ten replications data for each isotope counting signal. Signal to noise ratio (S/N) was determined by the various concentration, ranging from 0.5, 1, and 1.5 ppm and 5, 10, and 15 ppb for lithium analysis. The S/N ratio at the analyte concentration (1 ppm and 10 ppb) was demonstrated using the calibration samples signal and the background signal (water) before and after measuring those calibration samples. The purpose of background measurement is to ensure that the memory effect is insignificant. The S/N ratio for each signal counting was assured to be higher than 100 folds to omit the background correction. **Table 2.3** shows the S/N ratio

demonstration of ^{40}Ca and ^{7}Li analysis. Even the uncertainty value (%RSD) of calcium is larger than the lithium measurement, but the calculation of separation factor by a single collector ICP-MS was dependent on the counting uncertainty. However, the better measurement required a better accuracy. The improvement on the peri pump would solve the larger uncertainty problem.

Fig 2.17 The tune tap of H_2 gas mode

Fig 2.18 Full quant tap

Table 2.3 The example of S/N ratio demonstration of ^{40}Ca and ^{7}Li analysis

Sample	cps	σ	%RSD	BG (cps)[a]	BG (σ)[b]	S/N[c]
^{40}Ca calibration sample signal						
Ca 0 ppm (Water)[d]	39434	488	1.2%			
Ca 0.5 ppm	9100159	227993	2.5%			213
Ca 1 ppm	17011731	273451	1.6%	42676	3348	399
Ca 1.5 ppm	27894729	887553	3.2%			654
BG (Water)[d]	45918	264	0.6%			
^{7}Li calibration sample signal						
Li 0 ppb (Water)[d]	1475	8	0.5%			
Li 5 ppb	267595	934	0.3%			188
Li 10 ppb	539415	1272	0.2%	1425	80	379
Li 10 ppb	805412	1948	0.2%			565
BG (Water)[d]	1374	88	6.4%			

[a] Average BG count from water samples before and after calibration sample
[b] Standard deviation of BG count from water samples before and after calibration sample
[c] S/N ratio = C_{Sample} / C_{BG}: C = counting signal
[d] double distilled water

The isotope ratio (IR) was calculated by the counting signal of each isotope pair. For example, the average $^{48/40}$IR was calculated from each counting signal of ^{48}Ca and ^{40}Ca for each replication in calcium analysis. The IR is determined by the following equation 2.4.

$$^{H/L}IR = \frac{C_H}{C_L} \tag{2.4}$$

where IR is the isotope ratio (counting ratio) of concentrating isotope pair. The superscription (H/L) indicated the counting signal ratio from heavier isotope to lighter isotope. The C indicates the counting signal at a constant sample concentration. The

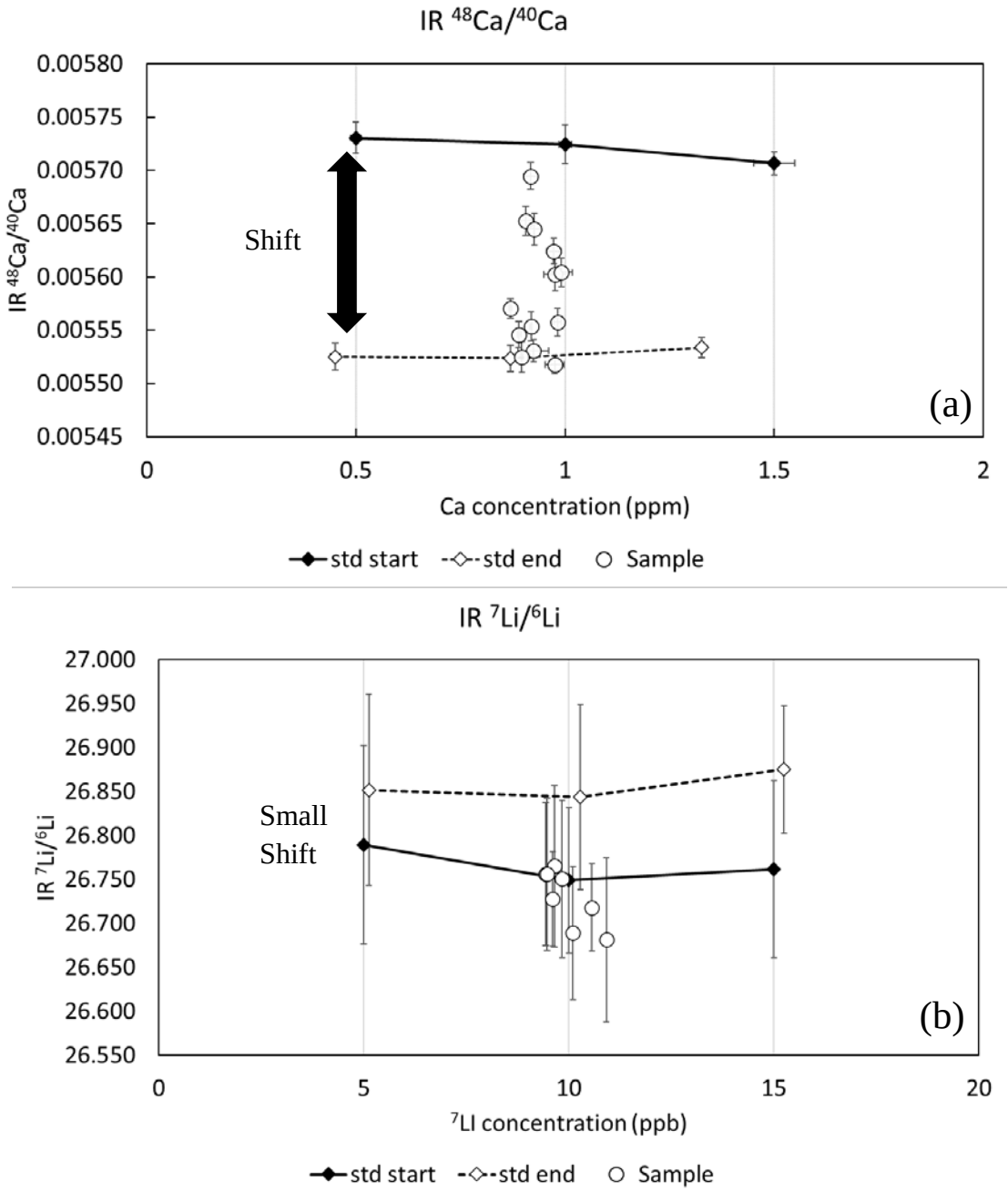

Fig 2.19 The example of measured concentration dependency of

(a) calcium and $^{48/40}$IR, (b) lithium and $^{7/6}$IR

next criteria to assure the data reliability is the observation of mass bias. As mentioned, mass bias depends on the self-induced matrix effect and time dependence. To avoid the self-induced matrix effect, we provided the measurement at the same concentration as much as possible. **Fig 2.19 (a)** shows the example of the measured concentration of calcium analysis between $^{48/40}$IR of calibration samples (0.5, 1, and 1.5 ppm) and the

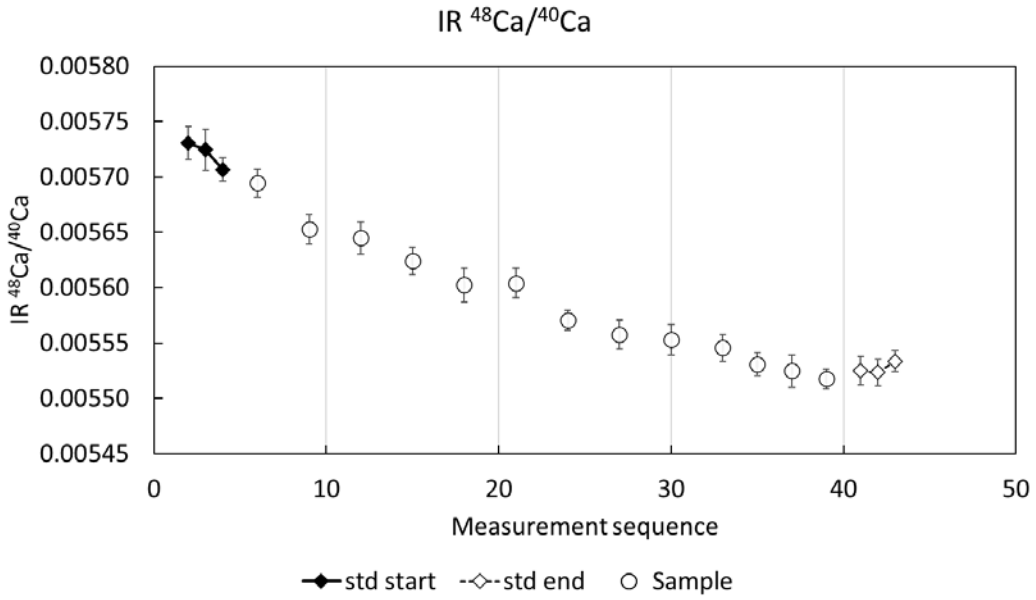

Fig 2.20 The example of measurement sequence and calcium and $^{48/40}$IR

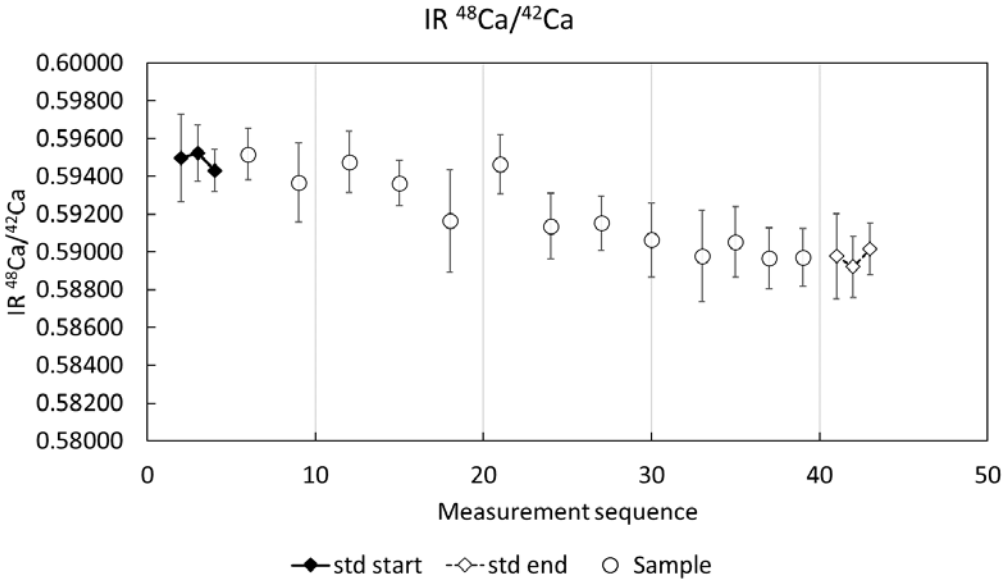

Fig 2.21 The example of measurement sequence and calcium $^{48/42}$IR

other feed samples at 1.0 ± 0.2 ppm. The sample was prepared according to the AAS results analysis. The result indicated the dependencies on IR was observed as increasing of calcium concentration as decreasing of IR. Here is why we need to prepare the sample at the same concentration. **Fig 2.19 (a)** also indicated the mass bias problem under the prolonged measurement. It was noted that the prolonged measurement was

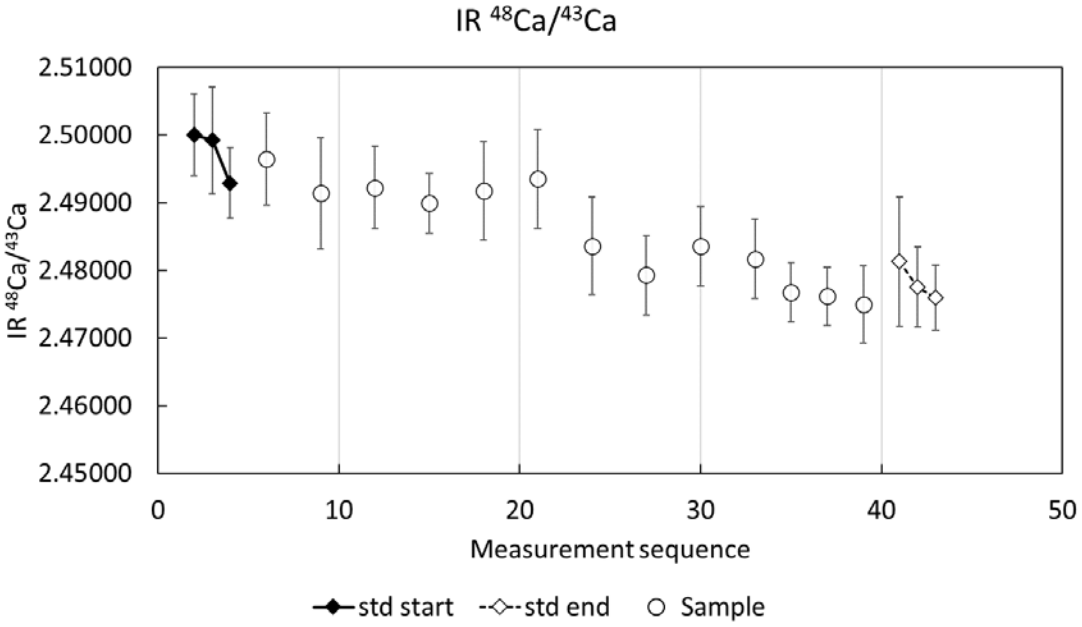

Fig 2.22 The example of measurement sequence and calcium $^{48/43}$IR

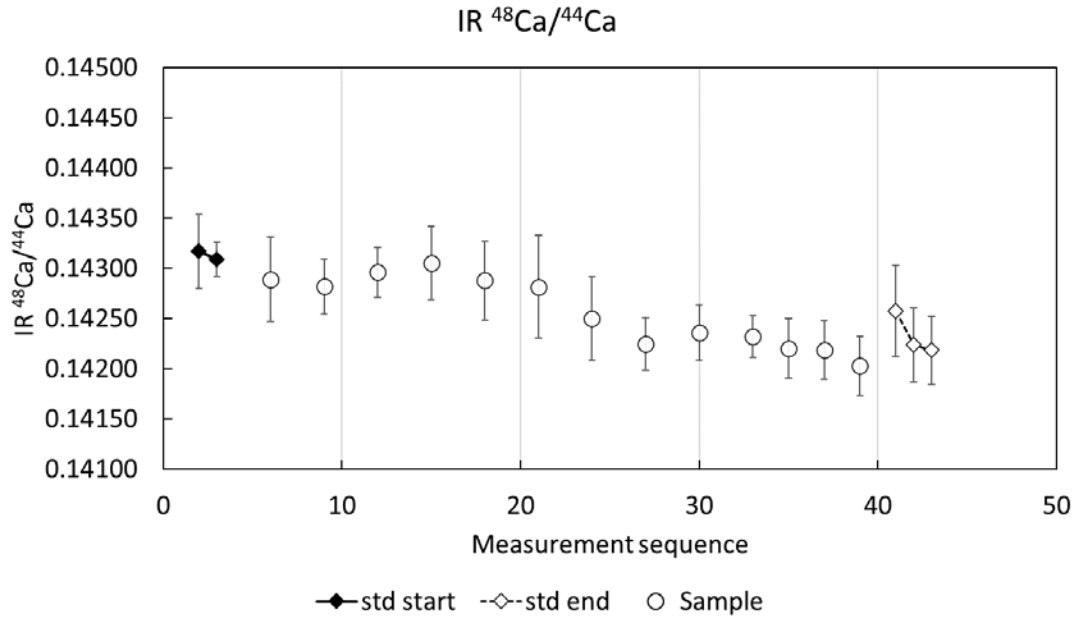

Fig 2.23 The example of measurement sequence and calcium $^{48/44}$IR

not significantly changed (within 1σ) in the case of lithium measurement (**Fig 2.19 (b)**). The IR of the calibration samples at the end after sample measurement (◇std end) were significantly shifted from the start calibration samples (◆std start). The magnitude of the drift was found to be -3.5%. **Fig 2.20** depicts the IR by the measurement sequence. It

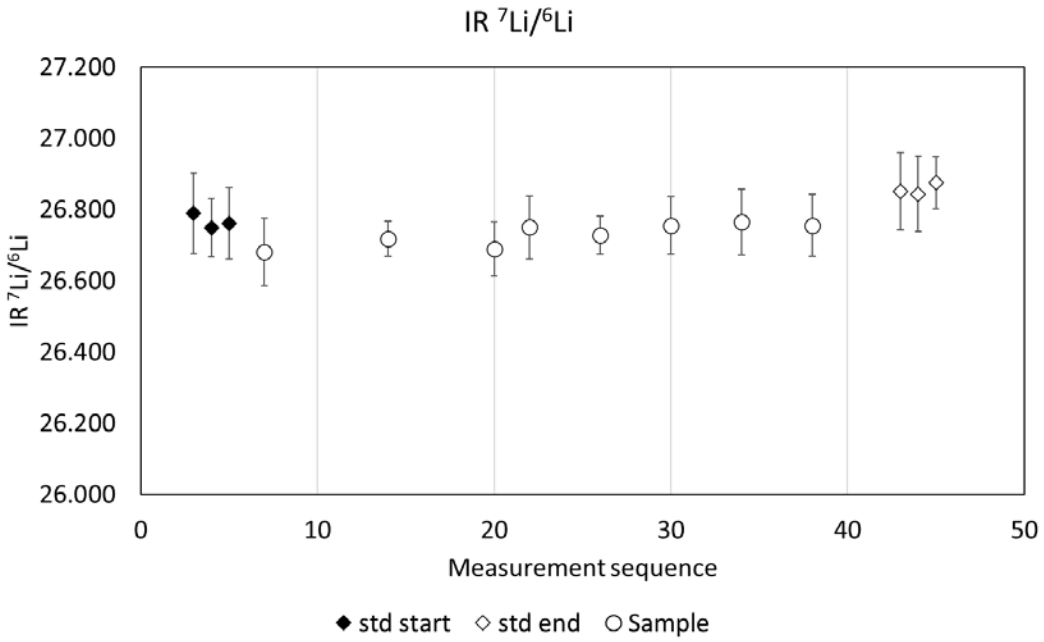

Fig 2.24 The example of measurement sequence and lithium $^{7/6}$IR

was found that the $^{48/40}$IR gradually decreased over the measurement times. The magnitude of the drift was found to be approximate – 3.5% / 40 = -0.0875% per sample. Each sample takes about 10 minutes of measurement. The example of other calcium isotope ratios, including ^{48}Ca/^{42}Ca, ^{48}Ca/^{43}Ca, and ^{48}Ca/^{44}Ca, are presented in **fig 2.21 to 2.23.** All the isotope analysis of calcium was gradually decreased over the prolonged measurement. The magnitude of the mass bias in the recession direction was -1.0%, -0.9%, and -0.6% for the analysis of ^{48}Ca/^{42}Ca, ^{48}Ca/^{43}Ca, and ^{48}Ca/^{44}Ca, respectively. Therefore, the feed sample bracketing sequence techniques could be applied to overcome the prolonged measurement problem and obtain the accurate separation factor (α) value. The same behavior was also observed in lithium analysis as well. The mass bias was found to be 0.35% (**Fig 2.24**). The mass bias was observed on every measurement but can be solved by using feed bracketing sequence techniques.

The calculation of the separation factor for each sample and concentrating isotope was carried out according to equation 2.3. This paragraph describes the uncertainty calculation by the following equations 2.5 and 2.6:

$$\boldsymbol{\alpha}_{\%\boldsymbol{RSD}} = \left(\sqrt{ \left(\frac{IR_{\%RSD\ sample}}{100}\right)^2 + \left(\frac{IR_{\%RSD\ Feed}}{100}\right)^2 } \right) \times 100 \quad (2.5)$$

$$\boldsymbol{\alpha}_{\boldsymbol{\sigma}} = \frac{\boldsymbol{\alpha} \times \boldsymbol{\alpha}_{\%\boldsymbol{RSD}}}{100} \quad (2.6)$$

where α_σ is the calculated uncertainty value of isotope separation factor (α) of 10 replications measured by ICP-MS.

The calcium standard sample from NIST (SRM915b) was measured compared to the calcium standard solution (Ca 1000) and $CaCl_2 \cdot 2H_2O$ (feed calcium source). It was noted that the $CaCl_2 \cdot 2H_2O$ (feed calcium source) used in this study contains two calcium stocks from different production lots. Therefore, the comparison measurement was carried out for both calcium sources. In this comparison, we measured using the NIST standard sample (SRM915b) as a bracketing sequence technique. The measurement order is shown in **Table 2.4**. This measurement aims to assure the natural isotope abundance of calcium source compared to the NIST sample. The relative difference in isotope abundance (δ) between calcium sources and the NIST standard sample was calculated in the following equation 2.7 and expressed in permil (‰) [120].

$$^{48}Ca/^{40}Ca\ \delta\ (‰) = \left(\frac{^{48}Ca/^{40}Ca_{IR_{sample}}}{^{48}Ca/^{40}Ca_{IR_{standard}}} - 1 \right) \times 1000 \quad (2.7)$$

where $IR_{standard}$ represents the average, a bracketing sequence of NIST (SRM915b) standard sample, and the IR_{sample} denotes the calcium sources and calcium standard solution (Ca 1000).

Table 2.4 A bracketing sequence technique using SRM 915b

Sample	
SRM 915b	
Ca 1000	δ (‰)
SRM 915b	
$CaCl_2 \cdot 2H_2O$ (1)	δ (‰)
SRM 915b	
$CaCl_2 \cdot 2H_2O$ (2)	δ (‰)
SRM 915b	

2.4.2. Calcium isotope analysis by TIMS (TIMS: TRITON X, and MAT261)

As a result, the calculated uncertainty value (σ) of the separation factor (α), measured by ICP-MS, was found to be approximately 0.003 – 0.005. The isotope fractionation of a single-stage isotope separation is usually tiny and requires a precise and accurate isotope measurement for comparison.

With the Tokyo Institute of Technologies (TIT) collaboration, Thermal Ionization Mass Spectrometry (TIMS) was carried out for precise calcium isotope composition measurement. We sent the feed sample and back-extracted samples (obtained from the 30% and 40% w/w extraction systems of calcium) to Prof. Masao Nomura for TIMS measurement (**Fig2.25**). The samples were diluted to the concentration, volume, and total mg of calcium shown in **Table 2.5**. Hydrogen iodide acid (HI) was added to convert the calcium chloride ($CaCl_2$) to calcium iodine (CaI_2). Afterwards, the sample was completely dried on the hot plate. The solid phase of calcium iodide was put in the filament for analysis.

Table 2.5 The details of samples sent to TIT for TIMS measurement comparison

Sample	Ca concentration (ppm)	Volume (mL)	Total Ca (mg)
Feed	2755	10	27.55
30% Back-extracted (BE)	2522	10	25.22
40% Back-extracted (BE)	2459	10	24.59

Fig 2.25 The samples sent to TIT for TIMS measurement.

2.5. Electrolytic enrichment and the measurement of tritium

This section denotes the electrolytic enrichment using SPE film for ultralow-level tritium enrichment and measurement. The electrolytic enrichment apparatus used in this research is SPE film with the SUS316 and DSA (dimensionally stable anode) as a cathode and anode electrode, respectively. The following shows the materials and instruments for tritium enrichment and measurement.

Materials and instruments

1) Solid polymer electrolyte (SPE) film
2) SUS316 electrode
3) DSA electrode
4) Reverse osmosis (RO) water purification system
5) 3 L laboratory bottle
6) Industrial cold air cooler, Suiden, (Japan)
7) Water circulating system
8) GL220 logger, Graphtec Corporation (Japan)
9) SA1-K-ROHS K-type sheet Thermocouple
10) Switchbot Thermo-Hygrometer
11) 20mL clear glass scintillation vial, WHEATON (US)
12) 20mL HDPE scintillation vial, WHEATON (US)
13) 500 mL wide-mouthed PP container, AS ONE CORPORATION (Japan)
14) ULTIMA GOLD, PerkinElmer (US)
15) Tritiated water sample for enrichment factor determination
16) Tritium standard reference material, Certificate number 20-C0132, Japan Radioisotope Association (JRIA) (Japan)
17) Liquid scintillation counter AccuFLEX LSC-LB7, Hitachi, Ltd. (Japan)

2.5.1. Improvement on electrolytic enrichment using SPF film

In this research, we aim to improve the enrichment and the measurement of the ultralow-level tritium. The enrichment process using SPE film was improved by the following. **Figs 2.26 and 2.27** show the overall improvement of the enrichment apparatus and reverse osmosis system.

1) We improve the enrichment process using SPE film by observing and stabilizing the temperature of the electrode. We installed the K-type thermocouples on the outside surface of the electric plates to measure the temperature change during the enrichment.
2) Thermocouples were also located on the air outlets to assure the performance of Peltier coolers. The Peltier coolers prevent the escaping of the water vapor, resulting in reliable results without the leak of tritium in water vapor form. The Peltier cooler has a cooling performance at lower than 0°C.
3) The water circulation system was applied to the water chamber and maintained the temperature at 14°C.
4) An industrial cold air circulation system was installed directly to the electric plate. The temperature of the electric plate was recorded before and after the installation.
5) The room temperature and room humidity were observed during the enrichment. The room temperature was stabilized at 20 to 25°C.
6) Reverse osmosis (RO) was applied instead of the atmospheric distillation to shorten the time required for the water purification process.

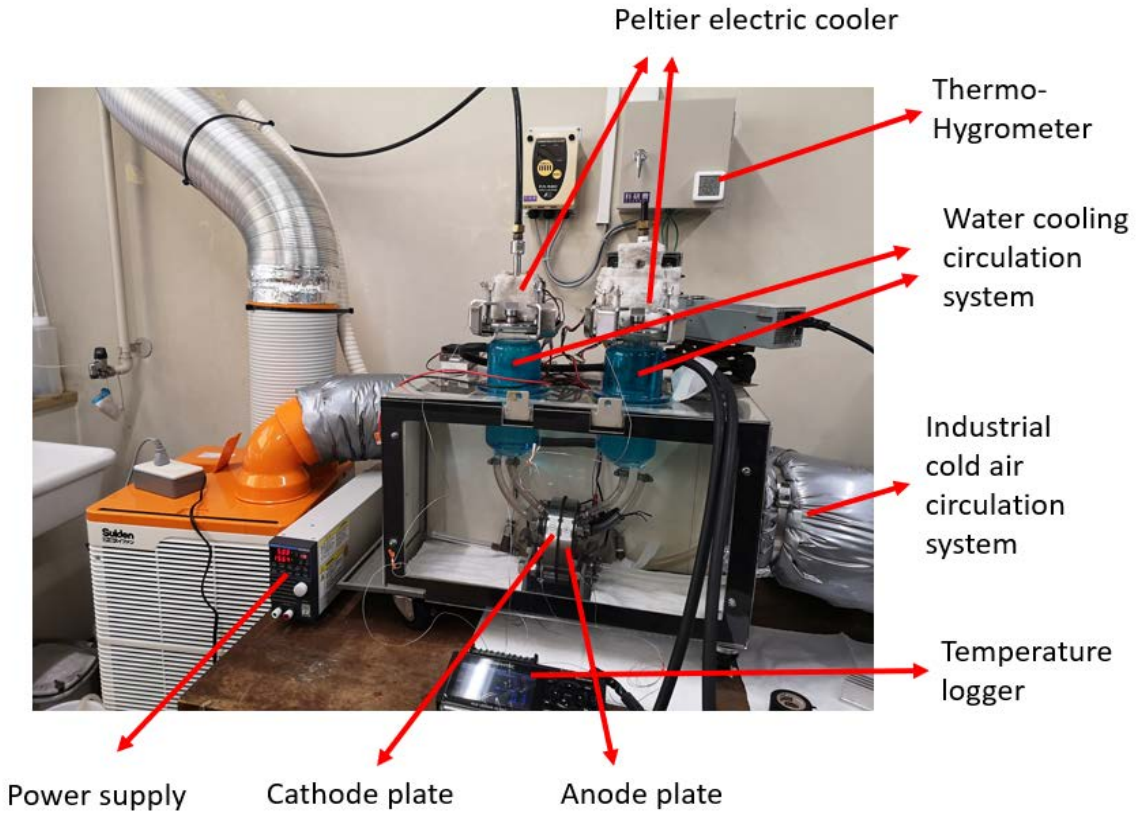

Fig 2.26 The overall improvement on the electrolytic enrichment apparatus using SPE film, including temperature logging, air circulation system, and water circulation system.

Fig 2.27 Reverse osmosis (RO) apparatus.

2.5.2. Enrichment processes

1) Water purification system using reverse osmosis (RO)

The water sample needs to be purified to eliminate the matrix effect of the dirty particle or ion content. Because the dirty particle causes severe damage to SPE film and enrichment apparatus but also affects the measurement of ultralow-level tritium measurement by liquid scintillation counting by blocking the scintillation light, results in the unreliable outcome. Atmospheric distillation is usually performed in several laboratories. However, it is a labor method that takes approximately 5 hours for 500 mL distillation. This research provides the reverse osmosis (RO) method, which is labor less than atmospheric distillation. **Fig 2.28** depicts the schematic diagram of RO apparatus, including 0.45 μm prefilter, double charcoal filters and RO filter. The final electrical conductivity (EC) is less than 30 μS/cm.

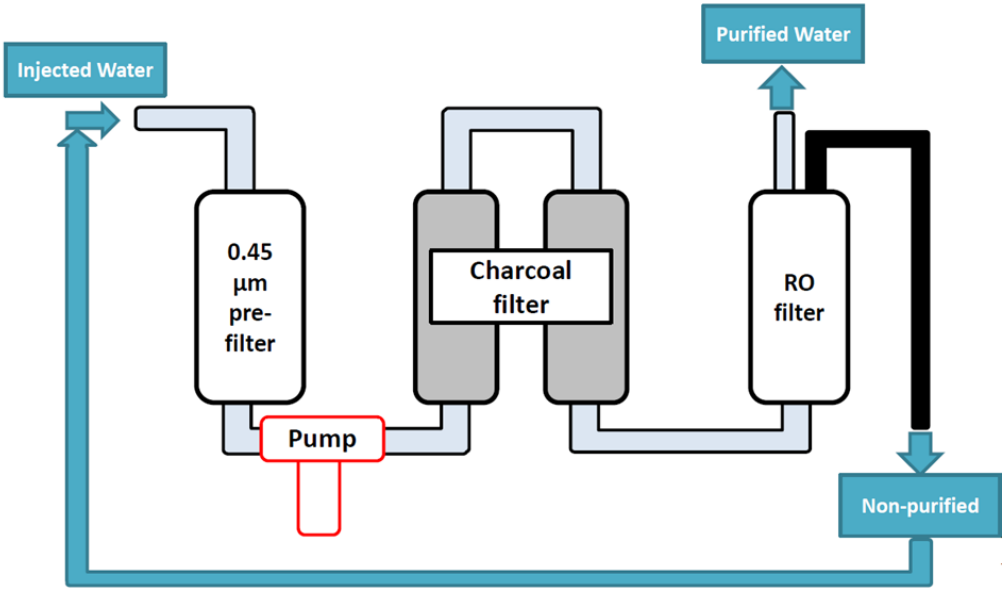

Fig 2.28 Schematic diagram of Reverse osmosis (RO) system.

2) Electrolytic enrichment

500 mL of purified water sample was introduced to the apparatus cell. The constant electric current was supplied at 30 A. The electrolytic enrichment took approximately 49.5 hours to electrolyte the initial volume of water from 500 mL to 10 mL. The calculation is shown in the following chemical reaction and equations 2.8 to 2.11.

$$Hydrolysis: H_2O \;\; -> \;\; 2H^+ \; + \; O_2/2 \; + \; 2e^- \tag{2.8}$$

1 mol H_2O give electric charge = $\frac{18\ g/mol}{2\times 9.65\times 10^4 \frac{C}{mol}} = 9.33 \times 10^{-5} C$ (2.9)

where 9.65×10^4 (C/mol) is the Faraday constant represents the magnitude of electric charge (C) per mole of electrons.

$$C \; = \; At \tag{2.10}$$

where C, A, and t represent the electric charge, electric current, and time (second), respectively. The hydrolysis of water per hour of 30 A constant electric current can be expressed in the following equation 2.11

$$Hydrolysis\ of \frac{water}{hour} = 9.33 \times 10^{-5}(C) \times At$$

$$Hydrolysis\ of \frac{water}{hour} = 9.33 \times 10^{-5}(C) \times 30(A) \times 3600(secs) \tag{2.11}$$

Therefore, 30 A could electrolyte water for 10.1 g/hr. The volume reduction of the initial water sample from 500 mL to 10 mL would take 490 g/10.1 g/hr. = 48.5 hrs. The enriched water sample had measured weight and collected in the 20mL clear glass scintillation vial; WHEATON (US) was then kept in the refrigerator to avoid evaporation.

3) Improvement on the temperature system of the apparatus

According to the Bigeleisen-Mayer equation [12, 25], the isotope separation depends on the temperature. The lower temperature, the higher isotope fractionation becomes. Therefore, the isotope fractionation could change based on the temperature as well. In the determination of enrichment factor of the electrolytic enrichment, describe in the following section, the tritiated water as a representation of the sample, was enriched, prepared a cocktail of non-enriched and enriched sample, and measured by LSC. The enrichment factor obtained from those sample was represented the apparatus condition. Therefore, to apply the enrichment factor to the whole samples, the stable condition of apparatus, especially temperature, need to be concerned.

The temperature control system, water and air circulation systems, were installed. Water coolant jacket was circulated around the apparatus cells, stabilizing the temperature at 14°C. Additional of the industrial air circulation system was put to cooldown the electric plate, directly. Moreover, the electronic cooler (Peltier) system was installed at the gases outlets to trap the water vapor and assure that there is no tritium escaped in term of the water vapor. Finally, the temperature logging system (GL220 logger, Graphtec Corporation (Japan)) was put to the Peltier and directly outside the electric plates to measure the temperature at the plates and assure the performance of the cooler during the enrichment periods.

4) Determination of enrichment factor using Tritiated water sample

The tritiated water sample was provided by Prof. Yoshimune Ogata from Nagoya University. This tritiated sample had a tritium activity concentration of approximately 20 Bq/L in July 2021. 500 mL of tritiated water was

enriched with the same condition as other samples. This sample was enriched at the beginning and end of the experiment to ensure the stability of the enrichment factor. The temperature was logging during the enrichment. At the same time, the other sample was controlled the constant temperature to employ the enrichment factor obtained from tritiated sample. Non-enriched tritiated water sample was prepared and measured directly. Along with the enriched tritiated water sample, the enrichment factor (α) was determined by tritium recovery factor (R) (equation 2.12 and 2.13)

$$R = \frac{T_f V_f}{T_i V_i} \tag{2.12}$$

$$\alpha = \frac{T_f}{T_i} \tag{2.13}$$

where T and V represent the tritium activity concentration (Bq/L) and volume of the water sample. The subscription *f* and *i* indicate the final and initial of the enrichment stage. Equation 2.12 can be applied to equation 2.14 to find the initial tritium concentration of the water sample (T_i).

$$T_i = \frac{T_f}{V_i/V_f \cdot R} \tag{2.14}$$

2.5.3. Tritium measurement by liquid scintillation counting (LSC)

A low background liquid scintillation counter carried out the measurement of the enriched sample; AccuFLEX LSC-LB7, Hitachi, Ltd. (Japan). The triple coincidence photomultiplier tube and an active-passive shield provide a tritium measurement sensitivity of less than 1 Bq/L.

1) Sample preparation and measurement conditions

The water sample was mixed homogeneously with a liquid scintillator (Ultima GOLD, PerkinElmer (US)) with the volume ratio between water sample and liquid scintillator at 10g/10g in the low diffusion 20 mL HDPE scintillation vial, WHEATON (US). To avoid a strange scintillation caused by chemiluminescence and photoluminescence, the cocktail samples were kept in the dark for 24 hours at a low temperature (10°C) and ultra-pure nitrogen gas was flowed to purge the radon gas in the measurement chamber (**Fig 2.29**).

The background sample is the tritium-free water samples collected at Tohno underground mine older than 1 million years. All samples were measured for 100 minutes, 10 replications, and 2 cycles.

Fig 2.29 Sample chamber of LSC-LB7.

2) Tritium calibration standard and ESCR measurement

In this research, an external standard channel ratio (ESCR) was carried out to determine counting efficiency using ^{133}Ba as a gamma ray

source. In order to obtain the correction curve, the ESCR calibration samples were prepared by adding JRIA standard tritium source with the activity of 201.5 Bq/g on May 25th, 2020. 1 gram of tritiated water was added to the calibration sample and mixed with the various ratio between water and liquid scintillator. **Table 2.6** shows the calibration samples preparation detail. The samples were measured for 10 minutes, 10 replications, and 10 cycles. The ESCR and counting efficiency are shown in **Fig 2.30**. The counting efficiency (%EFF) was calculated by equation 2.15.

$$\%Eff = \frac{H-CPS}{H-DPS} \times 100 \qquad (2.15)$$

where H-CPS and H-DPS indicate the counting signal and calculated tritium activity at the measurement date, respectively.

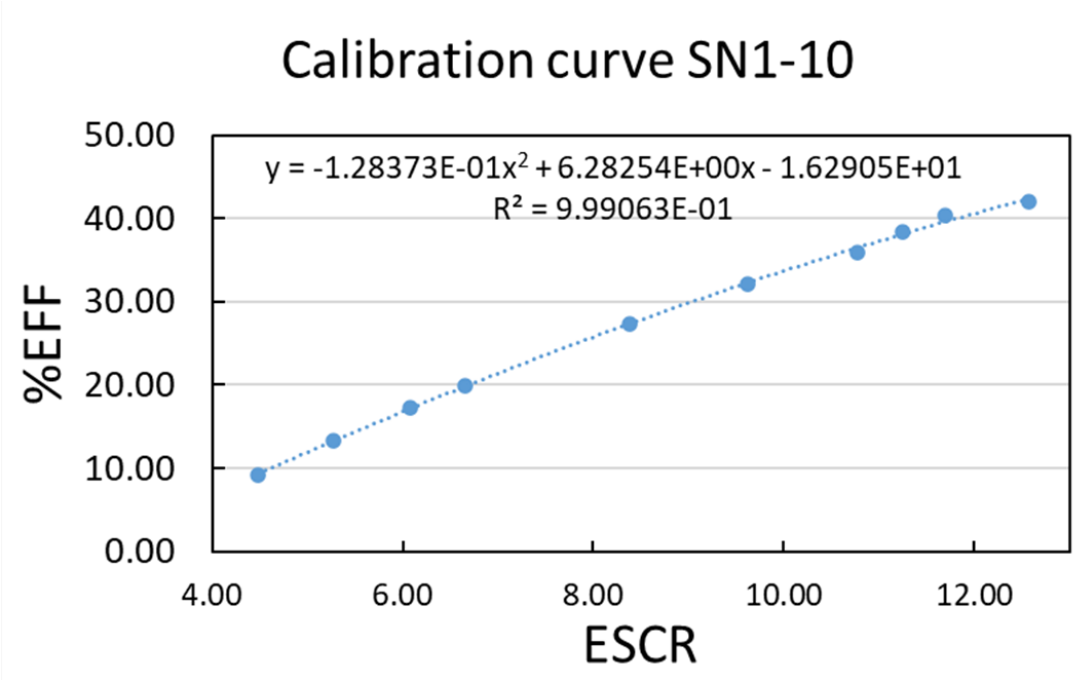

Fig 2.30 ESCR vs. counting efficiency (%EFF) calibration curve.

Table 2.6 Tritium calibration samples

Sample	HTO (g)	H_2O (g)	LS (g)	Total (g)
SN1	1.006	4.020	15.057	20.083
SN2	0.997	5.039	14.393	20.429
SN3	1.008	6.017	13.019	20.045
SN4	1.000	6.997	12.087	20.085
SN5	0.994	7.994	11.028	20.016
SN6	0.995	9.007	10.098	20.100
SN7	0.994	10.073	9.300	20.366
SN8	0.998	11.057	8.096	20.151
SN9	0.996	11.991	7.042	20.029
SN10	0.998	12.985	6.075	20.059

3) Data analysis

A full spectrum analyzed the measurement result from 0.005 – 19.995 keV (channel 1 – 3999) for both BG and samples. Cycle 1 and cycle 2 measurements were performed by individual calculation because the measurement date differed. Total counting signal from a full spectrum for each sample and BG used to calculate the measurement results by the equation 2.16.

$$T_f\left(\frac{Bg}{L}\right) = \left[\frac{N_s}{t_s} - \frac{N_b}{t_b}\right] \times \frac{1}{\%Eff} \times \frac{1}{V} \times \frac{10^5}{60} \qquad (2.16)$$

where T_f represents the sample tritium concentrations, N_s and N_b represent gross count from a full spectrum (channel 1 – 3999) analysis, and t_s and t_b represent measurement time, respectively. The subscriptions s and b indicate the sample and background sample (tritium free), respectively. A

quenching calibration curve determined the counting efficiency (%EFF) from the ESCR value. **Fig 2.31 to 2.34** show the example of the entire energy spectrum of BG, sample, non-enriched tritiated water, and enriched tritiated water, respectively. The signal obtained from the background signal usually came from the noise, and the signal from the enriched sample was found to be higher than the background itself. This information ensures that the enrichment plays a role in the ultralow-level tritium measurement.

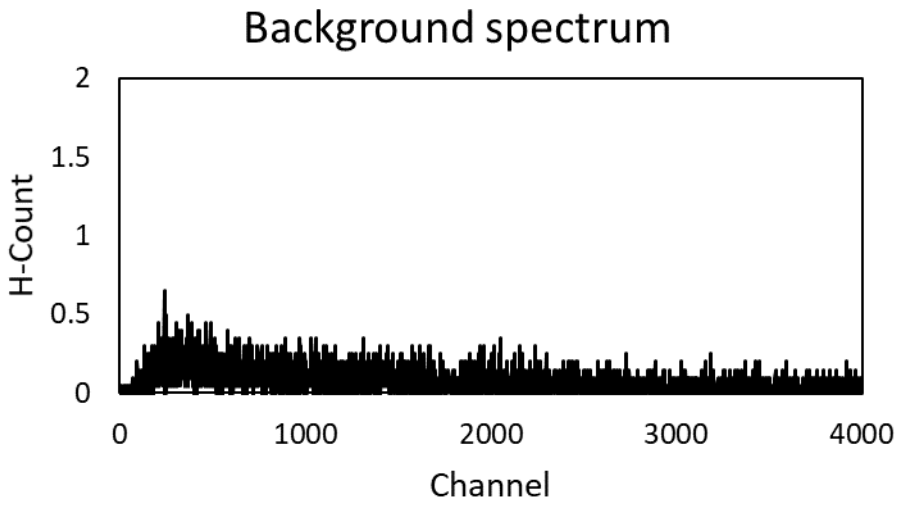

Fig 2.31 Background (tritium free) energy spectrum.

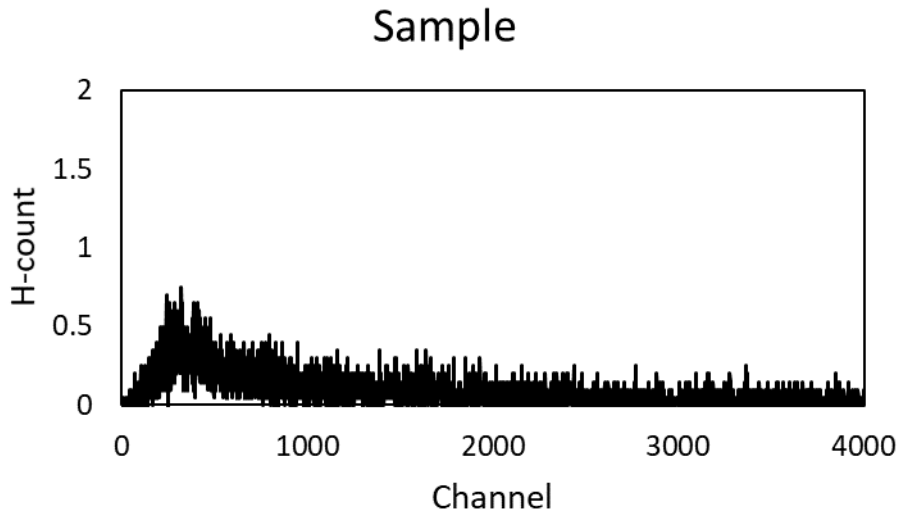

Fig 2.32 Sample energy spectrum.

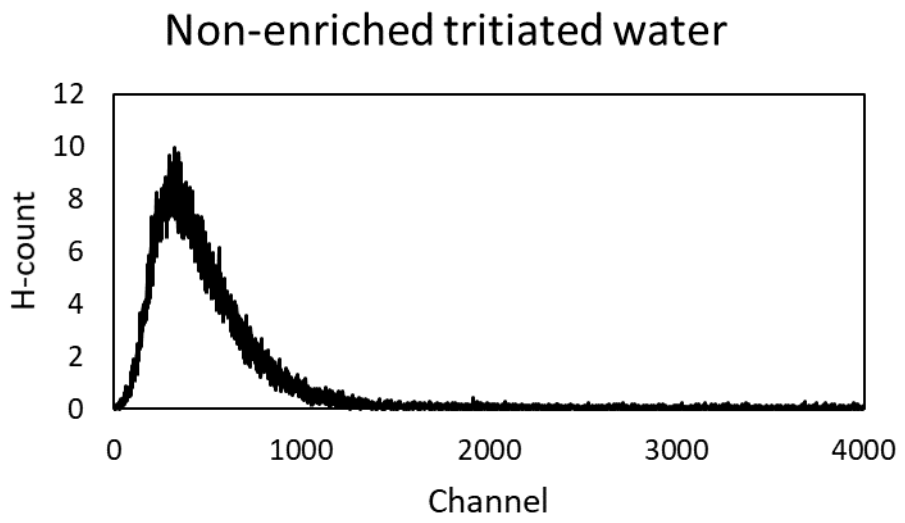

Fig 2.33 Non-enriched tritiated sample energy spectrum.

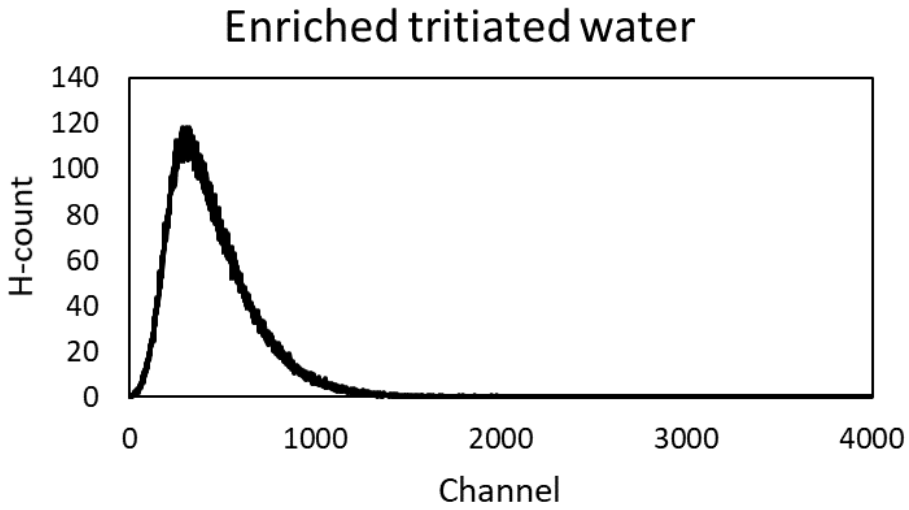

Fig 2.34 Enriched tritiated sample energy spectrum.

2.5.4. JSPS joint research project with Thailand

This research on the measurement of tritium aims to investigate the tritium levels in environmental water collected from the various region in Thailand. The JSPS, joint research project has been carried out along with the collaboration of the Department of Environmental Science and Technology, Osaka Sangyo University, Kasetsart University, Thailand Institute of Nuclear Technology (TINT), Thailand, Kyoto University, Kyoto, Japan, and Shinshu University, Nagano, Japan.

In the first year (2020), a tap water sample was collected from Bangkok and the metropolitan region, including the tap water treatment plants and tap water pump stations. All water samples were provided by the Metropolitan Waterworks Authority (MWA) of Thailand. **Fig 2.35** shows the sampling site in the first year of collaboration.

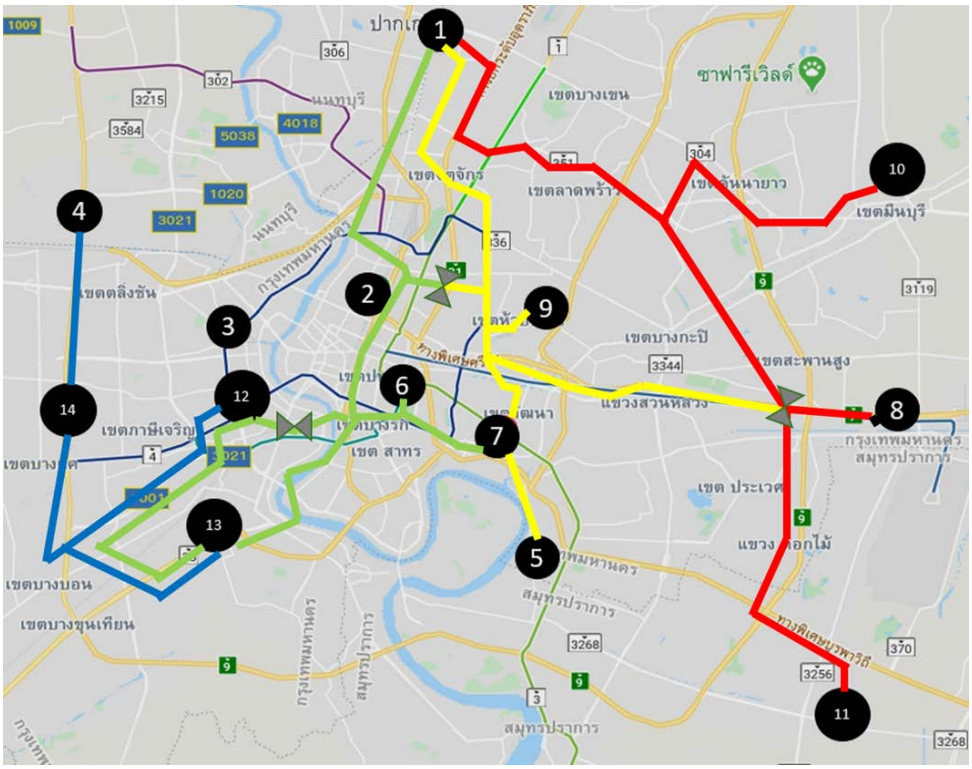

Fig 2.35 Tap water sampling site in Bangkok and metropolitan area in the first year of collaboration. The color lines between each point indicate the water flow and tap water distribution.

Table 2.7 indicate the sample name corresponding to the number in **Fig 2.35**. The second year (2021) has been carried out by extending the sample regions nationwide with the collaboration of the Provincial Waterworks Authority (PWA) of Thailand.

Table 2.7 The sampling site of tap water collected in Bangkok and metropolitan

Number	Sampling site
1	Bangkhen Water Treatment Plant
2	Samsen Water Treatment Plant
3	Thonburi Water Treatment Plant
4	Mahasawat Water Treatment Plant
5	Samrong Pump Station
6	Lumphini Pump Station
7	Khlong Toei Pump Station
8	Ladkrabang Pump Station
9	Latphrao Pump Station
10	Minburi Pump Station
11	Bang Phli Pump Station
12	Thaphra Pump Station
13	Ratburana Pump Station
14	Petchkasem Pump Station

On the other hand, the rainwater sample was collected monthly from Kasetsart University (Sri-Racha campus), Rayong, Thailand. **Fig 2.36** show the sampling site of second-year collaboration. The rainwater sampling site was extended at Chiang Mai in July 2021.

One liter of collected tap water sample for each location in July 2020 and 2021 and monthly rainwater samples were sent to Osaka Sangyo University, Japan and distributed to other universities. 100 mL of water sample was divided into wild mouth

PP bottle and transported to each university. The tritium was measured by TINT and OSU. Shinshu University and Kyoto University report the anion, cation, and oxygen isotope fractionation to identify the water sources.

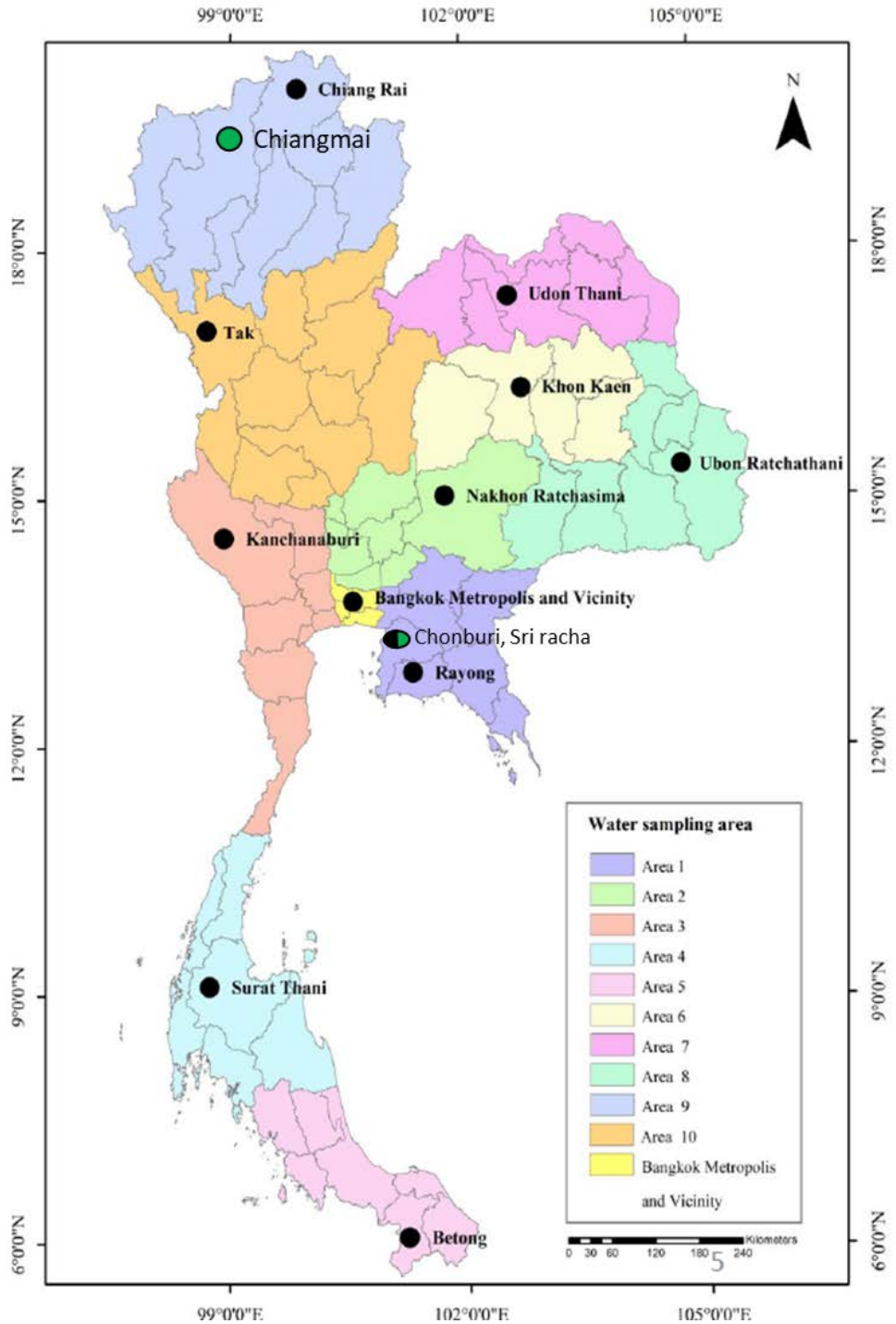

Fig 2.36 Nationwide tap water sampling site for the second year of collaboration.

● = tap water sampling site, ● = Rainwater sampling site

CHAPTER THREE: Result and discussion

3.1. Introduction

This chapter deals with the results and discussion following by the frame of study described in chapter two. The liquid-liquid extraction (LLE) was performed for calcium and lithium extraction. Section 3.2 deals with the isotope composition analysis of calcium and lithium, aiming to ensure that the measurement by ICP-MS is acceptable. Section 3.3 contains LLE results, including crown-ether extraction system, extraction time, aqueous phase concentration, acidity solvent (HCl), various volume ratio, extraction temperature, solid-liquid extraction, and multi-stage iteration and the prospect for the enrichment and isotope production. Section 3.3 presents the tritium result on the JSPS joint research project and plan.

3.2. Isotope composition analysis of calcium and lithium

This section presents the isotope analysis of calcium and lithium using the comparison of TIMS measurement and known lithium spike samples. This comparison aims to ensure that the measurement of calcium and lithium using ICP-MS is acceptable.

3.2.1. Calcium isotope composition analysis by ICP-MS

1) The variation of calcium isotope composition compared to SRM 915b

The comparison needs to be checked and verify the isotope composition compared to SRM 915b. This research used two calcium stocks from different production lots of $CaCl_2 \cdot 2H_2O$ (feed calcium source) and calcium standard solution (Ca 1000: FUJIFILM Wako Pure Chemical Industries, Ltd. (Japan)). The measurement sequence was set using SRM 915b as a bracketing sequence sample. The δ was calculated from the measured $^{48}Ca/^{40}Ca$ sample compared to the bracketing sequence sample expressed in permil (‰) (**Table 3.1**). The results indicated that the deviation

of calcium sample compared to SRM 915b is within 2σ of calculated δ. The finding indicated that the isotope composition of the calcium feed sample and calcium standard solution is the same as SRM 915b. However, the measurement of precise isotope composition is still required since the accuracy of reaction-cell ICP-MS was found to be approximately 3.6–3.8 ‰.

Table 3.1 The isotope measurement ($^{48}Ca/^{40}Ca$) of calcium sample compared to SRM 915b.

Measurement sequence	IR ($^{48}Ca/^{40}Ca$)	IR σ	Average bracketing sequence sample	σ	$^{48/40}\delta$ (‰) ± σ
SRM 915b	0.00555	0.00001			
Standard Ca 1000	0.00554	0.00001	0.00554	0.00002	-0.09±3.65
SRM 915b	0.00553	0.00001			
$CaCl_2 \cdot 2H_2O$ (1st stock)	0.00554	0.00001	0.00553	0.00002	1.33±3.82
SRM 915b	0.00552	0.00001			
$CaCl_2 \cdot 2H_2O$ (2nd stock)	0.00553	0.00001	0.00552	0.0002	1.77±3.68
SRM 915b	0.00552	0.00001			

2) Calcium isotope composition analysis by TIMS

The measurement of precise calcium isotope composition (TIMS) was carried out with the collaboration of Prof. Masao Nomura from Tokyo Institute of Technologies (TIT, Japan), aiming to compare with the data acquired from reaction-cell ICP-MS. **Table 3.2** and **Table 3.3** report the isotope composition of feed solution ($CaCl_2$) and back-extraction (BE) from 30% and 40% w/w extraction systems acquired from TIMS and reaction-cell ICP-MS (RC-ICP-MS), respectively. **Fig 3.1** depicts the calculated separation factor (α) per mass unit of the ICP-MS and TIMS (TRITON and MAT261).

Table 3.2 Isotope composition and separation factor of calcium samples measured by TIMS (TRITON and MAT261)

Isotope composition	Feed		30% BE		α (IR_{BE}/IR_{Feed}) 30% BE	40% BE		α (IR_{BE}/IR_{Feed}) 40% BE
	%	IR ($^{x}Ca/^{40}Ca$)	%	IR ($^{x}Ca/^{40}Ca$)		%	IR ($^{x}Ca/^{40}Ca$)	
TRITON								
^{40}Ca	0.96936	1.000000	0.96945	1.000000	1.00000	0.96938	1.000000	1.00000
^{42}Ca	0.00646	0.006666	0.00645	0.006657	0.99867	0.00646	0.006668	1.00033
^{43}Ca	0.00135	0.001395	0.00135	0.001388	0.99500	0.00135	0.001390	0.99593
^{44}Ca	0.02091	0.021570	0.02084	0.021499	0.99667	0.02090	0.021563	0.99967
^{48}Ca	0.00188	0.001944	0.00187	0.001931	0.99286	0.00188	0.001936	0.99586
MAT261								
^{40}Ca	0.96950	1.000000	0.96952	1.000000	1.00000	0.96952	1.000000	1.00000
^{42}Ca	0.00647	0.006674	0.00645	0.006656	0.99719	0.00647	0.006670	0.99935
^{43}Ca	0.00134	0.001387	0.00135	0.001388	1.00088	0.00134	0.001386	0.99934
^{44}Ca	0.02082	0.021624	0.02081	0.021465	0.99265	0.02096	0.021475	0.99311
^{48}Ca	0.00187	0.001939	0.00187	0.001928	0.99411	0.00188	0.001929	0.99490

Table 3.3 Separation factor of calcium samples measured by reaction-cell ICP-MS (RC-ICP-MS)

Isotope composition	Feed	30% BE	α±σ (IR_{BE}/IR_{Feed}) 30% BE	40% BE	α±σ (IR_{BE}/IR_{Feed}) 40% BE
	IR ($^{x}Ca/^{40}Ca$) (Counting ratio)	IR ($^{x}Ca/^{40}Ca$) (Counting ratio)		IR ($^{x}Ca/^{40}Ca$) (Counting ratio)	
RC-ICP-MS					
^{40}Ca	1.000000	1.000000	1.00000±0.00000	1.000000	1.00000±0.00000
^{42}Ca	0.009217	0.995664	0.99566±0.00484	0.997739	0.99774±0.00538
^{43}Ca	0.002191	0.997981	0.99798±0.00453	0.996829	0.99683±0.00489
^{44}Ca	0.038032	0.995899	0.99590±0.00515	0.997017	0.99702±0.00410
^{48}Ca	0.005361	0.991125	0.99113±0.00327	0.992867	0.99287±0.00631

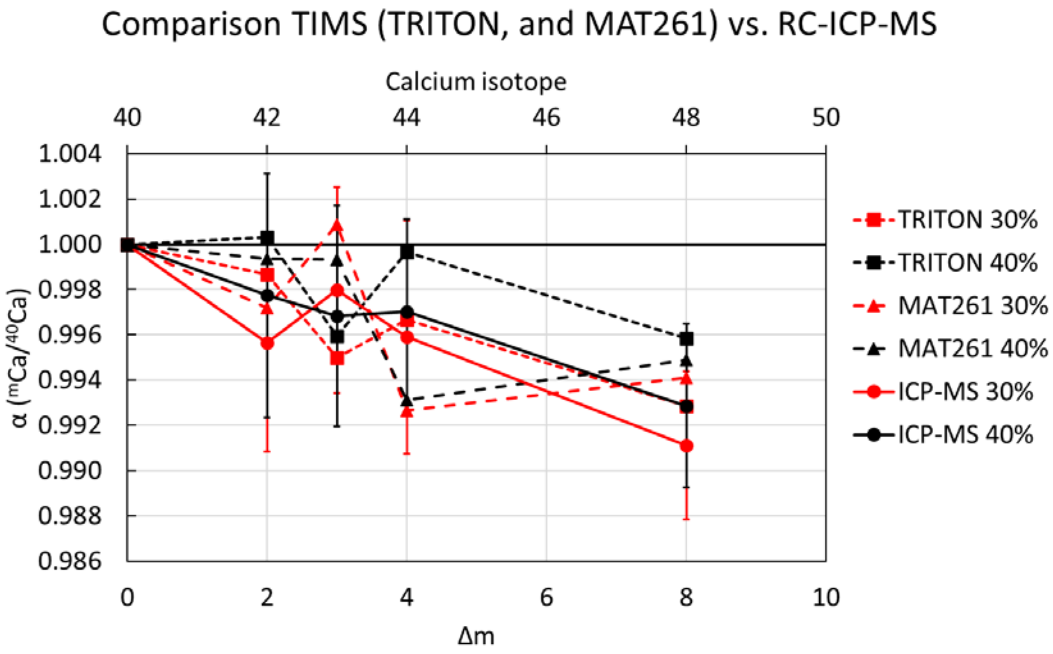

Fig 3.1 The calculated separation factor (α) per mass unit of the ICP-MS (Agilent 7900) and TIMS (TRITON and MAT261)

The results show that the separation factor obtained from ICP-MS and TIMS found to be the same magnitude (within 2σ) of RC-ICP-MS results, indicating that the measurement by reaction-cell ICP-MS is reliable. The correlation coefficient (CC) of the calculated separation factor between RC-ICP-MS to TRITON and MAT261 was strong at 0.742, 0.721 for 30% BE, and 0.735, 0.594 for 40% BE, respectively. It is noted that the uncertainty value of TIMS is less than 0.15% RSD

3.2.2. Lithium isotope composition analysis by ICP-MS

In order to assure the reliability of the measurement by ICP-MS, the spike lithium isotope composition was measured and compared to the lithium feedstock. Spike lithium samples with various ^{7}Li, 94.14%, 96.35%, and 98.20%, were obtained from the Tokyo Institute of Technology (TIT, Japan) (**Fig 3.2**). The samples were prepared and measured at 10 ppb concentration. The extrapolation was calculated to

find the isotope composition of the lithium feed sample. **Fig 3.3** indicates the isotope ratio of spike sample and feed sample. The LiCl used as feed solution was found to be at natural abundance (92.4% ^{7}Li, and 7.6% ^{6}Li). Moreover, these extrapolation results could be revealed the reliability of isotope analysis of lithium as well.

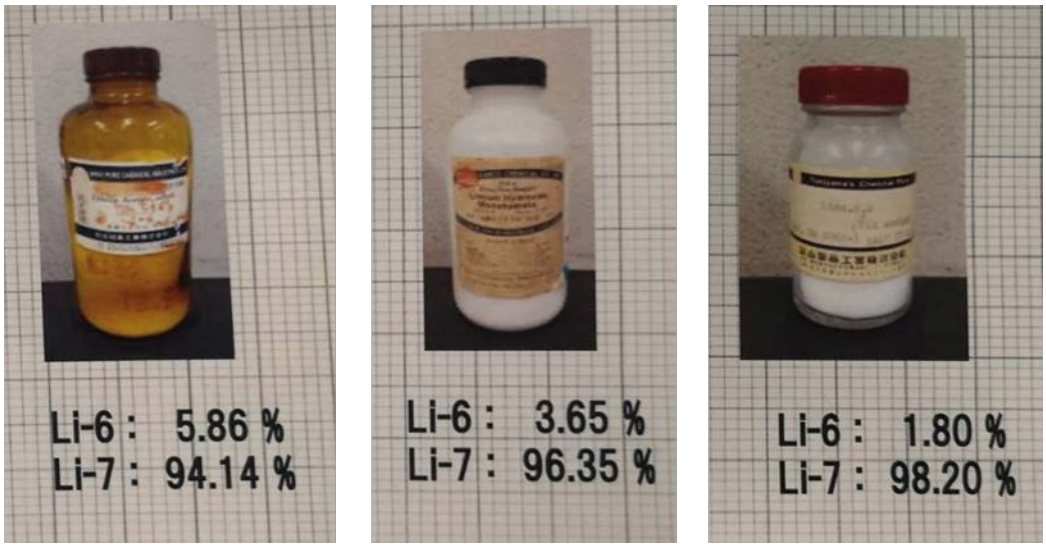

Fig 3.2 Lithium spike samples obtained from Tokyo Institute of Technology (TIT, Japan)

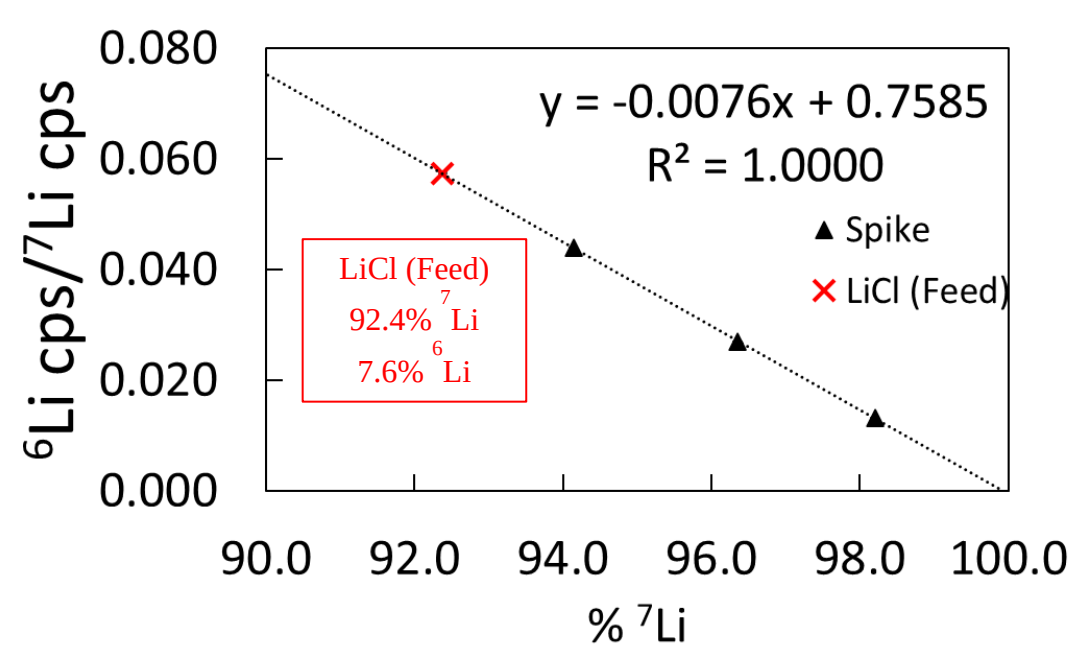

Fig 3.3 Identification of lithium feed abundance using various ^{7}Li spike samples

3.3. Chemical isotope separation for calcium and lithium using crown-ether

3.3.1. Presence and absence of crown-ether

This extraction system was carried out to assure the role of crown-ether on the liquid-liquid extraction of the aqueous and organic phases. 200 mL of 0.07M DC18C6 crown-ether dissolved in crown-ether. The absence of a crown-ether system was only chloroform as an organic phase. The aqueous phase is 20 mL of 3.3 M $CaCl_2$ (aq) (30% w/w system). The extraction time was 1 minute. The phase separation time was 10 minutes in the separation funnel. The water volume for back extraction is 1/10 of the volume ratio of water to organic phase after extraction. The back-extraction was performed twice to assure that all ion content was stripped to the water. The back-extraction represents the ion content in the organic phase (org). The distribution coefficient (D) was calculated by the concentration ratio of the back-extraction (organic) to extraction (aqueous). The results show in **table 3.4.** The result was found that the distribution coefficient (D) significantly increases to 0.0200 ± 0.0003 on the crown-ether system. The absence of a crown-ether system indicates that the distribution of calcium content in the organic solution is insignificant. The calcium content in back extraction was found to be insignificant at less than 4.8 ppm, while the presence of crown-ether was found to be 2522 ppm, measured by AAS. It was noted that the ion content measured by AAS has an uncertainty value of less than 1% RSD. The same behavior was observed in lithium extraction as well. These findings confirmed the chemical exchange reaction between ion and crown-ether and ensured the extraction under the presence of crown-ether.

Table 3.4 calcium and lithium content in feed, extraction, back extraction, and distribution coefficient (D)

Target	Crown -ether	Feed (M)	Extraction (M)	1st Back extraction (M)	2nd Back extraction (M)	D
Ca	○	3.3	3.1	0.06	0.00	0.0200±0.0003
	×	3.4	3.4	0.00	0.00	0.0000±0.0000
Li	○	8.4	7.7	0.25	0.00	0.0292±0.0001
	×	8.3	8.2	0.00	0.00	0.0000±0.0000

Jepson and DeWitt [99] firstly reported the liquid-liquid extraction of crown-ether in an organic system containing DC18C6 crown-ether. The result revealed that the extraction under 0.07M DC18C6 organic system and high aqueous phase concentration (5.11 to 7.1M) provided the maximum distribution coefficient at 0.0076. Compared to our results, the distribution coefficient under the presence of crown-ether extraction was found to be 0.0200±0.0003 at 3.3M feed calcium solution. Our finding shows the more significant distribution coefficient since the extraction system might differ from Jepson and DeWitt procedure, which did not report on the volume of organic solution. Moreover, in Jepson and DeWitt procedures, the mixing solution was shaken about 20 times and left overnight for phase separation, while our procedure was carried out by a strong magnetic separator to ensure the chemical reaction at equilibria. This might imply that the chemical reaction of their experiment might not be at equilibria.

In the case of lithium, K. Nishizawa et al. [104] reported the equilibria chemical exchange of lithium (LiCl) and in the organic solution contained B15C5 crown-ether to be 0.0029. The distribution coefficient was one order smaller than our finding (0.0292±0.0001). The reason was that the extraction system was different. K. Nishizawa used 20 mL of 0.186 M B15C5 and 20 mL of 8.0M LiCl (volume ratio (aq/org) = 1/1), while our experiment was 200 mL 0.07M DC18C6 and 20 mL 8.4M LiCl (volume ratio (aq/org) = 1/10). The content of crown-ether (mol) in our organic

solution (14.0 mmol) was greater than K. Nishizawa (3.7 mmol). This could explain why our finding has a larger distribution coefficient under the same initial aqueous phase concentration. The isotope composition and separation factor (α) will be discussed in the other section of this chapter.

3.3.2. Extraction time

This research carried out the liquid-liquid extraction with various extraction times, including 1 second (by shaking in separation funnel), 1, 10, 30, and 60 minutes using a magnetic stirrer. The organic phase is 200 mL 0.07M DC18C6, and the aqueous phase of 30% w/w extraction system. This experiment aims to identify the time required for equilibrium the chemical exchange reaction. The minimal time could also profit from the extraction and isotope enrichment production. The calcium distribution coefficient (D) and separation factor (α) shown in various extraction times are shown in table 3.5, **fig 3.4, and 3.5.** At the same time, lithium extraction shows in **table 3.6 and fig 3.6 and 3.7.** The distribution coefficient (D) results indicate that the chemical exchange between ion and crown-ether becomes equilibrium on a magnetic stirrer's extraction time of at least 1 minute. This finding is in good agreement with K. Nishizawa et al. [101] on the study of the isotope separation via liquid-liquid extraction of lithium isotope. Their finding indicated that the chemical equilibria of 5 seconds and isotope equilibria at 30 seconds by mixing stirrer. Compared to our experiments, the extraction time was studied from 1 second and 1 minute, implying that the extraction at 1 minute using a magnetic stirrer is sufficient for equilibria the chemical and isotope exchange. The finding could benefit the shortened time required for any other extraction. **Fig 3.8** shows the comparison between this research and K. Nishizawa et al. in terms of D and $\%^{6}Li$ in the organic phase.

Table 3.5 Calcium extraction on the various extraction time using a magnetic stirrer

Time	D	$^{48}Ca/^{40}Ca$ α_{org}	$^{48}Ca/^{42}Ca$ α_{org}	$^{48}Ca/^{43}Ca$ α_{org}	$^{48}Ca/^{44}Ca$ α_{org}
1 sec[a]	0.0064±0.0001	0.987±0.003	0.991±0.004	0.992±0.003	0.995±0.003
1 min	0.0182±0.0001	0.990±0.003	0.995±0.005	0.994±0.004	0.996±0.005
10 mins	0.0165±0.0001	0.993±0.003	0.995±0.004	0.993±0.004	0.995±0.003
30 mins	0.0167±0.0006	0.987±0.003	0.993±0.003	0.992±0.003	0.994±0.002
60 mins	0.0156±0.0001	0.985±0.004	0.993±0.005	0.993±0.004	0.994±0.003

[a] Shaken by hand

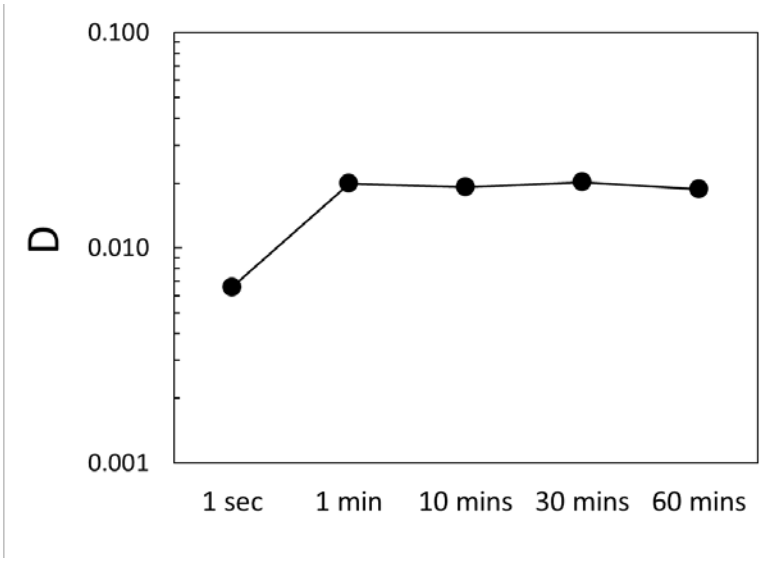

Fig 3.4 Distribution coefficient (D) of calcium on various extraction time

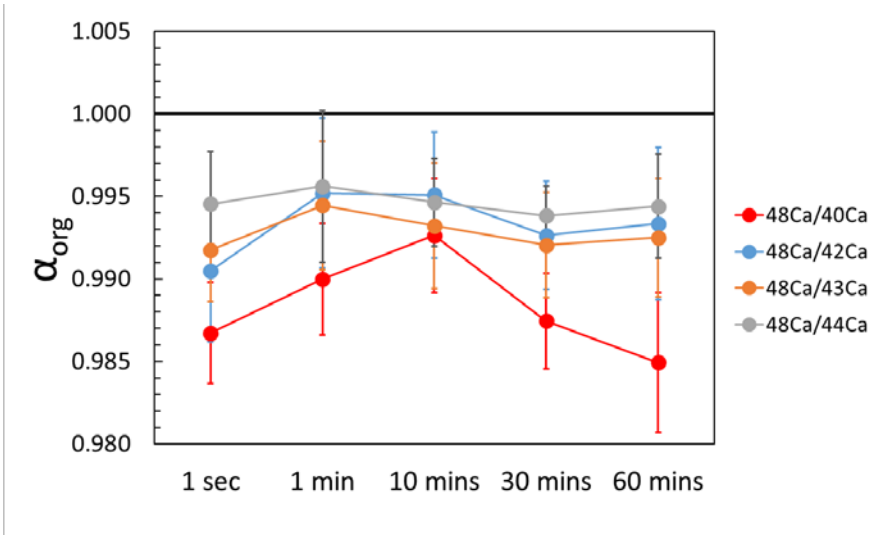

Fig 3.5 Isotope fractionation of calcium in organic phase on various mixing time

Table 3.6. Lithium extraction on the various extraction time using a magnetic stirrer

Time	D	$^{7}Li/^{6}Li$ α_{org}
1 sec[a]	0.0117±0.0000	0.993±0.004
1 min	0.0258±0.0002	0.988±0.004
10 mins	0.0272±0.0001	0.987±0.004
30 mins	0.0295±0.0002	0.989±0.005
60 mins	0.0279±0.0001	0.989±0.005

[a] Shaken by hand

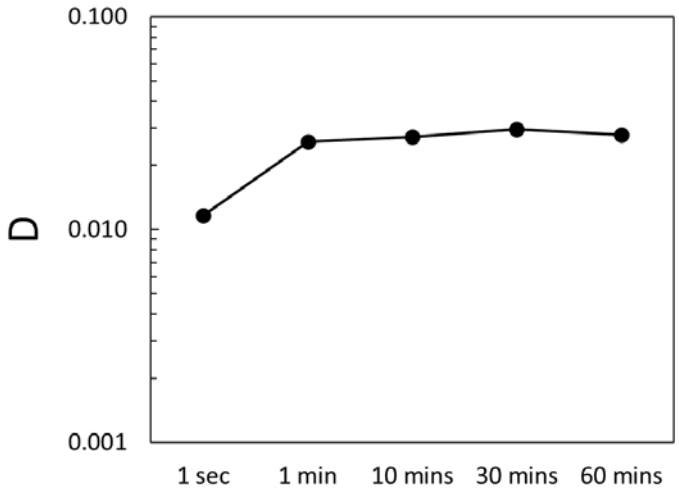

Fig 3.6 Distribution coefficient (D) of lithium on various extraction time

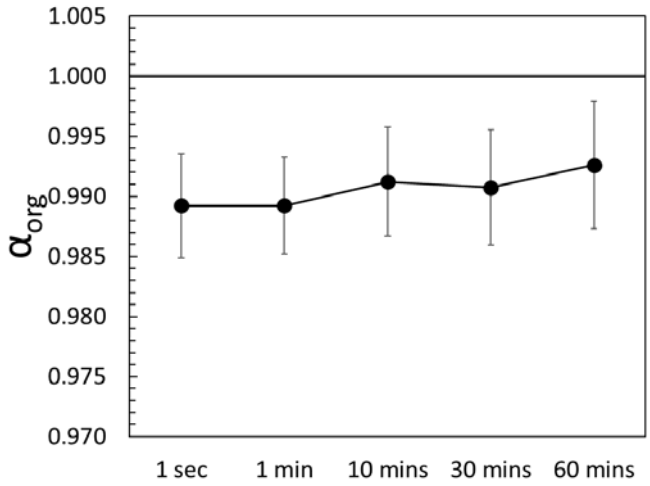

Fig 3.7 Isotope fractionation of lithium in organic phase on various mixing time

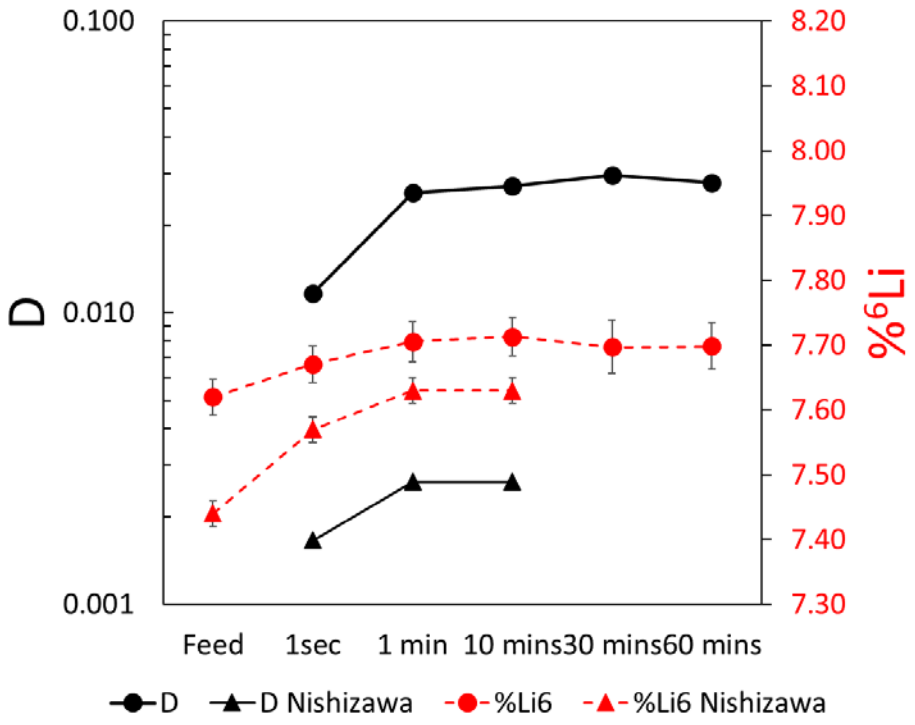

Fig 3.8 Comparison between this research and K. Nishizawa et al. on the isotope separation of lithium using B15C5 crown-ether

3.3.3. Aqueous phase concentration

It is well known that one of the most important parameters of liquid-liquid extraction is ion concentration in the aqueous phase. The calcium extraction concentration was investigated by the system of 10%, 15%, 20%, 25%, 30%, and 40% w/w (1.0 – 4.8 M) solution, while lithium was carried out under 10%, 15%, 20%, and 30% w/w (2.7 to 8.4 M). The other factors, such as crown-ether concentration, extraction time, and extraction temperature, are fixed at the same condition of 0.07M DC18C6, 1 minute extraction time, and room temperature. The calcium and lithium extraction results are shown in **table 3.7, table 3.8, and fig 3.9.** The results clearly show the dependency on the aqueous phase as an increase of aqueous phase concentration, the distribution coefficient also increases. However, the isotope fractionation of calcium and lithium in the organic phase was consistent (**Fig 3.10 and 3.11**). The result could be compared to one of K. Nishizawa et al. works on the effect of lithium content

in the extraction system [104]. The results revealed the same behavior on the distribution coefficient. However, the separation factor was inconsistent with K. Nishizawa work. In K. Nishizawa report, the result indicated the dependency of lithium isotope fractionation dependencies as an increasing of LiCl concentration, the separation factor of $^{6}Li/^{7}Li$ increases up to 1.045. The reason might be that the fractionation is dependent on the cavity size of the crown-ether. The crown-ether used in K. Nishizawa work is B15C5, which has a cavity size corresponding to the lithium ionic radius size. In contrast, our experiment is DC18C6 which has a larger cavity size and is more suitable for calcium extraction. Nonetheless, the total amount of crown-ether is also different. In this research, the crown-ether was found to be 14.0 mmol (200mL of 0.07M DC18C6 dissolve in chloroform), while the K. Nishizawa work was only 3.7 mmol (20mL of 0.186M B15C5 dissolve in chloroform). The difference might result in the distribution coefficient and the separation factor as well. **Fig 3.12** shows the comparison of lithium extraction results to K. Nishizawa works. Moreover, the mole ratio (η) also revealed the ion-crown complex to the total crown-ether in the extraction system, indicating the same behavior as the extraction under B15C5 crown-ether. The

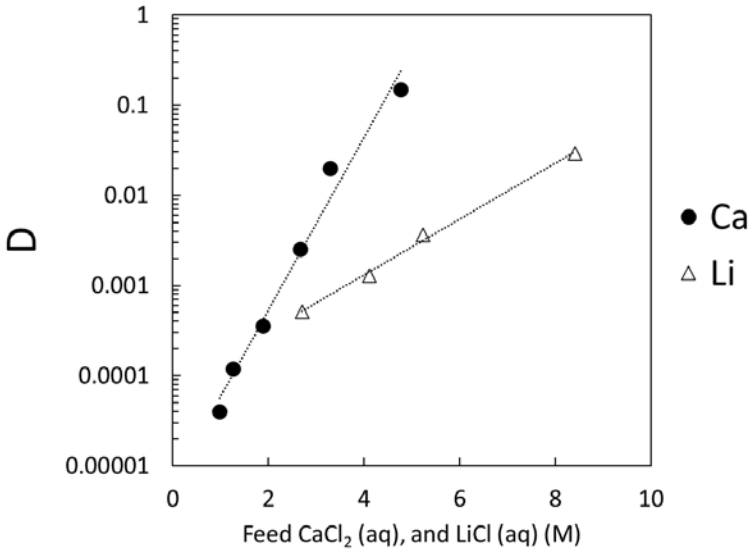

Fig 3.9 Distribution coefficient (D) of calcium and lithium extraction using 0.07M DC18C6 crown-ether under various feed concentration.

mole ratio (η) was directly related to the distribution coefficient (D), indicating that the ion exchange occurs through the ion-crown complex formation. At the same time, the mole ratio also demonstrated the activated crown-ether. For example, under the same concentration of calcium and lithium (2.7M), the mole ratio of calcium (0.009) is larger than lithium (0.002), indicating the ratio of calcium to crown-ether is approximately 1% while the lithium was 0.2%. This behavior also shows that the DC18C6 is appropriate to calcium more than lithium. The advantage of DC18C6 is that the low water solubility and our setup could provide the better lighter isotope (^{6}Li) separation and production due to the high distribution coefficient.

Table 3.7 Calcium extraction under the different aqueous phase concentration system

Aqueous phase		D	η	^{48}Ca/^{40}Ca	^{48}Ca/^{42}Ca	^{48}Ca/^{43}Ca	^{48}Ca/^{44}Ca
% w/w	$CaCl_2$ (M)			α_{org}	α_{org}	α_{org}	α_{org}
10	1.0	0.0000 ±0.0000	0.000	-	-	-	-
15	1.3	0.0001 ±0.0000	0.000	-	-	-	-
20	1.9	0.0004 ±0.0000	0.001	-	-	-	-
25	2.7	0.0025 ±0.0000	0.009	0.989 ±0.004	0.993 ±0.005	0.990 ±0.004	0.993 ±0.004
30	3.3	0.0200 ±0.0003	0.089	0.991 ±0.002	0.992 ±0.003	0.994 ±0.003	0.996 ±0.004
40	4.8	0.1480 ±0.0012	0.900	0.989 ±0.004	0.993 ±0.005	0.995 ±0.003	0.996 ±0.004

Table 3.8 Lithium extraction under the different aqueous phase concentration system

Aqueous phase		D	η	^{7}Li/^{6}Li
% w/w	LiCl (M)			α_{org}
10	2.7	0.0005±0.0000	0.002	0.991±0.004
15	4.1	0.0013±0.0000	0.007	0.990±0.003
20	5.2	0.0037±0.0000	0.025	0.988±0.003
30	8.4	0.0292±0.0001	0.324	0.991±0.003

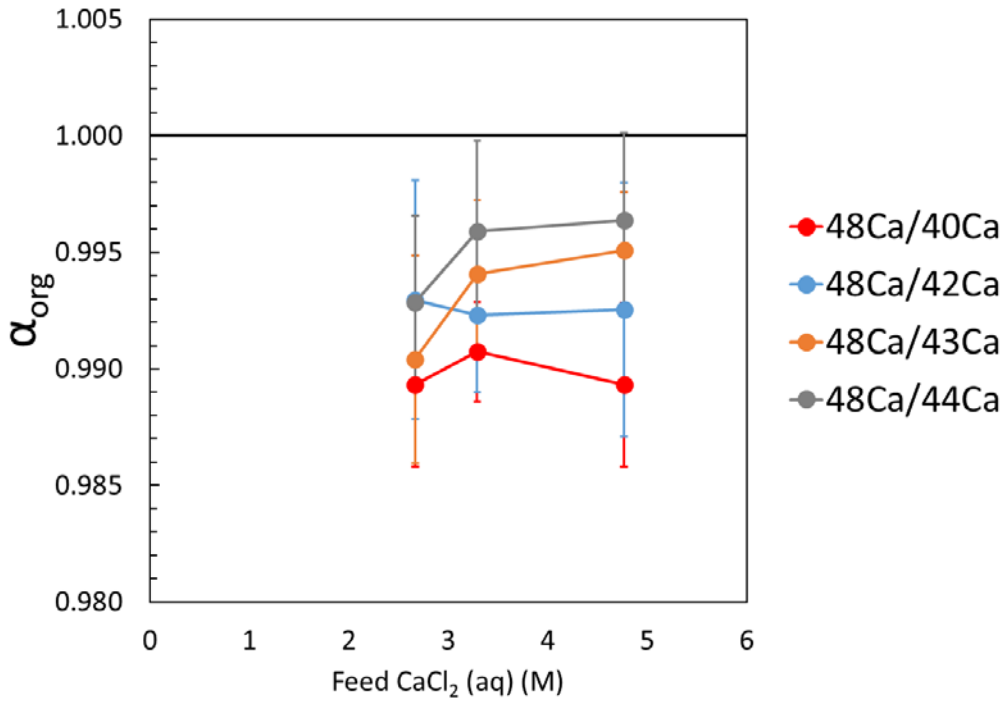

Fig 3.10 Separation factor (α_{org}) of calcium extraction using 0.07M DC18C6 crown-ether under various feed concentration.

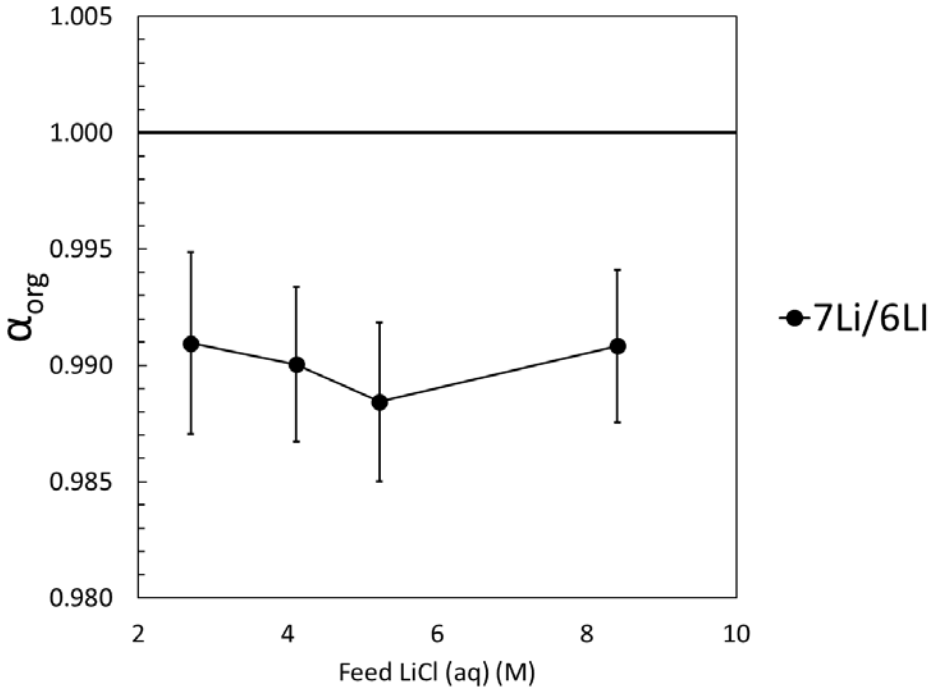

Fig 3.11 Separation factor (α_{org}) of lithium extraction using 0.07M DC18C6 crown-ether under various feed concentration.

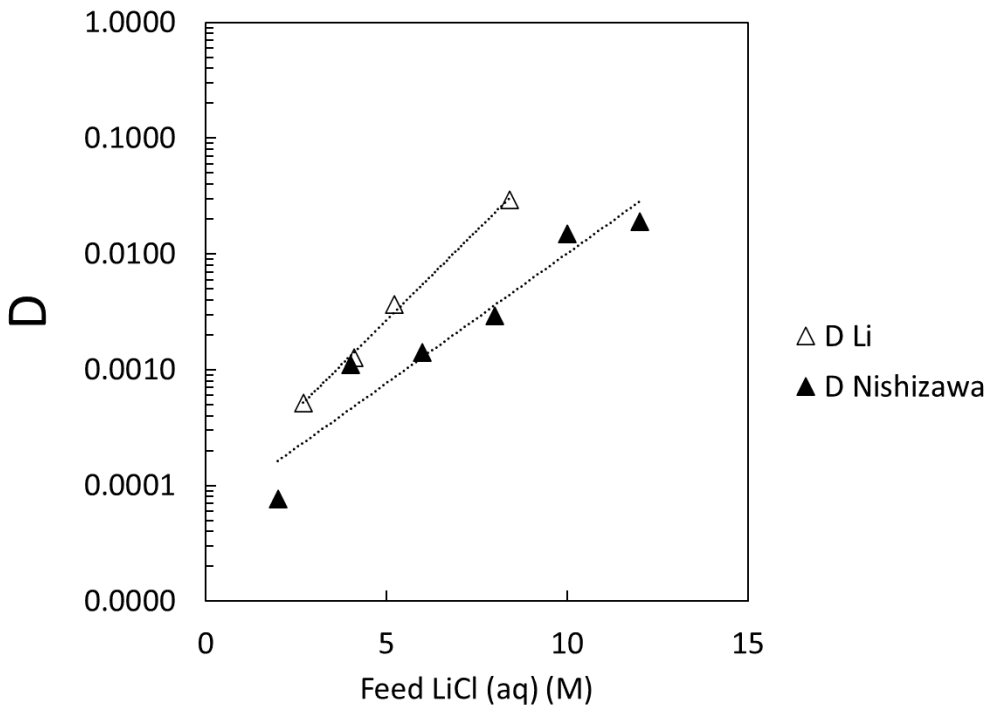

Fig 3.12 Distribution coefficient (D) of lithium extraction using 0.07M DC18C6 crown-ether under various feed concentration (Δ) compared to K. Nishizawa (▲) works under B15C5 crown-ether extraction system.

According to the results obtained from various aqueous phase concentrations, the appropriate concentration of the extraction system using liquid-liquid extraction and crown-ether was found to be higher than 25% w/w system for calcium and higher than 20% for lithium extraction. Therefore, the 30% w/w system extraction was employed in other extraction experiments. Although the 40% w/w $CaCl_2$ (aq) system provided the highest distribution coefficient, but 40% w/w is almost at maximum solubility of calcium chloride at room temperature (45% w/w). This reason led to the remaining calcium content in the organic solution after the back-extraction. Moreover, the requirement of the experiment is not on the production of the lighter isotope of calcium. However, the goal of this experiment is to assure the isotope effect under various concentrations. Therefore, the experiment at 40% w/w $CaCl_2$ (aq) system is not necessary.

3.3.4. Acidity solvent extraction system

In the crown-ether resin chromatographic method requires a high concentration of HCl or HBr solvent to observe the absorption of calcium to crown-ether [63, 64]. This experiment was carried out to investigate the extraction condition on the ion content under the presence of HCl acid. We expected the same behavior as the resin chromatographic method on increasing ion content distributed to crown-ether in the organic phase. This experiment was carried out by using the 12M hydrochloric acid (HCl, 35% – 37%, FUJIFILM Wako Pure Chemical Industries, Ltd. (Japan)) as a solvent instead of an aqueous solvent (pure water). In the calcium extraction, the acidity solvent was conducted by 10%, 20%, and 30% w/w $CaCl_2$ (HCl) (1.1 – 3.9M). On the other hand, the lithium experiment was conducted from 0.3%, 3%, and 30% w/w system (0.1 – 10.5M). The organic solvent was 200 mL 0.07 M DC18C6 dissolved in

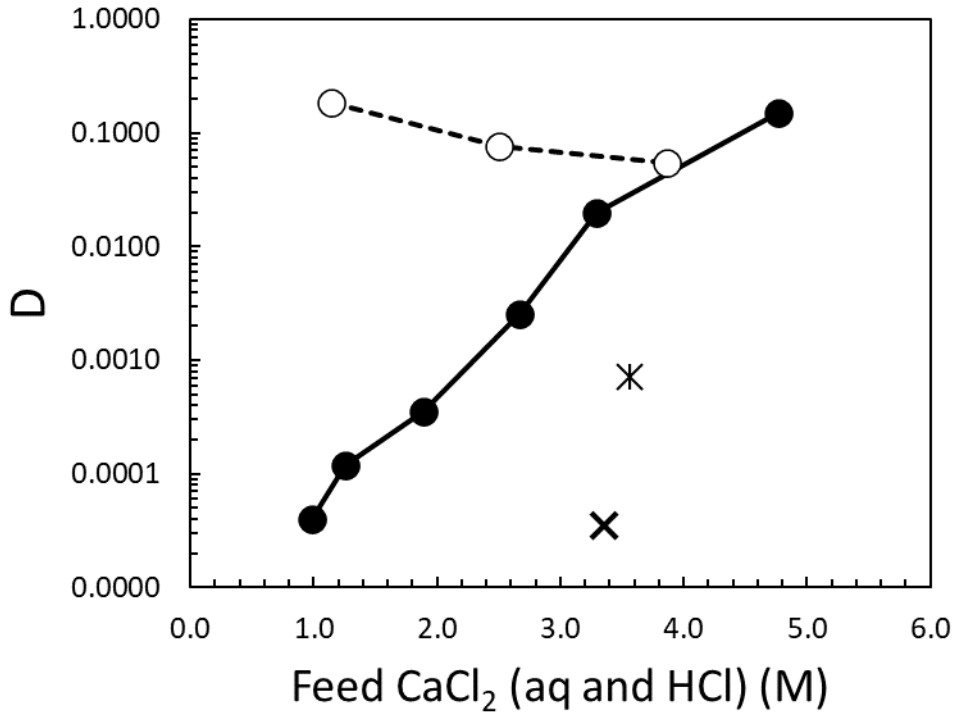

Fig 3.13 Distribution coefficient (D) of calcium extraction using 0.07M DC18C6 crown-ether under various feed concentration and the different solvent system, including water solvent (●) and 12M HCl solvent (○). The absence of crown-ether indicated by cross marks (✳ = HCl, × = aq)

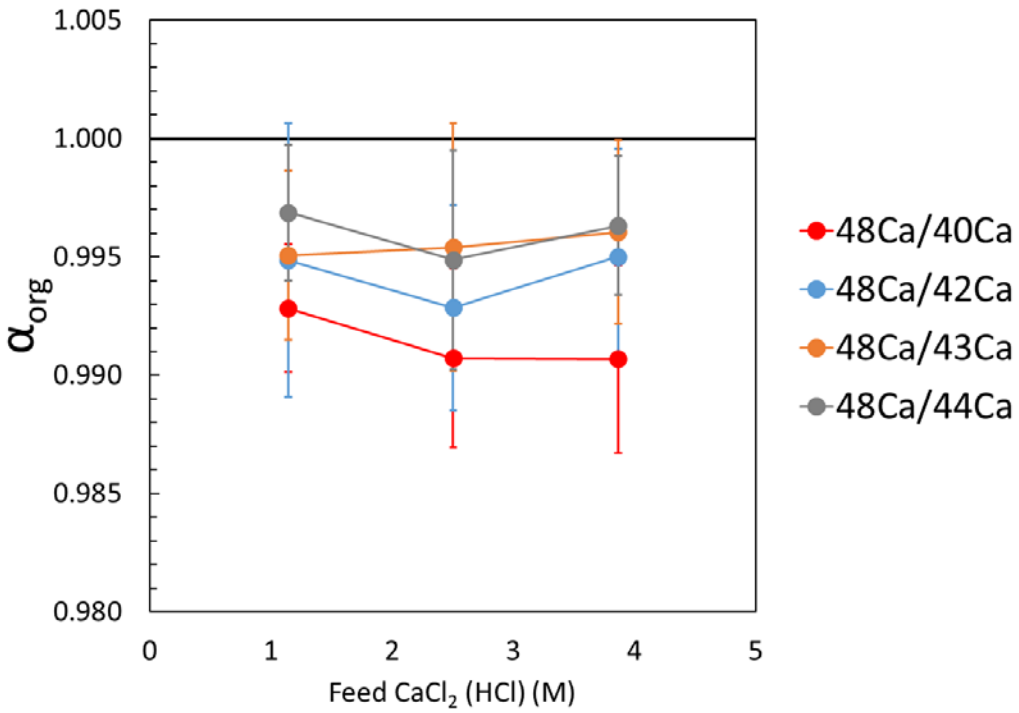

Fig 3.14 Separation factor (α) of calcium extraction using 0.07M DC18C6 crown-ether under the presence of 12M HCl acid as a solvent.

chloroform. The volume ratio of the aqueous and organic phase was fixed at 1/10. The extraction time was consistent at 1 minute and the phase separation time in the separation funnel was 10 minutes. Back-extraction solution obtained from the water solution at the same volume ratio and extraction time as the extraction step was processed. Additional absence of crown-ether and HCl solvent was performed to assure the extraction result. Eventually, the measurement of anion content (Cl^-) was conducted to investigate the contribution of anion to the crown-ether formation. The results of calcium extraction were displayed in **table 3.9, and fig 3.13 to fig 3.15**, comparing to the absence of acidity solvent. The results show the distribution coefficient dependency. This could be concluded that a high concentration of HCl acid resulted in the higher distribution of calcium content to crown-ether. Moreover, the dependency indicated that the HCl acid increased and was maintained at lower concentrations (10% and 20% w/w). The finding corresponded to the study of the band resin chromatographic method

of K. Hayasaka et al. [61]. The study of chromatographic method was conducted by the low concentration of calcium feed (0.02M) with the various concentrations of HCl from 0.5M to 9M. The results revealed that the high concentration of HCl increased the absorption of calcium to crown-ether. The mole ratio (η) indicated the contribution of calcium to crown-ether. Under the presence of 12M HCl acid, the formation of the ion-crown complex was increased and maintained at approximately 20.5 – 26.8% (**Fig 3.15**).

Table 3.9 Calcium extraction using 12M HCl acid as a solvent

Aqueous phase + 12M HCl		D	η	$^{48}Ca/^{40}Ca$	$^{48}Ca/^{42}Ca$	$^{48}Ca/^{43}Ca$	$^{48}Ca/^{44}Ca$
% $CaCl_2$ w/w	$CaCl_2$ (M)			α_{org}	α_{org}	α_{org}	α_{org}
10	1.1	0.1863 ±0.0028	0.205	0.993 ±0.003	0.995 ±0.006	0.995 ±0.004	0.997 ±0.003
20	2.5	0.0768 ±0.004	0.252	0.991 ±0.004	0.993 ±0.004	0.995 ±0.005	0.995 ±0.005
30	3.9	0.0546 ±0.0012	0.268	0.991 ±0.004	0.995 ±0.005	0.996 ±0.004	0.996 ±0.003
30[a]	3.6	0.0007 ±0.0000	0.000	-	-	-	-

[a] Absence of crown-ether extraction system

Another report from S. Nemoto et al. [63] on the calcium extraction under chromatographic method showed the consistent as the higher concentration of HCl acid, the higher absorption of calcium to crown-ether. However, it was revealed that the higher HCl acid, the lower isotope fractionation of calcium. S. Nemoto et al. also reported the MO-calculation based on the rpfr of Bigeleisen-Mayer equation, which supported the isotope fractionation. Those results were in good agreement with our finding on the distribution of calcium to crown-ether, but the advantage of liquid-liquid extraction is that the contribution of calcium is much higher (1.1 – 3.9M). Additionally, the resin chromatographic method under the HCl system showed the dependency of

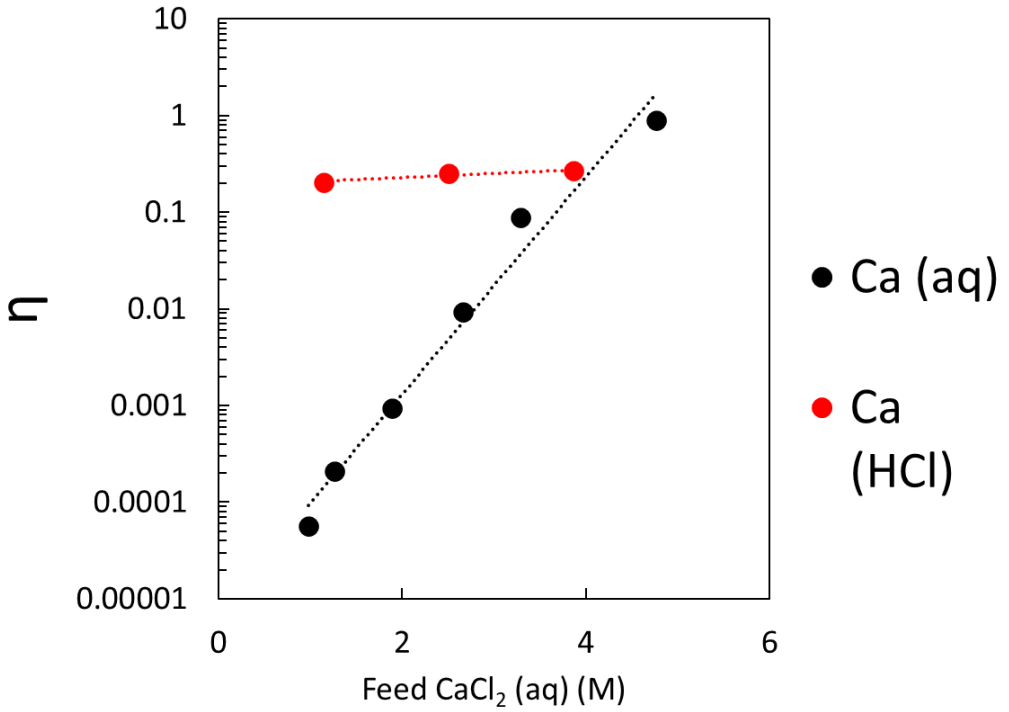

Fig 3.15 The mole ratio (η) of calcium extraction using 0.07M DC18C6 crown-ether under the present of 12M HCl acid as a solvent.

isotope fractionation that the higher concentration of HCl, resulted in the smaller fractionation. Moreover, the absence of HCl provided the higher rpfr value as well. The isotope fractionation of LLE was found to be the same as the aqueous solvent (**Table 3.9**). The reason might be that the conversion of calcium distributed to crown-ether was higher (0.14 – 0.19M) than resin chromatographic. Moreover, due to the enormous uncertainty value of ICP-MS, the difference in isotope fractionation between aqueous and HCl solvent might not be determined. The precise isotope measurement by TIMS is required. Moreover, research on the lower concentration of HCl acid and a small amount of aqueous phase might provide an exciting behavior on isotope fractionation.

The distribution coefficient of the absence crown-ether system under the presence of HCl solvent was found to be slightly higher but still lower than the 25% w/w $CaCl_2$ (aq) system. This behavior ensures that the distribution of calcium had occurred through ion-crown complex formation.

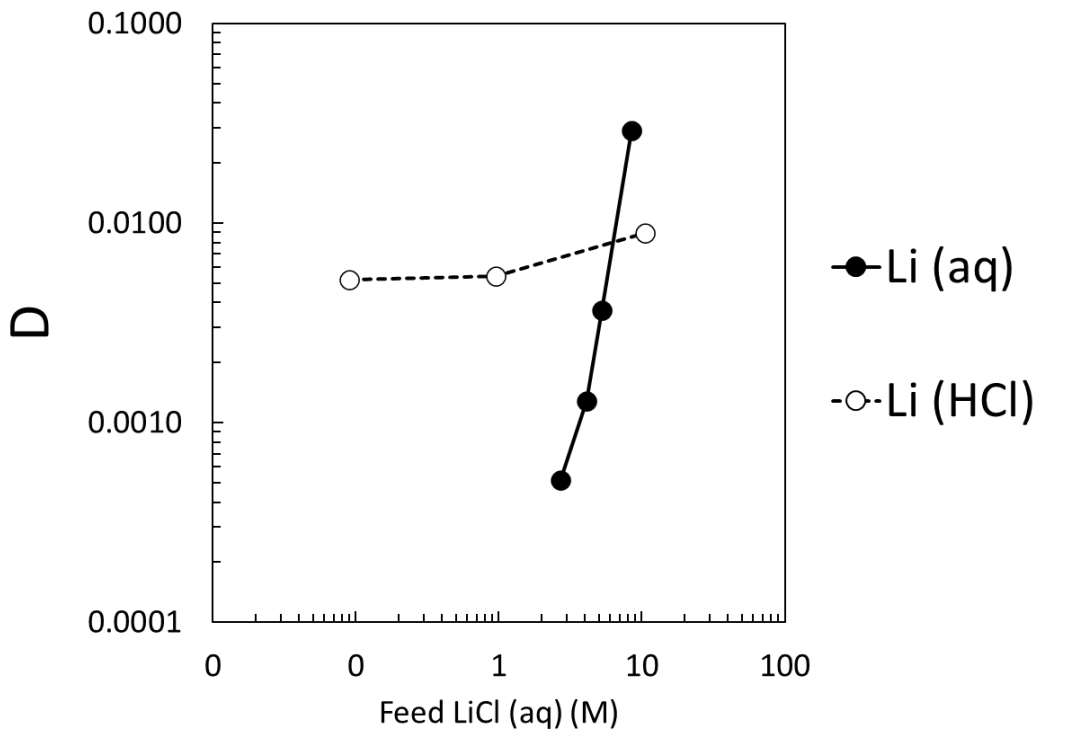

Fig 3.16 Distribution coefficient (D) of lithium extraction using 0.07M DC18C6 crown-ether under various feed concentration and the different solvent system, including water solvent (●) and 12M HCl solvent (○).

Table 3.10 Lithium extraction using 12M HCl acid as a solvent

Aqueous phase + 12M HCl		D	η	$^{7}Li/^{6}Li$
% LiCl w/w	LiCl (M)			α_{org}
0.3	0.1	0.0052±0.0001	0.001	0.996±0.005
3	1.0	0.0054±0.0001	0.008	0.994±0.006
30	10.5	0.0086±0.0001	0.140	0.990±0.004

Lithium results were denoted in **table 3.10 and fig 3.16 to 3.18**. The finding showed the same behavior as calcium extraction. However, because the cavity size of DC18C6 is not appropriate for lithium, the 12M HCl solvent does not increase the distribution coefficient at 30% LiCl w/w extraction system compared to the aqueous solvent. At the same time, the lower concentration trends to be increased and maintained the conversion as well.

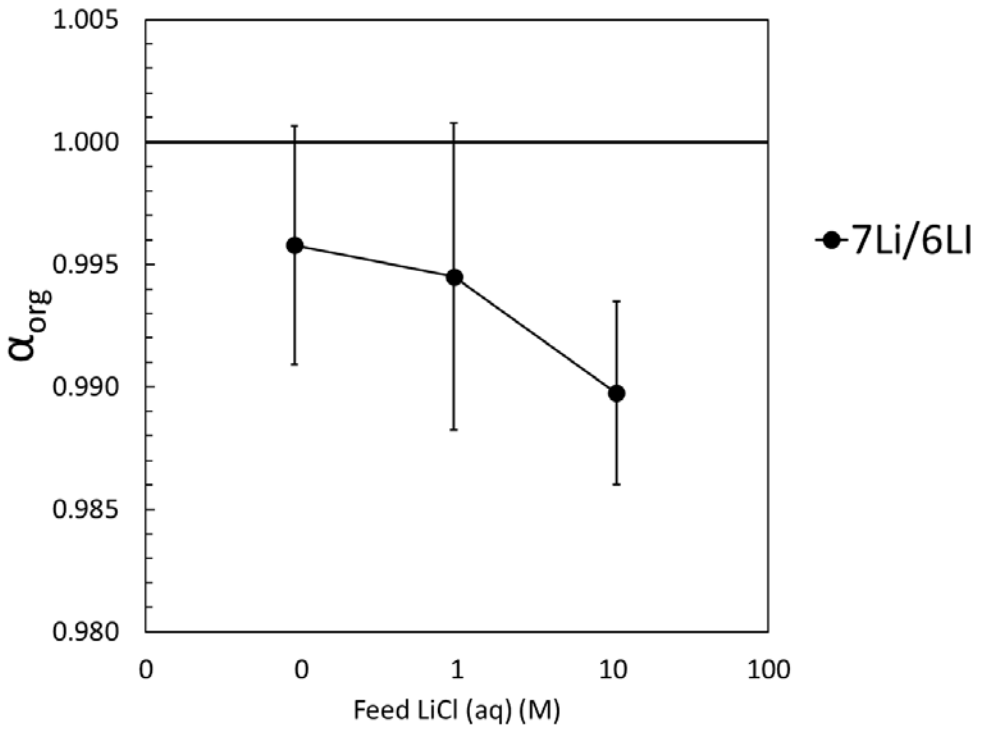

Fig 3.17 Separation factor (α) of lithium extraction using 0.07M DC18C6 crown-ether under the presence of 12M HCl acid as a solvent.

In terms of separation factor (α) under HCl acid solvent, the results show the trends as a higher lithium concentration, the higher isotope fractionation was observed. This behavior is consistent with K. Nishizawa et al.'s works [104] on the separation factor dependency under the high concentration of LiCl. Moreover, the mole ratio (η) was found to be dependent at low concentrations. However, it was noted that DC18C6 was not appropriate for lithium extraction.

In conclusion, the light isotope separation and production (^{6}Li) is possible under the current setup. The high concentration of – 1% fractionation of ^{7}Li/^{6}Li is promising for a single state using an ordinary water extraction system.

Additional measurement of anion contribution (Cl^-) was carried out by ion chromatography (IC) to investigate the role of Cl ion under the presence and absence of acidity solvent. Additional comparison measurement of calcium and lithium content (cation) between AAS and IC was carried out and compared by the represent samples

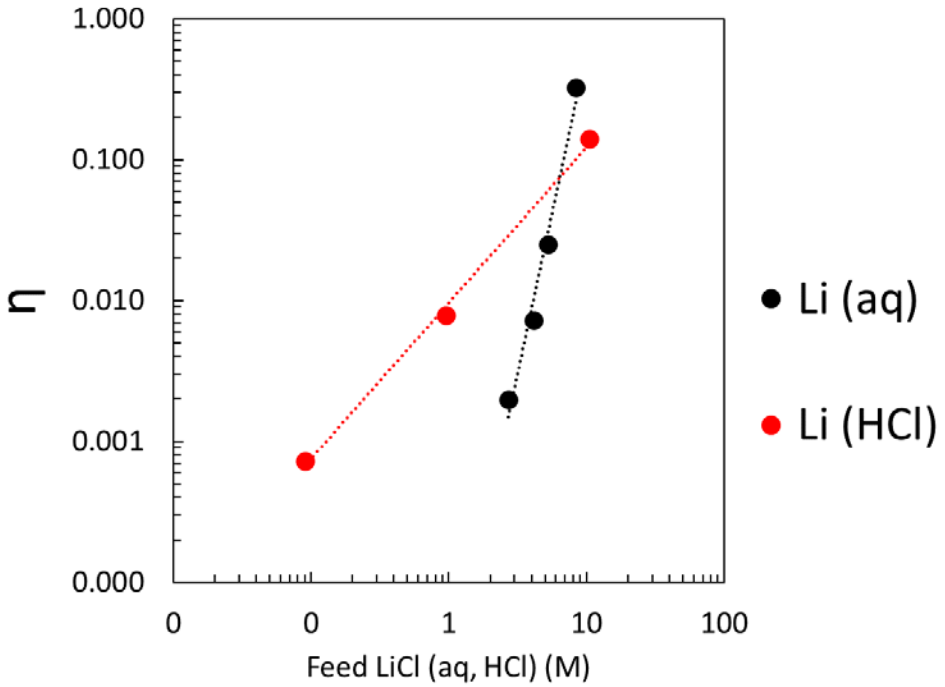

Fig 3.18 The mole ratio (η) of lithium extraction using 0.07M DC18C6 crown-ether under the present of 12M HCl acid as a solvent.

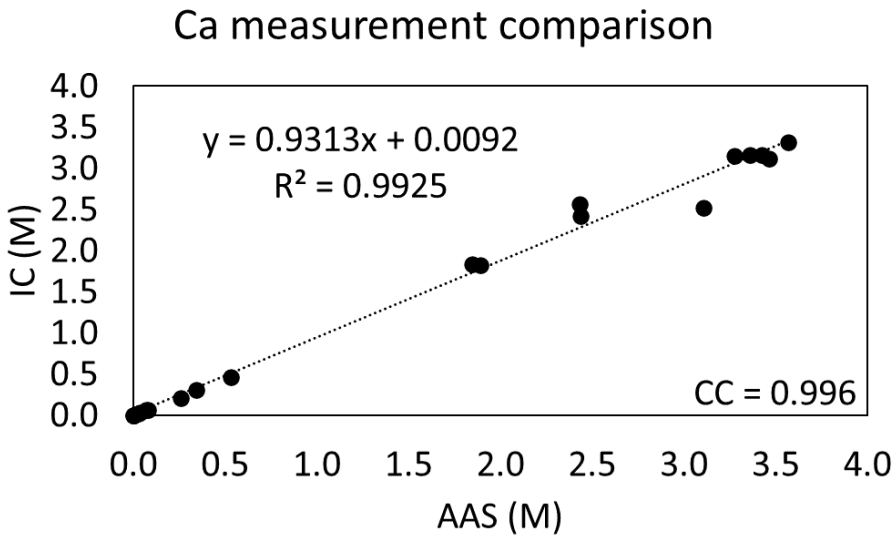

Fig 3.19 Comparison measurement of calcium content by AAS (horizontal) and IC (vertical)

assuring the chemical form of cation in the samples were only Ca^{2+} and Li^{+} ion. It was found that the cation content was comparable between those measurements. The correlation coefficient was very strong at 0.996 and 0.998 for calcium and lithium contents, respectively (**Fig 3.19, 3.20**). Therefore, the determination of cation content

could be conducted by the robust and rapid method, AAS measurement. The result was displayed by the concentration ratio between cation to anion. Calcium results were denoted in **table 3.11 and fig 3.21,** while lithium results were denoted in **table 3.12 and fig 3.22.**

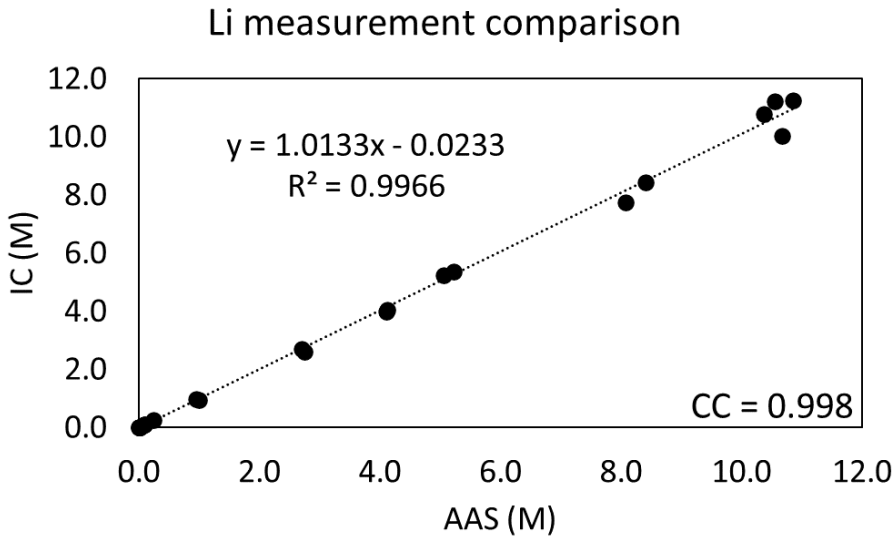

Fig 3.20 Comparison measurement of lithium content by AAS (horizontal) and IC (vertical)

Table 3.11. Calcium and chloride contents of calcium extraction by LLE using DC18C6 crown-ether measured by AAS and IC, respectively

% $CaCl_2$ w/w	Solv-ent	Feed			Extracted			Back extracted		
		Ca (M)	Cl (M)	Cl/Ca	Ca (M)	Cl (M)	Cl/Ca	Ca (mM)	Cl (mM)	Cl/Ca
10	Aq	1.2	2.5	2	1.2	2.6	2	0.14	0.30	2
15		1.9	4.0	2	1.8	3.7	2	0.30	0.68	2
20		2.4	5.1	2	2.4	4.8	2	2.15	4.58	2
30		3.4	7.3	2	3.4	6.8	2	69	141	2
30[a]		3.4	7.0	2	3.4	6.9	2	0.12	0.30	2
10	Aq + 12M HCl	1.1	11.7	10	0.8	9.4	12	142	620	4
20		2.5	12.8	5	2.3	11.4	5	174	722	4
30		3.9	13.2	3	3.4	11.9	3	187	772	4
30[a]		3.6	13.4	4	3.5	12.7	4	2.5	294	119

[a] Absence of crown-ether extraction system

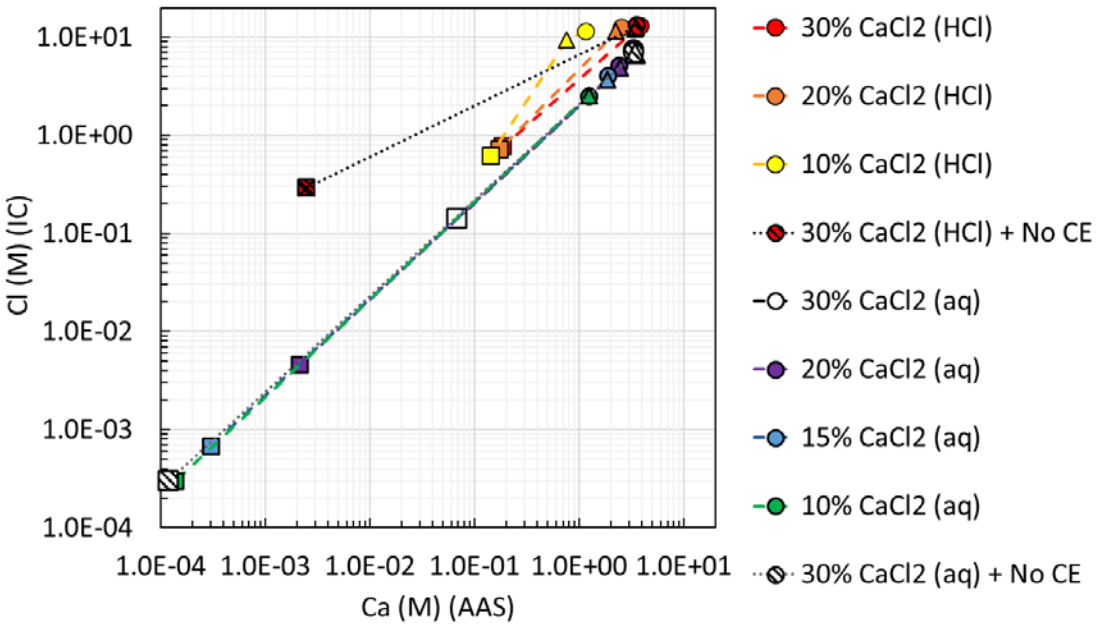

Fig 3.21 Cation and anion concentrations of calcium extraction using 0.07M DC18C6 crown-ether under the presence and absence of 12M HCl acid as a solvent. (● = Feed, ▲ = Extracted, ■ = Back Extracted)

Table 3.12. Lithium and chloride contents of calcium extraction by LLE using DC18C6 crown-ether measured by AAS and IC, respectively

% LiCl w/w	Solv-ent	Feed			Extracted			Back extracted		
		Li (M)	Cl (M)	Cl/Li	Li (M)	Cl (M)	Cl/Li	Li (mM)	Cl (mM)	Cl/Li
10	Aq	2.7	3.1	1	2.7	3.0	1	1.4	1.7	1
15		4.1	4.6	1	4.1	4.7	1	5.2	6.2	1
20		5.2	6.4	1	5.0	6.1	1	19	24	1
30		8.4	10.4	1	8.1	9.7	1	236	285	1
30[a]		8.4	8.6	1	8.1	8.6	1	0.04	0.03	1
0.3	Aq + 12M HCl	0.1	10.4	115	0.1	9.6	102	0.49	1332	2727
3		1.0	9.9	10	1.0	9.6	10	5.37	1398	260
30		10.5	13.0	1	10.7	10.8	1	95.57	1254	13
30[a]		10.8	12.8	1	10.4	11.9	1	1.50	123	82

[a] Absence of crown-ether extraction system

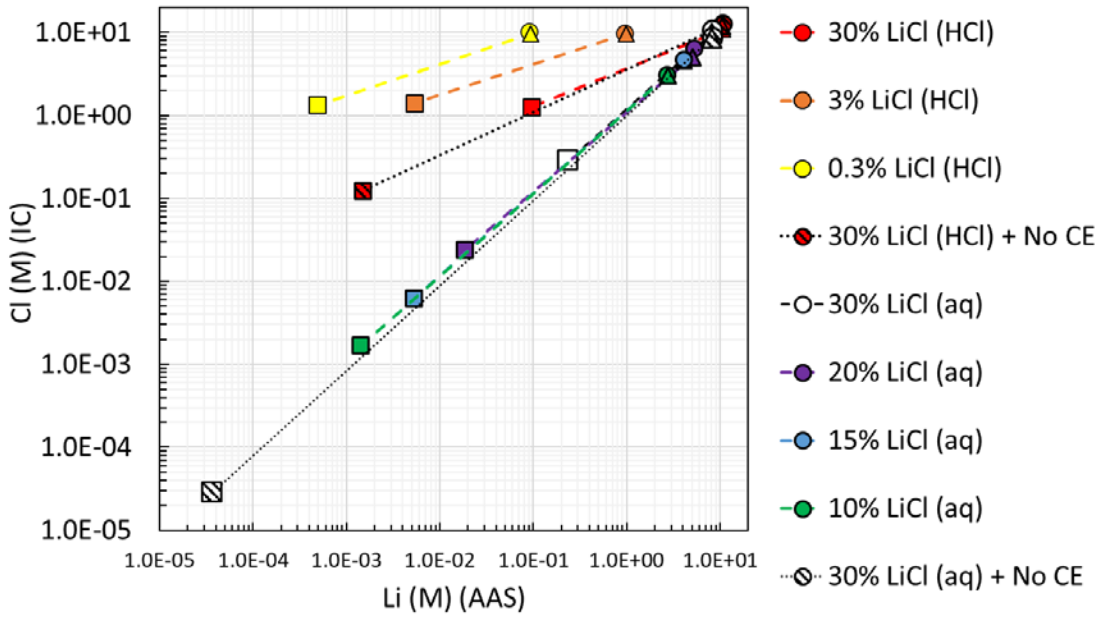

Fig 3.22 Cation and anion concentrations of lithium extraction using 0.07M DC18C6 crown-ether under the presence and absence of 12M HCl acid as a solvent. (● = Feed, ▲ = Extracted, ■ = Back Extracted)

All the aqueous extraction system results were found to be the same behavior. In the case of calcium extraction under the aqueous system, the concentration ratio between calcium to chloride in feed, extracted, and back-extracted was found to be constant at 1:2 (Ca:2Cl). On the other hand, the extraction under 12M HCl acid as a solvent, the concentration ratio (Ca:Cl) in the initial feed and the extracted solution depends on the calcium content. The concentration ratio in the back-extracted phase represented the ratio of the contributed ion-crown formation in the organic phase. The ratio indicated that under the presence of high concentration hydrochloric acid, the ratio of contributed ions forming the ion-crown complex was changed from 1:2 to 1:4. The finding was in good agreement with S. Nemoto et al. works [63] on the demonstration of the optimized structures of the calcium ion-benzo-18-crown-6 (B18C6) complex and calcium ion-benzo-15-crown-5 (B15C5) complex. S. Nemoto reported that the calcium ion located in the center of the B18C6 molecule and the distance between calcium ion

and six oxygen atoms are nearly the same. The anions contribution ($2Cl^-$), in the case of the absence of HCl acid, was found to be bonded to the calcium ion from one side and another side of the plane. Nonetheless, the extraction under the presence of HCl acid was suggested that the HCl atom interacts with the anion cap of the ion-crown complex molecule (**Fig 3.23)**. The formation of 1:4 ratio was expected to be increased with in increases of HCl concentration.

In terms of isotope fractionation, S Nemoto et al. [63] also evaluated the calcium isotope effect of calcium via the molecular orbital (MO) calculations in a qualitative

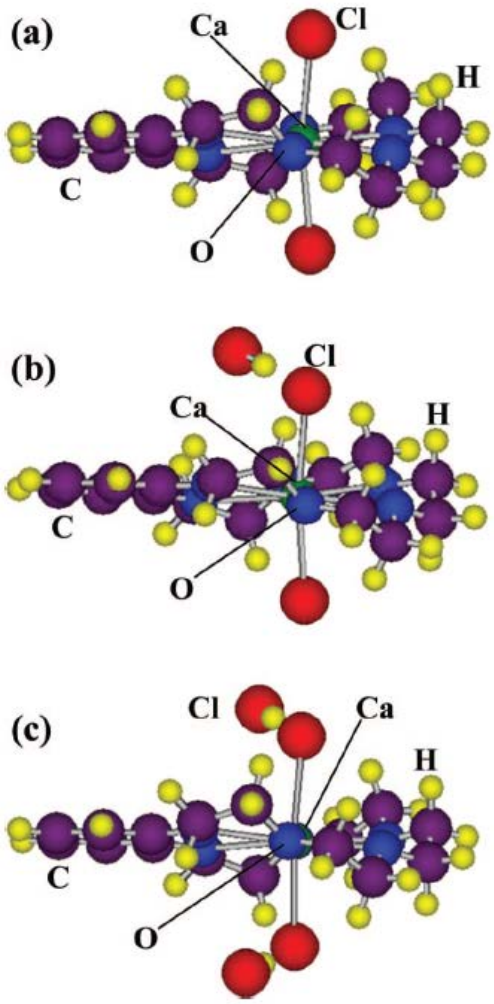

Fig 3.23 The optimized structures of calcium ion-benzo-18-crown-6 (B18C6) complex. (a) = without HCl contribution, (b, c) = HCl contributed to the formation with low and high concentration, respectively [63].

fashion. It was compared with the experimental value. The results indicated that a higher HCl acid concentration in the feed solution results in the minor isotope fractionation. Also, the appropriate crown-ether provided a better isotope fractionation than the smaller one (B15C5).

The same behavior was observed in the case of the aqueous extraction system of lithium as well. The concentration ratio between lithium and chloride was constant at 1:1. Nonetheless, a different behavior was observed in the case of lithium under the presence of HCl solvent. Even the high concentration of LiCl was carried out, the concentration ratio between lithium to chloride in the back-extracted solution was found to be 1:13. At the lower concentration, the behavior indicated that lithium content was slightly increased but different from the lower concentration in the case of calcium. The reason might be that the cavity size of DC18C6 crown-ether (2.6 – 3.2Å) is inappropriate to the lithium even the high concentration of HCl was occupied.

Additional simulation of the ions-crown complex was provided by Prof. Sunaga Ayaki, one of the collaborators from the Institute for Integrated Radiation and Nuclear Science, Kyoto University, Japan. The Program used in this simulation is Gaussian16 with the method of DFT(PBE1PBE), Basis set: Def2svp, and Symmetry: C1. The simulation was carried out to evaluate the formation of an ion-crown complex of calcium and lithium in the aqueous extraction system, along with the determination of the distance between the calcium/lithium to the six oxygen atoms in the crown-ether molecule (**Fig 3.24**). The simulation results correspond with our discovery on the Ca:2Cl:CE, and Li:Cl:CE ratio under the aqueous extraction system. It was indicated that the calcium-crown formation has a symmetry with the same distance between

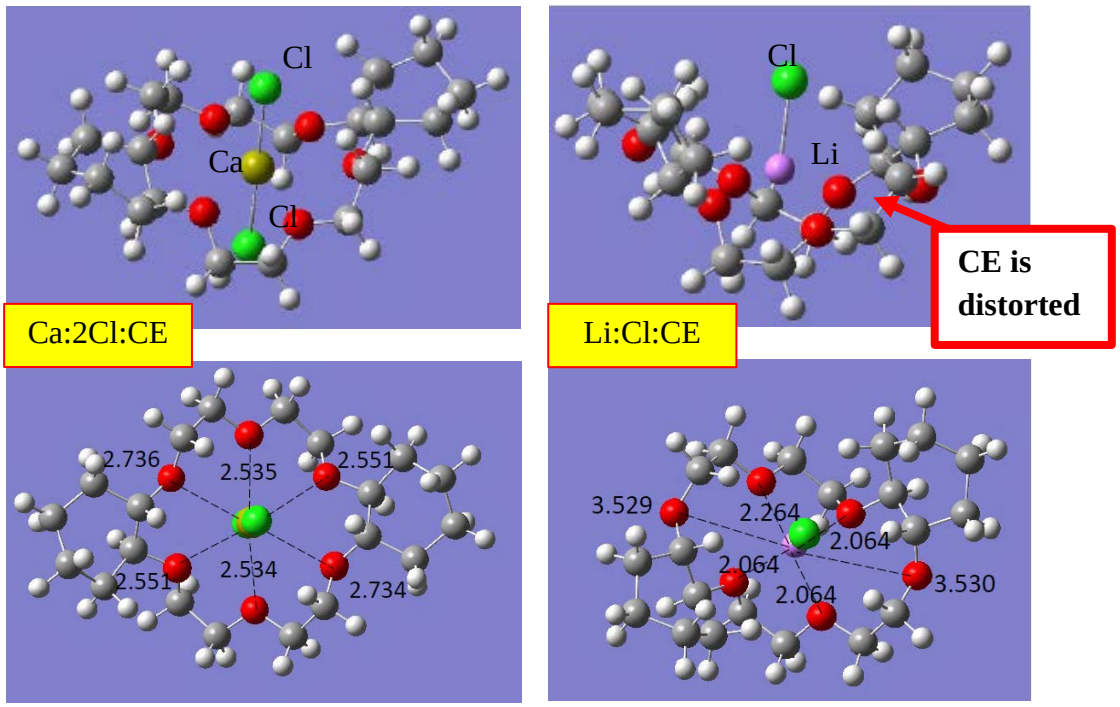

Symmetry with the same distance

CE was distorted. Four oxygen atoms and lithium atom are close to each other

Fig 3.24 The optimized structures of calcium ion-DC18C6 complex [Left]. The optimized structures of lithium ion-DC18C6 complex [Right].

calcium and six oxygen atoms in the ring. Two chloride atoms were bonded to the calcium ion from one side and another side of the plane. In contrast, the lithium-crown complex was found that the crown-ether is distorted, and only one chloride atom interacts with the lithium ion. The distance between lithium ion the oxygen atoms was asymmetry. Further study on the extraction system in the presence of HCl acid is in process.

3.3.5. Volume ratio extraction system

The various volume ratios of extraction conditions were investigated to find the optimal condition for the chemical exchange and calcium isotope fractionation. In this experiment, we extracted various organic phase amounts (0.07M DC18C6 dissolved in chloroform), including 10 mL, 100 mL, and 200 mL. At the same time, the aqueous

solution volume was 100 mL of 30% w/w $CaCl_2$ (aq). We expected to observe the isotope fractionation in the aqueous phase (enrichment). Since the volume of the aqueous solution is small (1 mL) and cannot be separated by separation funnel, we performed the phase separation by hydrophobic filter (Separation filter (No.2S) size 150Φmm, Advantech Toyo Co., Ltd. (Japan)). The aqueous and organic solution was mixed by a magnetic stirrer for 1 minute and immediately separated by a filter. The organic solution was back-extracted by 10 mL of pure water.

However, to ensure the extraction efficiency on the filter separation and isotope effect comparison, the various aqueous extraction concentrations were carried out. 10 mL of aqueous solution of 10% to 40% w/w $CaCl_2$ (aq) extraction systems was mixed with 100mL 0.07M DC18C6 dissolved in chloroform by magnetic stirrer. The mixing solution was separated by filter separation. Calcium content was stripped from the organic solution back to water by 10 mL of pure water. Because the extraction conditions are different with conventional LLE, the distribution coefficient could not be compared, and the indicating parameter is mole ratio (η) instead. The results show in **table 3.13 and fig 3.25.** It was noted that the 25% w/w system is lower than 100 ppm. The mass bias due to the organic solvent contaminant was observed and could not be reported.

Table 3.13 Filter LLE on calcium extraction on various aqueous phase concentration

Aqueous phase		η	$^{48}Ca/^{40}Ca$	$^{48}Ca/^{42}Ca$	$^{48}Ca/^{43}Ca$	$^{48}Ca/^{44}Ca$
% $CaCl_2$ w/w	$CaCl_2$ (aq) (M)		α_{org}	α_{org}	α_{org}	α_{org}
10	1.0	0.0000	-	-	-	-
15	1.6	0.0000	-	-	-	-
20	2.2	0.0001	-	-	-	-
25	2.8	0.0022	-	-	-	-
30	3.5	0.0653	0.990 ±0.002	0.995 ±0.005	0.993 ±0.002	0.996 ±0.003
40	5.1	0.8956	0.990 ±0.003	0.995 ±0.003	0.995 ±0.003	0.997 ±0.003

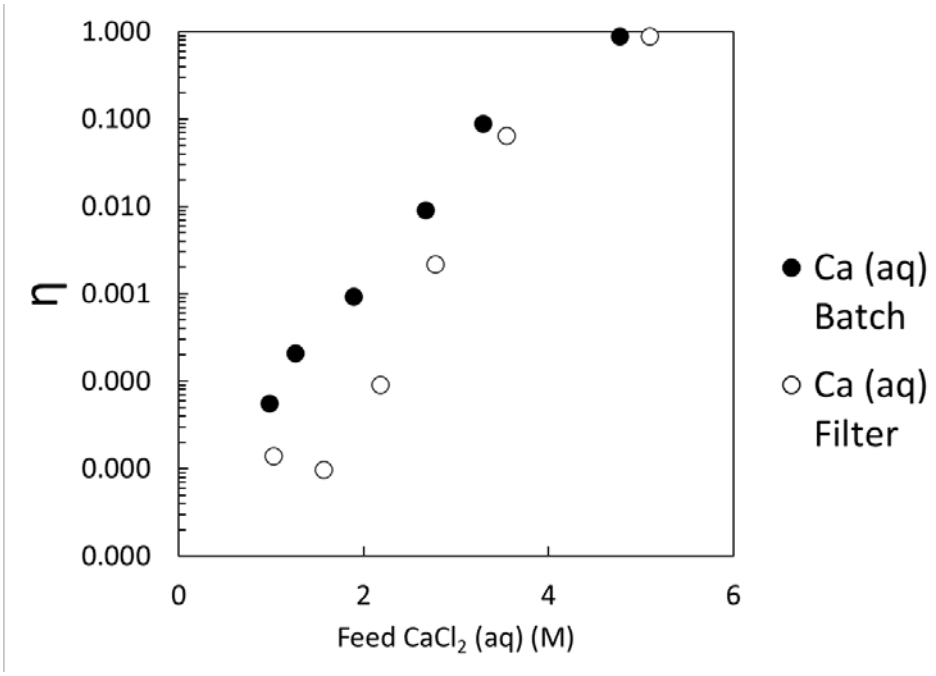

Fig 3.25 The mole ratio (η) of calcium extraction using 0.07M DC18C6 crown-ether on the conventional and filter separation techniques.

According to the results in **fig 3.23**, the mole ratio (η) indicated that the extraction results in the different separation techniques are slightly comparable. Particularly at the higher concentration of 30% to 40% w/w of feed concentration. This finding ensured that the separation techniques is insignificant on the extraction process. Moreover, the separation factor (α) was found to be constant at 0.990±0.002.

This experiment aims to observe the isotope effect on the aqueous phase (α_{aq}) where the heavier isotope was enriched. The volume ratio experiment was performed by the mentioned condition in the first paragraph of this section. The result shows in **table 3.14 and fig 3.26 – 3.27**.

The parameter that indicated the extraction dependencies is the ratio between extracted (raffinate) and feed. Under a large amount of organic solution (200mL), while the aqueous solvent is 1 mL, it was found that the ratio is smaller (0.7) compared to the small volume of the organic phase (0.93). This behavior was expected to be seen the isotope

fractionation in the aqueous phase due to a large amount of calcium (30% of feed) was extracted to the organic phase. The mole ratio (η) between ion-crown complex to the total crown-ether was found to be slightly smaller due to a large amount of total crown-ether in the extraction system. However, the result of the separation factor (α_{aq} and α_{org}) in **fig 3.27** shows the same behavior as conventional extraction with the volume ratio of 1/10 (20/200 mL). The reason might be that the single stage separation is insufficient and multi-stage iteration and precise isotope fractionation is required.

Table 3.14 Separation factor of calcium extraction on various volume ratio

Aq	Org	η	Extracted /Feed	K	$^{48}Ca/^{40}Ca$ α_{org}	$^{48}Ca/^{42}Ca$ α_{org}	$^{48}Ca/^{43}Ca$ α_{org}	$^{48}Ca/^{44}Ca$ α_{org}
mL	mL							
1	200	0.036	0.708	0.292	0.988 ±0.003	0.994 ±0.004	0.996 ±0.003	0.998 ±0.004
1	100	0.024	0.840	0.160	0.989 ±0.003	0.992 ±0.005	0.995 ±0.004	0.995 ±0.003
1	10	0.071	0.927	0.073	0.990 ±0.003	0.991 ±0.006	0.994 ±0.003	0.995 ±0.003
					$^{48}Ca/^{40}Ca$ α_{aq}	$^{48}Ca/^{42}Ca$ α_{aq}	$^{48}Ca/^{43}Ca$ α_{aq}	$^{48}Ca/^{44}Ca$ α_{aq}
					0.998 ±0.003	0.999 ±0.004	1.001 ±0.003	1.000 ±0.004
					1.001 ±0.003	1.001 ±0.005	1.001 ±0.004	1.001 ±0.002
					0.998 ±0.003	0.998 ±0.004	0.998 ±0.003	0.998 ±0.002

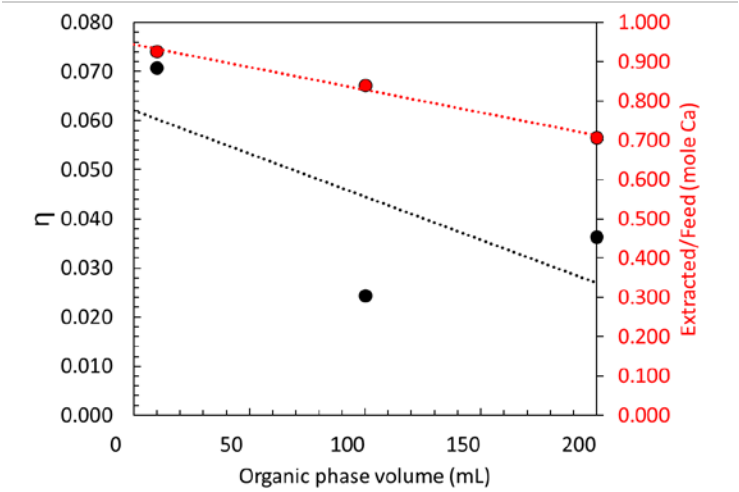

Fig 3.26 The mole ratio (η) and extracted to feed ratio of calcium extraction using 0.07M DC18C6 crown-ether on various volume ratio.

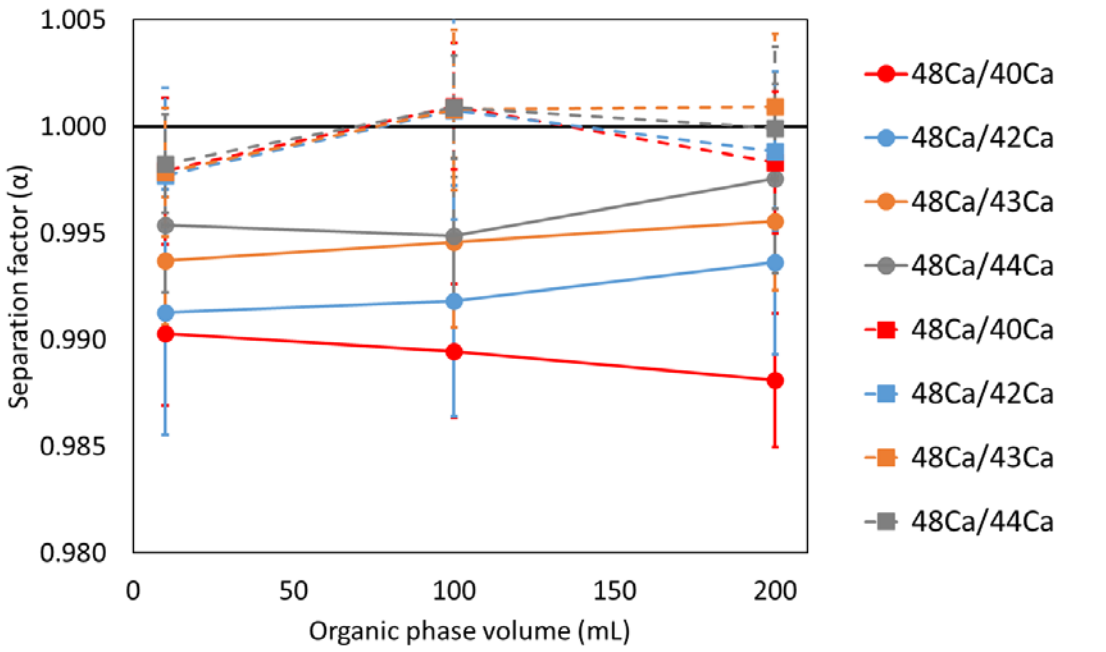

Fig 3.27 The separation factor (α) of calcium extraction using 0.07M DC18C6 crown-ether on various volume ratio. ● = α_{org} ■ = α_{aq}

In conclusion, the volume ratio results showed that even the smaller volume of aqueous could be applied for liquid-liquid extraction. Only the result on the extracted ratio (Extracted/Feed) is different depending on the initial ion volume in the feed. The higher extracted calcium was expected to have a more significant isotope fractionation on the extracted phase (raffinate). The extraction ratio was not significantly dependent on the separation factor in the organic phase (α_{org}) on the different volumes of organic solvents. The extraction ratio increases. The isotope fractionation in the extracted phase increases as well. **Fig 3.28** shows the preliminary calculated on the ^{48}Ca isotope abundance (%) in the aqueous phase (α_{aq}) on the extracted ratio, and α_{org} is equal to 0.990. The calculation value shows that the higher isotope fractionation observes when the large extraction ratio is occupied. The extracted ratio (K) was calculated by the following equation 3.1:

$$K = 1 - \frac{Extracted\ phase\ ion\ (mole)}{Feed\ ion\ (mole)} \quad (3.1)$$

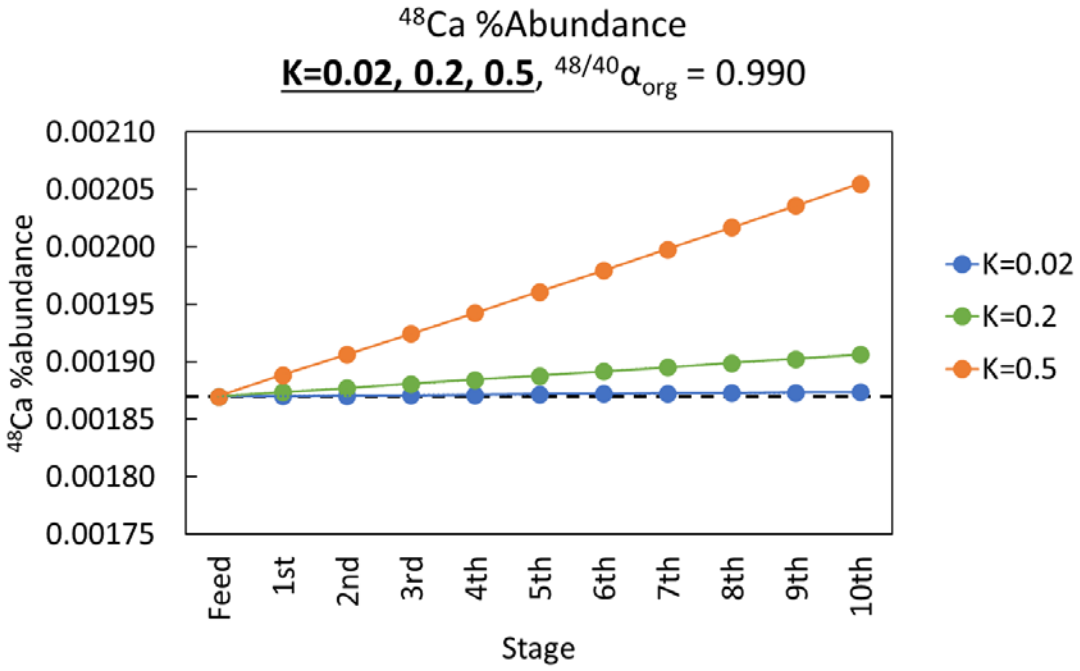

Fig 3.28 The calculated ^{48}Ca %abundance of calcium extraction on the various extracted ratio (K).

3.3.6. Extraction temperature

According to the finding of K Nishizawa et al. [101, 104] and Z. Zhang et al. [83] on the isotope separation of lithium using crown-ether liquid-liquid extraction and the organic liquid film method, and Bigeleisen approximation [25]. The results indicated that the extractant's extraction capacity for lithium ions and separation factor decreases as the temperature rises. This research also investigated the distribution coefficient and the isotope separation factor under the various extraction temperatures. The experiment conditions consisted of -15, 0, room temperature (22±0.5), and 45 °C extraction temperature. 30% w/w $CaCl_2$ (aq) and 0.07M DC18C6 dissolved in chloroform, with a volume ratio of 1/10, as an aqueous and organic phase was kept in the incubator with a constant temperature for 1 hour. The extraction process was conducted at room temperature for 1 minute and allowed for phase separation in the separation funnel for 10 minutes under the constant temperature condition. The back

extraction process was performed at room temperature by the same volume ratio as the extraction procedure. The results of extraction temperature dependencies show in **tables 3.15, and 3.16** and **fig 3.29 to 3.31** for calcium and lithium, respectively.

Table 3.15 Calcium extraction under various extraction temperature

Ext. Temp. °C	$CaCl_2$ (aq) (M)	D	η	$^{48}Ca/^{40}Ca$ α_{org}	$^{48}Ca/^{42}Ca$ α_{org}	$^{48}Ca/^{43}Ca$ α_{org}	$^{48}Ca/^{44}Ca$ α_{org}
-15	3.6	0.0339 ±0.0001	0.1565	0.987 ±0.003	0.992 ±0.004	0.992 ±0.003	0.994 ±0.003
0	3.6	0.0300 ±0.0009	0.1431	0.989 ±0.005	0.993 ±0.006	0.992 ±0.004	0.997 ±0.003
RT (22)	3.7	0.0230 ±0.0002	0.1150	0.990 ±0.003	0.992 ±0.004	0.992 ±0.004	0.993 ±0.003
45	3.6	0.0164 ±0.0001	0.0735	0.990 ±0.003	0.996 ±0.005	0.994 ±0.004	0.996 ±0.003

Table 3.16 Lithium extraction under various extraction temperature

Ext. Temp. °C	LiCl (aq) (M)	D	η	$^{7}Li/^{6}Li$ α_{org}
-15	7.87	0.0711 ±0.0002	0.6841	0.990±0.005
0	7.99	0.0449 ±0.0002	0.4640	0.994±0.004
RT (22)	8.61	0.0258 ±0.0002	0.3238	0.989±0.004
45	7.87	0.0148 ±0.0001	0.1563	0.994±0.005

The results of temperature dependency indicated that the distribution coefficient (D) increases as the temperature decrease. The same behavior was observed on both calcium and lithium extraction. This finding was in good agreement with K. Nishizawa et al. report on the study of lithium extraction using crown-ether and temperature difference, ranging from 0 – 40 °C [101]. The results revealed the same behavior as our finding. However, K. Nishizawa carried out the extraction by 2M LiI, was the most

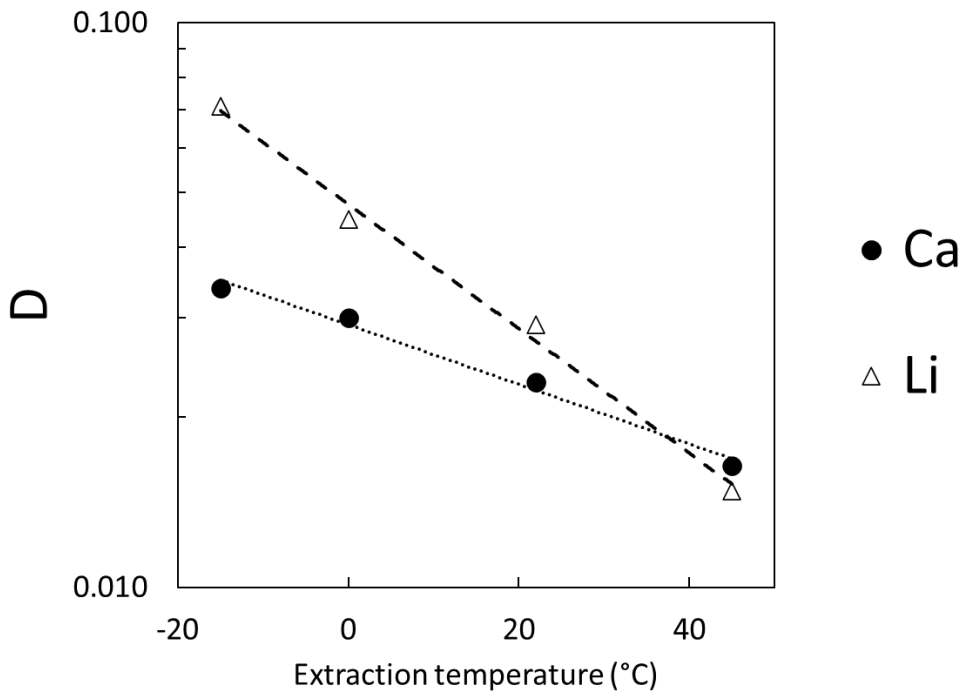

Fig 3.29 The distribution coefficient of calcium and lithium extraction on various extraction temperature

applicable species due to the high distribution coefficient (D) and a high concentration of B15C5 (0.186M) under the same volume of organic and aqueous phase (20mL/20mL). The results indicated the dependency on separation factor (α) up to 1.045 at 0 °C. According to **fig 3.30 and 3.31**, the separation factor was consistent at various temperatures. The precise isotope analysis of calcium is required to observe the difference in the isotope separation under the extraction temperature. In the case of lithium, the separation factor (α) was inconsistent with K. Nishizawa work. The reason that the species of lithium used in this research are LiCl which was reported to provide a small isotope effect compared to LiI. Moreover, the extraction conditions, such as crown-ether type (B15C5), concentration, and so on, differed from K. Nishizawa reported. In conclusion, the isotope fractionation should increase as the temperature decreased, according to the Bigeleisen-Mayer approximation. Despite the variation of separation factor on various temperatures could not be investigated by ICP-MS, the obtained separation factor trended to be as the lower temperature, resulted to the more fractionation becomes (**fig 3.30 and 3.31)**.

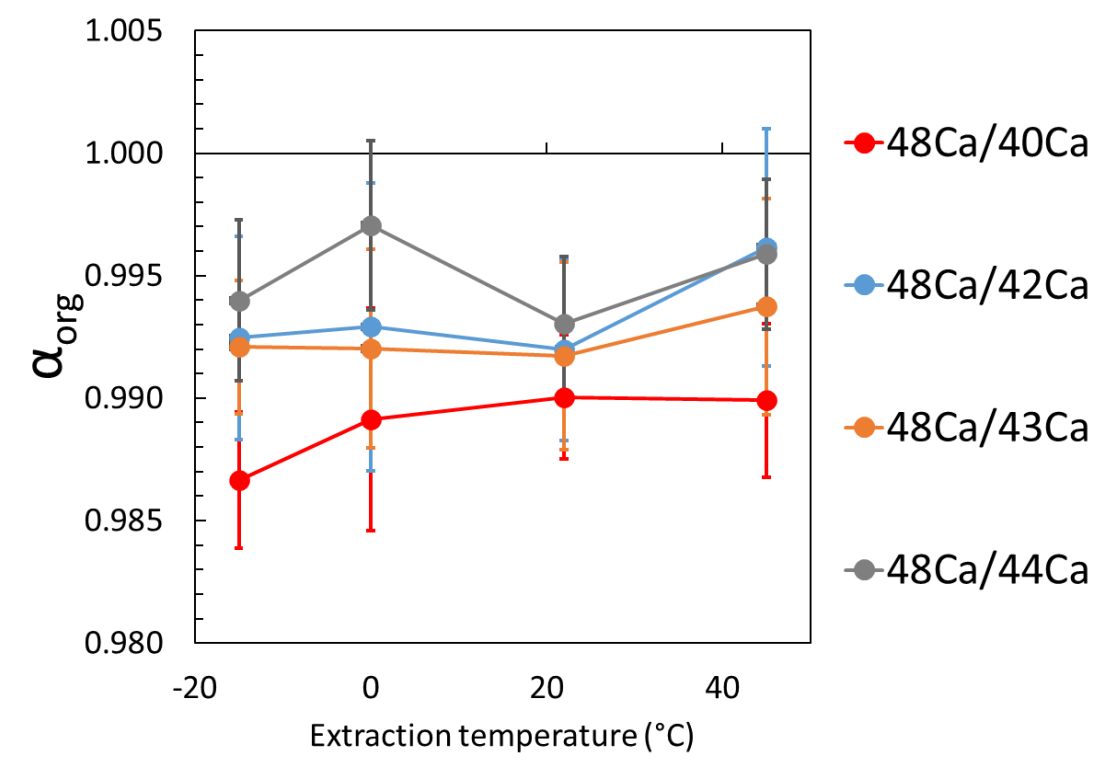

Fig 3.30 The separation factor (α_{org}) of calcium extraction on various extraction temperature

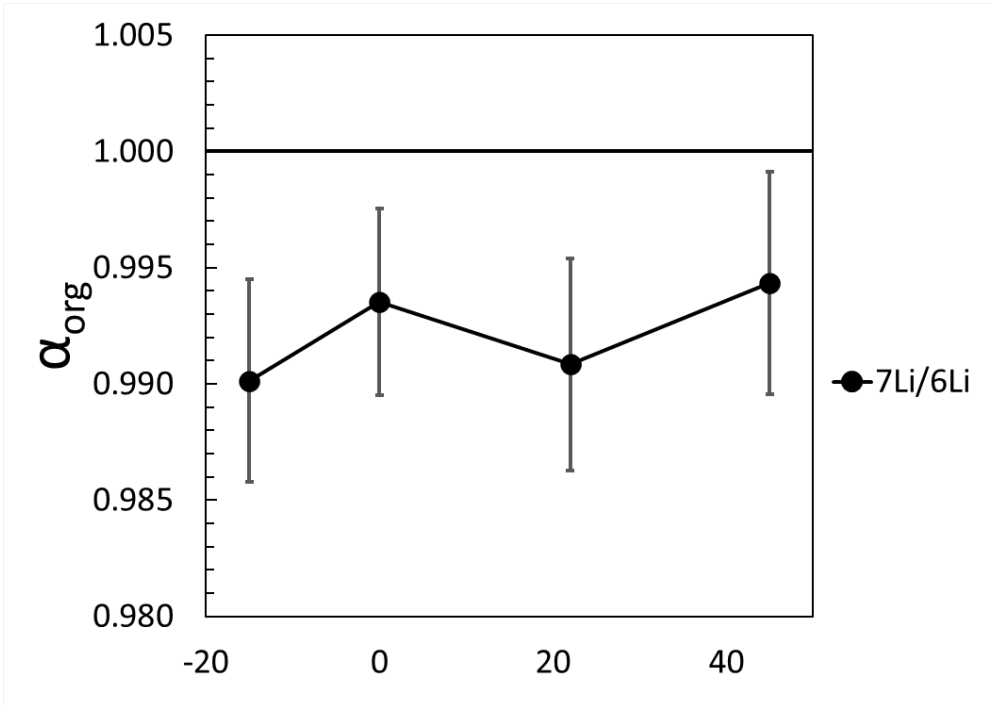

Fig 3.31 The separation factor (α_{org}) of lithium extraction on various extraction temperature

3.3.7. Solid-liquid extraction (SLE)

This experiment aims to investigate the chemical reaction between calcium in the solid phase to crown-ether dissolved in the organic solution. The finding could be applied to the water-soluble crown-ether, such as 18C6 crown-ether, which is approximately 10 times cheaper than DC18C6 crown-ether. We experimented using filter separation techniques and a low-level vacuum system (**Fig 3.32**). The solid phase of 1gram $CaCl_2 \cdot 2H_2O$ as a calcium feed was mixed with the organic phase, 20mL 0.07M DC18C6, for 1 minute using a glass rod and separated by the filter. The organic phase was back-extracted by 20mL of pure water. The remaining solid phase on the filter was mixed with the new organic phase containing crown-ether to ensure the same chemical reaction. The extraction process was repeated three times. The same

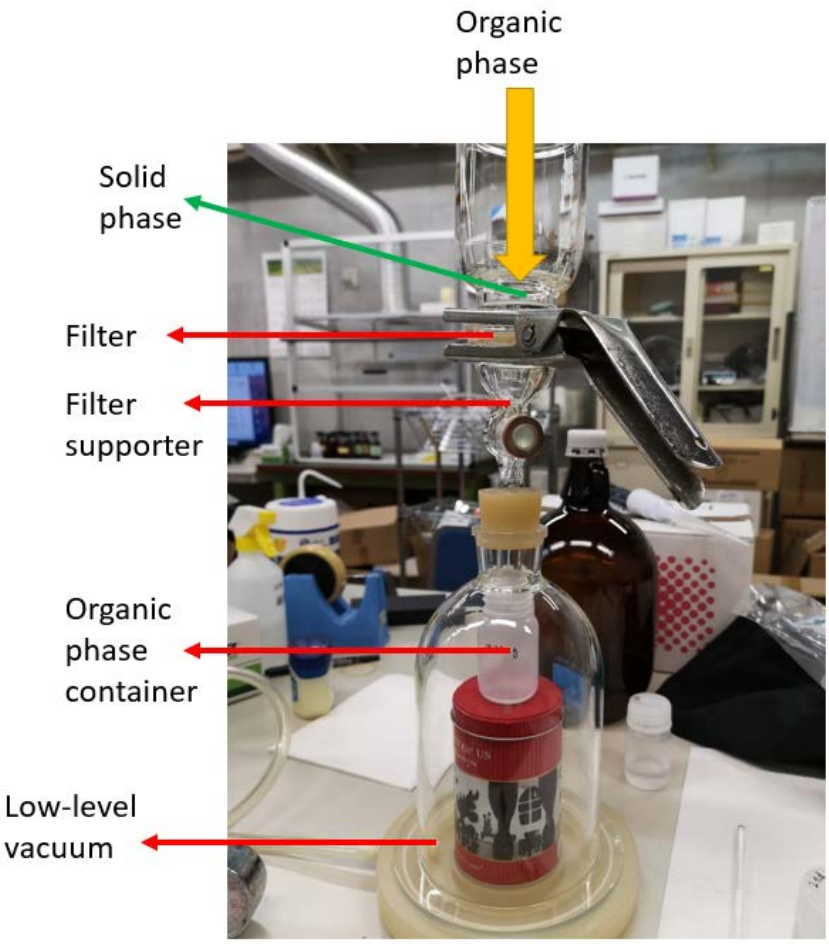

Fig 3.32 Low vacuum filter separation system for solid-liquid extraction

extraction process was conducted without a crown-ether extraction system. The calcium content in organic solutions shows in **table 3.16 and fig 3.33.** The calcium content in back-extracted samples confirmed the chemical reaction between the solid calcium phase and DC18C6 crown-ether. Moreover, the mole ratio (η) was highest at 0.8421, while the liquid-liquid extraction was approximately 0.0957 and 0.2677 under the absence and presence of HCl acid at 30% w/w feed extraction system.

Table 3.16 Solid-liquid extraction of calcium

$CaCl_2 \cdot 2H_2O$ (g)	mmol crown-ether	1st Iteration		2nd Iteration		3rd Iteration	
		Ca (mmol)	η	Ca (mmol)	η	Ca (mmol)	η
1	1.4	1.175	0.8421	0.787	0.5638	0.605	0.4334
1	0.0	0.000	0.0000	0.000	0.0000	0.000	0.0000

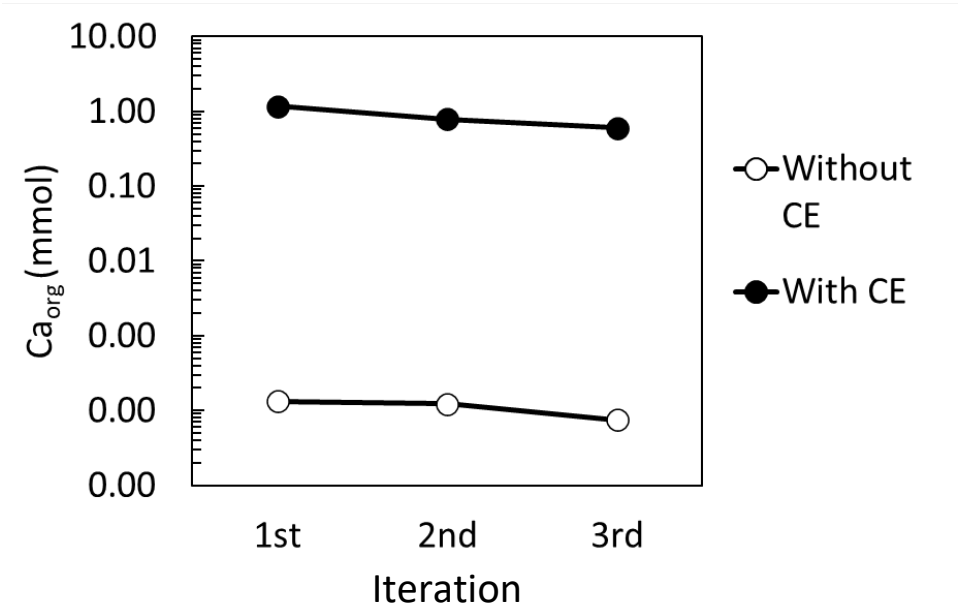

Fig 3.33 Low vacuum filter separation system for solid liquid extraction

High extraction efficiency was observed, and the multistage extraction was easy to be performed. The iteration experiment of solid-liquid extraction was carried out under the same conditions as the previous experiment, except that the initial solid phase was increased to 2 grams to ensure sufficient extraction. Additionally, water-soluble crown-ether, 18C6, was prepared at the same conditions as DC18C6. The multistage

iteration was carried out for five iterations. After each extraction, the solid phase was sampled for 0.1 g and dissolved in 50 mL pure water. The organic phase was mixed with 20 mL pure water for back extraction. All of the remaining solid phase was dissolved in pure water at the final iteration. **Fig 3.34** shows the solid-liquid extraction procedures for each iteration stage. The result is shown in **table 3.17**. It is noted that ICP-MS conducted the preliminary isotope measurement of calcium without reaction gas. Therefore, the isotope analysis could be measured only for ^{48}Ca and ^{43}Ca. The separation factor (α) was reported by $^{48}Ca/^{43}Ca$ for both solid and organic phase (**Fig 3.35 – 3.36**). The result indicated that even the large extraction amount could be obtained from solid-liquid extraction, but the isotope fractionation was not observed in both organic and aqueous species. The reason is that the isotope effect occurs in the chemical exchange of cation to the crown-ether. The calcium species need to be ion or solution for the isotope separation by crown-ether LLE. In conclusion, the SLE increased calcium content extraction, but no isotope effect was observed. Therefore, SLE is inappropriate for isotope separation and mass production. The same behavior

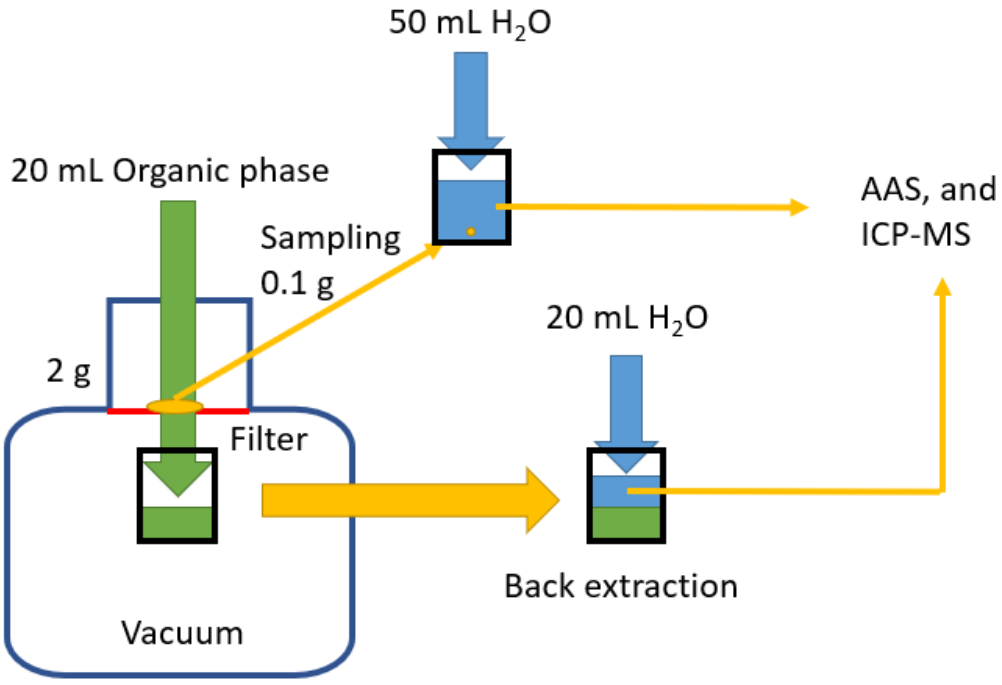

Fig 3.34 The solid-liquid extraction procedures.

was also observed from water-soluble crown-ether (18C6). Further research on the countermeasure of 18C6 or other types of crown-ether is required for a cost-effective manner.

Table 3.17 Solid-liquid extraction of calcium on 5 iteration stages

Stage	20 mL 0.07M DC18C6			20 mL 0.07M 18C6		
	Ca (mmol)	η	$^{48}Ca/^{43}Ca$ α	Ca (mmol)	η	$^{48}Ca/^{43}Ca$ α
Feed (1g)	13.60	-	-	13.60	-	-
S1	0.56	-	1.001±0.002	0.52	-	0.998±0.003
S2	0.64	-	1.000±0.002	0.51	-	1.000±0.003
S3	0.65	-	1.000±0.002	0.46	-	0.999±0.002
S4	0.52	-	1.000±0.002	0.46	-	1.000±0.003
S5	5.74	-	0.999±0.003	6.21	-	0.999±0.003
Org1	1.25	0.895	1.000±0.002	0.85	0.604	1.001±0.002
Org2	1.34	0.955	1.001±0.002	1.01	0.722	1.000±0.002
Org3	1.18	0.845	1.000±0.002	0.94	0.674	1.001±0.002
Org4	0.90	0.643	1.001±0.002	1.07	0.766	0.998±0.002
Org5	0.52	0.374	0.999±0.002	0.82	0.584	1.000±0.002
Conversion	13.32			12.85		
Recovery	97.88%			94.45%		

S = solid phase, Org = organic phase
Conversion = total S1-S5 and Org1-Org5
Recovery = conversion/feed

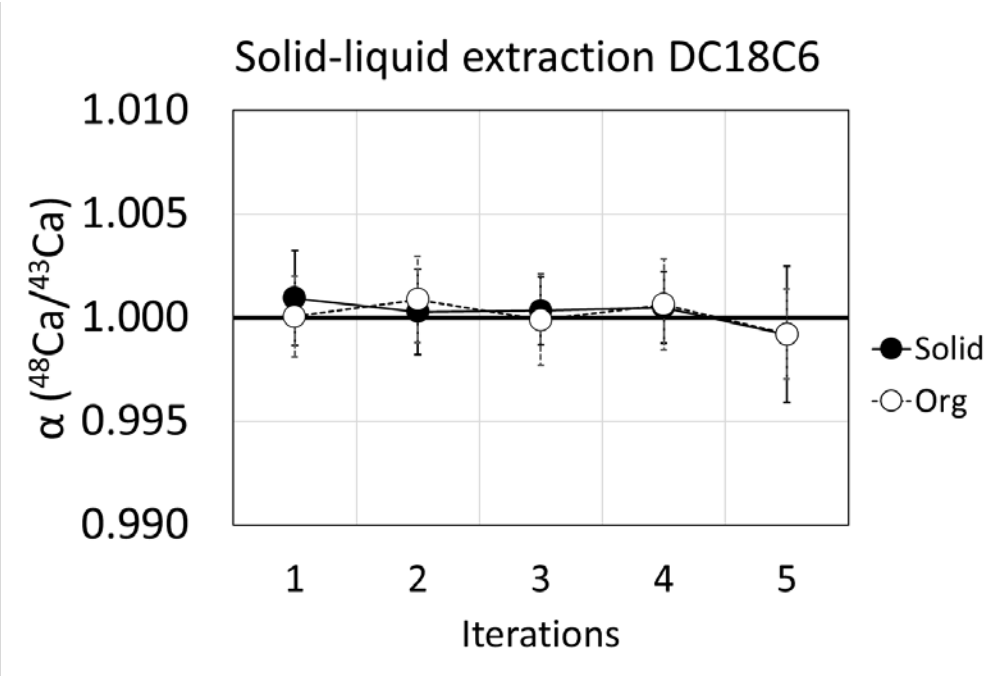

Fig 3.35 The separation factor (α) of solid-liquid extraction and a multistage iteration using DC18C6.

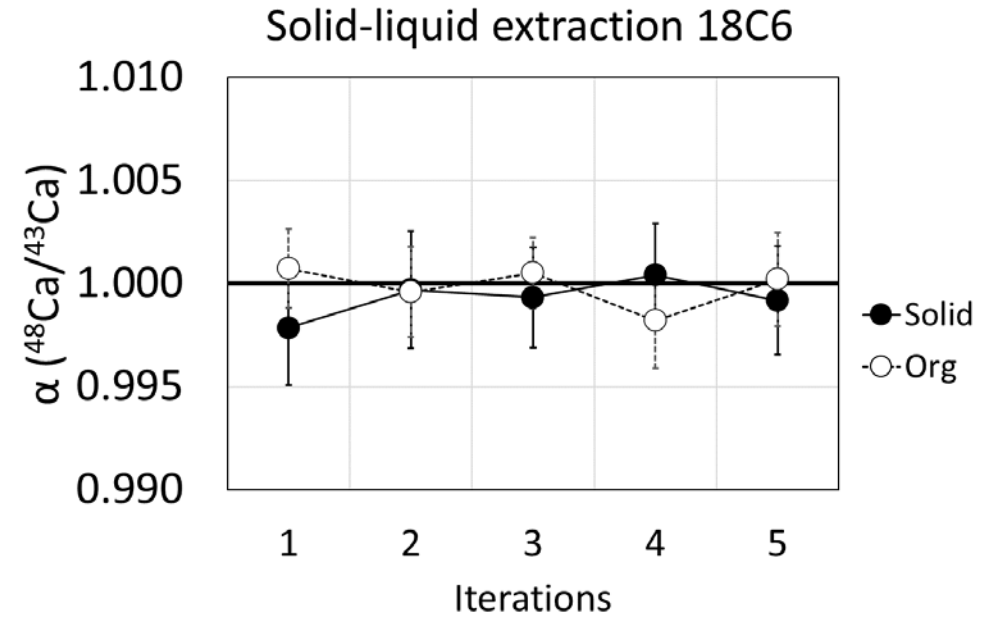

Fig 3.36 The separation factor (α) of solid-liquid extraction and a multistage iteration using 18C6.

3.3.8. Multistage iteration

This research aims to investigate the enrichment of ^{48}Ca toward the study of neutrinoless double beta decay ($0\nu\beta\beta$). According to the above result, the isotope fractionation was confirmed as a depleted (approximately -1%) at the organic phase. However, the obtained result on single-stage liquid-liquid extraction seems insufficient to observe the enrichment in the aqueous phase. A multistage iteration is required.

The preliminary separation factor of aqueous phase (α_{aq}), where the heavier isotope was enriched, and the isotope abundance of $^{48}Ca/^{40}Ca$ on multistage separation was shown in **fig 3.37**. The isotope composition was analyzed by TIMS with the collaboration of Prof. Masao Nomura. The result indicated the separation factor (α) of 1.0010±0.0003. Hence, the enrichment coefficient (ε) appeared to be 1.0±0.3 ‰. The result appears to be approximately one order smaller compared to the separation factor measured by ICP-MS on organic phase ($^{48/40}\alpha_{org}$ = 0.989±0.004, ε (‰) = (0.989 – 1)

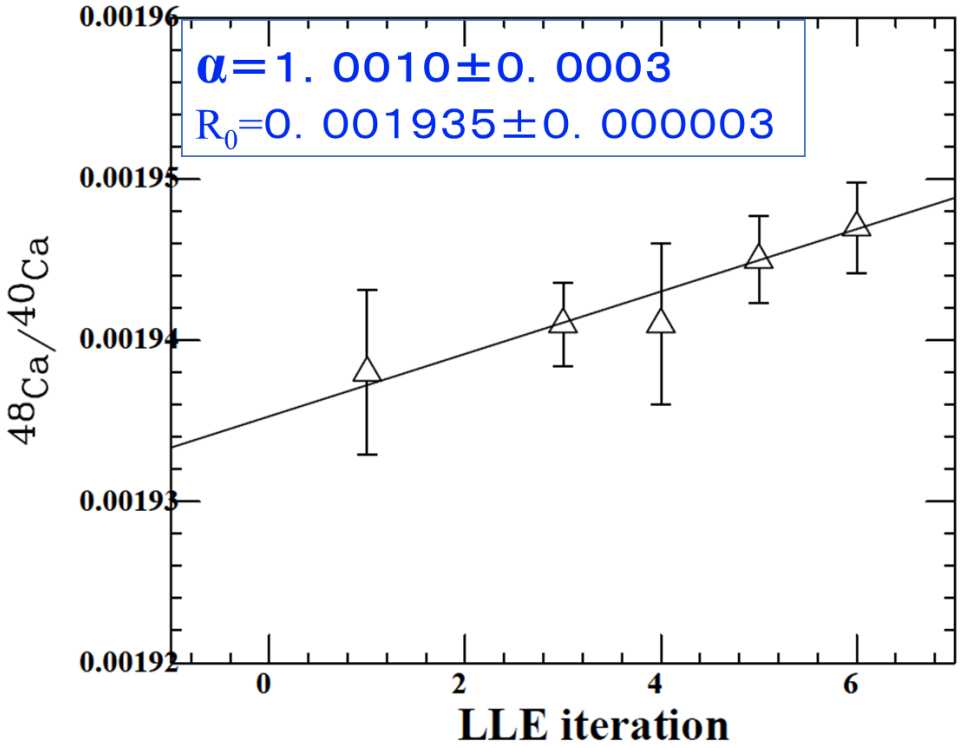

Fig 3.37 The separation factor aqueous phase (α_{aq}) of liquid-liquid extraction by 30% w/w system as an initial feed concentration. The organic solution was 200mL 0.07M DC18C6: R_0 = natural ratio of $^{48}Ca/^{40}Ca$.

×1000 = -11‰). The reason is that the distributed calcium to the organic solution was approximately 2% at 30% w/w $CaCl_2$ (aq) extraction system. To increase the distribution of calcium to the organic phase, a large amount of crown-ether was required.

Nonetheless, the crown-ether (DC18C6) used in this experiment is costly material (≈2000$ / 100 grams). Therefore, the larger amount of crown-ether is problematic. Even the organic solution could be reused, but the extractant loss could be a problem on the cost-effective procedure. Another option is to study the smaller amount of feed solution. The large extraction ratio (K) occupies by reducing the feed content while the concentration is maintained. The extraction conditions were conducted according to the obtained result to study the enrichment in the aqueous phase. The criteria to observe the trace of enrichment are the following.

- According to the calculation in **fig 3.28,** the small amount of calcium could provide the larger isotope fractionation in the aqueous phase. Hence, a small amount of calcium feed solution is required.
- The extraction time result indicated that the chemical reaction and isotope exchange reached equilibrium after 1 minute of mixing with a magnetic stirrer.
- A large amount of crown-ether provided a larger distribution coefficient, according to the comparison between our finding and K. Nishizawa et al. [101] on the extraction of lithium isotope using B15C5.
- The multistage iteration should be carried out as much as possible and investigate the isotope effect for each iteration stage. However, the total amount of calcium decreases as the iteration stage increases. Another factor that needs to be concerned is the initial calcium concentration. According to the finding, we usually performed by 30% w/w extraction system. Despite that the 40% w/w provides a larger

distribution coefficient, the investigation showed that single stage back-extraction is insufficient to recover the calcium from the organic phase. Therefore, 30% w/w extraction is more appropriate for LLE.

- The extraction under the presence of high concentration HCl acid (12M) provided the advancement on the extracted amount of calcium but and needs a careful safety procedure. The optimal concentration of HCl acid as a solvent and the concentration of $CaCl_2$ is still lacking and needs to be investigated before mass production.
- The extraction temperature was also provided with the distribution coefficient dependencies. As a distribution coefficient increases when the temperature decreases. However, carrying out the multistage iteration at a low temperature was problematic. Additional equipment or designed experiment are required.

We conducted the multistage iteration by 2 mL 3.5M $CaCl_2$ (aq) (30% w/w) system and 20 mL 0.07M DC18C6 dissolved in chloroform as an aqueous and organic phase, respectively. The separation technique was carried out by filter separation under the low-level vacuum chamber. The aqueous and organic phase was mixed by a magnetic stirrer. 10 mL of pure water was used to strip the calcium content from an organic solution of each stage. During the extraction, the extracted aqueous phase was sampled for the measurement of the calcium content and isotope composition of 0.1 mL each. **Table 3.18** shows the results of multistage iteration of calcium extraction. **Fig 3.38** depicts the separation factor of the aqueous phase (α). The isotope fractionation was observed in the aqueous phase. It was noted that the ^{40}Ca could not be reported since the mass bias was found to be out of the bracketing sequence sample's uncertainty value and needed to be remeasured. However, the maximum isotope separation of $^{48}Ca/^{42}Ca$ was found to be 1.004±0.004 at the 4^{th} iteration stage.

Therefore, we estimated the isotope effect of $^{48}Ca/^{40}Ca$ by the following equation 3.2. The $^{48/40}$est. α_{aq} was found to be 1.006.

$$^{48/40}est.\alpha_{aq} = \left[\left(\frac{^{48}}{^{42}}\alpha_{aq} - 1\right) \times \frac{8}{6}\right] + 1 \quad (3.2)$$

$$^{48/40}est.\alpha_{aq} = \left[(1.004 - 1) \times \frac{8}{6}\right] + 1 = 1.006$$

Table 3.18 Multistage iteration on filter LLE of calcium extraction using 2 mL of $CaCl_2$ (aq) as an initial feed (30%w/w)

Stage	D	$^{48}Ca/^{40}Ca$ est. α	$^{48}Ca/^{42}Ca$ α	$^{48}Ca/^{43}Ca$ α	$^{48}Ca/^{44}Ca$ α
Aq1	-	1.000	0.999 ±0.004	0.999 ±0.003	1.000 ±0.004
Aq2	-	1.003	1.002 ±0.005	1.001 ±0.004	1.000 ±0.004
Aq3	-	1.005	1.003 ±0.004	1.001 ±0.004	1.000 ±0.004
Aq4	-	1.006	1.004 ±0.004	1.002 ±0.003	1.002 ±0.004
Org1	0.00313 ±0.00002	0.992	0.994 ±0.003	0.994 ±0.004	0.996 ±0.002
Org2	0.00267 ±0.00003	0.990	0.992 ±0.004	0.993 ±0.004	0.995 ±0.003
Org3	0.00342 ±0.00003	0.996	0.997 ±0.006	0.999 ±0.005	0.998 ±0.004
Org4	0.01115 ±0.00017	0.998	0.998 ±0.005	1.001 ±0.004	0.999 ±0.003

It was noted that the distribution coefficient at the 4th iteration was significantly increased since the leaking of the filter was reused several times. However, the primary purpose of this experiment was to investigate and confirm the isotope enrichment at the aqueous phase. The distribution coefficient (D) was in good agreement at approximately one order lower than the conventional LLE since to total among of crown-ether is one order smaller. The mole ratio (η) was maintained at the same amount

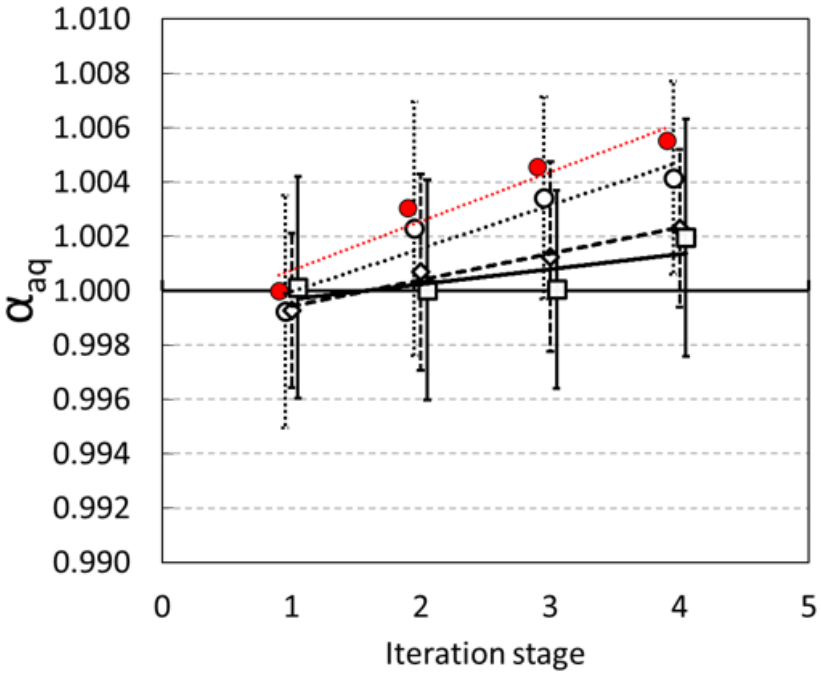

Fig 3.38 The separation factor aqueous phase (α_{aq}) of multistage filter liquid-liquid extraction by 2mL 30% w/w system as an initial feed concentration. The organic solution was 20mL 0.07M DC18C6.
● = $^{48}Ca/^{40}Ca$ (est.), ○ = $^{48}Ca/^{42}Ca$, ◇ = $^{48}Ca/^{43}Ca$, □ = $^{48}Ca/^{44}Ca$

value as conventional LLE, indicating that the extraction was dominated by concentration more than total calcium content in the feed. Therefore, these results emphasized the extraction as high concentration, but a low amount of calcium resulted in a high extraction ratio (K). However, since the extraction was conducted by sampling method, we could not measure the remaining volume after the extraction, and the remaining calcium and extraction ratio (K) could not be determined. However, the recovery of the calcium content in aqueous phase after 4th iteration is less than 10% (0.2 mL) and could not be continue to the 5th iteration, implying that the initial feed of 2 mL is impractical for separation and mass production.

We also conducted the batch LLE using 500mL of separation funnel. The initial of feed was 5 mL of $CaCl_2$ (aq) and $CaCl_2$ (HCl) (30% w/w). The extraction under the

presence of HCl acid could potentially provide the higher extraction ratio compared to aqueous solvent. The higher extraction ratio (K) was expected to increase the isotope fractionation in the extracted aqueous phase, according to the calculation in **fig 3.28**. The organic solution was 100 mL of 0.07M DC18C6. The mixed solution was stirred

Table 3.19 Multistage iteration on batch LLE of calcium extraction using 5 mL of $CaCl_2$ (aq) as an initial feed (30%w/w)

Stage	D	Ca (mmol)	$^{48}Ca/^{40}Ca$ α	$^{48}Ca/^{42}Ca$ α	$^{48}Ca/^{43}Ca$ α	$^{48}Ca/^{44}Ca$ α
Feed	-	18.3	-	-	-	-
Aq1	-	16.2	0.999± 0.004	1.000± 0.005	1.001± 0.004	1.001± 0.004
Aq2	-	15.2	1.001± 0.004	0.998± 0.004	1.002± 0.004	1.000± 0.004
Aq3	-	13.5	0.999± 0.004	0.999± 0.004	0.997± 0.003	1.000± 0.003
Aq4	-	12.4	1.001± 0.004	1.000± 0.005	1.001± 0.004	1.001± 0.004
Aq5	-	9.5	1.001± 0.004	0.999± 0.003	0.999± 0.004	0.996± 0.004
Aq6	-	9.2	1.004± 0.004	1.004± 0.004	1.001± 0.005	0.999± 0.004
Org1	0.0230± 0.0002	0.8	0.992± 0.004	0.994± 0.004	0.995± 0.004	0.996± 0.003
Org2	0.0132± 0.0001	0.4	0.994± 0.005	0.997± 0.006	0.995± 0.004	0.995± 0.003
Org3	0.0078± 0.0001	0.2	0.992± 0.003	0.994± 0.005	0.996± 0.005	0.996± 0.004
Org4	0.0068± 0.0001	0.2	1.002± 0.005	1.001± 0.005	1.003± 0.005	1.004± 0.004
Org5	0.0061± 0.0000	0.1	1.000± 0.003	1.000± 0.006	0.999± 0.005	1.000± 0.004
Org6	0.0025± 0.0000	0.1	1.000± 0.004	0.999± 0.006	0.999± 0.004	1.002± 0.004

Aq = aqueous phase
Org = organic phase

by magnetic stirrer for 1 minute and allowed for phase separation in the separation

funnel for 10 minutes. The separated organic solution was stripped for back extraction by 10 mL of pure water. All the extraction processes were carried out at room temperature (22.0±0.5 °C). The iteration was carried out on the extracted aqueous phase for 6 times.

Table 3.20 Multistage iteration on batch LLE of calcium extraction using 5 mL of $CaCl_2$ (HCl) as an initial feed (30%w/w)

Stage	D	Ca (mmol)	$^{48}Ca/^{40}Ca$ α	$^{48}Ca/^{42}Ca$ α	$^{48}Ca/^{43}Ca$ α	$^{48}Ca/^{44}Ca$ α
Feed	-	21.3	-	-	-	-
Aq1	-	14.3	1.002± 0.003	1.001± 0.007	1.001± 0.005	1.002± 0.003
Aq2	-	9.9	1.005± 0.004	1.007± 0.005	1.002± 0.003	1.002± 0.003
Aq3	-	8.3	1.004± 0.004	1.003± 0.008	1.001± 0.004	1.000± 0.004
Aq4	-	7.2	1.006± 0.003	1.003± 0.005	1.001± 0.005	1.004± 0.005
Aq5	-	6.5	1.006± 0.004	1.004± 0.006	1.005± 0.006	1.005± 0.005
Aq6	-	5.5	1.007± 0.004	1.005± 0.006	1.006± 0.003	1.005± 0.004
Org1	0.1579± 0.0007	5.2	0.995± 0.003	0.995± 0.005	0.998± 0.004	0.996± 0.003
Org2	0.0948± 0.0009	2.4	0.997± 0.005	0.996± 0.005	0.997± 0.003	0.999± 0.003
Org3	0.0810± 0.0008	1.9	0.995± 0.004	1.000± 0.006	0.996± 0.003	0.996± 0.004
Org4	0.0258± 0.0002	0.6	0.998± 0.004	0.994± 0.005	0.998± 0.004	0.998± 0.004
Org5	0.0117± 0.0001	0.2	1.006± 0.003	1.003± 0.007	1.004± 0.005	1.004± 0.004
Org6	0.0079± 0.0002	0.1	1.002± 0.004	1.004± 0.004	1.001± 0.003	1.001± 0.003

Aq = aqueous phase
Org = organic phase

During the iteration, 0.1 mL of aqueous phase was sampling to measure the calcium content and isotope composition. The results of calcium content and isotope composition of each stage show in **table 3.19, 3.20, fig 3.39, and 3.40**.

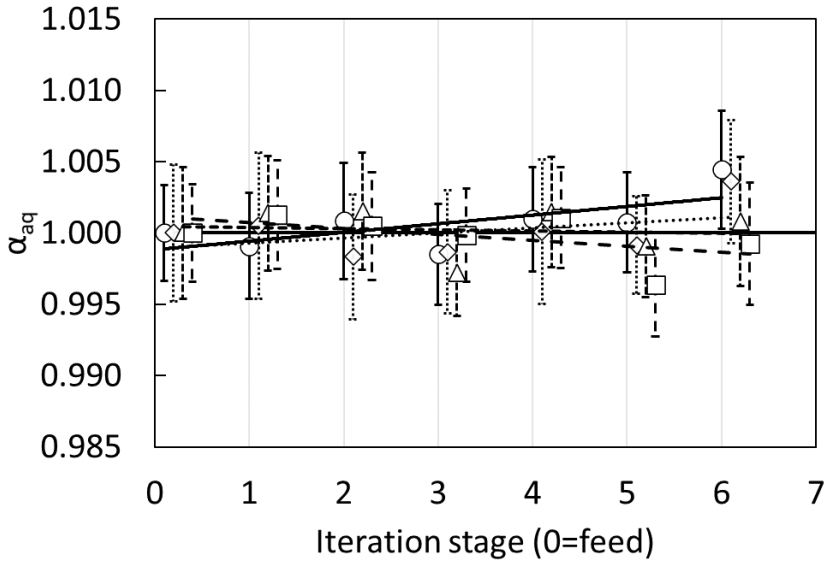

Fig 3.39 The separation factor of aqueous phase (α_{aq}) on multistage extraction by **5mL $CaCl_2$ (aq) (30% w/w)** system as an initial feed concentration.
The organic solution was 20mL 0.07M DC18C6.
○ = $^{48}Ca/^{40}Ca$, ◇ = $^{48}Ca/^{42}Ca$, △ = $^{48}Ca/^{43}Ca$, □ = $^{48}Ca/^{44}Ca$

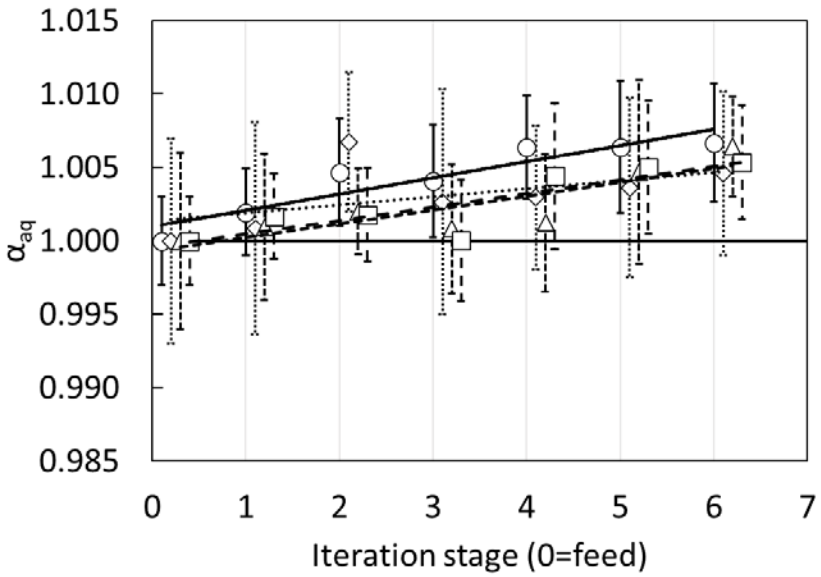

Fig 3.40 The separation factor of aqueous phase (α_{aq}) on multistage extraction by **5mL $CaCl_2$ (HCl) (30% w/w)** system as an initial feed concentration.
The organic solution was 20mL 0.07M DC18C6.
○ = $^{48}Ca/^{40}Ca$, ◇ = $^{48}Ca/^{42}Ca$, △ = $^{48}Ca/^{43}Ca$, □ = $^{48}Ca/^{44}Ca$

According to the batch iteration, when the feed was 5 mL, the separation via separation funnel is possible. Moreover, the extraction system under the presence of 12M HCl increased the extraction amount of calcium. Total extracted of calcium to organic phase was increased up to 10.4 mmol, which corresponded to 48.8% of the initial feed. In contrast with the aqueous solvent, the total calcium extracted to the organic phase was only 1.89 mmol (10.4% of feed). The remaining of calcium after the 6^{th} iteration was 5.5 and 9.2 mmol for HCl and aqueous solvent, respectively. This implied that the extraction could be extended more than 6 times. The distribution coefficient at the 6^{th} iteration, however, indicated that the extracted amount of calcium was very small because the calcium concentration in the aqueous phase was gradually decreased over the iterations, implying that the number of iterations could only be increased a few more times.

In terms of separation factor, the isotope fractionation of $^{48}Ca/^{40}Ca$ in the aqueous phase (head) was increased up to 1.007±0.004 under the presence of 12M HCl. The aqueous solvent was found to be 1.004±0.004 at 6^{th} iteration stage. This behavior indicated the enrichment of the heavier isotope of ^{48}Ca. In conclusion, the presence of HCl acid increase the extraction amount of calcium and when the initial feed was small and the extraction ratio (K) was large, the isotope fractionation in aqueous phase was observed.

3.3.9. Prospect for the enrichment by LLE

According to the above finding, the result confirmed that LLE provided the isotope separation using crown-ether as an extractant. Moreover, the LLE can provide the extraction at high calcium or lithium concentration, resulting in the potentially practical for isotope enrichment and mass production via multistage iteration. However, the current result on the multistage extraction is limited by the recovery of calcium

amount. A further experiment was required at the same condition and higher crown-ether content for mass production. The following paragraph describes the key element of isotope separation and mass production via multistage iteration or cascade enrichment.

According to the finding on **fig 3.39 – 3.40**, the enrichment of ^{48}Ca to the number of iteration stage was determined by the following equation 3.3 and 3.4 for aqueous and HCl solvent, respectively.

$$^{48/40}\alpha_{aq} = 0.99882e^{0.00061x} \quad (3.3)$$

$$^{48/40}\alpha_{aq} = 1.00099e^{0.00110x} \quad (3.4)$$

where x represents the number of iteration stages. Regardless of the recovery amount of calcium content, the required iterations were approximately 3793, and 2112 stages to achieve the ten times enrichment of ^{48}Ca compared to ^{40}Ca. The number of iteration stage when 2mL of $CaCl_2$ (aq) was used as an initial feed (**fig 3.38**) the number of iteration stage was corresponded to 1273 (equation 3.5)

$$^{48/40}est.\alpha_{aq} = 0.99894e^{0.00181x} \quad (3.5)$$

Since the initial feed was smaller (2mL), the extracted ratio (K) was significantly larger and resulting in the more isotope fractionation on the aqueous phase.

Nonetheless, the recovery amount of calcium is one of the most important obstacles to isotope enrichment and mass production. The following **fig 3.41** indicates the preliminary calculated under the condition of organic phase separation factor (α_{org}) = 0.990, feed = 7 mmol, extraction ratio (K) = 0.2, 10 iteration stages, 20mL 0.07M DC18C6, and regardless the sampling and lost during the extraction. It was found that after the 10th iteration, the remaining head stage was approximately 1.17 mmol of

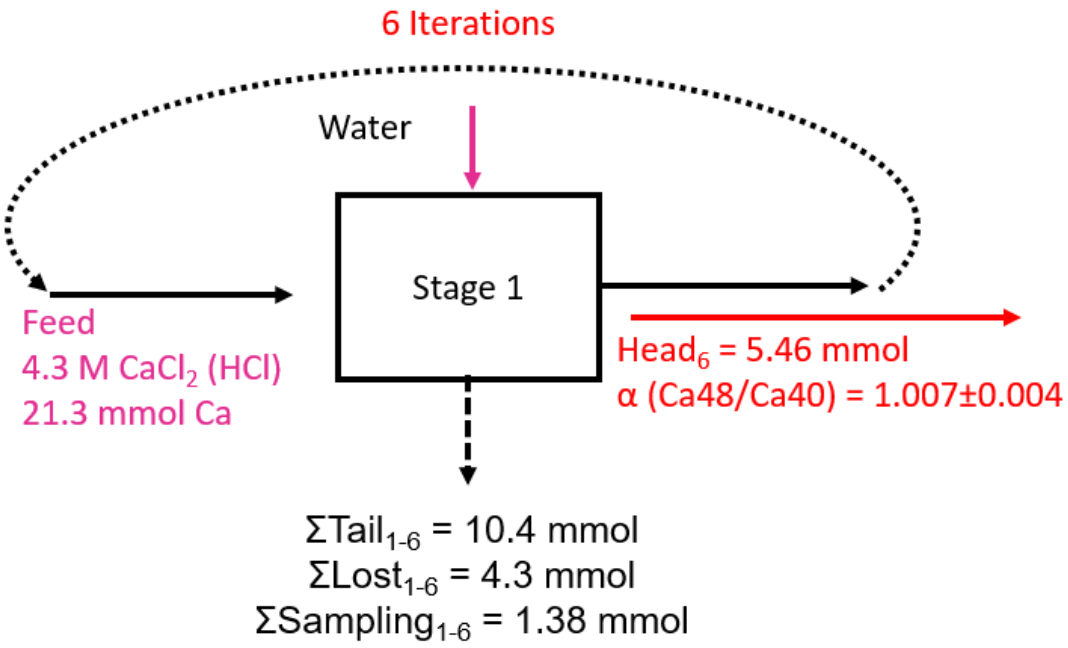

Fig 3.41 The calculated of isotope enrichment and mass production of calcium extraction. The number of substage was 10 substages.

calcium. Most of the calcium was extracted in the tail stage. Therefore, additional parallel enrichment was required for the mass production of the next stage iteration shown in **fig 3.42**. This is the basic idea of cascade enrichment and production.

In conclusion, isotope separation of calcium by chemical exchange using DC18C6 crown-ether was potentially possible. Compared to other isotope enrichment such as crown-ether resin chromatographic method, the report from S. Umehara et al. [61] indicated the enrichment coefficient (ε) of 3.04±0.11 ‰ of 200 m migration length with the ten days of operation. At the same time, K. Hayasaka et al. [62] reported the enrichment coefficient (ε) to be 1.9‰. In contrast, S. Nemoto et al. [63] revealed to be 6.0±1.0 ‰. All the resin chromatographic methods required problematic handling of a high concentration of HCl acid and prolonged operation. On the other hand, we reported the same estimated enrichment coefficient of $^{48}Ca/^{40}Ca$ at 6 ‰ under 4th iterations using filter separation, which can be complete within 2 hours. More importantly, LLE provided the high conversion depending on the appropriate ratio of calcium to crown-

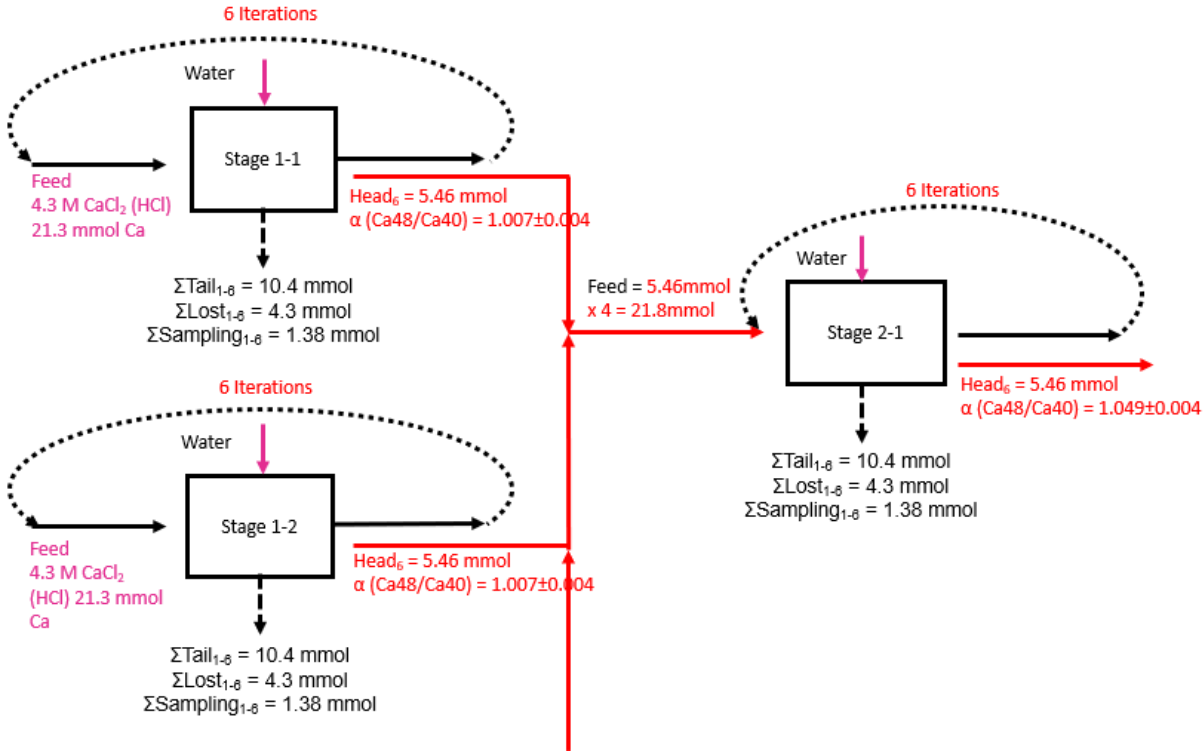

Fig 3.42 The example for the cascade isotope enrichment via chemical exchange isotope separation of calcium extraction using crown-ether

ether. A further experiment on the same volume ratio but a larger volume of aqueous and organic was required to establish the enrichment feasibility. Additionally, we confirmed the contribution of HCl acid on the extraction via LLE. The additional HCl's multistage iteration could provide a larger extraction ratio and greatly fractionate the isotope in the aqueous phase. According to the calculation, we expected the enrichment of ^{48}Ca of LLE using HCl compared to an aqueous solvent.

3.3.10. Calcium and lithium isotope effect evaluation

According to the TIMS measurement, with the help from Prof. Nomura, Tokyo Tech, Japan (section 3.2.1). We could acquire the precise isotope measurement of calcium isotope composition. The following describes the isotope effect evaluation of nuclear mass effect, nuclear field effect, and spin shift.

T. Fujii et al. [17] evaluated the isotope effect of titanium (Ti) using isotope pair evaluation. Therefore, the same evaluation was applied to our experimental result. **Table 3.21** indicates the contributed factors, including isotope pair, changes in mean-square nuclear charge radii ($\delta \langle r^2 \rangle$ (fm^2)), isotope mass contribution ($\Delta M/MM'$), separation factor (α_{org}), separation coefficient ε (α_{org}-1), and mass effect. The linear mass effects were obtained from the normalization of the heaviest isotope pair of $^{48}Ca/^{40}Ca$, which has almost the same value of change in mean square nuclear charge radii: $\delta (r^2)$ (fm^2), due to the same double magic number.

Table 3.21. Calcium isotope effect evaluation

Isotope	Pair (x/40)	$\delta\langle r^2 \rangle$ (fm^2) x-40 [18]	$\Delta M/MM'$	TRITON 30%BE sample $\alpha_{org}\pm\sigma$	ε (α_{org}-1)	Mass effect
39	39/40	-0.127	-0.0006	-		0.0009
40	40/40	0.000	0.0000	1.0000±0.0000	0.0000	0.0000
41	41/40	0.003	0.0006	-		-0.0009
42	42/40	0.215	0.0012	0.9987±0.0002	-0.0013	-0.0018
43	43/40	0.125	0.0017	0.9950±0.0008	-0.0050	-0.0027
44	44/40	0.283	0.0023	0.9967±0.0005	-0.0033	-0.0036
45	45/40	0.119	0.0028	-		-0.0045
46	46/40	0.124	0.0033	-		-0.0054
47	47/40	0.005	0.0037	-		-0.0062
48	48/40	-0.004	0.0042	0.9929±0.0011	-0.0071	-0.0071
50	50/40	0.276	0.0050	-		-0.0089

The obtained results of the separation coefficient for each isotope pair ($^{48}Ca/^{40}Ca$, $^{44}Ca/^{40}Ca$, $^{43}Ca/^{40}Ca$, and $^{42}Ca/^{40}Ca$) are shown in **fig 3.43**. The linear tendency of mass effect breakdown was observed in ^{43}Ca since it has the odd number isotope, and 7/2 nuclear spin. The contribution of nuclear mass effect, nuclear field

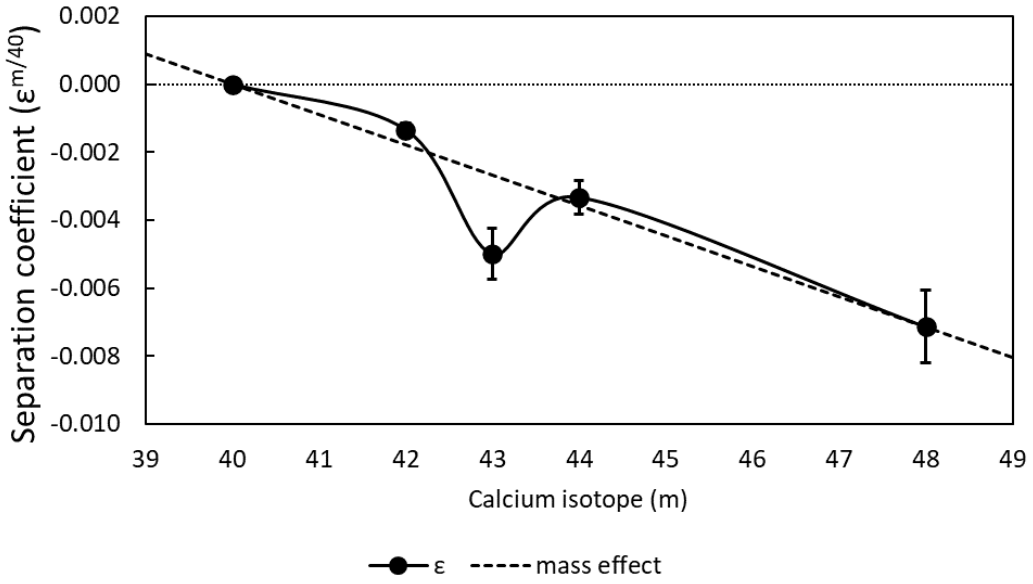

Fig 3.43. Separation coefficient (ε) of calcium isotope effect obtained from the TRITON measurement of the back-extraction sample, represent the isotope effect of calcium in the organic phase. The dash line indicates the linear tendency of nuclear mass effect.

effect, and nuclear spin effect could be written in the following simple relation shows in equation 3.6 – 3.10 [25].

$$\varepsilon_{x/40} = a\left(\frac{\Delta M}{MM'}\right)_{x/40} + b\delta(r^2)_{x/40} + ln\, K_{hf} \tag{3.6}$$

$$\varepsilon_{48/40} = a\left(\frac{\Delta M}{MM'}\right)_{48/40} + b\delta(r^2)_{48/40} \tag{3.7}$$

$$\varepsilon_{44/40} = a\left(\frac{\Delta M}{MM'}\right)_{44/40} + b\delta(r^2)_{44/40} \tag{3.8}$$

$$\varepsilon_{43/40} = a\left(\frac{\Delta M}{MM'}\right)_{43/40} + b\delta(r^2)_{43/40} + ln\, K_{hf43} \tag{3.9}$$

$$\varepsilon_{42/40} = a\left(\frac{\Delta M}{MM'}\right)_{42/40} + b\delta(r^2)_{42/40} \tag{3.10}$$

According to the isotope pair evaluation, a, b, and ln K_{hf43} represent the scaling factor of nuclear mass effect, nuclear field effect, and hyperfine splitting (nuclear spin effect) of odd number isotope, respectively, which were evaluated using the use of four isotope pairs. The results show in **table 3.22**. The scaling factor of nuclear mass effect is -1.68851, the nuclear field effect is 0.00206, and the hyperfine splitting (nuclear spin effect) of ^{43}Ca is -0.0024.

Table 3.22. Scaling factor of nuclear mass effect (a), nuclear field effect (b), and nuclear spin effect (ln K_{hf43})

a	b	ln K_{hf43}
-1.68851	0.00206	-0.00239

The contribution ratio of nuclear mass effect, nuclear field effect, and nuclear spin effect are shown in **table 3.23**. The results indicated that the nuclear mass effect dominated the calcium isotope effect more than the nuclear field effect, except ^{43}Ca, which was also contributed by the nuclear spin effect. Compared with the previous work of R. Hazama et al. [100], the contribution ratio of nuclear field effect and nuclear spin effect to the nuclear mass effect were found in good agreement. The nuclear field effect to the mass effect of ^{48}Ca/^{40}Ca was reported to be mass effect dominated (0.02±0.48). The other isotopes pair were compared based on the ^{48}Ca. However, the trend of contribution ratio corresponded to this work. The ^{43}Ca also showed the breakdown of the linear tendency of mass effect, which was contributed by the nuclear spin effect (^{43}Ca/^{48}Ca: ln K_{hf43}/ aΔM/MM' = 0.64±1.35).

Table 3.23. Contribution ratio of nuclear field effect, nuclear spin effect to nuclear mass effect.

Isotope pair	bδ<r^2>/aΔM/MM'	ln K_{hf43}/aΔM/MM'
This work		
^{42}Ca/^{40}Ca	-0.221	-
^{43}Ca/^{40}Ca	-0.088	0.811
^{44}Ca/^{40}Ca	-0.152	-
^{48}Ca/^{40}Ca	0.001	-
R. Hazama [100]		
^{40}Ca/^{48}Ca	0.02±0.48	-
^{44}Ca/^{48}Ca	0.62±1.31	-
^{43}Ca/^{48}Ca	0.22±0.88	0.64±1.35

In the case of lithium, because lithium has only two isotopes, ^{6}Li and ^{7}Li, the isotope pair evaluation is inapplicable. The evaluation method requires experimental data under various temperatures. **Table 3.24. and fig 3.44** shows the separation coefficient (ε (α_{org}-1)) under the various temperature (1/T), ranging from -15°C to 45°C (section 3.36). The extrapolation on the origin point represents when the temperature approaches infinity, the separative effect is disappeared. The second order polynomial was evaluated based on the Bigeleisen's new theory in the equation 1.8.

Table 3.24. Lithium isotope effect

1/T (K)	°C	$\delta \langle r^2 \rangle$ $(fm^2)7/6$ [18]	ΔM/MM'	$\alpha_{org}\pm\sigma$	ε (α_{org}-1)
0.003876	-15	-0.731	0.0238	0.990±0.005	-0.010
0.003663	0			0.994±0.004	-0.006
0.00339	22			0.991±0.003	-0.009
0.003145	45			0.994±0.005	-0.006

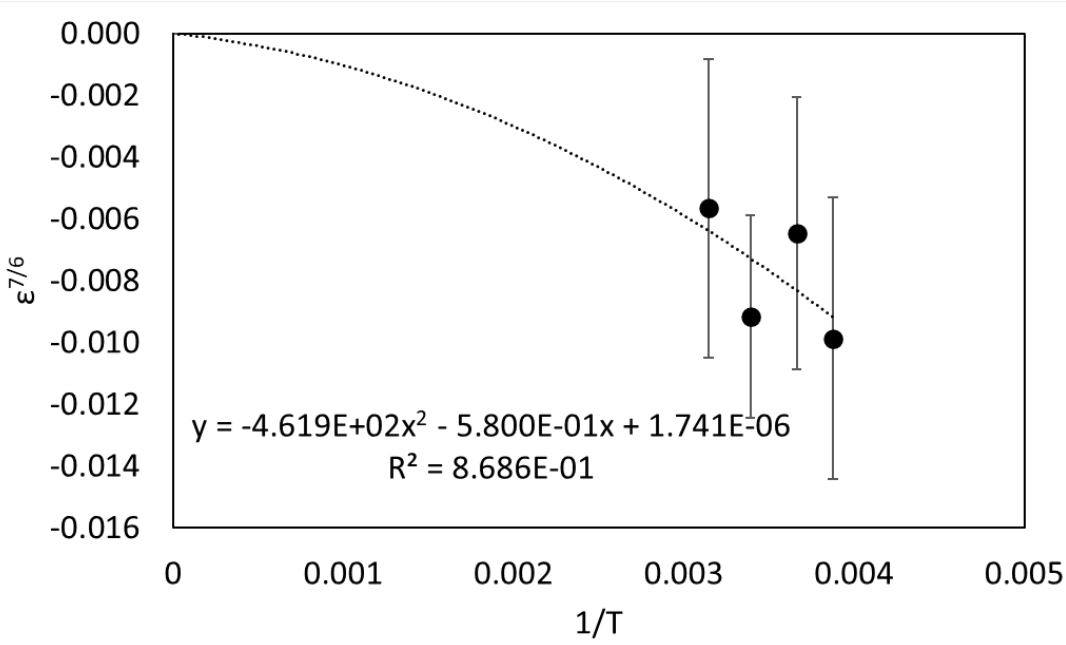

Fig 3.44. Separation coefficient of lithium based on the various extraction temperature ranging from -15 °C to 45°C

$$y = (-4.619 \times 10^{2})x^{2} - (5.800 \times 10^{-1})x + 1.741 \times 10^{-6} \qquad (3.11)$$

According to the above equation 3.11 and Bigeleisen's new theory, the scaling factor of nuclear mass effect (a) is revealed to be -4.619×10^{2} and -5.800×10^{-1} for nuclear field effect (b). The additional nuclear spin effect was found to be 1.741×10^{-6}. The contribution ratio of nuclear field and nuclear spin to the nuclear mass effect shows in **table 3.25.** The results indicated that the isotope shift was greatly dominated by the nuclear mass effect corresponding to the calcium isotope effect. The value of contribution ratio of $^{48}Ca/^{40}Ca$ was overwhelming in the nuclear mass effect due to the parabolic behavior of ^{48}Ca and ^{40}Ca which have double magic number isotope. The past research on the isotope exchange reaction, which described the nuclear mass effect, nuclear field effect, and nuclear spin effect were shown with an addition of this work in **table 3.26**.

Table 3.25. Contribution ratio of nuclear field effect, nuclear spin effect to nuclear mass effect of lithium.

Isotope pair	$b\delta\langle r^2\rangle/a\Delta M/MM'$	$\ln K_{hf43}/a\Delta M/MM'$
$^{7}Li/^{6}Li$	-0.039	1.58×10^{-7}

Table 3.26. The past research described about the nuclear mass effect, nuclear filed shift effect and nuclear spin effect.

Elements	Separation method	Ref.
Sr, Ti, Cr, Ni	Solvent extraction	16 ,17, 20, 24
Ca, Li	Solvent extraction (liquid-liquid method)	This work
Zn, Gd, Sr	Liquid chromatography	19, 22, 23
Yb	Amalgam method	21

3.4. Electrolytic enrichment of tritium

3.4.1. The measurement of tritium by LSC-LB7

The tritium calibration sample by ESCR was prepared and measured to determine the tritium counting efficiency (%EFF). The counting efficiency of calibration sample SN1 to SN10 is shown in **table 3.27**. The %EFF was calculated by the tritium standard (known activity: DPS on October 22nd, 2020) and count per second (CPS). It is noted that the difference between each calibration sample is the ratio of quenching agent (HTO + H_2O) to liquid scintillator (ULTIMA GOLD) as mentioned in chapter 2. **Fig 3.45** indicated the quenching calibration curve of ESCR mode. **Fig 3.46** shows the energy spectrum due to the quenching effect. All calibration and water samples were obtained from a full spectrum ranging from 0.005 – 19.995 keV (channel 1 – 3999).

Table 3.27 Tritium calibration samples measurement by ESCR mode

Sample	ESCR	H-CPS	H-DPS (Oct. 22, 2020)	%EFF
SN1	12.58	83.29	198.0	42.07
SN2	11.69	79.24	196.2	40.39
SN3	11.24	76.08	198.5	38.34
SN4	10.77	70.58	196.9	35.84
SN5	9.63	63.05	195.8	32.21
SN6	8.39	53.62	195.8	27.38
SN7	6.66	38.93	195.6	19.91
SN8	6.08	33.81	196.5	17.20
SN9	5.27	26.03	196.1	13.27
SN10	4.48	18.14	196.5	9.23

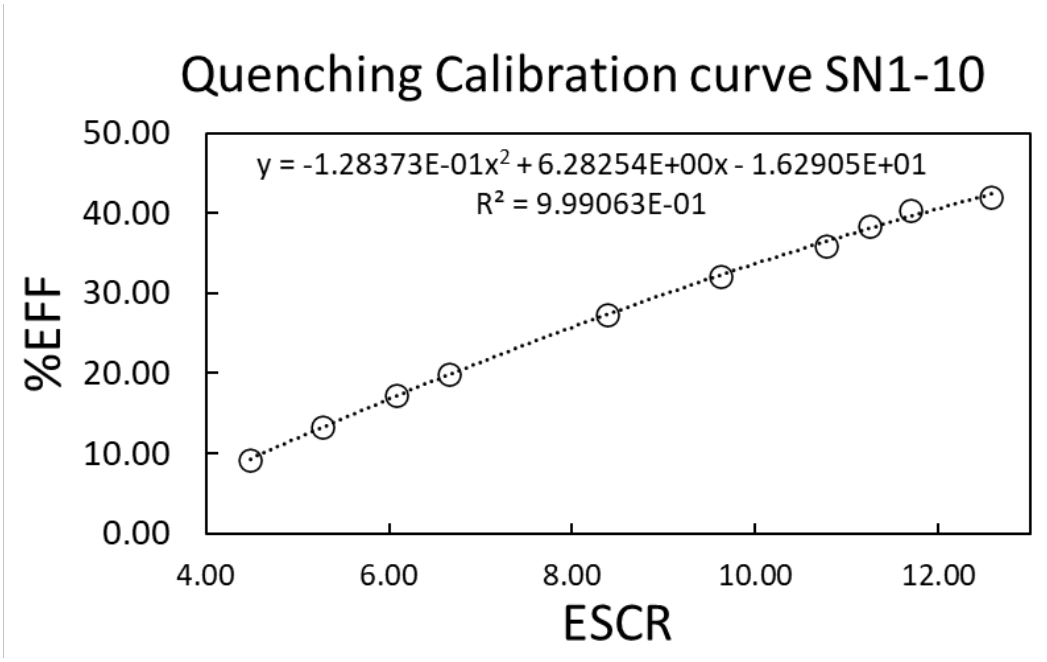

Fig 3.45 Quenching calibration curve of tritium measurement using ESCR mode

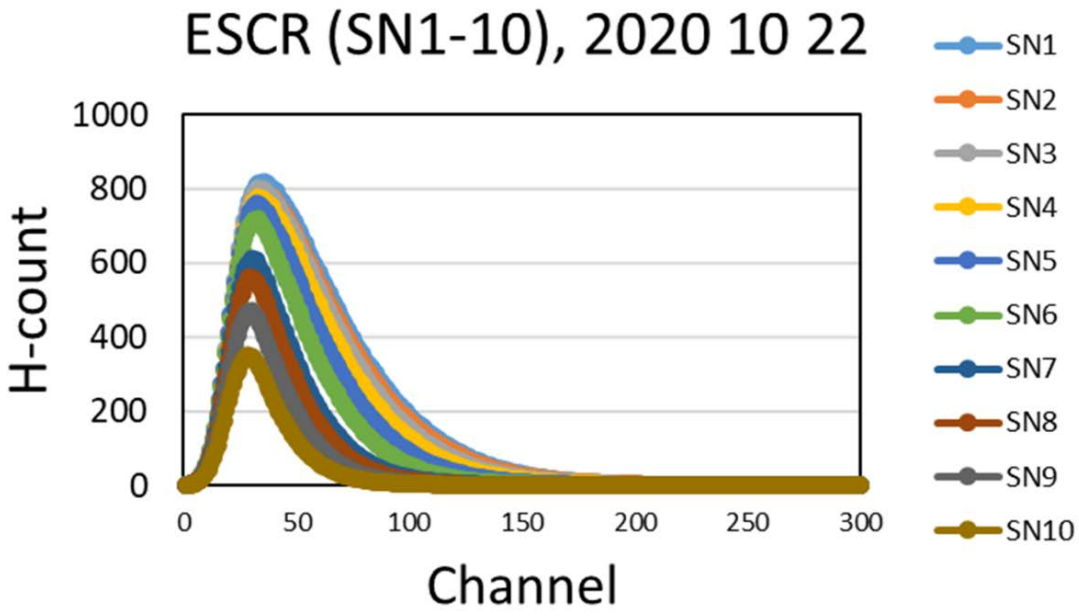

Fig 3.46 Quenching calibration curve of tritium measurement using ESCR mode

3.4.2. Improvement on the temperature system of the apparatus

The temperature system was installed to stabilize the temperature and assure the enrichment factor during the enrichment periods. **Fig 3.47** depicts the thermocouples located at the Peltier and electric plates. The Peltier should be lower than 0 °C to avoid the water vapor. **Fig 3.48** shows the temperature logging at the cathode plate during the enrichment. The red line indicates the temperature before the installation of air circulation system. The green line shows the temperature when the air system was applied. The temperature logging indicated that the temperature at the cathode plate was decreased from 36.7 °C to 24.0 °C. The maximum temperature was also decreased from 73.9 °C to 36.0 °C. All of the enriched sample was measured the temperature change to assure that the enrichment factor obtained from tritiated water could applied to those sample. The results on the obtained enrichment factor shows in the next section.

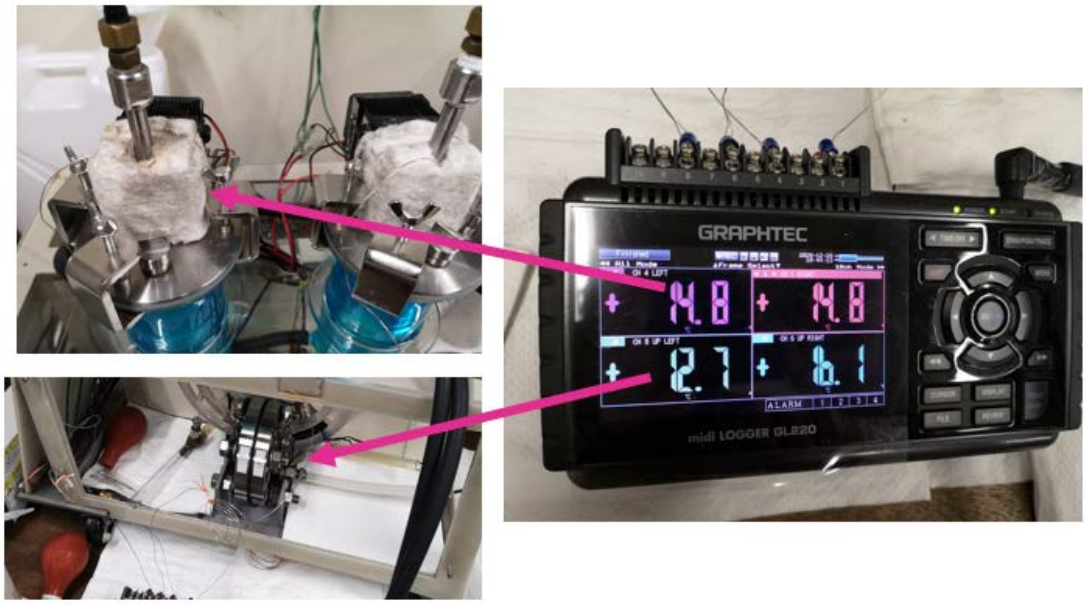

Fig 3.47 The temperature logging system on the Peltier and the electric plates.

3.4.3. Determination of tritium enrichment factor

30A of consistent electric current was applied to enrich 500mL of the tritiated sample. Enrichment factor (α) determined by the non-enriched tritiated water (HTO)

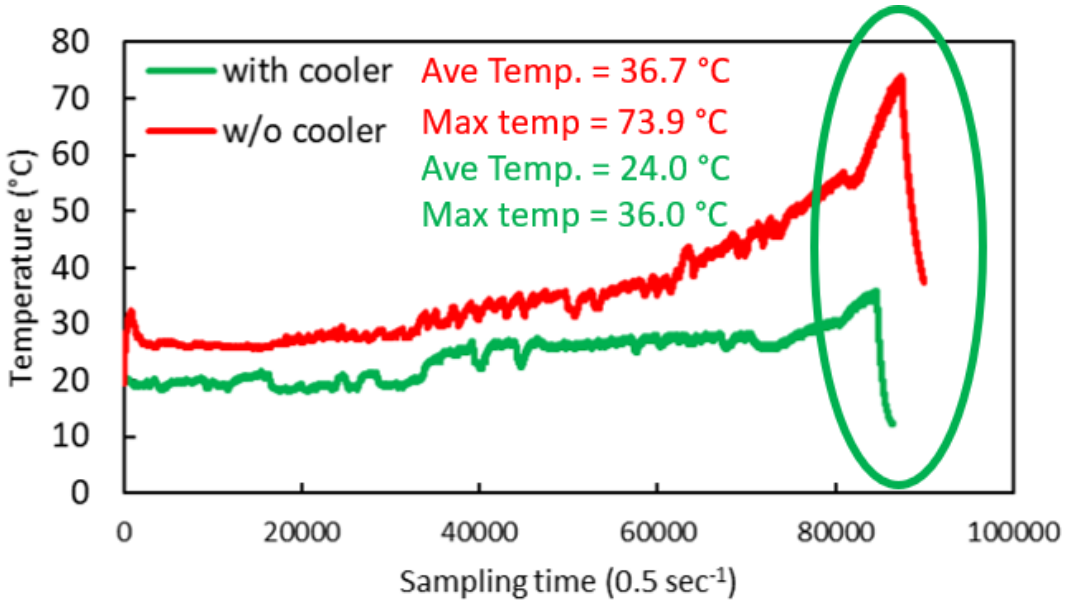

Fig 3.48 Temperature before (red) and after (green) the installation of air circulation system

and enriched tritiated water (E-HTO) results via tritium recovery factor (R) (3.12), which also depends on the volume reduction factor (V_i/V_f). Equations 3.13 and 3.14 were used to determine the initial concentration of tritium in the unknown water sample and enrichment factor, respectively.

$$R = \frac{T_f V_f}{T_i V_i} \tag{3.12}$$

$$T_i = \frac{T_f}{\left(\frac{V_i}{V_f}\right)R} \tag{3.13}$$

$$\alpha = \frac{T_f}{T_i} \tag{3.14}$$

Table 3.28 shows the measurement result of non-enriched tritiated and enriched tritiated water samples, used to determine the tritium enrichment factor of our SPE electrolytic apparatus (before the installation of air circulation system). The calculated separation factor (α) and tritium recovery factor are shown in the following calculation. The enrichment factor under 500 mL of our SPE film apparatus using 30A was found to be 13.75±2.38 to 14.01±1.80. **Table 3.29** denotes the same condition but after the air

circulation system was installed. The enrichment factor was increased up to 15.83±0.99 and 16.16±0.97.

Table 3.28 The measurement results of non-enriched and enriched tritiated water sample for the determination of tritium enrichment factor (α) (before air circulation system was installed)

Sample	Cycle	H-CPS	SD	%RSD	ESCR	V_f (mL)	V_i (mL)	%EFF	T_f (Bq/L)
BG	1	309.4	27.9	9.0	8.15	-	10.06	26.38	-
HTO		4070.7	62.8	1.5	8.50	-	10.03	27.84	225±21
E-HTO		50525.9	213.5	0.4	8.19	11.89	500	26.54	3147±20
BG	2	331.2	40.3	12.2	7.97	-	10.06	25.63	
HTO		4157.6	72.8	1.7	8.40	-	10.03	27.42	232±29
E-HTO		50535.0	208.3	0.4	8.10	11.89	500	26.18	3190±28

Cycle 1 $$R = \frac{3147 \times 11.89}{225 \times 500} = 0.33$$

Cycle 2 $$R = \frac{3190 \times 11.89}{232 \times 500} = 0.33$$

Cycle 1 $$\alpha = \frac{3147}{225} = 14.01 \pm 1.80$$

Cycle 2 $$\alpha = \frac{3190}{232} = 13.75 \pm 2.38$$

Table 3.29 The measurement results of non-enriched and enriched tritiated water sample for the determination of tritium enrichment factor (α) (after air circulation system was installed)

Sample	Cycle	H-CPS	SD	%RSD	ESCR	V_f (mL)	V_i (mL)	%EFF	T_f (Bq/L)
BG	1	305.9	18.3	6.0	8.38	-	-	27.39	-
HTO		662.4	27.1	4.1	8.58	-	-	28.18	21±2
E-HTO		5892.1	99.2	1.7	8.51	12.20	500	27.89	334±21
BG	2	305.7	17.8	5.8	8.24	-	-	26.85	
HTO		649.6	20.9	3.2	8.51	-	-	27.88	21±1
E-HTO		5781.9	79.3	1.4	8.40	12.20	500	27.47	333±20

Cycle 1 $$R = \frac{334 \times 12.20}{21 \times 500} = 0.39$$

Cycle 2 $$R = \frac{333 \times 11.89}{21 \times 500} = 0.33$$

Cycle 1 $\alpha = \frac{334}{21} = 15.83 \pm 0.99$

Cycle 2 $\alpha = \frac{333}{21} = 16.16 \pm 0.97$

3.4.4. Status of JSPS joint research project with Thailand

As mentioned in chapter 2, the goal of the tritium experiment is for the joint research collaboration on the nationwide tritium concentration of Thailand water samples, including tap water, rainwater, and ground water.

The tritium measurement in the Thailand water sample was mainly measured by the Thailand Institute of Nuclear Technology (TINT). However, the comparison was performed once a year by our laboratory. July tap water was sent to Japan and distributed to other collaborators from Shinshu University and Kyoto University to measure oxygen isotope composition and other trace elements. The first year of collaboration is July 2020. Tap water samples was collected in Bangkok and the metropolitan area. **Fig 3.49** depicts the sampling location. The results of tritium

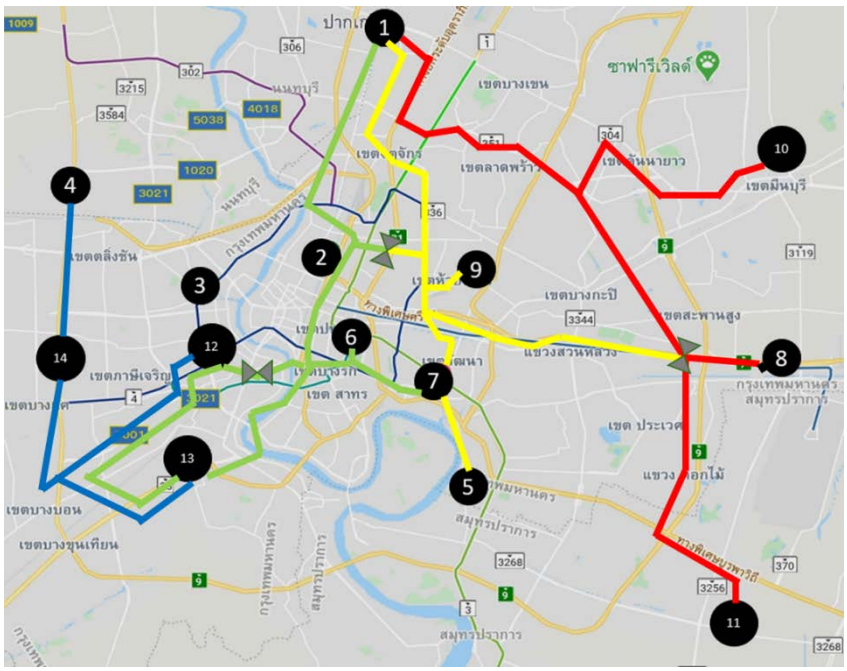

Fig 3.49 Tap water sampling site in Bangkok and metropolitan area in the first year of collaboration. The color lines between each point indicate the water flow and distribution.

concentration in July 2020 tap water samples measured by Osaka Sangyo University (OSU) and TINT were shown in **table 3.30. fig 3.50** shows the comparison between OSU and TINT result.

Table 3.30. Tritium concentration in July 2020 tap water

TTW	Sample	TINT		OSU	
		Bq/L	σ	Bq/L	σ
TTW1	1. Bangkhen Water Treatment Plant	0.22	0.04	0.22	0.04
TTW2	2. Samsen Water Treatment Plant	0.18	0.04	0.19	0.03
TTW3	3. Thonburi Water Treatment Plant	0.26	0.02	0.13	0.02
TTW4	4. Mahasawat Water Treatment Plant	0.15	0.02	0.08	0.01
TTW5	5. Samrong Pump Station	0.22	0.04	0.11	0.02
TTW6	6. Lumphini Pump Station	0.22	0.04	0.26	0.04
TTW7	7. Khlong Toei Pump Station	0.19	0.04	0.27	0.04
TTW8	8. Ladkrabang Pump Station	0.19	0.02	0.24	0.04
TTW9	9. Latphrao Pump Station	0.18	0.02	0.25	0.04
TTW10	10. Minburi Pump Station	0.21	0.04	0.30	0.05
TTW11	11. Bang Phli Pump Station	0.19	0.04	0.24	0.04
TTW12	12. Thaphra Pump Station	0.18	0.02	0.21	0.03
TTW13	13. Ratburana Pump Station	0.19	0.04	0.27	0.05
TTW14	14. Petchkasem Pump Station	0.19	0.04	0.18	0.03

Fig 3.50 indicated some mismatches of measure tritium concentration in the July 2020 tap water sample collected from Bangkok and the metropolitan area. Therefore, the inter comparison between Thailand and Japan sides was required. We sent the known tritiated sample to the Thailand laboratory and the third party for intercomparison by the in-house direct measurement method with the quantitative limit of detection at 15 Bq/L. However, **fig 3.51** shows the comparison on cycle two measurement, and more consistent results were observed, except the samples TTW3 to TTW5. The reason might be the measurement condition is unstable and need a careful condition, such as consistent room temperature.

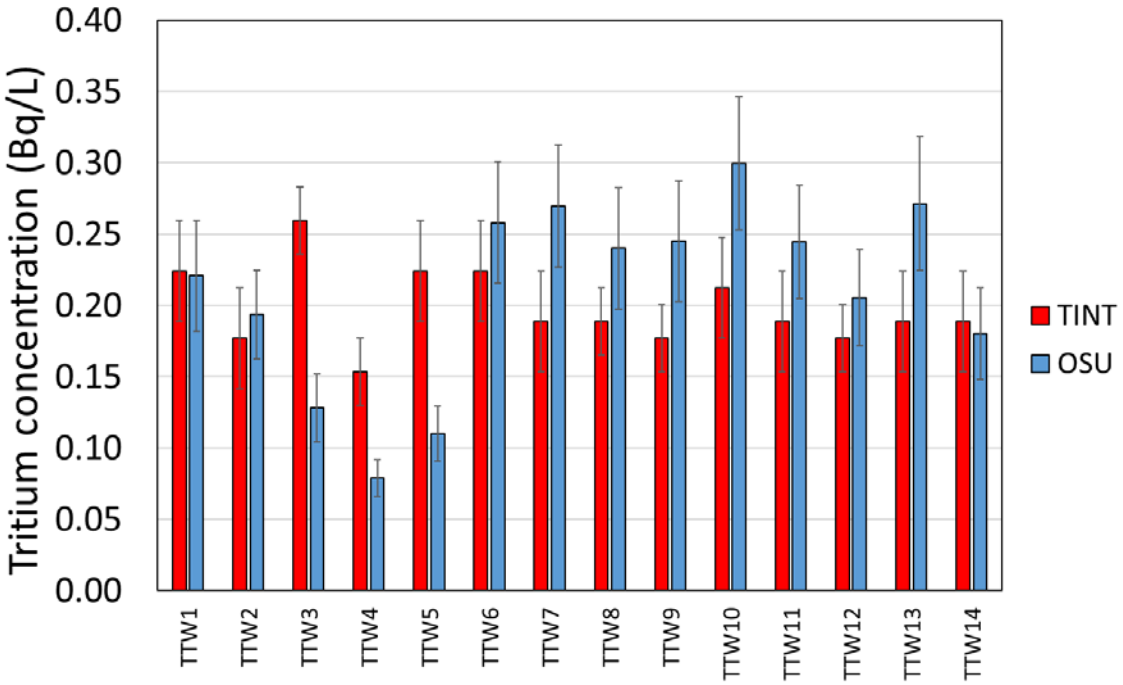

Fig 3.50 Tritium concentration in July 2020 tap water measured by OSU and TINT

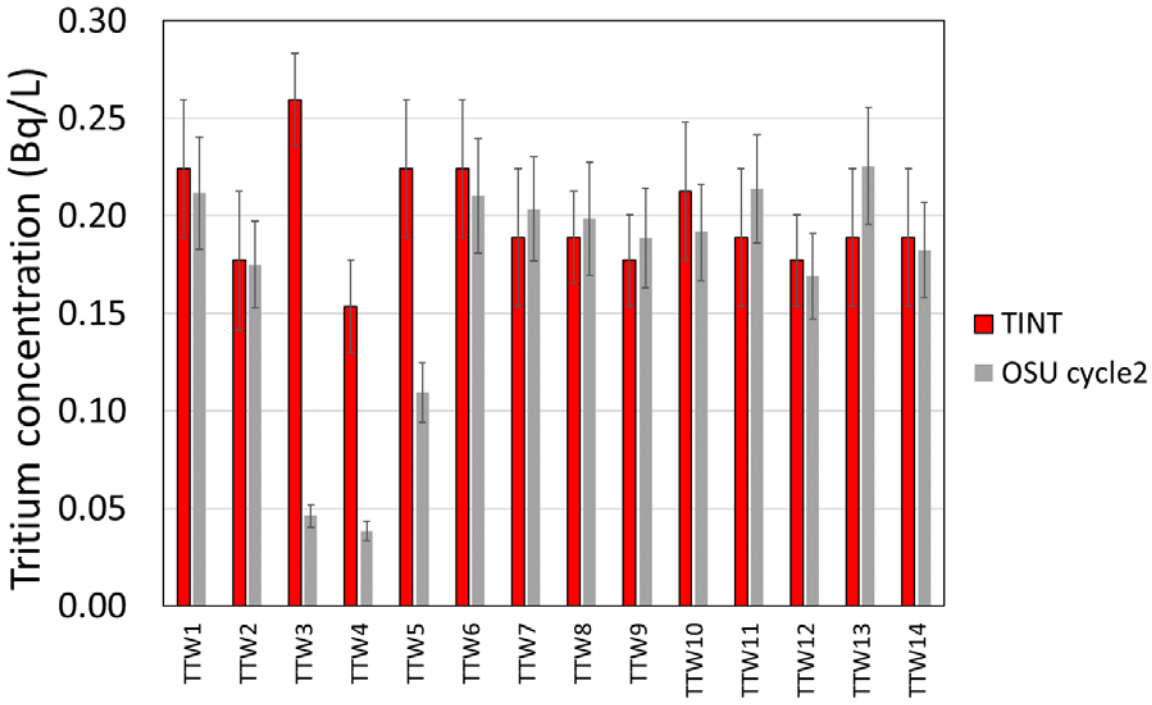

Fig 3.51 Tritium concentration in July 2020 tap water measured by OSU (cycle 2) and TINT

Fig 3.52 shows the locality dependent on tritium measurement, the correlation coefficient (CC) between tritium concentration and locality was found to be -0.060 and

0.542 for latitude and longitude, respectively. However, the sampling area was only 0.4 degrees different in latitude and longitude. Therefore, the result might not be reliable.

Additional measurement was carried out by Shinshuu University and Kyoto University on the measurement of tap water samples along with the rainwater sample collected from Kasetsart University (Sri Racha campus), Rayong, Thailand. The instruments contain pH and EC meters, water isotope analyzer (Picarro) L-2130-i, Automatic titration system, cation analyzer (IC (Thermo) ICS-1500), and anion

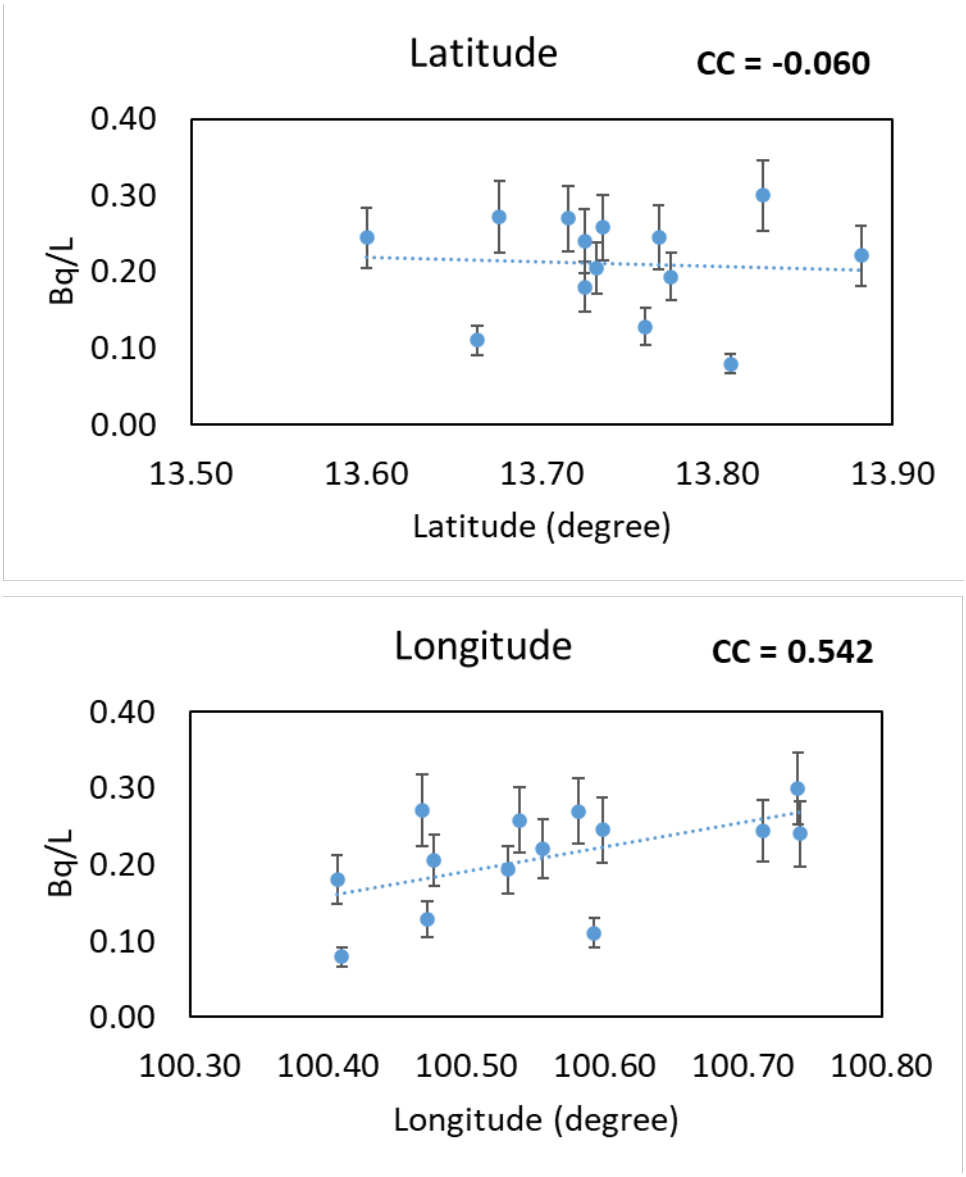

Fig 3.52 Locality dependencies on tritium concentration and sampling areas.

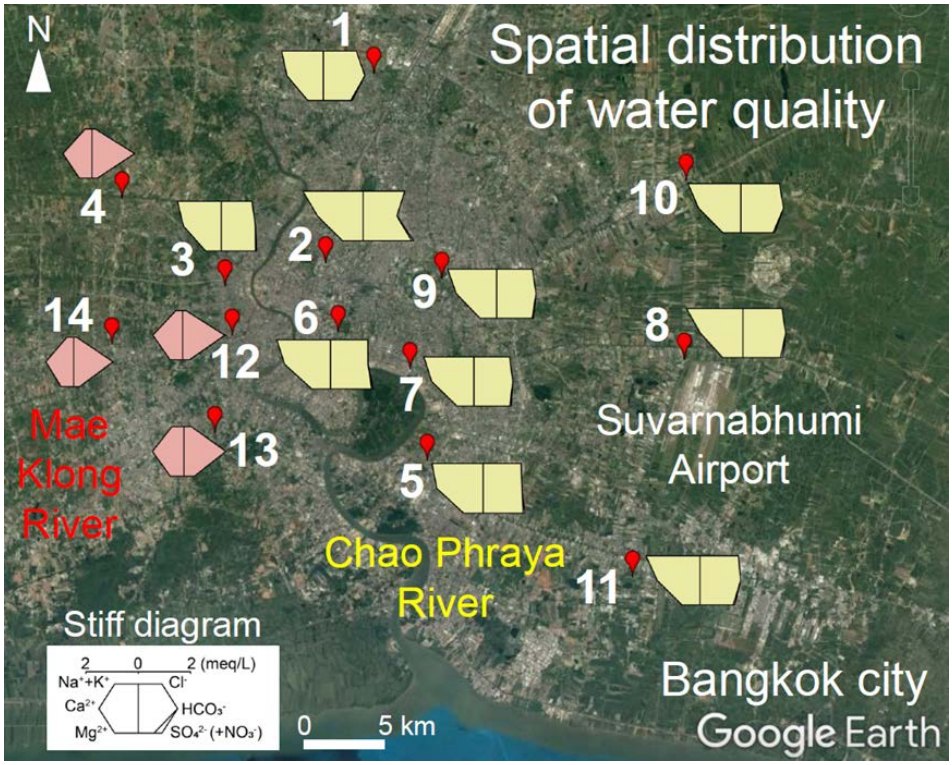

Fig 3.53 Stiff diagram of tap water quality.

analyzer (IC (Thermo) ICS-2100). The major anion compositions in rainwater found that the principal component is NO^{3-} and SO_4^{2-}, which may be delivered from air pollutants. The electrical conductivity of tap water samples collected in Bangkok was different in two water sources include Chao Phraya River and Mae Klong River. The indicators of water quality consist of Stiff diagram (**Fig 3.53**). Stiff diagram showed the Mae Klong River source characterized by calcium and bicarbonate water type. As for Chao Phraya River, the water sample characterized to be sodium, chloride, and sulfate ion. The stable isotopic composition results showed that each water types have different origins of water (**Fig 3.54**).

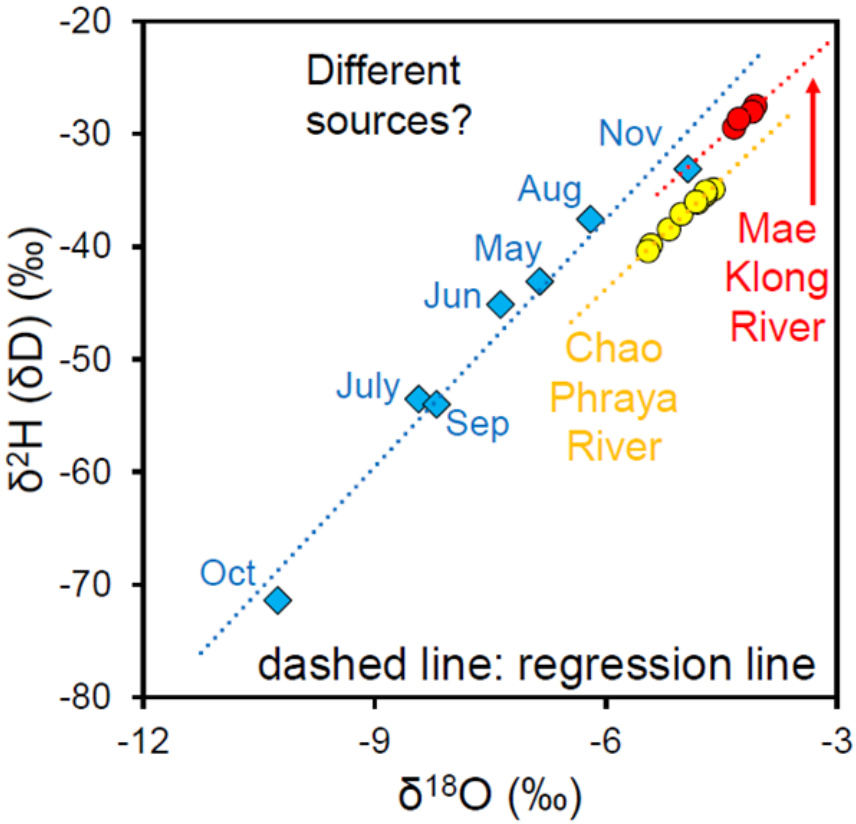

Fig 3.54 The stable isotopic composition results of tap water and rainwater sample

3.4.5. Future collaboration plan

As mentioned in the results, the first-year collaboration was conducted on the tap water sample collected only in Bangkok and the metropolitan area. The second-year collaboration aims to extend the water sampling region nationwide. **Fig 3.55 and table 3.31** show the tap water sample's sampling and rainwater sample from Sri Racha and Chiangmai. At present, the samples are under enrichment and measurement process.

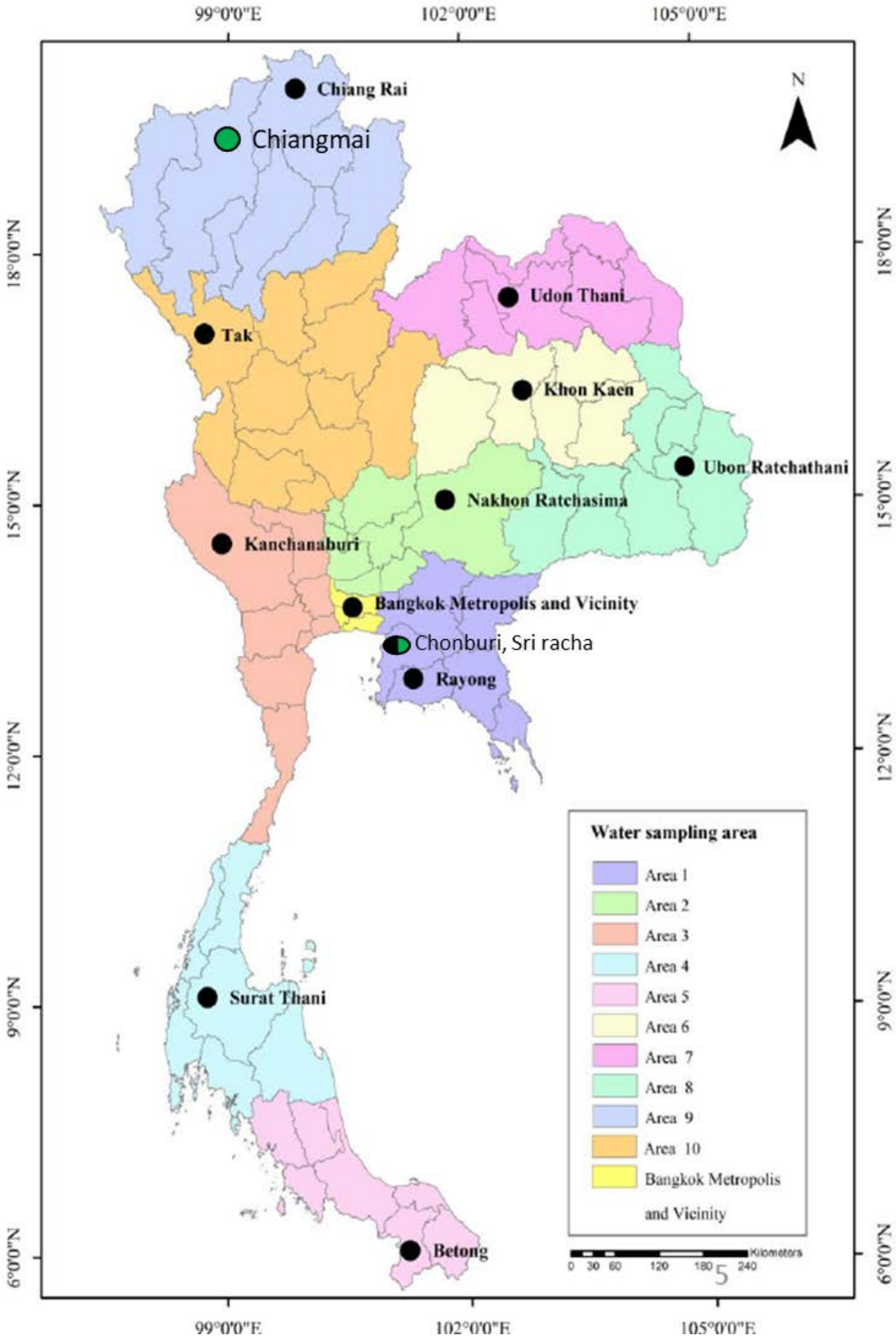

Fig 3.55 Nationwide tap water sampling site for the second year of collaboration.

● = tap water sampling site, ● = Rainwater sampling site

Table 3.31 Sampling region of nationwide tap water and rainwater

Tap water July 2021	Location
1	Rayong
2	Chonburi
3	Nakhon Ratchasima
4	Kanchanaburi
5	Surat Thani
6	Yala
7	Khon Kaen
8	Udon Thani
9	Ubon Ratchathani
10	Chiang Rai
11	Tak
Rainwater	**Location**
May-20	Sri racha 2020
Jun-20	
Jul-20	
Aug-20	
Sep-20	
Oct-20	
Apr-21	Sri racha 2021
May-21	
Jun-21	
Jul-21	
Aug-21	
Jul-21	Chiang-Mai 2021
Aug-21	

CHAPTER FOUR: Conclusion

Isotope separation via chemical exchange using DC18C6 crown-ether was carried out to investigate the isotope enrichment of calcium-48 (^{48}Ca). This research aimed to find a cost-effective way to enrich ^{48}Ca for the study of neutrinoless double beta decay ($0\nu\beta\beta$) in CANDLES (CAlcium fluoride for studies of Neutrino and Dark matters by Low Energy Spectrometer) project. Liquid-liquid extraction (LLE) was carried out to investigate the isotope separation and enrichment mass production. LLE has the advantage of accessing the high concentration of ion content, which was suitable for the isotope separation mass production compared to other methods, such as crown-ether resin chromatographic. The initial feed concentration of LLE was approximately 30% w/w concentration (3.3 M $CaCl_2$ (aq), while the resin chromatography was less than 0.1M [61 – 63]. Moreover, the resin chromatographic method needed to operate for at least 1 to 10 days depending on several factors, such as migration length, flow rate, calcium concentration, and the additional high HCl acid. On the other hand, the liquid-liquid extraction under the appropriate condition could be finished with several multistage iterations within a few hours. Those obstacles indicated that the crown-ether resin chromatographic method was inapplicable for the isotope separation and mass production of ^{48}Ca isotope compared to LLE. Nonetheless, the LLE required a design experiment on the multistage iteration or cascade enrichment to acquire the isotope enrichment and mass production. Simultaneously, the extraction of lithium was carried out using the same conditions.

Reaction-cell ICP-MS was used to analyze calcium isotope composition and compared to TIMS. The calculated separation factor (α) obtained from reaction-cell ICP-MS was in a good agreement with the TIMS result, indicating that the measurement by ICP-MS is reliable under the addition of H_2 gas as a reaction gas. Moreover, careful correction using bracketing

sequence sample was applied to avoid the mass bias during the prolonged measurement. At the same time, lithium isotope composition was carried out to assure the measurement reliability by spike lithium samples at various concentrations of ^{7}Li, including 94.14%, 96.35%, and 98.20%. The results demonstrated that our lithium sample was naturally abundant, and the variation of isotope composition was reliable.

Several fundamental factors to study the isotope separation was performed, including the presence and absence of crown-ether, various extraction time, aqueous phase concentration, acidity solvent, volume ratio extraction system, extraction temperature, solid-liquid extraction, and multistage iteration.

The result indicated the dependency on the presence and absence of crown-ether on the extraction system. Without crown-ether, there was no cation extracted to the organic phase, and the distribution coefficient (D) of both calcium and lithium was found to be 0. This finding assured that the crown-ether plays a role in the extraction process as a host-guest molecule by electrostatic attraction. As for the extraction time experiment, the chemical exchange was equilibria at least 1 minute by magnetic stirrer for both calcium and lithium extraction. The distribution coefficient (D) was consistent at 1 minute to 1 hour extraction system. The result was consistent with K Nishizawa et al. [101] reported on lithium isotope separation via B15C6 crown-ether study. The result indicated that at least 30 seconds is required to equilibria the chemical exchange reaction. However, K. Nishizawa found the dependency of separation factor (α) of ^{7}Li/^{6}Li up to 0.990 ± 0.002. Our finding indicated that all of the separation factor results were consistent at approximately -1.2% of isotope fractionation ($^{7/6}\alpha$ = 0.988±0.004), consistent with K. Nishizawa reported. The reason might be that our conditions were in a larger crown-ether content, resulting in a higher distribution coefficient. All of the separation factors were constant at every extraction time. We aimed to observe the isotope fractionation and the significant contribution of ion content to establish mass production. Therefore, we need to

study by the large among of crown-ether and maintain the advantage of high conversion LLE simultaneously. In conclusion, 1 minute extraction was sufficient and ensured that the chemical and isotope reaction was at equilibria.

The study of aqueous phase concentration was conducted by the $CaCl_2$ (aq) and LiCl (aq), ranging from 10% w/w to 40% w/w extraction system. The distribution coefficient (D) was increased up to 0.1480±0.0012 and 0.0292±0.0001 for 40% w/w $CaCl_2$(aq) and 30% w/w LiCl (aq) extraction system, respectively. The separation factor (α_{org}) was consistent at 0.989±0.004 to 0.991±0.002 and 0.988±0.003 to 0.991±0.003 for calcium and lithium, respectively. Despite that, the 40% w/w extraction system provided the highest conversion under the same isotope fractionation, but 40% w/w of the aqueous phase was almost the highest solubility of $CaCl_2$ (aq). Therefore, the extraction at high concentration might lead to the colloidal substances problem and only one-time back extraction might be insufficient to strip the calcium ion back to the water. The result of the aqueous phase was in a good agreement with another work of K. Nishizawa et al. [104]. The higher the aqueous phase concentration, the distribution coefficient was increased. However, K. Nishizawa found the separation factor (α) dependency on the high concentration as well. In contrast, our finding did not show the separation factor (α) dependency. The reason was that the amount of crown-ether contributed to this present work was much larger than K. Nishizawa works. The advantage was that a large amount of lighter enriched lithium isotope could be promising and suitable for lighter isotope separation and enrichment. Another reason that the separation factor dependency was not observed was that the crown-ether used in this research was not appropriate to lithium extraction. On the other hand, the calcium extraction was also not observed the dependency. The separation factor (α_{org}) was consistent at 0.989±0.004 to 0.991±0.002 and 0.988±0.003 to 0.991±0.003 for calcium ($^{48}Ca/^{40}Ca$) and lithium ($^{7}Li/^{6}Li$), respectively. At the presence of HCl solvent, the distribution coefficient increased from 0.0200±0.0003 to 0.0546±0.0012 with the

absence and presence of HCl acid at the same 30% w/w $CaCl_2$ (aq) extraction system. For lithium, the distribution coefficient increased from 0.0292±0.0001 to 0.0086±0.0001 at 30% w/w LiCl extraction system. The separation factor was consistent at 0.991±0.004 to 0.993±0.003 and 0.990±0.004 for both calcium and lithium extraction. The lithium separation factor showed a slight increase at the higher concentration under HCl acid from 0.996±0.005 to 0.990±0.004 under 0.3% and 30% w/w LiCl (HCl) extraction system. Moreover, the most important extraction under HCl was that the HCl acid increased and maintained the ion-crown formation even the low feed calcium or lithium concentration. This finding could be explained by the contribution of the anion (Cl^-) on the formation of crown-complex. Compared to the study of S. Nemoto et al. [63] on the resin chromatographic method and the determination of the optimized structures of calcium ion-benzo-18-crown-6 (B18C6) complex, it was found that the measured ion corresponded to the formation provided by S. Nemoto. The formation of the calcium ion-crown complex under high concentration HCl acid was found to be Ca:4Cl:CE. On the other hand, lithium extraction was inconsistent at Li:13Cl:CE. The simulation provided by Prof. Sunaga Ayaki, one of the collaborators from the Institute for Integrated Radiation and Nuclear Science, Kyoto University, Japan, suggested that the extraction with the absence of HCl acid had the ratio of Ca:2Cl:CE and Li:1Cl:CE and the crown-ether was distorted under the formation with lithium ion. In conclusion, HCl could improve the extraction of calcium and lithium content. To establish the mass production, further study on the multistage iteration for the isotope enrichment and mass production was required. However, the production under the presence of hard handling reagent was problematic. Therefore, we conducted the rest of the experiment using an aqueous solvent at a 30% w/w of the feed extraction system.

The volume ratio and filter LLE experiment were carried out to investigate the extraction under the small aqueous solution. This experiment was expected to observe the separation factor in the aqueous phase, where the heavier isotope was enriched. The smaller

volume (1mL) of aqueous needed to be separated by filter separation since the separation using the separation funnel was inappreciable. The extraction efficiency was determined by the mole ratio (η) and found to be comparable with conventional LLE. However, the single-stage separation was insufficient to overcome the uncertainty value of ICP-MS measurement (approximately 4‰).

Multistage iteration was carried out under an aqueous solvent. The results showed the enrichment of ^{48}Ca in the aqueous phase. The maximum separation factor (α) of $^{48}Ca/^{42}Ca$ was found to be 1.004±0.004 after the 4th iteration. The separation factor of $^{48}Ca/^{40}Ca$ was estimated to be 1.006 (ε = 6.00 ‰). However, the recovery amount of calcium in aqueous phase was less than 10% (0.2mL), which was not suitable for enrichment and mass production. Compared to crown-ether resin chromatographic, the enrichment coefficient (ε) reported by S. Nemoto, S Umehara, and K. Hayasaka [61 – 63] was found to be 3.04 ‰, 1.90‰, and 6.0±1.0, respectively. The recovery of calcium was much smaller compared to LLE. Our extraction via the LLE indicated the higher and comparable value of enrichment coefficient (ε) compared to the crown-ether resin chromatographic method plus the larger recovery amount of calcium content. Nonetheless, we also conducted the extraction with the presence and absence of 12M HCl acid with the larger feed volume at 5mL for 6th iteration. The separation was carried out by batch LLE using separation funnel. It was found that the recovery amount of calcium content was 5.5 and 9.2 mmol for HCl and aqueous solvent, respectively. This indicated that the recovery amount of aqueous phase was 50.4% and 25.6% of the initial feed, which suitable for the mass production vis cascade iteration.

LLE provided a higher conversion of ion content and was more suitable for isotope enrichment and mass production since the higher contribution of calcium content was allowed. To establish mass production, additional research on the higher volume of crown-ether content and a large amount of calcium in the aqueous phase is required. However, the calcium content

was decreased over the multistage iteration. We also provided the preliminary iteration based on the observed parameter to find the appropriate enrichment procedure in the section 3.3.9.

Additional experiments were carried out, including the extraction temperature dependency (-15 to 45°C) and solid-liquid extraction (SLE). The temperature effect was found that the distribution coefficient increased as temperature decreased. At the same time, the separation factor was consistent at the same at 0.987±0.003 to 0.990±0.003, and 0.989±0.004 to 0.994±0.004 for calcium and lithium extraction, respectively. An additional study of K. Nishizawa et al. [101] was reported on the study of lithium extraction using crown-ether and temperature difference. The results revealed the same behavior as our finding. However, the results indicated the dependency on separation factor (α) up to 1.045 at 0 °C. The reason might be that the setup of K. Nishizawa was the high concentration of B15C5 crown-ether, the volume ratio of 1/1, and the LiI, which provided the highest separation factor among lithium species. In the study of SLE, the comparison between DC18C6 and 18C6, water-soluble type crown-ether, was determined. It was found that SLE provided a higher mole ratio (η) than LLE for both DC18C6 and 18C6 crown-ether. However, the separation factor was not observed in solid and organic phases. These results indicated that the selectively crown-ether separation is required a cation to form the ion-crown complex via electrostatic attraction. Further study on the use of cost-effectively crown-ether, 18C6, was required to improve mass production effectively.

The evaluation of calcium and lithium isotope effect was identified. The scaling factor of Bigeleisen's new theory was revealed the contribution ratio of nuclear field effect, and nuclear spin effect to the nuclear mass effect. In the case of calcium, isotope pair evaluation was applied. The contribution of isotope shifts mostly came from the mass effect, especially $^{48}Ca/^{40}Ca$ which has double magic number, known as parabolic behavior. The finding emphasized the isotope exchange via crown-ether was a powerful method for the separation of

^{48}Ca from the most abundance of ^{40}Ca. Moreover, the obtained value also showed the contribution of hyperfine splitting in the odd number isotope, ^{43}Ca. The dominated in the mass effect was in good agreement with the calculation of R. Hazama [100]. On the other hand, the lithium, which has only two isotopes, was evaluated by the experimental value from various extraction temperature. The results indicated the strongly isotope shift from the nuclear mass effect as the calcium effect.

The SPE film was used as a hydrogen ion carrier to study the electrolytic enrichment of tritium. The advantage of SPE film compared to alkali electrolyte is that the SPR film did not require the pretreatment procedure. The enrichment factor is not limited depending on the water volume. The large electric current was allowed since the produced gases were separated and significantly improved the safety of the enrichment. However, the enrichment using SPE film apparatus could only be performed one by one, while the alkali electrolyte could be connected in a series for several sample enrichment simultaneously.

This research improved the SPE apparatus and the logging of temperature deviation to assure the enrichment factor obtained from the tritiated water sample. Additionally, the water and air circulation systems were installed to stabilize the plate temperature during the enrichment. The temperature at the cathode plate was decreased from 36.7 °C to 24.0 °C. The maximum temperature was also decreased from 73.9 °C to 36.0 °C. All of the enriched sample was measured the temperature change to assure that the enrichment factor obtained from tritiated water could applied to those sample. The average enrichment factor before and after the installation of air circulation system was increased from 13.9±0.2 to 16.0±0.2. Compared to the previous works of Ogata Y, et al [127] the enrichment factor was reported to be 10.8±1.2 under the same electrode, temperature, and initial volume of water sample. Our improvement on the temperature stabilization system enhanced about 1.5 time of the enrichment factor

reported Y. Ogata, et al. The temperature logging on the cathode plate could assure the reliable of the obtained enrichment factor by the represented sample of tritiated water as well.

This research was toward the international joint research project between the Department of Applied Radiation and Isotope, Kasetsart University, and Thailand Institute of Nuclear Technology (TINT), Thailand and Department of Environmental Science and Technology, Osaka Sangyo University. The water samples collected from Bangkok and metropolitan areas, Thailand, were sent and distributed to Japan. The water sample consists of July 2020 tap water and rainwater samples collected from Sri-Racha, Rayong. The determination of tritium concentration was carried out by liquid scintillation counting (LSC LB-7). The concentration in July tap water samples was found to be comparable with the results measured by TINT. The tritium result in tap water ranged from 0.10±0.01 to 0.36±0.03 Bq/L. However, additional intercomparison is in a process to compare ultralow-level tritium measurement. However, the locality dependency was not observed since the sampling area was closed to each other. Shinshu University and Kyoto University collaboration performed additional measurements of the trace elements. The result clearly showed the difference in water sources from Mae Klong River and Chao Phraya River. The stiff diagram showed the Mae Klong River source characterized by calcium and bicarbonate water type. As for the Chao Phraya River, the water sample was characterized to be sodium, chloride, and sulfate ion. The stable isotopic composition results showed that each water type has different water origins.

The second-year collaboration between Thailand and Japan aimed to extend the sampling area nationwide. At present, the July 2021 tap water samples collected from 11 locations of Thailand and rainwater sample is under enrichment and measurement processes.

Reference

[1] Thomson, J. J. (1897). Discovery of the electron. *Philosophical Magazine, 44*, 93.

[2] Debierne, A. (1911). RADIOACTIVITY. 2. *Journal of the American Chemical Society, 33*(8), 1388-1402.

[3] Soddy, F. (1921). The Atomic Volume of Isotopes. *Nature, 107*(2680), 41-42.

[4] Chadwick, J. (1932). Possible existence of a neutron. *Nature, 129*(3252), 312-312.

[5] Bleakney, W., & Gould, A. J. (1933). The relative abundance of hydrogen isotopes. *Physical Review, 44*(4), 265.

[6] Wolfsberg, M., Van Hook, W. A., Paneth, P., & Rebelo, L. P. N. (2009). *Isotope effects: in the chemical, geological, and bio sciences*: Springer Science & Business Media.

[7] Graph of isotopes by type of nuclear decay Retrieved from https://upload.wikimedia.org/wikipedia/commons/c/c4/Table_isotopes_en.svg

[8] Kohen, A., & Limbach, H.-H. (2005). *Isotope effects in chemistry and biology*: cRc Press.

[9] Rahmani, P. (2017) Study of the Primary Isotope Dependence of the Secondary Kinetic Isotope Effects and Hammett Correlations in Hydride Transfer Reactions in Solution. *Southern Illinois University Edwardsville*.

[10] Sen, A., & Kohen, A. (2010). Enzymatic tunneling and kinetic isotope effects: chemistry at the crossroads. *Journal of Physical Organic Chemistry, 23*(7), 613-619.

[11] Bigeleisen, J., & Mayer, M. G. (1947). Calculation of equilibrium constants for isotopic exchange reactions. *The Journal of Chemical Physics, 15*(5), 261-267.

[12] Fujii, Y., Nomura, M., Okamoto, M., Onitsuka, H., Kawakami, F., & Takeda, K. (1989). An anomalous isotope effect of 235U in U (IV)-U (VI) chemical exchange. *Zeitschrift für Naturforschung A*, *44*(5), 395-398.

[13] CHEN, J., Nomura, M., Fujii, Y., Kawakami, F., & Okamoto, M. (1992). Gadolinium isotope separation by cation exchange chromatography. *Journal of Nuclear Science and Technology*, *29*(11), 1086-1092.

[14] Nishizawa, K., Nakamura, K., Yamamoto, T., & Masuda, T. (1993). Zinc isotope effects in complex formation with a crown ether. *Solvent Extraction and Ion Exchange*, *11*(3), 389-394.

[15] Oi, T., Ogino, H., Hosoe, M., & Kakihana, H. (1992). Fractionation of strontium isotopes in cation-exchange chromatography. *Separation science and technology*, *27*(5), 631-643.

[16] Nishizawa, K., Satoyama, T., Miki, T., Yamamoto, T., & Hosoe, M. (1995). Strontium isotope effect in liquid-liquid extraction of strontium chloride using a crown ether. *Journal of nuclear science and technology*, *32*(12), 1230-1235.

[17] Fujii, T., Inagawa, J., & Nishizawa, K. (1998). Influences of nuclear mass, size, shape and spin on chemical isotope effect of titanium. *Berichte der Bunsengesellschaft für physikalische Chemie*, *102*(12), 1880-1885.

[18] Angeli, I., & Marinova, K. P. (2013). Table of experimental nuclear ground state charge radii: An update. *Atomic Data and Nuclear Data Tables*, *99*(1), 69-95.

[19] Nishizawa, K., Maeda, Y., Kawashiro, F., Fujii, T., Yamamoto, T., & Hirata, T. (1998). Contributions of nuclear size and shape, nuclear mass, and nuclear spin to enrichment factors of zinc isotopes in a chemical exchange reaction by a cryptand. *Separation Science and Technology*. *33*(14), 2101-2112

[20] Fujii, T., Suzuki, D., Gunji, K., Watanabe, K., Moriyama, H., & Nishizawa, K. (2002). Nuclear field shift effect in the isotope exchange reaction of chromium (III) using a crown ether. *The Journal of Physical Chemistry A*, *106*(30), 6911-6914.

[21] Dembiński, W., Poniński, M., & Fiedler, R. (1998). Preliminary results of the studies on fractionation of ytterbium isotopes in Yb (III)-acetate/Yb-amalgam system. *Separation science and technology*, *33*(11), 1693-1701.

[22] Ismail, I. M., Fukami, A., Nomura, M., & Fujii, Y. (2000). Anomaly of 155Gd and 157Gd isotope effects in ligand exchange reactions observed by ion exchange chromatography. *Analytical chemistry*, *72*(13), 2841-2845.

[23] Shibahara, Y., Nishizawa, K., Yasaka, Y., & Fujii, T. (2002). STRONTIUM ISOTOPE EFFECT IN DMSO–WATER SYSTEM BY LIQUID CHROMATOGRAPHY USING A CRYPTAND POLYMER. *Solvent extraction and ion exchange*, *20*(1), 67-79.

[24] Nishizawa, K., Miki, T., Ikeda, R., Fujii, T., Yamamoto, T., & Nomura, M. (1997). Isotopic enrichment of nickel in aqueous solution/crown ether system. *Journal of the Mass Spectrometry Society of Japan*, *45*(4), 521-527.

[25] Bigeleisen, J. (1996). Nuclear size and shape effects in chemical reactions. Isotope chemistry of the heavy elements. *Journal of the American Chemical Society*, *118*(15), 3676-3680.

[26] Fujii, T., (2004). **異常同位体効果**, Retrieved from http://jsac.jp/bunseki/pdf/bunseki2004/izumi200402.pdf

[27] Liu, Q., Tossell, J. A., & Liu, Y. (2010). On the proper use of the Bigeleisen–Mayer equation and corrections to it in the calculation of isotopic fractionation equilibrium constants. *Geochimica et Cosmochimica Acta*, *74*(24), 6965-6983.

[28] Awan, I. Z., & Khan, A. Q. (2015). Uranium-The Element: Its Occurrence and Uses. *Journal of the Chemical Society of Pakistan, 37*(6).

[29] Grenthe, I., Drożdżyński, J., Fujino, T., Buck, E. C., Albrecht-Schmitt, T. E., & Wolf, S. F. (2008). Uranium *The chemistry of the actinide and transactinide elements* (pp. 253-698): Springer.

[30] Carvalho, F. P. (2017). Mining industry and sustainable development: time for change. *Food and Energy Security, 6*(2), 61-77.

[31] Nuclear explained , The nuclear fuel cycle Retrieved from https://www.eia.gov/energyexplained/nuclear/the-nuclear-fuel-cycle.php

[32] Hore-Lacy, I. (2016). *Uranium for nuclear power: Resources, mining and transformation to fuel.*

[33] Isotope Separation Methods, atomic heritage foundation Retrieved from https://www.atomicheritage.org/history/isotope-separation-methods

[34] Villani, S. (1979). *Uranium enrichment*, Springer, p 15

[35] Whitaker, J. (2005). Uranium enrichment plant characteristics: A training manual for the IAEA,‖ Oak Ridge National Laboratory. *ORNL/TM*-2005/43

[36] Medical uses of radioactive calcium. Review of an IAEA programme to promote the applications of calcium-47, *IAEA Bulletin; ISSN 0020-6067*; CODEN IAEBAB; v. 5(1); p. 15-17

[37] Schmitt, A.-D., Cobert, F., Bourgeade, P., Ertlen, D., Labolle, F., Gangloff, S., . . . Stille, P. (2013). Calcium isotope fractionation during plant growth under a limited nutrient supply. *Geochimica et Cosmochimica Acta, 110*, 70-83.

[38] Gupta, R. K., Săndulescu, A., & Greiner, W. (1977). Synthesis of Fermium and Transfermium elements using Calcium-48 beam. *Zeitschrift für Naturforschung A, 32*(7), 704-707.

[39] Kajita, T. (2016). Nobel Lecture: Discovery of atmospheric neutrino oscillations. *Reviews of Modern Physics, 88*(3), 030501.

[40] Esposito, S., Majorana Jr, E., Van der Merwe, A., & Recami, E. (2003). *Ettore Majorana: Notes on Theoretical Physics* (Vol. 133): Springer Science & Business Media.

[41] Dolinski, M. J., Poon, A. W., & Rodejohann, W. (2019). Neutrinoless double-beta decay: status and prospects. *Annual Review of Nuclear and Particle Science, 69*, 219-251.

[42] Ajimura, S., Chan, W., Ichimura, K., Ishikawa, T., Kanagawa, K., Khai, B., . . . Matsuoka, K. (2021). Low background measurement in CANDLES-III for studying the neutrinoless double beta decay of Ca 48. *Physical Review D, 103*(9), 092008.

[43] Agostini, M., Bakalyarov, A., Balata, M., Barabanov, I., Baudis, L., Bauer, C., . . . Bezrukov, L. (2018). Improved limit on neutrinoless double-β decay of ge 76 from GERDA phase ii. *Physical review letters, 120*(13), 132503.

[44] Aalseth, C. E., Abgrall, N., Aguayo, E., Alvis, S., Amman, M., Arnquist, I. J., . . . Barbeau, P. (2018). Search for Neutrinoless Double-β Decay in Ge 76 with the Majorana Demonstrator. *Physical review letters, 120*(13), 132502.

[45] Arnold, R., Augier, C., Baker, J., Barabash, A., Brudanin, V., Caffrey, A., . . . Etienvre, A. (2006). Limits on different majoron decay modes of 100Mo and 82Se for neutrinoless double beta decays in the NEMO-3 experiment. *Nuclear Physics A, 765*(3-4), 483-494.

[46] Argyriades, J., Arnold, R., Augier, C., Baker, J., Barabash, A., Basharina-Freshville, A., . . . Caffrey, A. (2010). Measurement of the two neutrino double

beta decay half-life of Zr-96 with the NEMO-3 detector. *Nuclear Physics A, 847*(3-4), 168-179

[47] Arnold, R., Augier, C., Baker, J., Barabash, A., Basharina-Freshville, A., Blondel, S., . . . Busto, J. (2015). Results of the search for neutrinoless double-β decay in Mo 100 with the NEMO-3 experiment. *Physical Review D, 92*(7), 072011.

[48] Barabash, A., Belli, P., Bernabei, R., Cappella, F., Caracciolo, V., Cerulli, R., . . . Incicchitti, A. (2018). Final results of the Aurora experiment to study 2 β decay of Cd 116 with enriched Cd 116 WO 4 crystal scintillators. *Physical Review D, 98*(9), 092007.

[49] Arnaboldi, C., Brofferio, C., Bucci, C., Capelli, S., Cremonesi, O., Fiorini, E., . . . Pedretti, M. (2003). A calorimetric search on double beta decay of 130Te. *Physics Letters B, 557*(3-4), 167-175.

[50] Alduino, C., Alessandria, F., Alfonso, K., Andreotti, E., Arnaboldi, C., Avignone III, F., . . . Banks, T. (2018). First Results from CUORE: A Search for Lepton Number Violation via 0 ν β β Decay of Te 130. *Physical review letters, 120*(13), 132501.

[51] Gando, A., Gando, Y., Hachiya, T., Hayashi, A., Hayashida, S., Ikeda, H., . . . Koga, M. (2016). Search for Majorana neutrinos near the inverted mass hierarchy region with KamLAND-Zen. *Physical review letters, 117*(8), 082503.

[52] Albert, J., Anton, G., Badhrees, I., Barbeau, P., Bayerlein, R., Beck, D., . . . Cao, G. (2018). Search for neutrinoless double-beta decay with the upgraded EXO-200 detector. *Physical review letters, 120*(7), 072701.

[53] Arnold, R., Augier, C., Baker, J., Barabash, A., Basharina-Freshville, A., Blondel, S., . . . Busto, J. (2016). Measurement of the 2 ν β β decay half-life of Nd 150

and a search for 0 ν β β decay processes with the full exposure from the NEMO-3 detector. *Physical Review D, 94*(7), 072003.

[54] Kwiatkowski, A., Brunner, T., Holt, J., Chaudhuri, A., Chowdhury, U., Eibach, M., . . . Horoi, M. (2014). New determination of double-β-decay properties in 48 Ca: High-precision Q β β-value measurement and improved nuclear matrix element calculations. *Physical Review C, 89*(4), 045502.

[55] Kishimoto, T, Study of 48Ca Double Beta Decay by CANDLES Retrieved from https://www.rcnp.osakau.ac.jp/~umehara/dbdnm07/presentation/Kishimoto.pdf

[56] Love, L. (1973). Electromagnetic Separation of Isotopes at Oak Ridge: An informal account of history, techniques, and accomplishments. *Science, 182*(4110), 343-352.

[57] Yergey, A. L., & Yergey, A. K. (1997). Preparative scale mass spectrometry: A brief history of the calutron. *Journal of the American Society for Mass Spectrometry, 8*(9), 943-953.

[58] Kornoukhov, N. (2010). Status of $^{40}Ca^{100}MoO_4$ single crystals growing for AMORE Collanoration Retrieved from https://slidetodoc.com/status-of-40-ca-100-mo-o-4/

[59] Zucker, D., & Drury, J. (1964). Separation of calcium isotopes in an amalgam system. *The Journal of Chemical Physics, 41*(6), 1678-1681.

[60] Saito, S, Yanase, S, and Oi, T,. (2011). Calcium isotope effects accompanying electrochemical insertion of calcium into graphite from electrolyte solution. *Radioisotopes, 60*(7), 265-274.

[61] Umehara, S., Kishimoto, T., Kakubata, H., Nomura, M., Kaneshiki, T., Suzuki, T., . . . Nemoto, S. (2015). A basic study on the production of enriched isotope ^{48}Ca

by using crown-ether resin. *Progress of Theoretical and Experimental Physics,* 2015(5).

[62] Hayasaka, K., Kaneshiki, T., Nomura, M., Suzuki, T., & Fujii, Y. (2008). Calcium ion selectivity and isotope effects studied by using benzo-18-crown-6 resins. *Progress in Nuclear Energy, 50*(2-6), 510-513.

[63] Nemoto, S., Suga, K., Fukuda, Y., Nomura, M., Suzuki, T., & Oi, T. (2012). Calcium isotope fractionation in liquid chromatography with crown ether resins. *Journal of Nuclear Science and Technology, 49*(4), 425-437.

[64] Sato, T., & Oi, T. (2015). Calcium isotope fractionation in liquid chromatography with benzo-18-crown-6 resin in aqueous hydrobromic acid medium. *Journal of Nuclear Science and Technology, 52*(5), 641-650.

[65] Kemp, G. (1998). Capillary electrophoresis: a versatile family of analytical techniques. *Biotechnology and applied biochemistry, 27*(1), 9-17.

[66] Kobayashi, N., Fujii, Y., & Okamoto, M. (1982). Calcium isotope enrichment by means of counter-current electromigration using an ion-exchange resin as migration medium. *Journal of Chromatography A, 252*, 121-130.

[67] Kishimoto, T., Matsuoka, K., Fukumoto, T., & Umehara, S. (2015). Calcium isotope enrichment by means of multi-channel counter-current electrophoresis for the study of particle and nuclear physics. *Progress of Theoretical and Experimental Physics,* 2015(3).

[68] Nabiev, S. S., Sukhanov, L., Gaponov, Y. V., & Inzhechik, L. (2001). Electrooptical separation of Ca isotopes for nuclear-physics experiments. *Physics of Atomic Nuclei, 64*(9), 1541-1548.

[69] Matsuoka, K., Niki, H., Ogawa, I., Shinki, Y., Kawashima, Y., & Matsumura, K. (2020). The laser Isotope separation (LIS) methods for the enrichment of 48*Ca. J. Phys.: Conf. Ser.* 1468 012199

[70] Tomascak, P. B., Magna, T., & Dohmen, R. (2016). *Advances in lithium isotope geochemistry*: Springer.

[71] Abdou, M. A. (1983). *Tritium breeding in fusion reactors.* Paper presented at the Nuclear data for science and technology.

[72] Euro fusion (2017), Tritium: a challenging fuel for fusion Retrieved from https://fusion4freedom.com/tritium-challenging-fuel-fusion/

[73] Dolan, T. J. (2017). *Molten salt reactors and thorium energy*: Woodhead Publishing.

[74] US Department of Energy Nuclear Energy Research Advisory Committee, Retrieved from https://en.wikipedia.org/wiki/Molten_salt_reactor

[75] Okuyama, K., Okada, I., & Saito, N. (1973). The isotope effects in the isotope exchange equilibria of lithium in the amalgam-solution system. *Journal of Inorganic and Nuclear Chemistry, 35*(8), 2883-2895.

[76] Brooks, S. C., & Southworth, G. R. (2011). History of mercury use and environmental contamination at the Oak Ridge Y-12 Plant. *Environmental pollution, 159*(1), 219-228.

[77] Ban, Y., Nomura, M., & Fujii, Y. (2002). Chromatographic separation of lithium isotopes with silica based monobenzo-15-crown-5 resin. *Journal of Nuclear Science and Technology, 39*(3), 279-281.

[78] Kim, D., Jeon, Y., Eom, T., Suh, M., & Lee, C. (1991). Lithium isotope separation on a monobenzo-15-crown-5 resin. *Journal of Radioanalytical and Nuclear Chemistry, 150*(2), 417-426.

[79] Arisawa, T., Maruyama, Y., Suzuki, Y., & Shiba, K. (1982). Lithium isotope separation by laser. *Applied Physics B, 28*(1), 73-76.

[80] Saleem, M., Hussain, S., Rafiq, M., & Baig, M. (2006). Laser isotope separation of lithium by two-step photoionization. *Journal of applied physics, 100*(5), 053111.

[81] Zhou, H. X., & Szabo, A. (1995). Microscopic formulation of Marcus' theory of electron transfer. *The Journal of Chemical Physics, 103*(9), 3481-3494.

[82] Black, J. R., Umeda, G., Dunn, B., McDonough, W. F., & Kavner, A. (2009). Electrochemical isotope effect and lithium isotope separation. *Journal of the American Chemical Society, 131*(29), 9904-9905.

[83] Wang, M., Sun, J., Zhang, P., Huang, C., Zhang, Q., Shao, F., . . . Jia, Y. (2020). Lithium isotope separation by electromigration. *Chemical Physics Letters, 746*, 137290.

[84] Sun, H., Jia, Y., Liu, B., Jing, Y., Zhang, Q., Shao, F., & Yao, Y. (2019). Separation of lithium isotopes by using solvent extraction system of crown ether-ionic liquid. *Fusion Engineering and Design, 149*, 111338.

[85] Zhu, W., Jia, Y., Zhang, Q., Sun, J., Jing, Y., & Li, J. (2019). The effect of ionic liquids as co-extractant with crown ether for the extraction of lithium in dichloromethane-water system. *Journal of Molecular Liquids, 285*, 75-83.

[86] Hoshino, T., & Terai, T. (2011). Basic technology for 6Li enrichment using an ionic-liquid impregnated organic membrane. *Journal of nuclear materials, 417*(1-3), 696-699.

[87] Hoshino, T., & Terai, T. (2011). High-efficiency technology for lithium isotope separation using an ionic-liquid impregnated organic membrane. *Fusion Engineering and Design, 86*(9-11), 2168-2171.

[88] Rezaee, M., Yamini, Y., & Faraji, M. (2010). Evolution of dispersive liquid–liquid microextraction method. *Journal of Chromatography A*, *1217*(16), 2342-2357.

[89] Dmitrienko, S. G., Apyari, V. V., Tolmacheva, V. V., & Gorbunova, M. V. (2020). Dispersive Liquid–Liquid Microextraction of Organic Compounds: An Overview of Reviews. *Journal of Analytical Chemistry*, *75*(10), 1237-1251.

[90] Davoudi, M., & Mallah, M. H. (2013). Enrichment of 6Li using dispersive liquid–liquid microextraction as a highly efficient technique. *Annals of Nuclear Energy*, *62*, 499-503.

[91] Mallah, M., & Davoudi, M. (2012). Evaluation of lithium separation by dispersive liquid–liquid microextraction using benzo-15-crown-5. *Journal of Radioanalytical and Nuclear Chemistry*, *293*(1), 247-254.

[92] Aguilar, M., & Cortina, J. L. (Eds.). (2008). *Solvent extraction and liquid membranes: Fundamentals and applications in new materials*. CRC Press.

[93] Pedersen, C. J. (1971). Macrocyclic polyethers for complexing metals. *Aldrichimica Acta*, *4*(1).

[94] Pedersen, C. J. (1988). The discovery of crown ethers. *Science*, *241*(4865), 536-540.

[95] Izatt, R. (Ed.). (2012). *Synthetic multidentate macrocyclic compounds*. Elsevier.

[96] Wong, K. H., Konizer, G., & Smid, J. (1970). Binding of cyclic polyethers to ion pairs of carbanion alkali salts. *Journal of the American Chemical Society*, *92*(3), 666-670.

[97] Truter, M. R., & Pedersen, C. J. (1971). Cryptates. *Endeavour*, *30*(111), 142.

[98] Pedersen, C. J., Poonia, N. S., Bajaj, A. V., Izatt, R. M., Bradshaw, J. S., Nielsen, S. A., ... & Debabrata, S. (1967). Thermodynamic and kinetic data for cation-macrocycle interaction. *Chem. Rev.*, *89*, 7017-7036.

[99] Jepson, B. E., & DeWitt, R. (1976). Separation of calcium isotopes with macrocyclic polyether calcium complexes. *Journal of Inorganic and Nuclear Chemistry*, *38*(6), 1175-1177.

[100] Hazama, R., Tatewaki, Y., Kishimoto, T., Matsuoka, K., Endo, N., Kume, K., ... & Tanimizu, M. (2007). Challenge on Ca-48 enrichment for candles double beta decay experiment. *arXiv preprint arXiv*:0710.3840.

[101] Nishizawa, K., Ishino, S. I., Watanabe, H., & Shinagawa, M. (1984). Lithium isotope separation by liquid-liquid extraction using benzo-15-crown-5. *Journal of nuclear science and technology*, *21*(9), 694-701.

[102] Moynier, F., Fujii, T., Telouk, P., & Albarede, F. (2008). Isotope separation of Te in chemical exchange system with dyclohexano-18-crown-6. *Journal of Nuclear Science and Technology*, *45*(sup6), 10-14.

[103] Heumann, K. G., & Schiefer, H. P. (1980). Calcium isotope separation on an exchange resin having cryptand anchor groups. *Angewandte Chemie International Edition in English*, *19*(5), 406-407.

[104] Nishizawa, K., & Takano, T. (1988). Extractive separation of lithium isotopes using benzo-15-crown-5. Effect of salt concentration. *Separation Science and Technology*, *23*(6-7), 751-757.

[105] Nishizawa, K., Fujii, T., (2001). Isotope separations of potassium and rubidium in chemical exchange system with dicyclohexano-18-crown-6. *Journal of Radioanalytical and Nuclear Chemistry*, *249*(3), 569-571.

[106] Tokeshi, M., Minagawa, T., Uchiyama, K., Hibara, A., Sato, K., Hisamoto, H., & Kitamori, T. (2002). Continuous-flow chemical processing on a microchip by combining microunit operations and a multiphase flow network. *Analytical Chemistry*, *74*(7), 1565-1571.

[107] Hisamoto, H., Saito, T., Tokeshi, M., Hibara, A., & Kitamori, T. (2001). Fast and high conversion phase-transfer synthesis exploiting the liquid–liquid interface formed in a microchannel chip. *Chemical Communications*, (24), 2662-2663.

[108] Gross, J. H. (2006). *Mass spectrometry: a textbook*. Springer Science & Business Media.

[109] De Hoffmann, E., & Stroobant, V. (2007). *Mass spectrometry: principles and applications*. John Wiley & Sons.

[110] May, T. W., & Wiedmeyer, R. H. (1998). A table of polyatomic interferences in ICP-MS. *ATOMIC SPECTROSCOPY-NORWALK CONNECTICUT-*, *19*, 150-155.

[111] Ohno, T., Hirono, M., Kakuta, S., & Sakata, S. (2018). Determination of strontium 90 in environmental samples by triple quadrupole ICP-MS and its application to Fukushima soil samples. *Journal of Analytical Atomic Spectrometry*, *33*(6), 1081-1085.

[112] Tanner, S. D., Baranov, V. I., & Bandura, D. R. (2002). Reaction cells and collision cells for ICP-MS: a tutorial review. *Spectrochimica Acta Part B: Atomic Spectroscopy*, *57*(9), 1361-1452.

[113] Amr, M. A. (2012). The collision/reaction cell and its application in inductively coupled plasma mass spectrometry for the determination of radioisotopes: A literature review. *Adv. Appl. Sci. Res*, *3*(4), 2179-2191.

[114] Okada, S., & Momoshima, N. (1993). Overview of tritium: characteristics, sources, and problems. *Health physics*, *65*(6), 595-609.

[115] Tadros, C. V., Hughes, C. E., Crawford, J., Hollins, S. E., & Chisari, R. (2014). Tritium in Australian precipitation: A 50 year record. *Journal of hydrology*, *513*, 262-273.

[116] Gonfiantini, R. (1978). Standards for stable isotope measurements in natural compounds. *Nature*, *271*(5645), 534-536.

[117] Matsumoto, T., Maruoka, T., Shimoda, G., Obata, H., Kagi, H., Suzuki, K., ... & Aggarwal, P. (2013). Tritium in Japanese precipitation following the March 2011 Fukushima Daiichi nuclear plant accident. *Science of the total environment*, *445*, 365-370.

[118] Muranaka, T., & Shima, N. (2012). Electrolytic enrichment of tritium in water using SPE film. *Edited by Janis Kleperis and Vladimir Linkov*, 141.

[119] Saito, M., Takata, S., Nishiki, Y., Shimizu, H., & Hayashi, T. (1996). Tritium enrichment by electrolysis using solid polymer electrolyte. *Radioisotopes (Tokyo)*, *45*(5), 285-292.

[120] Wieser, M. E., Buhl, D., Bouman, C., & Schwieters, J. (2004). High precision calcium isotope ratio measurements using a magnetic sector multiple collector inductively coupled plasma mass spectrometer. *Journal of Analytical Atomic Spectrometry*, *19*(7), 844-851.

[121] Atomic Absorption Spectroscopy (AAS) Retrieved from http://www.zoefact.com/science/chemistry/atomic-absorption-spectroscopy-aas.html

[122] Instruction manuals, AA-6800 series, Shimadzu

[123] Operation manuals, Dionex Aquion Ion Chromatography System, Thermo Scientific

[124] Andrén, H., Rodushkin, I., Stenberg, A., Malinovsky, D., & Baxter, D. C. (2004). Sources of mass bias and isotope ratio variation in multi-collector ICP-MS: optimization of instrumental parameters based on experimental observations. *Journal of Analytical Atomic Spectrometry*, *19*(9), 1217-1224.

[125] Mason, T. F., Weiss, D. J., Horstwood, M., Parrish, R. R., Russell, S. S., Mullane, E., & Coles, B. J. (2004). High-precision Cu and Zn isotope analysis by plasma source mass spectrometry Part 2. Correcting for mass discrimination effects. *Journal of Analytical Atomic Spectrometry*, *19*(2), 218-226.

[126] Ingle, C. P., Sharp, B. L., Horstwood, M. S., Parrish, R. R., & Lewis, D. J. (2003). Instrument response functions, mass bias and matrix effects in isotope ratio measurements and semi-quantitative analysis by single and multi-collector ICP-MS. *Journal of Analytical Atomic Spectrometry*, *18*(3), 219-229.

[127] Kishi, Y., Kawabata, K., Shi, H., & Thomas, R. (2004). Reduction of carbon-based interferences in organic compound analysis by dynamic reaction cell ICP MS. *SPECTROSCOPY-SPRINGFIELD THEN EUGENE THEN DULUTH-*, *19*, 14-23.

[128] Ogata, Y., Sakuma, Y., Ohtani, N., & Kotaka, M. (2004). Characteristics analysis of electrolytic tritium separation using solid polymer electrolyte (*No. KEK-PROC--2004*-8)

Appendix

1. The preparation of NIST standard reference material (SRM915b), calcium and lithium feed solution

   1.1. SRM915b (NIST standard ($CaCO_3$) in 0.1 M HNO_3)

   Prepare 0.1M HNO_3 solution from 68% HNO_3 (ρ = 1.41 g/mL)

$$M = \frac{\frac{0.68 \times 1.41\ (g)}{63.01\ \left(\frac{g}{mol}\right)}}{1 \times 10^{-3}\ L} = 15.2\ M$$

   100 mL of 0.1 M HNO_3

$$V_1(mL) = \frac{0.1\ M \times 100\ mL}{15.2\ M} = 0.657\ mL$$

   - Put the water in a 100 mL volumetric flask.
   - Add 0.657 mL of 68% HNO3
   - Adjust the volume by adding water to 100 mL

   Prepare NIST standard ($CaCO_3$) in 0.1 M HNO_3

   Calcium: Target concentration: 1000 ppm, Volume = 100 mL

$$HNO_3\ (aq) \rightarrow\ H^+ + NO_3^-$$

$$CaCO_3\ (s) \rightarrow\ Ca^{2+} + CO_3^{2-}$$

$$1000\ \left(\frac{mg}{L}\right) of\ Ca\ = \frac{1000\ \left(\frac{mg}{L}\right)}{40.078\ \left(\frac{g}{mol}\right)} \times \frac{1\ L}{1000\ mL}$$

$$100\ mL\ of\ 1000\ \left(\frac{mg}{L}\right) of\ Ca = \ 0.0250\ \left(\frac{mol}{L}\right) \times 100\ mL = 2.5\ mmol$$

$$2.5\ mmol\ of\ Ca = \ 2.5\ (mmol) \times 40.078\ \left(\frac{g}{mol}\right) = 100\ mg\ of\ Ca$$

$$mg\ of\ Ca\ in\ CaCO_3\ (s) = \frac{40.078\ \left(\frac{g}{mol}\right)}{100.0869\ \left(\frac{g}{mol}\right)} = 0.4$$

$$100\ mg\ of\ Ca\ in\ CaCO_3\ (s) = \frac{100\ mg}{0.4} = 250\ mg\ of\ CaCO_3\ (s)$$

- Dissolve 250 mg of CaCO3 (s) in 100 mL 0.1 M HNO_3

1.2. Calcium feed solution as reference material.

Prepare feed solution for 1000 ppm from $CaCl_2 \cdot 2H_2O$ (s) in 0.1 M HNO3 in 0.1 M HNO_3

Calcium: Target concentration: 1000 ppm, Volume = 100 mL

$$HNO_3\ (aq) \rightarrow\ H^+ + NO_3^-$$

$$CaCl_2\ (aq) \rightarrow\ Ca^{2+} + 2Cl^-$$

$$1000\ \left(\frac{mg}{L}\right) of\ Ca\ =\ \frac{1000\ \left(\frac{mg}{L}\right)}{40.078\ \left(\frac{g}{mol}\right)} \times \frac{1\ L}{1000\ mL}$$

$$100\ mL\ of\ 1000\ \left(\frac{mg}{L}\right) of\ Ca =\ 0.0250\ \left(\frac{mol}{L}\right) \times 100\ mL = 2.5\ mmol$$

$$2.5\ mmol\ of\ Ca =\ 2.5\ (mmol) \times 40.078\ \left(\frac{g}{mol}\right) = 100\ mg\ of\ Ca$$

$$mg\ of\ Ca\ in\ CaCl_2 \cdot 2H_2O = \frac{40.078\ \left(\frac{g}{mol}\right)}{147.01\ \left(\frac{g}{mol}\right)} = 0.2726$$

$$100\ mg\ of\ CaCl_2 \cdot 2H_2O = \frac{100\ mg}{0.2726} = 366\ mg\ of\ CaCl_2 \cdot 2H_2O$$

- Dissolve 366 mg of CaCl2·2H2O (s) in 100 mL 0.1 M HNO3

1.3. The feed solution of various concentrations ranged from 10% to 40% w/w $CaCl_2$ (aq) and LiCl (aq)

Calcium feed was prepared from $CaCl_2 \cdot 2H_2O$ (s)

%w/w (Solvent)	$CaCl_2 \cdot 2H_2O$ (g)	Solvent (mL)	Calculated Ca concentration(M)
10% $CaCl_2$ (aq)	6.11	40 mL H_2O	0.97
15% $CaCl_2$ (aq)	9.22	40 mL H_2O	1.52
20% $CaCl_2$ (aq)	14.42	40 mL H_2O	2.12
25% $CaCl_2$ (aq)	19.80	40 mL H_2O	2.75
30% $CaCl_2$ (aq)	26.37	40 mL H_2O	3.46
40% $CaCl_2$ (aq)	45.07	40 mL H_2O	4.97
10% $CaCl_2$ (12M HCl)	6.30	35 mL 12M HCl	1.09
20% $CaCl_2$ (12M HCl)	14.88	35 mL 12M HCl	2.30
30% $CaCl_2$ (12M HCl)	27.23	35 mL 12M HCl	3.65

Calculation

$$Ca\ (M) = \frac{\left(g\ of\ CaCl_2 \cdot\ 2H_2O \times \frac{40.078}{147.01}\right) g}{40.078\ g/mol} \times \frac{1000}{\frac{g}{\rho}\ (mL)}$$

where 40.078 and 147.01 are the Ca and $CaCl_2 \cdot 2H_2O$ (s) molecular weights. g and ρ represent the total solutions weight and density.

$$CaCl_2\ (\%\ w/w) = \frac{\left(g\ of\ CaCl_2 \cdot\ 2H_2O \times \frac{110.98}{147.01}\right) g}{(g\ of\ CaCl_2 \cdot\ 2H_2O + g\ of\ solvent)\ g} \times 100$$

Lithium feed was prepared from LiCl (s)

%w/w (Solvent)	LiCl (g)	Solvent (mL)	Calculated Li concentration(M)
10% LiCl (aq)	5	45 mL H_2O	2.77
15% LiCl (aq)	7.5	42.5 mL H_2O	4.16
20% LiCl (aq)	10	40 mL H_2O	5.54
30% LiCl (aq)	15	35 mL H_2O	8.32
30% LiCl (12M HCl)	15	29.66 mL 12M HCl	8.51
3% LiCl (12M HCl)	Diluted 1/10 from 30% LiCl (12M HCl)		0.85
0.3% LiCl (12M HCl)	Diluted 1/10 from 3% LiCl (12M HCl)		0.09

Calculation

$$Li\ (M) = \frac{\left(g\ of\ LiCl \times \frac{6.941}{42.394}\right) g}{6.941\ g/mol} \times \frac{1000}{\frac{g}{\rho}\ (mL)}$$

where 6.941 and 42.394 are the Li and LiCl (s) molecular weights. g and ρ represent the total solutions weight and density.

$$LiCl\ (\%\ w/w) = \frac{\left(g\ of\ LiCl \times \frac{6.941}{42.394}\right) g}{(g\ of\ LiCl + g\ of\ solvent)\ g} \times 100$$

2. The preparation of crown-ether organic solution

The crown-ether dissolved in the organic solution was prepared at the final volume of 200 mL.

<u>0.07M DC18C6 in organic solvent (chloroform: $CHCl_3$)</u>

$$DC18C6\ (M) = \frac{g\ or\ crown-ether\ (g)}{MW\ \left(\frac{g}{mol}\right)} \times \frac{1000}{200\ mL}$$

$$DC18C6\ (M) = \frac{5.2\ (g)}{372.5\ \left(\frac{g}{mol}\right)} \times \frac{1000}{200\ mL} = \ 0.07\ M$$

- Dissolve 5.2 g of DC18C6 in chloroform
- Adjust the volume to 200 mL by using a volumetric flask

<u>0.07M 18C6 in organic solvent (chloroform: $CHCl_3$)</u>

$$18C6\ (M) = \frac{g\ or\ crown-ether\ (g)}{MW\ \left(\frac{g}{mol}\right)} \times \frac{1000}{200\ mL}$$

$$18C6\ (M) = \frac{3.74\ (g)}{264.112\ \left(\frac{g}{mol}\right)} \times \frac{1000}{200\ mL} = \ 0.07\ M$$

- Dissolve 3.74 g of 18C6 in chloroform
- Adjust the volume to 200 mL by using a volumetric flask

3. Preparation of ICP-MS sample

0.15 mL of 68% HNO_3 was added to all of the sample before the measurement.

$$g\ of\ 68\%\ HNO_3 = 0.15\ mL \times 1.51 \frac{g}{ml} = 0.2265$$

$$g\ of\ HNO_3 = 0.2265 \times 0.68 = 0.154\ g$$

$$g\ of\ HNO_3 = 0.2265 \times 0.68 = 0.154\ g$$

$$\%w/w\ HNO_3 in\ 10\ g\ of\ sample = \frac{0.154\ g}{(10 + 0.154)} \times 100 = 1.5\%$$

5% HNO_3 (aq) was used to eliminate the memory effect during the measurement.

Preparation 100 mL of 5% HNO_3 from 68% HNO_3

$$5\ g\ of\ HNO_3 = \frac{5}{0.68} = 7.35\ g$$

$$100mL\ of\ 5\%\ HNO_3(aq) = \frac{5}{7.35 + (100 - 7.35)} \times 100 = 5\%$$

- Take 7.35 g of 68% HNO_3 to 92.65 mL of H_2O

4. Preparation of eluent for ion chromatography

Anion: 4.5mM Solium Carbonate solution and 0.5mM Sodium Hydrogen carbonate solution

- Mix 4.5 mL of 1M Solium Carbonate solution and 0.5mL of 1M Sodium Hydrogen carbonate solution in 1L volumetric flask
- Adjust the volume by adding water to 1L

Cation: 30mM Methanesulfonic Acid solution

- Mix 15 mL of 2M Methanesulfonic Acid solution in 1L volumetric flask
- Adjust the volume by adding water to 1L

5. Experimental details

5.1. Presence and absence of DC18C6 crown-ether

Target	DC18C6	Crown-ether			Feed (30% w/w)			Aq			Org (BE)		
	Crown-ether	M	mL	mmol	M	mL	mmol	M	mL	mmol	M	mL	mmol
Ca	○	0.07	187	13.1	3.29±0.04	18.7	61.5	3.15±0.05	18.4	57.8	0.06±0.00	18.4	1.2
	×	0	188	0	3.36±0.03	18.8	63.9	3.39±0.01	18.5	63.0	0.00±0.00	18.5	0.0
Li	○	0.07	133	9.3	8.41±0.02	13.3	111.9	8.07±0.02	13.1	106.0	0.24±0.00	12.8	3.0
	×	0	193	0	8.41±0.02	19.3	162.3	8.41±0.02	19.0	158.7	0.00±0.00	18.9	0.0

5.2. Extraction time

Target	Time	Crown-ether			Feed (30% w/w)			Aq			Org (BE)		
		M	mL	mmol	M	mL	mmol	M	mL	mmol	M	mL	mmol
Ca	1 sec	0.07	129	9.0	3.44±0.02	12.9	44.3	3.42±0.01	12.84	43.9	0.02±0.00	12.5	0.3
	1 min	0.07	126	8.8	3.44±0.02	12.6	43.3	3.38±0.04	12.34	41.7	0.07±0.00	12.3	0.8
	10 mins	0.07	123	8.6	3.44±0.02	12.3	42.3	3.33±0.03	11.95	39.7	0.06±0.00	11.9	0.8
	30 mins	0.07	119	8.3	3.44±0.02	11.9	40.9	3.15±0.01	11.53	36.3	0.06±0.00	11.4	0.7
	60 mins	0.07	115	8.0	3.44±0.02	11.5	39.5	3.37±0.02	11.25	37.9	0.06±0.00	11.0	0.7
Li	1 sec	0.07	170	11.9	8.61±0.02	17.0	146.4	8.50±0.01	16.30	138.6	0.10±0.00	16.6	1.6
	1 min	0.07	165	11.5	8.61±0.02	16.5	142.1	8.48±0.06	16.45	139.5	0.22±0.00	16.2	3.6
	10 mins	0.07	160	11.2	8.61±0.02	16.0	137.8	8.25±0.02	15.92	131.4	0.22±0.00	15.8	3.5
	30 mins	0.07	182	12.7	8.65±0.02	18.2	157.4	8.13±0.04	18.36	149.3	0.24±0.00	18.3	4.4
	60 mins	0.07	176	12.3	8.65±0.03	17.6	152.2	8.15±0.03	17.50	142.7	0.23±0.00	17.4	4.0

Extraction time (cont.)

Target	Time	$^{48}Ca/^{40}Ca$		$^{48}Ca/^{42}Ca$		$^{48}Ca/^{43}Ca$		$^{48}Ca/^{44}Ca$	
		α_{aq}	α_{org}	α_{aq}	α_{org}	α_{aq}	α_{org}	α_{aq}	α_{org}
Ca	1 sec	0.995±0.003	0.987±0.003	0.995±0.005	0.991±0.004	0.998±0.004	0.992±0.003	0.997±0.004	0.995±0.003
	1 min	0.998±0.003	0.990±0.003	1.000±0.004	0.995±0.005	0.998±0.003	0.994±0.004	0.999±0.003	0.996±0.005
	10 mins	1.003±0.003	0.993±0.003	0.994±0.005	0.995±0.004	0.996±0.003	0.993±0.004	0.997±0.003	0.995±0.003
	30 mins	0.998±0.003	0.987±0.003	0.999±0.004	0.993±0.003	0.998±0.004	0.992±0.003	0.999±0.002	0.994±0.002
	60 mins	0.993±0.004	0.985±0.004	0.998±0.005	0.993±0.005	0.999±0.003	0.993±0.004	0.996±0.002	0.994±0.003

Target	Time	$^{7}Li/^{6}Li$	
		α_{aq}	α_{org}
Li	1 sec	0.997±0.004	0.989±0.004
	1 min	1.001±0.004	0.989±0.004
	10 mins	0.999±0.005	0.991±0.005
	30 mins	1.000±0.005	0.991±0.005
	60 mins	1.004±0.004	0.993±0.005

5.3. Aqueous phase concentration and HCl solvent system

Target	%w/w	Solvent	Crown-ether			Feed			Aq			Org (BE)		
			M	mL	mmol	M	mL	mmol	M	mL	mmol	M	mL	mmol
Ca	10	Aq	0.07	200	14.0	0.98±0.01	20.0	19.6	0.96±0.00	20.0	19.3	0.00±0.00	20.5	0.0
	15		0.07	196	13.7	1.26±0.00	19.6	24.7	1.23±0.01	18.2	22.3	0.00±0.00	19.5	0.0
	20		0.07	192	13.4	1.89±0.02	19.2	36.3	1.85±0.02	19.0	35.1	0.00±0.00	19.0	0.0
	25		0.07	132	9.2	2.67±0.03	13.2	35.2	2.59±0.02	13.2	34.1	0.01±0.00	12.9	0.1
	30		0.07	187	13.1	3.29±0.04	18.7	61.5	3.15±0.05	18.4	57.8	0.06±0.00	18.4	1.2
	40		0.07	180	12.6	4.77±0.02	18.0	85.8	4.14±0.01	17.2	71.4	0.61±0.00	18.4	11.3
	10	Aq +	0.07	200	14.0	1.14±0.01	20.0	22.9	0.76±0.01	24.0	18.3	0.14±0.00	20.1	2.9
	20	12M	0.07	190	13.3	2.51±0.01	19.0	47.6	2.26±0.01	18.5	41.9	0.17±0.00	19.2	3.3
	30	HCl	0.07	186	13.0	3.87±0.02	18.6	71.9	3.44±0.03	17.8	61.2	0.19±0.00	18.5	3.5
Li	10	Aq	0.07	153	10.7	2.70±0.01	15.3	41.3	2.75±0.01	14.9	40.9	0.00±0.00	14.9	0.0
	15		0.07	149	10.4	4.11±0.01	14.9	61.3	4.11±0.00	14.7	60.4	0.01±0.00	14.3	0.1
	20		0.07	144	10.1	5.23±0.02	14.4	75.3	5.05±0.03	14.2	71.7	0.02±0.00	13.7	0.3
	30		0.07	133	9.3	8.41±0.02	13.3	111.9	8.07±0.02	13.1	106.0	0.24±0.00	12.8	3.0
	0.3	Aq +	0.07	145	10.1	0.09±0.00	14.5	1.3	0.09±0.00	13.9	1.3	0.00±0.00	15.0	0.0
	3	12M	0.07	140	9.8	0.95±0.00	14.0	13.3	0.99±0.01	13.3	13.2	0.01±0.00	14.3	0.1
	30	HCl	0.07	134	9.4	10.55±0.04	13.4	141.4	10.67±0.01	12.6	134.9	0.10±0.00	13.7	1.3

Aqueous phase concentration and HCl solvent system (cont.)

Target	%w/w	Solvent	$^{48}Ca/^{40}Ca$		$^{48}Ca/^{42}Ca$		$^{48}Ca/^{43}Ca$		$^{48}Ca/^{44}Ca$	
			α_{aq}	α_{org}	α_{aq}	α_{org}	α_{aq}	α_{org}	α_{aq}	α_{org}
Ca	25	Aq	0.999±0.04	0.989±0.04	0.998±0.05	0.993±0.05	1.000±0.03	0.990±0.04	0.998±0.04	0.993±0.04
	30		1.001±0.04	0.991±0.02	1.001±0.05	0.992±0.03	1.002±0.04	0.994±0.03	1.002±0.03	0.996±0.04
	40		1.000±0.03	0.989±0.04	1.001±0.04	0.993±0.05	1.001±0.02	0.995±0.03	1.001±0.03	0.996±0.04
	10	Aq + 12M	1.001±0.04	0.993±0.03	1.001±0.05	0.995±0.06	1.002±0.04	0.995±0.04	1.001±0.04	0.997±0.03
	20	HCl	1.000±0.03	0.991±0.04	1.000±0.05	0.993±0.04	1.001±0.06	0.995±0.05	0.999±0.05	0.995±0.05
	30		0.999±0.03	0.991±0.04	1.000±0.04	0.995±0.05	1.000±0.03	0.996±0.04	1.001±0.03	0.996±0.03

Target	%w/w	Solvent	$^{7}Li/^{6}Li$	
			α_{aq}	α_{aq}
Li	10	Aq	1.001±0.05	0.991±0.04
	15		1.003±0.05	0.990±0.03
	20		0.999±0.04	0.988±0.03
	30		0.999±0.04	0.991±0.03
	0.3	Aq + 12M	1.000±0.04	0.996±0.05
	3	HCl	0.998±0.06	0.994±0.06
	30		0.998±0.04	0.990±0.04

Comparison measurement of AAS and IC

Ca sample	AAS (M)	IC (M)
1	0.03	0.03
2	0.03	0.02
3	0.01	0.01
4	0.34	0.31
5	0.26	0.21
6	0.08	0.07
7	3.28	3.15
8	3.11	2.53
9	0.53	0.46
10	3.57	3.32
11	3.46	3.12
12	0.00	0.00
13	1.89	1.83
14	1.85	1.84
15	0.00	0.00
16	2.43	2.57
17	2.44	2.42
18	0.00	0.00
19	3.36	3.17
20	3.43	3.17
21	0.07	0.06
CC	0.996	

Li sample	AAS (M)	IC (M)
1	0.1	0.1
2	0.1	0.1
3	0.0	0.0
4	1.0	1.0
5	1.0	1.0
6	0.0	0.0
7	10.5	11.2
8	10.7	10.0
9	0.1	0.1
10	10.8	11.3
11	10.4	10.8
12	0.0	0.0
13	2.7	2.7
14	2.7	2.6
15	0.0	0.0
16	4.1	4.1
17	4.1	4.0
18	0.0	0.0
19	5.2	5.4
20	5.0	5.2
21	0.0	0.0
22	8.4	8.4
23	8.1	7.7
24	0.2	0.2
CC	0.998	

5.4. Filter separation LLE on various aqueous phase concentration

Target	%w/w	Solvent	Crown-ether			Feed			Aq			Org (BE)		
			M	mL	mmol	M	mL	mmol	M	mL	mmol	M	mL	mmol
Ca	10	Aq	0.07	100	7.0	1.02±0.00	10	10.2	0.99±0.00	9.9	9.8	0.00±0.00	10.1	0.0
	15		0.07	100	7.0	1.56±0.00	10	15.6	1.55±0.02	9.9	15.3	0.00±0.00	10.0	0.0
	20		0.07	100	7.0	2.18±0.00	10	21.8	2.08±0.01	9.7	20.1	0.00±0.00	9.9	0.0
	25		0.07	100	7.0	2.78±0.02	10	27.8	2.81±0.01	9.5	26.8	0.00±0.00	9.9	0.0
	30		0.07	100	7.0	3.54±0.01	10	35.4	3.41±0.01	9.4	32.2	0.05±0.00	10.0	0.5
	40		0.07	100	7.0	5.09±0.03	10	50.9	4.37±0.04	9.0	39.5	0.62±0.01	10.2	6.3

Target	%w/w	Solvent	$^{48}Ca/^{40}Ca$		$^{48}Ca/^{42}Ca$		$^{48}Ca/^{43}Ca$		$^{48}Ca/^{44}Ca$	
			α_{aq}	α_{org}	α_{aq}	α_{org}	α_{aq}	α_{org}	α_{aq}	α_{org}
Ca	30	Aq	0.998±0.002	0.990±0.002	0.999±0.005	0.995±0.005	0.999±0.003	0.993±0.002	0.999±0.004	0.996±0.003
	40		0.999±0.003	0.990±0.003	1.001±0.003	0.995±0.003	0.999±0.003	0.995±0.003	1.001±0.004	0.997±0.003

5.5. Volume ratio extraction system (Filter LLE)

Target	Volume Ratio (Org/Aq)	Crown-ether			Feed			CE/Ca Feed	Aq			Org (BE)		
		M	mL	mmol	M	mL	mmol		M	mL	mmol	M	mL	mmol
Ca	200/1	0.07	200	14.0	3.56 ±0.02	1	3.56	3.92	3.36 ±0.01	0.8	2.5	0.05 ±0.00	10.0	0.5
	100/1	0.07	100	7.0	3.56 ±0.02	1	3.56	1.96	3.14 ±0.03	1.0	3.0	0.02 ±0.00	10.0	0.2
	10/1	0.07	10	7.0	3.56 ±0.02	1	3.56	0.20	3.43 ±0.03	1.0	3.3	0.01 ±0.00	8.9	0.0

Volume ratio extraction system (Filter LLE) (cont.)

Target	Volume Ratio (Org/Aq)	$^{48}Ca/^{40}Ca$		$^{48}Ca/^{42}Ca$		$^{48}Ca/^{43}Ca$		$^{48}Ca/^{44}Ca$	
		α_{aq}	α_{org}	α_{aq}	α_{org}	α_{aq}	α_{org}	α_{aq}	α_{org}
Ca	200/1	0.998±0.003	0.988±0.003	0.999±0.004	0.994±0.004	1.001±0.003	0.996±0.003	1.000±0.004	0.998±0.004
	100/1	1.001±0.003	0.989±0.003	1.001±0.005	0.992±0.005	1.001±0.004	0.995±0.004	1.001±0.002	0.995±0.003
	10/1	0.998±0.003	0.990±0.003	0.998±0.004	0.991±0.006	0.998±0.003	0.994±0.003	0.998±0.002	0.995±0.003

5.6. The calculated ^{48}Ca %abundance of calcium extraction on the various extracted ratio (K = 0.02, 0.2, 0.5)

Ca isotope	K	% Abundance vs. iteration stage of aqueous phase										
		Feed	1	2	3	4	5	6	7	8	9	10
^{40}Ca	0.02	0.96941	0.96941	0.96940	0.96940	0.96940	0.96939	0.96939	0.96939	0.96939	0.96938	0.96938
^{42}Ca		0.00647	0.00647	0.00647	0.00647	0.00647	0.00647	0.00647	0.00647	0.00647	0.00647	0.00647
^{43}Ca		0.00135	0.00135	0.00135	0.00135	0.00135	0.00135	0.00135	0.00135	0.00135	0.00135	0.00135
^{44}Ca		0.02086	0.02086	0.02086	0.02087	0.02087	0.02087	0.02087	0.02088	0.02088	0.02088	0.02088
^{46}Ca		0.00004	0.00004	0.00004	0.00004	0.00004	0.00004	0.00004	0.00004	0.00004	0.00004	0.00004
^{48}Ca		0.00187	0.00187	0.00187	0.00187	0.00187	0.00187	0.00187	0.00187	0.00187	0.00187	0.00187
^{40}Ca	0.20	0.96941	0.96938	0.96935	0.96932	0.96929	0.96926	0.96923	0.96920	0.96917	0.96914	0.96911
^{42}Ca		0.00647	0.00647	0.00648	0.00648	0.00648	0.00649	0.00649	0.00649	0.00650	0.00650	0.00650
^{43}Ca		0.00135	0.00135	0.00135	0.00135	0.00135	0.00136	0.00136	0.00136	0.00136	0.00136	0.00136
^{44}Ca		0.02086	0.02088	0.02090	0.02093	0.02095	0.02097	0.02099	0.02101	0.02103	0.02106	0.02108
^{46}Ca		0.00004	0.00004	0.00004	0.00004	0.00004	0.00004	0.00004	0.00004	0.00004	0.00004	0.00004
^{48}Ca		0.00187	0.00187	0.00188	0.00188	0.00188	0.00189	0.00189	0.00190	0.00190	0.00190	0.00191
^{40}Ca	0.50	0.96941	0.96925	0.96911	0.96896	0.96881	0.96866	0.96851	0.96836	0.96821	0.96806	0.96790
^{42}Ca		0.00647	0.00649	0.00650	0.00652	0.00654	0.00656	0.00657	0.00659	0.00661	0.00662	0.00664
^{43}Ca		0.00135	0.00136	0.00136	0.00137	0.00137	0.00138	0.00138	0.00139	0.00139	0.00140	0.00140
^{44}Ca		0.02086	0.02097	0.02108	0.02119	0.02130	0.02140	0.02151	0.02162	0.02173	0.02184	0.02195
^{46}Ca		0.00004	0.00004	0.00004	0.00004	0.00004	0.00004	0.00004	0.00004	0.00004	0.00004	0.00004
^{48}Ca		0.00187	0.00189	0.00191	0.00192	0.00194	0.00196	0.00198	0.00200	0.00202	0.00204	0.00206

The calculated ^{48}Ca %abundance of calcium extraction on the various extracted ratio (K = 0.02, 0.2, 0.5) (count.)

Ca isotope	K	% Abundance vs. iteration stage of organic (BE) phase										
		Feed	1	2	3	4	5	6	7	8	9	10
^{40}Ca	0.02	-	0.96956	0.96956	0.96956	0.96955	0.96955	0.96955	0.96954	0.96954	0.96954	0.96954
^{42}Ca		-	0.00645	0.00645	0.00645	0.00645	0.00645	0.00645	0.00645	0.00645	0.00646	0.00646
^{43}Ca		-	0.00134	0.00134	0.00134	0.00134	0.00134	0.00135	0.00135	0.00135	0.00135	0.00135
^{44}Ca		-	0.02075	0.02075	0.02075	0.02076	0.02076	0.02076	0.02076	0.02076	0.02077	0.02077
^{46}Ca		-	0.00004	0.00004	0.00004	0.00004	0.00004	0.00004	0.00004	0.00004	0.00004	0.00004
^{48}Ca		-	0.00185	0.00185	0.00185	0.00185	0.00185	0.00185	0.00185	0.00185	0.00185	0.00185
^{40}Ca	0.20	-	0.96956	0.96953	0.96950	0.96947	0.96944	0.96941	0.96938	0.96935	0.96932	0.96929
^{42}Ca		-	0.00645	0.00646	0.00646	0.00646	0.00647	0.00647	0.00647	0.00648	0.00648	0.00648
^{43}Ca		-	0.00134	0.00135	0.00135	0.00135	0.00135	0.00135	0.00135	0.00135	0.00135	0.00135
^{44}Ca		-	0.02075	0.02077	0.02079	0.02081	0.02084	0.02086	0.02088	0.02090	0.02092	0.02094
^{46}Ca		-	0.00004	0.00004	0.00004	0.00004	0.00004	0.00004	0.00004	0.00004	0.00004	0.00004
^{48}Ca		-	0.00185	0.00186	0.00186	0.00186	0.00187	0.00187	0.00187	0.00188	0.00188	0.00188
^{40}Ca	0.50	-	0.96956	0.96941	0.96926	0.96911	0.96897	0.96882	0.96867	0.96852	0.96837	0.96822
^{42}Ca		-	0.00645	0.00647	0.00649	0.00650	0.00652	0.00654	0.00656	0.00657	0.00659	0.00661
^{43}Ca		-	0.00134	0.00135	0.00136	0.00136	0.00137	0.00137	0.00138	0.00138	0.00139	0.00139
^{44}Ca		-	0.02075	0.02086	0.02097	0.02108	0.02118	0.02129	0.02140	0.02151	0.02162	0.02173
^{46}Ca		-	0.00004	0.00004	0.00004	0.00004	0.00004	0.00004	0.00004	0.00004	0.00004	0.00004
^{48}Ca		-	0.00185	0.00187	0.00189	0.00191	0.00192	0.00194	0.00196	0.00198	0.00200	0.00202

The calculated ^{48}Ca %abundance of calcium extraction on the various extracted ratio (K = 0.02, 0.2, 0.5) (count.)

Ca isotope	K	Separation factor (α_{aq}) vs. iteration stage of aqueous phase										
		Feed	1	2	3	4	5	6	7	8	9	10
$^{48}Ca/^{40}Ca$	0.02	1.000	1.000	1.000	1.001	1.001	1.001	1.001	1.001	1.002	1.002	1.002
$^{48}Ca/^{42}Ca$		1.000	1.000	1.000	1.000	1.001	1.001	1.001	1.001	1.001	1.001	1.001
$^{48}Ca/^{43}Ca$		1.000	1.000	1.000	1.000	1.000	1.001	1.001	1.001	1.001	1.001	1.001
$^{48}Ca/^{44}Ca$		1.000	1.000	1.000	1.000	1.000	1.000	1.001	1.001	1.001	1.001	1.001
$^{48}Ca/^{46}Ca$		1.000	1.000	1.000	1.000	1.000	1.000	1.000	1.000	1.000	1.000	1.000
$^{48}Ca/^{40}Ca$	0.20	1.000	1.002	1.004	1.006	1.008	1.010	1.012	1.014	1.016	1.018	1.020
$^{48}Ca/^{42}Ca$		1.000	1.001	1.003	1.004	1.006	1.007	1.008	1.010	1.011	1.013	1.014
$^{48}Ca/^{43}Ca$		1.000	1.001	1.002	1.003	1.005	1.006	1.007	1.008	1.009	1.010	1.011
$^{48}Ca/^{44}Ca$		1.000	1.001	1.002	1.003	1.004	1.004	1.005	1.006	1.007	1.008	1.009
$^{48}Ca/^{46}Ca$		1.000	1.000	1.001	1.001	1.002	1.002	1.003	1.003	1.003	1.004	1.004
$^{48}Ca/^{40}Ca$	0.50	1.000	1.010	1.020	1.030	1.040	1.049	1.060	1.070	1.080	1.090	1.101
$^{48}Ca/^{42}Ca$		1.000	1.007	1.014	1.021	1.028	1.035	1.042	1.049	1.056	1.063	1.071
$^{48}Ca/^{43}Ca$		1.000	1.006	1.011	1.017	1.023	1.028	1.034	1.040	1.045	1.051	1.057
$^{48}Ca/^{44}Ca$		1.000	1.005	1.009	1.013	1.018	1.022	1.026	1.031	1.035	1.040	1.044
$^{48}Ca/^{46}Ca$		1.000	1.002	1.004	1.006	1.008	1.010	1.013	1.015	1.017	1.019	1.021

The calculated ^{48}Ca %abundance of calcium extraction on the various extracted ratio (K = 0.02, 0.2, 0.5) (count.)

Ca isotope	K	Separation factor (α_{org}) vs. iteration stage of organic (BE) phase										
		Feed	1	2	3	4	5	6	7	8	9	10
$^{48}Ca/^{40}Ca$	0.02		0.990	0.990	0.990	0.991	0.991	0.991	0.991	0.991	0.992	0.992
$^{48}Ca/^{42}Ca$			0.993	0.993	0.993	0.993	0.993	0.994	0.994	0.994	0.994	0.994
$^{48}Ca/^{43}Ca$			0.994	0.994	0.994	0.995	0.995	0.995	0.995	0.995	0.995	0.995
$^{48}Ca/^{44}Ca$			0.995	0.996	0.996	0.996	0.996	0.996	0.996	0.996	0.996	0.996
$^{48}Ca/^{46}Ca$			0.998	0.998	0.998	0.998	0.998	0.998	0.998	0.998	0.998	0.998
$^{48}Ca/^{40}Ca$	0.20		0.990	0.992	0.994	0.996	0.998	1.000	1.002	1.004	1.006	1.008
$^{48}Ca/^{42}Ca$			0.993	0.994	0.996	0.997	0.998	1.000	1.001	1.003	1.004	1.005
$^{48}Ca/^{43}Ca$			0.994	0.995	0.996	0.998	0.999	1.000	1.001	1.002	1.003	1.004
$^{48}Ca/^{44}Ca$			0.995	0.996	0.997	0.998	0.999	1.000	1.001	1.002	1.003	1.003
$^{48}Ca/^{46}Ca$			0.998	0.998	0.999	0.999	1.000	1.000	1.000	1.001	1.001	1.002
$^{48}Ca/^{40}Ca$	0.50		0.990	1.000	1.010	1.019	1.029	1.039	1.049	1.059	1.069	1.079
$^{48}Ca/^{42}Ca$			0.993	1.000	1.007	1.014	1.021	1.028	1.035	1.042	1.049	1.056
$^{48}Ca/^{43}Ca$			0.994	1.000	1.006	1.011	1.017	1.022	1.028	1.034	1.039	1.045
$^{48}Ca/^{44}Ca$			0.995	1.000	1.004	1.009	1.013	1.017	1.022	1.026	1.031	1.035
$^{48}Ca/^{46}Ca$			0.998	1.000	1.002	1.004	1.006	1.008	1.010	1.012	1.014	1.017

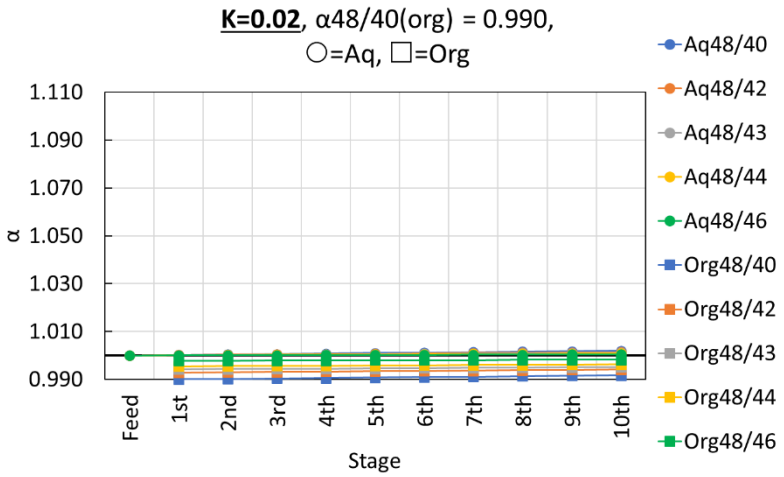
K=0.02, α48/40(org) = 0.990,
○=Aq, □=Org
1.110
1.090
1.070
1.050
1.030
1.010
0.990
α
Feed
1st
2nd
3rd
4th
5th
6th
7th
8th
9th
10th
Stage
Aq48/40
Aq48/42
Aq48/43
Aq48/44
Aq48/46
Org48/40
Org48/42
Org48/43
Org48/44
Org48/46

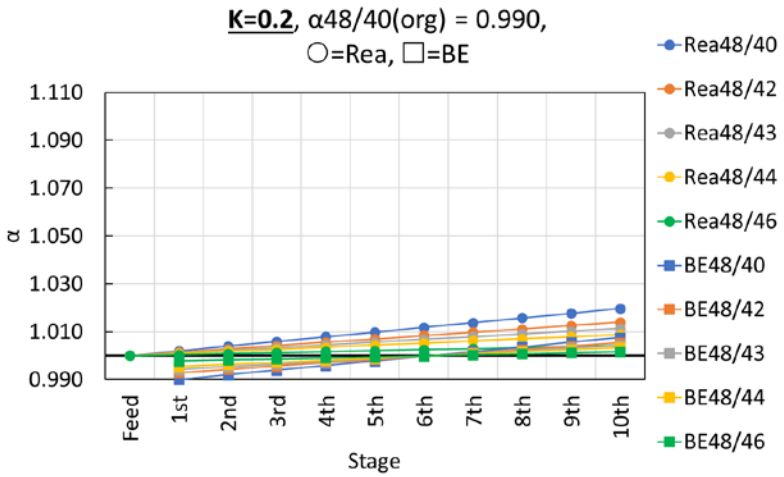
K=0.2, α48/40(org) = 0.990,
○=Rea, □=BE
1.110
1.090
1.070
1.050
1.030
1.010
0.990
α
Feed
1st
2nd
3rd
4th
5th
6th
7th
8th
9th
10th
Stage
Rea48/40
Rea48/42
Rea48/43
Rea48/44
Rea48/46
BE48/40
BE48/42
BE48/43
BE48/44
BE48/46

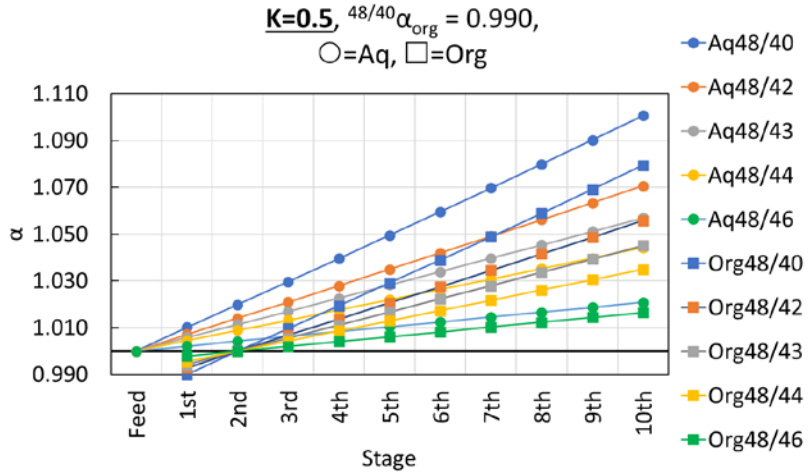
K=0.5, 48/40αorg = 0.990,
○=Aq, □=Org
1.110
1.090
1.070
1.050
1.030
1.010
0.990
α
Feed
1st
2nd
3rd
4th
5th
6th
7th
8th
9th
10th
Stage
Aq48/40
Aq48/42
Aq48/43
Aq48/44
Aq48/46
Org48/40
Org48/42
Org48/43
Org48/44
Org48/46

5.7. Extraction temperature

Target	Temp.	Crown-ether			Feed (30% w/w)			Aq			Org (BE)		
		M	mL	mmol	M	mL	mmol	M	mL	mmol	M	mL	mmol
Ca	-15	0.070	100	7.0	3.60±0.01	10	36.0	3.32±0.01	9.37	31.1	0.11±0.00	9.7	1.1
	0	0.070	100	7.0	3.60±0.01	10	36.0	3.29±0.09	9.55	31.4	0.10±0.00	10.1	1.0
	RT (22)	0.070	100	7.0	3.68±0.02	10	36.8	3.43±0.03	9.84	33.8	0.08±0.00	10.2	0.8
	45	0.070	100	7.0	3.60±0.01	10	36.0	3.15±0.01	9.30	29.3	0.05±0.00	9.9	0.5
Li	-15	0.070	170	11.9	7.87±0.01	17.0	133.7	6.75±0.02	15.6	105.6	0.48±0.00	16.9	8.1
	0	0.070	194	13.5	7.99±0.01	19.4	155.1	7.30±0.02	18.7	136.6	0.33±0.00	19.2	6.3
	RT (22)	0.070	133	9.3	8.41±0.02	13.3	111.9	8.07±0.02	13.1	106.0	0.24±0.00	12.8	3.0
	45	0.070	176	12.3	7.87±0.01	17.6	138.4	7.45±0.03	17.2	128.0	0.11±0.00	17.4	1.9

Target	Temp.	$^{48}Ca/^{40}Ca$		$^{48}Ca/^{42}Ca$		$^{48}Ca/^{43}Ca$		$^{48}Ca/^{44}Ca$	
		α_{aq}	α_{org}	α_{aq}	α_{org}	α_{aq}	α_{org}	α_{aq}	α_{org}
Ca	-15	0.999±0.003	0.987±0.003	1.001±0.005	0.992±0.004	1.000±0.004	0.992±0.003	1.000±0.003	0.994±0.003
	0	0.998±0.003	0.989±0.005	0.999±0.005	0.993±0.006	0.999±0.004	0.992±0.004	1.001±0.003	0.997±0.003
	RT (22)	0.999±0.003	0.990±0.003	1.000±0.007	0.992±0.004	1.000±0.004	0.992±0.004	1.000±0.003	0.993±0.003
	45	0.998±0.003	0.990±0.003	1.000±0.005	0.996±0.005	0.999±0.005	0.994±0.004	1.000±0.004	0.996±0.003

Target	Temp.	$^{7}Li/^{6}Li$	
		α_{aq}	α_{aq}
Li	-15	1.002±0.005	0.990±0.005
	0	1.002±0.005	0.994±0.004
	RT (22)	0.999±0.004	0.991±0.003
	45	1.004±0.005	0.994±0.005

5.8. Solid-liquid extraction

Sample	Solid-liquid extraction by DC18C6 crown-ether					Solid-liquid extraction by 18C6 crown-ether				
	M	mL	mmol	$^{43}Ca/^{48}Ca$ α_{aq}	$^{43}Ca/^{48}Ca$ α_{org}	M	mL	mmol	$^{43}Ca/^{48}Ca$ α_{aq}	$^{43}Ca/^{48}Ca$ α_{org}
Feed	-	-	13.6	-	-	-	-	13.6	-	-
S1	0.01	50	0.6	1.001	-	0.01	50	0.5	0.998	-
S2	0.01	50	0.6	1.000	-	0.01	50	0.5	1.000	-
S3	0.01	50	0.6	1.000	-	0.01	50	0.5	0.999	-
S4	0.01	50	0.5	1.000	-	0.01	50	0.5	1.000	-
S5	0.11	50	5.7	0.999	-	0.12	50	6.2	0.999	-
Org1	0.06	20	1.3	-	1.000	0.04	20	0.8	-	1.001
Org2	0.07	20	1.3	-	1.001	0.05	20	1.0	-	1.000
Org3	0.06	20	1.2	-	1.000	0.05	20	0.9	-	1.001
Org4	0.05	20	0.9	-	1.001	0.05	20	1.1	-	0.998
Org5	0.03	20	0.5	-	0.999	0.04	20	0.8	-	1.000

5.9. Multi-stage iteration (Filter separation with 2mL $CaCl_2$ (aq) (30%w/w) as a Feed)

Target	Iteration	Crown-ether			Feed (30% w/w)			Aq			Org (BE)		
		M	mL	mmol	M	mL	mmol	M	mL	mmol	M	mL	mmol
Ca	Feed	0.07	20	0.14	3.52±0.03	2.0	7.0	-	-	-	-	-	-
	1st	0.07	20	0.14	-	-	-	3.47±0.02	-	-	0.01±0.00	9.9	0.1
	2nd	0.07	20	0.14	-	-	-	3.14±0.03	-	-	0.01±0.00	8.6	0.1
	3rd	0.07	20	0.14	-	-	-	3.17±0.02	-	-	0.01±0.00	9.7	0.1
	4th	0.07	20	0.14	-	-	-	2.94±0.00	-	-	0.03±0.00	10.1	0.3

Target	Iteration	$^{48}Ca/^{40}Ca$ (est.)		$^{48}Ca/^{42}Ca$		$^{48}Ca/^{43}Ca$		$^{48}Ca/^{44}Ca$	
		α_{aq}	α_{org}	α_{aq}	α_{org}	α_{aq}	α_{org}	α_{aq}	α_{org}
Ca	1st	1.000	0.992	0.999±0.004	0.994±0.003	0.999±0.003	0.994±0.004	1.000±0.004	0.996±0.002
	2nd	1.003	0.990	1.002±0.005	0.992±0.004	1.001±0.004	0.993±0.004	1.000±0.004	0.995±0.003
	3rd	1.005	0.996	1.003±0.004	0.997±0.006	1.001±0.004	0.999±0.005	1.000±0.004	0.998±0.004
	4th	1.006	0.998	1.004±0.004	0.998±0.005	1.002±0.003	1.001±0.004	1.002±0.004	0.999±0.003

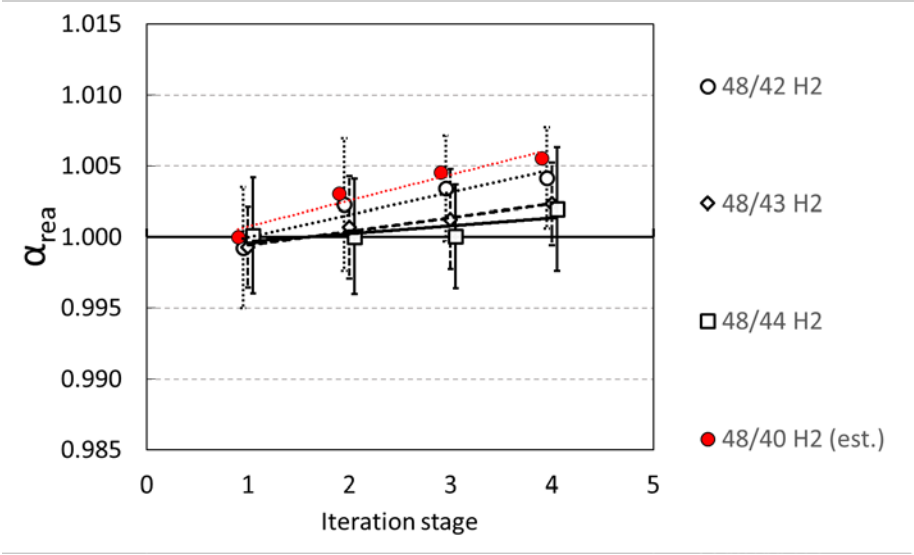

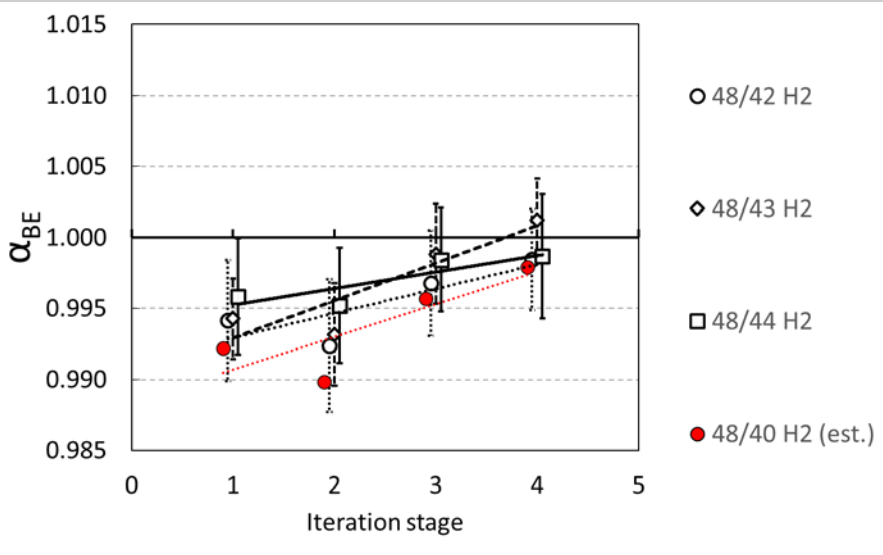

Multi-stage iteration (Batch separation with 5mL $CaCl_2$ (aq) (30%w/w) as a Feed)

Target	Iteration	Crown-ether			Feed (30% w/w)			Aq			Org (BE)		
		M	mL	mmol	M	mL	mmol	M	mL	mmol	M	mL	mmol
Ca	Feed	0.07	100	7.00	3.66±0.01	5.0	18.3	-	-	-	-	-	-
	1st	0.07	100	7.00	-	-	-	3.41±0.01	4.76	16.2	0.08±0.00	10.17	0.8
	2nd	0.07	100	7.00	-	-	-	3.28±0.02	4.63	15.2	0.04±0.00	10.28	0.4
	3rd	0.07	100	7.00	-	-	-	3.13±0.01	4.32	13.5	0.02±0.00	10.15	0.2
	4th	0.07	100	7.00	-	-	-	2.95±0.02	4.19	12.4	0.02±0.00	10.02	0.2
	5th	0.07	100	7.00	-	-	-	2.37±0.00	3.99	9.5	0.01±0.00	9.88	0.1
	6th	0.07	100	7.00	-	-	-	2.49±0.02	3.70	9.2	0.01±0.00	9.69	0.1

Target	Iteration	$^{48}Ca/^{40}Ca$ (est.)		$^{48}Ca/^{42}Ca$		$^{48}Ca/^{43}Ca$		$^{48}Ca/^{44}Ca$	
		α_{aq}	α_{org}	α_{aq}	α_{org}	α_{aq}	α_{org}	α_{aq}	α_{org}
Ca	1st	0.999±0.004	0.992±0.004	1.000±0.005	0.994±0.004	1.001±0.004	0.995±0.004	1.001±0.004	0.996±0.003
	2nd	1.001±0.004	0.994±0.005	0.998±0.004	0.997±0.006	1.002±0.004	0.995±0.004	1.000±0.004	0.995±0.003
	3rd	0.999±0.004	0.992±0.003	0.999±0.004	0.994±0.005	0.997±0.003	0.996±0.005	1.000±0.003	0.996±0.004
	4th	1.001±0.004	1.002±0.005	1.000±0.005	1.001±0.005	1.001±0.004	1.0030.005	1.001±0.004	1.004±0.004
	5th	1.001±0.004	1.000±0.003	0.999±0.003	1.000±0.006	0.999±0.004	0.999±0.005	0.996±0.004	1.000±0.004
	6th	1.004±0.004	1.000±0.004	1.004±0.004	0.999±0.006	1.001±0.005	0.999±0.004	0.999±0.004	1.002±0.004

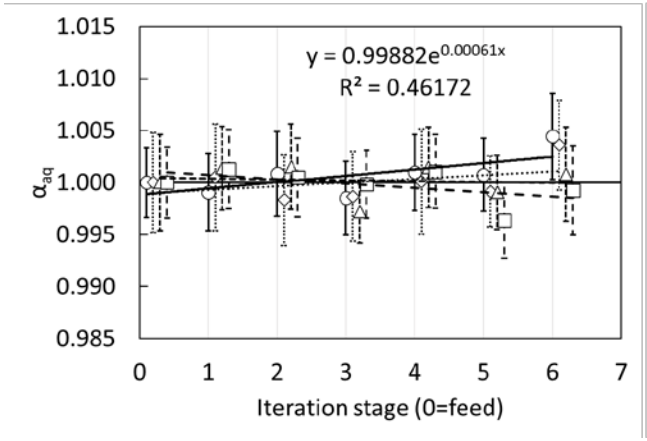

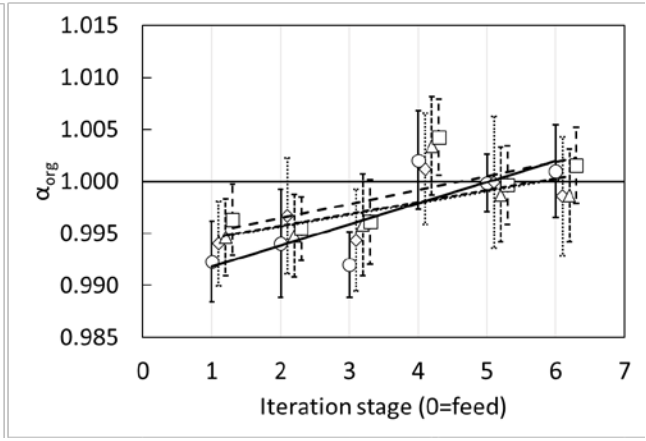

Multi-stage iteration (Batch separation with 5mL $CaCl_2$ (HCl) (30%w/w) as a Feed)

Target	Iteration	Crown-ether			Feed (30% w/w)			Aq			Org (BE)		
		M	mL	mmol	M	mL	mmol	M	mL	mmol	M	mL	mmol
Ca	Feed	0.07	100	7.00	4.27±0.02	5.0	21.3	-	-	-	-	-	-
	1st	0.07	100	7.00	-	-	-	3.08±0.01	4.65	14.3	0.49±0.00	10.63	5.2
	2nd	0.07	100	7.00	-	-	-	2.47±0.00	4.00	9.9	0.23±0.00	10.28	2.4
	3rd	0.07	100	7.00	-	-	-	2.29±0.02	3.62	8.3	0.19±0.00	10.25	1.9
	4th	0.07	100	7.00	-	-	-	2.13±0.01	3.41	7.2	0.05±0.00	10.08	0.6
	5th	0.07	100	7.00	-	-	-	2.01±0.02	3.22	6.5	0.02±0.00	9.95	0.2
	6th	0.07	100	7.00	-	-	-	1.87±0.05	2.91	5.5	0.01±0.00	9.97	0.1

Target	Iteration	$^{48}Ca/^{40}Ca$ (est.)		$^{48}Ca/^{42}Ca$		$^{48}Ca/^{43}Ca$		$^{48}Ca/^{44}Ca$	
		α_{aq}	α_{org}	α_{aq}	α_{org}	α_{aq}	α_{org}	α_{aq}	α_{org}
Ca	1st	1.002±0.003	0.995±0.003	1.001±0.007	0.995±0.005	1.001±0.005	0.998±0.004	1.002±0.003	0.996±0.003
	2nd	1.005±0.004	0.997±0.005	1.007±0.005	0.996±0.005	1.002±0.003	0.997±0.003	1.002±0.003	0.999±0.003
	3rd	1.004±0.004	0.995±0.004	1.003±0.008	1.000±0.006	1.001±0.004	0.996±0.003	1.000±0.004	0.996±0.004
	4th	1.006±0.003	0.998±0.004	1.003±0.005	0.994±0.005	1.001±0.005	0.998±0.004	1.004±0.005	0.998±0.004
	5th	1.006±0.004	1.006±0.003	1.004±0.006	1.003±0.007	1.005±0.006	1.004±0.005	1.005±0.005	1.004±0.004
	6th	1.007±0.004	1.002±0.004	1.005±0.006	1.004±0.004	1.006±0.003	1.001±0.003	1.005±0.004	1.001±0.003

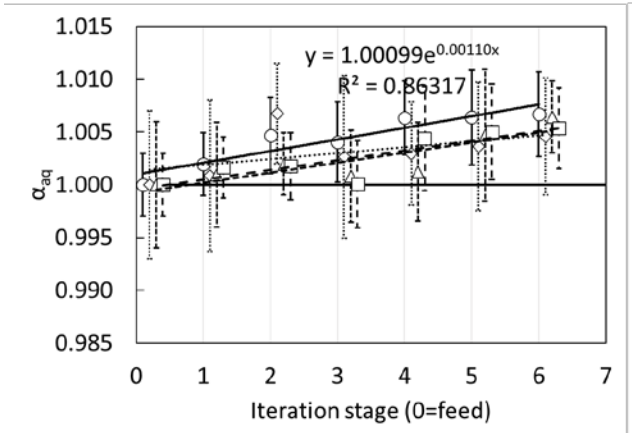

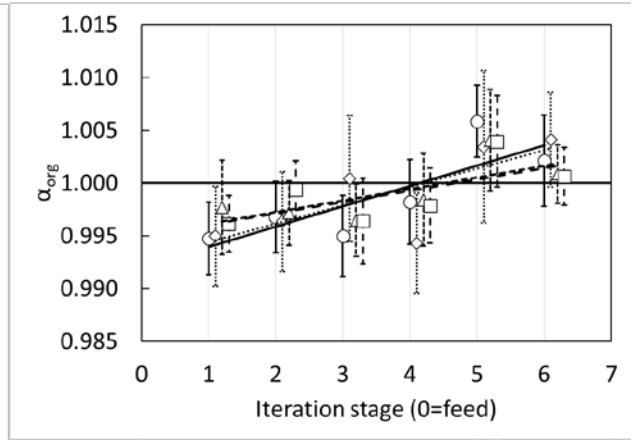

5.10. July 2020 Thailand's tap water tritium results (cycle 1)

Sample	Gross count	SD	%RSD	ESCR	V_f (mL)	V (mL)	%EFF	T_f (Bq/L)	V_i/V_f V_i = 500 mL	T_i (Bq/L)	Collected date	Measured date	Tritium concentration (Bq/L)	SD
BG	309.4	27.9	9.0	8.15	-	10.06	26.38	-				1-Nov-20		
HTO	4070.7	62.8	1.5	8.50	-	10.03	27.84	225				2-Nov-20	225	20.51
E-HTO	50525.9	213.5	0.4	8.19	11.89	10.02	26.54	3147	42.05	225		3-Nov-20	3147	283.67
TTW1	370.3	25.7	6.9	8.63	10.51	10.00	28.38	3.58	47.57	0.23	9-Jul-20	3-Nov-20	0.23	0.03
TTW2	356.2	18.1	5.1	8.56	12.54	10.04	28.07	2.77	39.87	0.21	9-Jul-20	4-Nov-20	0.21	0.02
TTW3	358.2	22.7	6.3	8.59	11.98	10.05	28.19	2.87	41.74	0.21	9-Jul-20	5-Nov-20	0.21	0.02
TTW4	340.4	12.4	3.6	8.60	11.74	9.98	28.24	1.83	42.59	0.13	9-Jul-20	5-Nov-20	0.13	0.01
TTW5	335.1	18.2	5.4	8.59	11.95	9.99	28.21	1.52	41.84	0.11	17-Jul-20	6-Nov-20	0.11	0.01
TTW6	381.8	18.1	4.7	8.69	11.87	9.99	28.60	4.22	42.12	0.30	17-Jul-20	7-Nov-20	0.31	0.03
TTW7	385.1	15.6	4.0	8.38	11.94	10.02	27.34	4.61	41.88	0.33	16-Jul-20	8-Nov-20	0.34	0.03
TTW8	381.6	25.3	6.6	8.38	10.48	10.02	27.35	4.39	47.71	0.28	9-Jul-20	8-Nov-20	0.28	0.03
TTW9	373.7	24.7	6.6	8.43	12.66	9.98	27.56	3.90	39.49	0.30	13-Jul-20	9-Nov-20	0.30	0.03
TTW10	387.0	14.3	3.7	8.47	14.29	9.99	27.73	4.67	34.99	0.40	13-Jul-20	10-Nov-20	0.41	0.04
TTW11	372.0	19.4	5.2	8.66	12.26	9.97	28.48	3.67	40.78	0.27	15-Jul-20	10-Nov-20	0.28	0.03
TTW12	362.5	20.5	5.7	8.53	12.43	9.96	27.96	3.18	40.23	0.24	15-Jul-20	11-Nov-20	0.24	0.03
TTW13	394.1	27.0	6.9	8.37	10.00	9.97	27.31	5.19	50.00	0.31	14-Jul-20	12-Nov-20	0.32	0.04
TTW14	357.1	26.4	7.4	8.60	10.34	9.98	28.25	2.82	48.36	0.17	17-Jul-20	13-Nov-20	0.18	0.02

July 2020 Thailand’s tap water tritium results (cycle 2)

Sample	Gross count	SD	%RSD	ESCR	V_f (mL)	V (mL)	%EFF	T_f (Bq/L)	V_i/V_f V_i = 500 mL	T_i (Bq/L)	Collected date	Measured date	Tritium concentration (Bq/L)	SD
BG	331.2	40.3	12.2	7.97	-	10.06	25.77	0				14-Nov-20		
HTO	4157.6	72.8	1.7	8.40	-	10.03	27.53	232		232	2-Nov-20	15-Nov-20	232	28.53
E-HTO	50535.0	208.3	0.4	8.10	11.89	10.02	26.26	3190	42.05	232	3-Nov-20	15-Nov-20	3190	388.59
TTW1	384.7	23.43	6.1	8.45	10.51	10.00	27.85	3.23	47.57	0.21	9-Jul-20	16-Nov-20	0.21	0.03
TTW2	368	13.61	3.7	8.38	12.54	10.04	27.50	2.24	39.87	0.17	9-Jul-20	17-Nov-20	0.17	0.02
TTW3	341.4	13.52	4.0	8.41	11.98	10.05	27.56	0.62	41.74	0.05	9-Jul-20	18-Nov-20	0.05	0.01
TTW4	339.8	17.93	5.3	8.41	11.74	9.98	27.65	0.52	42.59	0.04	9-Jul-20	18-Nov-20	0.04	0.01
TTW5	355.5	24.06	6.8	8.45	11.95	9.99	27.75	1.47	41.84	0.11	17-Jul-20	19-Nov-20	0.11	0.02
TTW6	379.1	25.64	6.8	8.58	11.87	9.99	28.35	2.84	42.12	0.21	17-Jul-20	20-Nov-20	0.21	0.03
TTW7	375.4	18.73	5.0	8.28	11.94	10.02	27.07	2.73	41.88	0.20	16-Jul-20	20-Nov-20	0.20	0.03
TTW8	380.3	30.29	8.0	8.28	10.48	10.02	27.09	3.03	47.71	0.19	9-Jul-20	21-Nov-20	0.20	0.03
TTW9	370.1	21.95	5.9	8.35	12.66	9.98	27.41	2.39	39.49	0.18	13-Jul-20	22-Nov-20	0.19	0.03
TTW10	366.4	15.25	4.2	8.38	14.29	9.99	27.55	2.15	34.99	0.19	13-Jul-20	22-Nov-20	0.19	0.02
TTW11	378.2	17.02	4.5	8.58	12.26	9.97	28.35	2.79	40.78	0.21	15-Jul-20	23-Nov-20	0.21	0.03
TTW12	367.4	15.85	4.3	8.49	12.43	9.96	27.98	2.18	40.23	0.17	15-Jul-20	24-Nov-20	0.17	0.02
TTW13	389.6	20.91	5.4	8.30	10.00	9.97	27.16	3.61	50.00	0.22	14-Jul-20	25-Nov-20	0.23	0.03
TTW14	378.7	21.13	5.6	8.56	10.34	9.98	28.23	2.83	48.36	0.18	17-Jul-20	25-Nov-20	0.18	0.02